



UNIVERSITAT DE
BARCELONA

Regulation of lipid and redox metabolism in X-linked Adrenoleukodystrophy (X-ALD): therapeutic implications

Leire Goicoechea Barrenechea

ADVERTIMENT. La consulta d'aquesta tesi queda condicionada a l'acceptació de les següents condicions d'ús: La difusió d'aquesta tesi per mitjà del servei TDX (www.tdx.cat) i a través del Dipòsit Digital de la UB (diposit.ub.edu) ha estat autoritzada pels titulars dels drets de propietat intel·lectual únicament per a usos privats emmarcats en activitats d'investigació i docència. No s'autoritza la seva reproducció amb finalitats de lucre ni la seva difusió i posada a disposició des d'un lloc aliè al servei TDX ni al Dipòsit Digital de la UB. No s'autoritza la presentació del seu contingut en una finestra o marc aliè a TDX o al Dipòsit Digital de la UB (framing). Aquesta reserva de drets afecta tant al resum de presentació de la tesi com als seus continguts. En la utilització o cita de parts de la tesi és obligat indicar el nom de la persona autora.

ADVERTENCIA. La consulta de esta tesis queda condicionada a la aceptación de las siguientes condiciones de uso: La difusión de esta tesis por medio del servicio TDR (www.tdx.cat) y a través del Repositorio Digital de la UB (diposit.ub.edu) ha sido autorizada por los titulares de los derechos de propiedad intelectual únicamente para usos privados enmarcados en actividades de investigación y docencia. No se autoriza su reproducción con finalidades de lucro ni su difusión y puesta a disposición desde un sitio ajeno al servicio TDR o al Repositorio Digital de la UB. No se autoriza la presentación de su contenido en una ventana o marco ajeno a TDR o al Repositorio Digital de la UB (framing). Esta reserva de derechos afecta tanto al resumen de presentación de la tesis como a sus contenidos. En la utilización o cita de partes de la tesis es obligado indicar el nombre de la persona autora.

WARNING. On having consulted this thesis you're accepting the following use conditions: Spreading this thesis by the TDX (www.tdx.cat) service and by the UB Digital Repository (diposit.ub.edu) has been authorized by the titular of the intellectual property rights only for private uses placed in investigation and teaching activities. Reproduction with lucrative aims is not authorized nor its spreading and availability from a site foreign to the TDX service or to the UB Digital Repository. Introducing its content in a window or frame foreign to the TDX service or to the UB Digital Repository is not authorized (framing). Those rights affect to the presentation summary of the thesis as well as to its contents. In the using or citation of parts of the thesis it's obliged to indicate the name of the author.



UNIVERSITAT DE
BARCELONA

Programa de Doctorat en Biomedicina

**Regulation of lipid and redox metabolism in X-
linked Adrenoleukodystrophy (X-ALD):
therapeutic implications**

Memòria presentada per Leire Goicoechea Barrencechea per optar al grau
de doctora per la Universitat de Barcelona

Doctorand

Leire Goicoechea Barrencechea

Directora

Aurora Pujol Onofre

Tutor

Francesc Villarroya Gombau

Stephane
Fourcade-DNI:
x6284111m

Firmado digitalmente por
Stephane Fourcade-DNI:
x6284111m
Número de reconocimiento (DN):
cn=Stephane Fourcade-DNI,
x6284111m, o, ou,
email=fourcade@idb3.cat, c=ES
Fecha: 2021.03.29 12:06:39 +0200

Co-director

Stéphane Fourcade Guillou



UNIVERSITAT DE
BARCELONA

Programa de Doctorat en Biomedicina

**Regulation of lipid and redox metabolism
in X-linked Adrenoleukodystrophy (X-ALD):
therapeutic implications**

Memòria presentada per Leire Goicoechea Barrenechea per optar al grau
de doctora per la Universitat de Barcelona

Tesi realitzada al laboratori de malalties neurometabòliques de l'Institut d'Investigació
Biomèdica de Bellvitge (IDIBELL)

Doctorand
Leire Goicoechea Barrenechea

Directora
Aurora Pujol Onofre

Tutor
Francesc Villarroya Gombau

Co-director
Stéphane Fourcade Guillou

AGRADECIMIENTOS (ACKNOWLEDGMENTS)

Ya está. Ya ha llegado el día que tantas veces hemos imaginado. Al principio se ve como algo muy lejano, ¡pero es que el tiempo pasa tan rápido! (Supongo que eso es buena señal, no??). Realizar la tesis ha sido una experiencia gratificante y muy enriquecedora, tanto a nivel profesional como personal, un camino duro, sin duda, con muchos altibajos y obstáculos que superar, pero es que dicen, que lo bueno se hace esperar. Gracias a todos los que habéis formado parte de este proceso y habéis hecho vuestra aportación a esta aventura.

En primer lugar, quiero agradecer a mi directora, Aurora Pujol, por haberme dado la oportunidad de realizar la tesis en este laboratorio. En estos años con ella, he aprendido a ser minuciosa en los detalles, ser independiente y “buscarte la vida”, hacer muchas preguntas, pero sobretodo, la importancia que tiene creer en lo que haces y más aun si cabe, saber demostrarlo. También me gustaría dar las gracias a Stéphane, mi codirector y supervisor durante todos estos años. Gracias por el seguimiento y la ayuda concedida, por aguantar mis correos (quizás un poco extensos algunas veces....) y por estar pendiente. Sin duda, parte de esta tesis se debe a tu esfuerzo. Gracias también a Francesc por tutorizar esta tesis.

Al igual, me gustaría agradecer a todas las agencias y entidades financiadoras que han hecho posible la realización de esta tesis.

Hasta aquí he nombrado las personas que pueden ser las caras más visibles de lo que es esta tesis doctoral, pero todo esto no hubiera sido posible sin el trabajo realizado por todo el equipo formado por el grupo X-ALD. O mejor dicho la familia X-ALD; porque al final hemos sido como una familia, no solo por las horas que hemos pasado juntos, ¡que no han sido pocas!, sino por la piña que se crea entre nosotros y el apoyo mutuo que nos hemos dado. Empezando por mis maestros, Pablo y Janani. Fue una suerte teneros cerca en mis inicios para explicarme cómo funcionaba todo y poder adaptarme mejor. También a Devesh, que por su madurez, siempre tenía sabios consejos a mano e intentaba guiarte. Ahora cada uno está en un lugar diferente, pero sé que aun puedo acudir a vosotros cuando lo necesite. Los más seniors, Montse y Stéphane, o el “consell de savis” que decíamos, a los que acudíamos cuando teníamos dudas sobre técnicas, protocolos, resultados, etc., y podíamos pasar horas debatiendo. Gracias Montse por todas las gestiones y trámites que haces; pedidos, proyectos, contratos (¡y he tenido unos cuantos!), compras, etc., tareas que, por desgracia, muchas veces pasan inadvertidas, pero sin las cuales no se podría llevar a cabo nuestro trabajo. A Nath, gracias por tu ayuda, apoyo y consejos, sobre todo al final, cuando más me hacía falta. Mucha suerte en tu nueva etapa, estoy segura de que saldrán cosas bonitas! Agatha, aunque lo que haces me queda un poco lejano y a veces abstracto, siempre que he acudido a ti me has ayudado con las dudas que tenía. Agustí y Valentina, a vosotros también os queda poquito para acabar. ¡Mucho ánimo en la recta final!

Y qué decir de los técnicos, Juanjo y Cris, quienes con su trabajo nos hacen el día a día más fácil. Juanjo, una persona activa, alegre, cercana, charlatana, pero sobretodo, siempre dispuesto a ayudar. No importa lo que sea, él siempre intentará buscar una solución para arreglarlo. Cris, tu amabilidad y disponibilidad para colaborar en todo lo que se te plantea es increíble. Aun me impresiona tu capacidad de positivismo y mostrar

siempre una sonrisa. Ojalá todo tu trabajo se vea recompensado. Gracias también por las sesiones de “terapia” (¡a veces mutuas!) de los últimos meses.

Edgard, que aunque ya no sea parte de X-ALD, yo lo sigo incluyendo. No lo puedes evitar, sigues teniendo la “esencia” X-ALD! Junto con Laura y Valentina, cuando las guardias se lo permiten, hemos creado un vínculo de amistad que hemos compartido no solo dentro del laboratorio, sino también fuera. Para mí vuestro apoyo ha sido muy necesario en esta etapa y quiero daros las gracias por todos los buenos momentos que hemos compartido. Nos queda pendiente ir al famoso carnaval de Torelló! Laura, la meva professora particular de català, potser tu ets la que més m'ha hagut d'aguantar. Una tècnica, que ara no vaig a esmentar per a això ja hi ha la tesi jaja, va fer que comencéssim a treballar juntes i des de llavors no hem parat fins ara. Et he de donar gràcies especialment ja que has aguantat les meves "xapes" científiques, i no tan científiques. Però bé, així amenitzàvem les llargues hores en cultius mà a mà, no? Et quedes a el front, però ja has demostrat de sobres que vals per això i no tinc cap dubte que ho faràs genial. Zorte on eta animo!

A la nueva generación que viene por delante, Lorenzo e Irene, no he podido conocerlos mucho, pero por lo poco que he visto, estoy segura de que haréis un buen trabajo.

Gracias a toda la gente que forma “Genética Molecular”: Virginia, Mercè, Sara, Julián, Xavi, Josep, Atila, Ana, Esther, que me habéis ayudado siempre que he necesitado algo. Y qué decir de Antonia y Javi, a los que tantas veces habré ido a “quejarme” de que esto está roto, de que falta aquello, pedir lo otro, etc.... Y ellos siempre responden con una inmensa amabilidad y dispuestos a echar una mano. Perdona Javi por todas las veces que habrás tenido que llamar/bajar al almacén para comprobar si ha llegado ese pedido tan “urgente” que estamos esperando! No me quiero olvidar de Olga, que con su entrada cantarina y risueña, alegraba las mañanas de cultivos. Quizás por eso no tuve en cuenta que se pasó tres años llamándome Laia/Laura! Al resto de predocs de genética, Clara, Carmen, Dimitri, David, Jeremy, Xènia, Ana, Imma, Silvia, compañeros que hacen que el día a día sea más divertido y llevadero. Tengo que decir que sin esta gente mi doctorado no hubiera sido el que ha sido. No han sido solo compañeros de trabajo, sino también amigos. En breves muchos de vosotros también os enfrentaréis a esto, y espero poder estar ahí para verlo, pero lo que de verdad espero es, mantener vuestra amistad a pesar de que nuestros caminos se separen.

Llegué a Barcelona recién acabada la carrera, donde conocí a un grupo de amigos incondicionales. Me habían dicho que los amigos que haces en la universidad duran para toda la vida. No sé si será verdad, pero de momento, no me puedo quejar. Con dos de ellas, Maialen y Naroa, empecé mi viaje en Barcelona, en aquel piso en Sagrera. Un buen año el que pasamos allí, sin lugar a dudas. Maialen se marchó hace ya un tiempo, pero nuestra relación sigue siendo la misma y ella ha seguido mostrándome su apoyo durante estos años. Naroa, que aun anda por aquí, ánimo, ya no queda nada! Hau baño gauza zailagoak gainditu dituzu. Izan gogoan zerk ekarri zintun hona, eta gogoratu, lehenengo gu!

A los amigos que hice en el Máster durante mi primer año en Barcelona, gracias por todas las risas y buenos ratos que hemos pasado, y que tanto hacían falta en algunos

momentos. Gente con la que puedes hablar de ciencia, irte de cañas, a una discoteca, a la montaña, ¡o hasta de ruta gastronómica!

Quiero dar las gracias también a mis amigas del País Vasco, mi kuadrilla, que aunque sea en la distancia, siempre han estado ahí cuando las he necesitado. Las he visto mucho menos de lo que me hubiera gustado desde que me vine a Barcelona, pero sé que pase lo que pase y a pesar de los años, nos seguiremos tratando como si el tiempo no hubiera pasado. Iera, Ana, Ane, Gaxi, Arce, Jani, Amaia, Mire, Alon, Gil. Milesker danoi!

A Natalia, Mireia y la ya mencionada Clara, gracias por acogerme y haber confiado en mí para formar parte de ese épico “Can Cacauet”. Desde el primer minuto me sentí arropada por vosotras y rápidamente hicisteis que me sintiera una más. ¡Mira como son las cosas que, siempre vacilábamos con que Clara era un miembro adoptado en X-ALD y al final es ella quien me ha acogido a mí! Merci per tot!! Gracias también a Natalia por tu característica amabilidad, generosidad y ternura.

Por último, ¡no me olvido de mi familia! Tengo claro que yo no sería quién soy si no fuera por mis padres. Ellos fueron los que me inculcaron la importancia de valerse por uno mismo y de la constancia y esfuerzo en el trabajo. Han intentado entender, y yo explicarles en repetidas ocasiones, cómo funciona este mundo nuestro de la ciencia. Y aunque no estoy segura de si lo han conseguido, porque la verdad es que hay cosas que no son fáciles de entender para alguien que es ajeno a ello, junto con mis dos hermanos, Aitor y Goretti, siempre han estado ahí mostrándome su cariño y apoyo. Eskerrik asko, bihotz bihotzez! Por último, quiero dedicar unas palabras a mis abuelos, que tanto significan para mí. Mila esker jasotako animo guztiengatik!

Summary

X-linked adrenoleukodystrophy (X-ALD) is a rare neurometabolic disease characterized by the loss of function of the peroxisomal transporter ABCD1, which leads to an accumulation of very long-chain fatty acids (VLCFA), inducing the production of mitochondrial reactive oxygen species. Clinical phenotypes in humans range from adrenal insufficiency to fatal inflammatory cerebral demyelination. *Abcd1*-null mice (*Abcd1*⁻ mice) develop late-onset axonal degeneration in the spinal cord and locomotor disability resembling the most common phenotype in humans, adrenomyeloneuropathy (AMN). Oxidative stress and mitochondrial dysfunction are key common features in X-ALD patients as well as in *Abcd1*⁻ mouse.

In this thesis, we sought to explore novel therapeutic targets that would contribute to better understand the pathophysiology of the disease, based on the existing knowledge on these common hallmarks of X-ALD. First, we identified a lipidic imbalance in the X-ALD mouse models (*Abcd1*⁻ and *Abcd1*/*Abcd2*^{-/-} mice), characterized by the presence of lipid droplet (LD) accumulation, due to overactivation of the mTOR/SREBP-1c axis and its target genes (Chapter I). Next, we studied the effect of pharmacological doses of biotin in redox homeostasis and lipid metabolism in the X-ALD mouse models and fibroblasts derived from healthy subjects and X-ALD patients. In a second study, we investigated the role of E2F1, a transcription factor essential for cell cycle and metabolic homeostasis, in X-ALD pathophysiology. To address this objective, we studied E2F1 expression in the X-ALD mouse models. We found out an increase of E2F1, both at mRNA and protein level, in the spinal cord from *Abcd1*⁻ and *Abcd1*/*Abcd2*^{-/-} mice. Finally, we explored the therapeutic potential of targeting E2F1 in X-ALD mice. We followed a genetic approach by crossing E2F1-deficient mice with the X-ALD mouse models (Chapter II). Both therapeutic strategies, the pharmacological intervention with high-dose biotin and the genetic inactivation of E2F1, led to an amelioration of i) mitochondrial dysfunction, ii) bioenergetic failure, iii) oxidative damage iv) dysregulated inflammatory profile, and most importantly, v) halted axonal degeneration and behavioural abnormalities in X-ALD mice (Chapters I and II). Collectively, these findings reveal an impairment of the mTOR/SREBP-1c axis that controls lipid homeostasis in X-ALD, as well as point to E2F1 as a candidate for the impaired mitochondrial activity and antioxidant response in X-ALD. Finally, the results

of this doctoral thesis indicate that therapies based on correcting lipid accumulation and redox imbalance may be valuable strategies to treat X-ALD and other neurodegenerative disorders which share general dysregulation of lipid metabolism, impaired redox homeostasis, mitochondrial dysfunction, and neuroinflammation among their hallmarks.

Resumen

La adrenoleucodistrofia ligada al cromosoma X (X-ALD) es una enfermedad neurometabólica rara caracterizada por la pérdida de función del transportador peroxisomal ABCD1. Como consecuencia se acumulan ácidos grasos de cadena muy larga, que inducen la producción de especies reactivas de oxígeno en la mitocondria. El fenotipo clínico en humanos es variable, desde la insuficiencia suprarrenal hasta la desmielinización inflamatoria cerebral que suele ser fatal. Los ratones deficientes para el gen *Abcd1* (ratones *Abcd1*⁻) desarrollan una degeneración axonal de aparición tardía en la médula espinal e incapacidad locomotora, un fenotipo que se asemeja al más común en humanos, la adrenomieloneuropatía (AMN). El estrés oxidativo y la disfunción mitocondrial son características claves en los pacientes con X-ALD, así como en el modelo de ratón.

En esta tesis, buscamos explorar nuevas dianas terapéuticas que contribuyan a una mejor comprensión de la fisiopatología de la enfermedad, basándonos en el conocimiento existente sobre estas alteraciones en X-ALD. En primer lugar, identificamos un desequilibrio lipídico en los modelos de ratón X-ALD (*Abcd1*⁻ y *Abcd1*⁻/*Abcd2*^{-/-}), caracterizado por la acumulación de gotas lipídicas (o lipid droplets, LD), debido a la sobreactivación del eje mTOR/SREBP-1c y sus genes diana (Capítulo I). Después, estudiamos el efecto que tiene la dosis farmacológica de biotina en la homeostasis redox y el metabolismo de los lípidos en los modelos de ratón X-ALD y en fibroblastos derivados de individuos sanos y pacientes con X-ALD. En un segundo estudio, investigamos el papel de E2F1, un corregulador transcripcional esencial para el ciclo celular y la homeostasis metabólica, en la fisiopatología de X-ALD. Para abordar este objetivo, estudiamos la expresión de E2F1 en el modelo de ratón *Abcd1*⁻. Descubrimos un aumento de E2F1, a nivel de mRNA y proteína, en la médula espinal de ratones *Abcd1*⁻ y *Abcd1*⁻/*Abcd2*^{-/-}. Finalmente, exploramos el potencial terapéutico de la administración de dosis farmacológicas de biotina (Capítulo I)/silenciar E2F1 (Capítulo II) en ratones X-ALD. Para el último abordaje, seguimos una aproximación genética, cruzando ratones deficientes en E2F1 con modelos de ratón X-ALD (Capítulo II). En ambos casos, la intervención terapéutica conllevó a una mejora de i) la

disfunción mitocondrial, ii) el fallo bioenergético, iii) el daño oxidativo iv) la perturbación del perfil inflamatorio, y, lo que es más importante, detuvo la degeneración axonal y previno las alteraciones del comportamiento en ratones X-ALD (Capítulos I y II). En conjunto, estos hallazgos revelan un deterioro del eje mTOR/SREBP-1c que controla la homeostasis de los lípidos, y apuntan a E2F1 como candidato plausible para la regulación del metabolismo oxidativo, así como de la respuesta antioxidante en X-ALD. Finalmente, los resultados derivados de esta tesis doctoral indican que las terapias basadas en corregir la acumulación de lípidos y el desequilibrio redox pueden ser estrategias valiosas para tratar la X-ALD y otros trastornos neurodegenerativos que compartan la desregulación general del metabolismo de los lípidos, la homeostasis redox alterada, la disfunción mitocondrial y la neuroinflamación entre sus señas de identidad.

TABLE OF CONTENTS

List of tables	25
List of figures	27
List of abbreviations	31
1 Introduction	39
1.1 Peroxisomes: function and diseases	39
1.1.1 Peroxisome overview	39
1.1.2 Peroxisome functions	39
1.1.3 Peroxisomal ABC transporters	41
1.1.4 Peroxisomal disorders	42
1.2 General aspects of X-linked adrenoleukodystrophy	43
1.2.1 History	43
1.2.2 Clinical features	45
1.2.3 Biochemical and molecular diagnosis	47
1.2.4 Genetics and biochemistry	48
1.2.4.1 X-ALD mutations and modifier genes	48
1.2.4.2 Origin of VLCFA	51
1.2.4.3 Biochemical aspects of X-ALD	51
1.2.5 Therapeutic strategies	52
1.2.6 Animal models	55
1.2.7 The role of VLCFA in the pathogenesis of X-ALD	57
1.3 Hallmarks of X-ALD	58
1.3.1 Redox dyshomeostasis	58

1.3.1.1	Role of ROS in X-ALD	59
1.3.2	Mitochondrial dysfunction	61
1.3.2.1	Mitochondrial functions	61
1.3.2.2	Mitochondria and the central nervous system	62
1.3.2.3	Mitochondrial dysfunction associated to neurodegeneration	63
1.3.2.3.1	Mitochondrial dysfunction in X-ALD	64
1.3.2.4	Mitochondrial biogenesis	65
1.3.2.4.1	Upstream metabolic sensors	66
1.3.2.4.2	Regulation of mtDNA transcription and replication	66
1.3.2.4.3	Regulation of nuclear-encoded mitochondrial genes	67
1.3.2.4.4	Mitochondrial biogenesis impairment in neurodegeneration ...	69
1.3.3	Neuroinflammation	70
1.3.3.1	Microglial dysfunction in X-ALD	72
1.3.4	Proteostasis impairment	74
1.3.4.1	Ubiquitin-proteasome system	74
1.3.4.2	Autophagic flux	75
1.3.5	ER stress	75
1.3.6	Lipidic imbalance: new member in the family?	76
1.3.6.1	Lipids and the central nervous system	76
1.3.6.2	Lipid-derived neurodegeneration in the CNS	77
1.3.6.2.1	Lipid-derived neurodegeneration in X-ALD	81

1.4 Biotin: physiological functions and therapeutic potential	83
1.5 E2F1: cycling through metabolism	88
1.5.1 The E2Fs transcription factors family	88
1.5.2 Metabolic functions of E2F1	92
1.5.3 E2F1 in the CNS	95
1.5.4 The role of E2F1 in BM-derived cells	96
1.5.4.1 The origin of microglia	96
1.5.4.1.1 CD34 ⁺ cells	99
1.5.4.2 Bone Marrow Transplantation in X-ALD	100
1.5.4.3 The role of E2F1 in BM-derived HSCs	101
2 Aim and objectives	107
3 Materials and Methods	113
3.1 Human samples	113
3.1.1 Evaluation of intracellular ROS	113
3.1.2 Evaluation of reduced glutathione	114
3.1.3 Inner mitochondrial membrane potential quantification by flow cytometry 114	
3.2 Mouse experiments	114
3.2.1 Mouse strains	114
3.2.1.1 X-ALD mice	115
3.2.1.2 Generation of <i>Abcd1</i> ⁻ / <i>E2f1</i> ⁻ and <i>Abcd1</i> ⁻ / <i>Abcd2</i> ⁻ / <i>E2f1</i> ⁻ mice	115
3.2.2 Biotin administration	116
3.2.3 Bone marrow transplantation	117
3.2.3.1 Bone marrow extraction, processing and injection	117

3.2.3.2 Irradiation	118
3.2.3.3 Recipient mice follow up	118
3.2.3.4 Chimerism determination	119
3.3 Quantitative real-time PCR	120
3.4 Immunoblotting	124
3.5 High-resolution respirometry	126
3.6 ATP measurement	127
3.7 Lipidomic analysis	128
3.8 LPC 26:0 absolute quantification	128
3.9 Triglyceride level measurement	129
3.10 Oil red O staining and quantification of lipid droplets (LD)	130
3.11 Immunohistochemistry (IHC)	130
3.12 Behavioural test	131
3.12.1 Horizontal bar cross test	131
3.12.2 Treadmill test	132
3.12.3 Hindlimbs clasping test	133
3.13 Statistical analysis	133
4 Results	139
4.1 Chapter I: high-dose biotin restores redox balance, energy and lipid homeostasis, and axonal health in a model of adrenoleukodystrophy	139
4.1.1 Biotin counteracts redox imbalance in human fibroblasts	139
4.1.2 High-dose biotin rescues mitochondrial biogenesis and energy failure in <i>Abcd1</i> ⁻ mice	140

4.1.3 Increased triglyceride levels in the spinal cord of <i>Abcd1</i> ⁻ mice and restoration by high-dose biotin	141
4.1.4 Increased size and number of lipid droplets (LDs) accumulated in motor neurons of <i>Abcd1</i> ⁻ / <i>Abcd2</i> ^{-/-} mice and restoration by high-dose biotin	147
4.1.5 Transcriptional dysregulation of lipid homeostasis in <i>Abcd1</i> ⁻ mice spinal cord and restoration by high-dose biotin	148
4.1.6 Lipid imbalance is not an early event in X-ALD mice.....	153
4.1.7 High-dose biotin prevents locomotor deficits in <i>Abcd1</i> ⁻ / <i>Abcd2</i> ^{-/-} mice ...	155
4.1.8 High-dose biotin prevents axonal degeneration in <i>Abcd1</i> ⁻ / <i>Abcd2</i> ^{-/-} mice .	155
4.2 Chapter II: study of the role of transcription factor E2F1 in X-ALD pathophysiology: neuroprotective effect of E2F1 deletion in X-ALD mouse models .	161
4.2.1 E2F1 expression is elevated in <i>Abcd1</i> ⁻ mice spinal cord	161
4.2.2 E2F1 deletion prevents mitochondrial depletion and bioenergetic failure in X-ALD mice	161
4.2.3 Loss of E2F1 prevents inflammatory imbalance in <i>Abcd1</i> ⁻ mice spinal cord	163
4.2.4 E2F1 deletion restores lipid homeostasis in <i>Abcd1</i> null mice	164
4.2.5 E2F1 deletion restores redox homeostasis in <i>Abcd1</i> null mice	170
4.2.6 E2F1 deficiency halts axonal degeneration and neurological symptoms of <i>Abcd1</i> ⁻ / <i>Abcd2</i> ^{-/-} mice	171
4.2.7 <i>Abcd1</i> ⁻ / <i>Abcd2</i> ^{-/-} / <i>E2f1</i> ^{-/-} bone marrow-derived cells are equally engrafted in WT and <i>Abcd1</i> ⁻ / <i>Abcd2</i> ^{-/-} mice	176

4.2.8 Bone marrow transplantation with <i>Abcd1</i> ⁻ / <i>Abcd2</i> ⁻ / <i>E2f1</i> ⁻ cells in <i>Abcd1</i> ⁻ / <i>Abcd2</i> ⁻ mice	178
4.2.9 <i>Abcd1</i> ⁻ / <i>Abcd2</i> ⁻ / <i>E2f1</i> ⁻ bone marrow-derived cells are successfully engrafted in <i>Abcd1</i> ⁻ / <i>Abcd2</i> ⁻ mice	179
4.2.10 Bone marrow transplantation with <i>Abcd1</i> ⁻ / <i>Abcd2</i> ⁻ / <i>E2f1</i> ⁻ cells prevents locomotor disability in <i>Abcd1</i> ⁻ / <i>Abcd2</i> ⁻ mice	182
4.2.11 Bone marrow transplantation with <i>Abcd1</i> ⁻ / <i>Abcd2</i> ⁻ / <i>E2f1</i> ⁻ cells halts axonal degeneration in <i>Abcd1</i> ⁻ / <i>Abcd2</i> ⁻ mice	182
5 Discussion	189
5.1 Chapter I	189
5.2 Chapter II	195
5.3 Global discussion	203
6 Conclusions	213
7 Bibliography	219
Appendix 1	257

LIST OF TABLES

Table 1 List of quantitative RT-PCR probes used in this thesis	122
Table 2 List of Sybr Green primers used in this thesis	123
Table 3 List of primary antibodies used in this thesis	125
Table 4 List of secondary antibodies used in this thesis	125
Table 5 Scoring system for the hindlimbs clasping test	134

LIST OF FIGURES

Figure 1 Comparison and interplay of peroxisomal and mitochondrial fatty acid β -oxidation in humans	41
Figure 2 Typical white matter lesions in a ccALD patient	46
Figure 3 Model recapitulating the noxious effects of VLCFA excess on mitochondria, redox homeostasis and proteolytic machineries in X-ALD	83
Figure 4 Schematic representation of the acetyl-CoA carboxylase reaction	84
Figure 5 Schematic representation of the structure of the E2F family members	90
Figure 6 Schematic overview of the molecular regulation of cell cycle	91
Figure 7 Macrophages and microglia in the CNS	98
Figure 8 Characterization of E2F1 knockout mice	116
Figure 9 “E2F1 KO” gradient	120
Figure 10 E2F1 PCR amplification cycle determination	120
Figure 11 Biotin prevents ROS production of mitochondrial origin in X-ALD patients’ fibroblasts	142
Figure 12 Biotin normalizes GSH levels in X-ALD patients’ fibroblasts	144
Figure 13 High-dose biotin rescues mitochondrial biogenesis and prevents energetic failure in <i>Abcd1</i> ⁻ mice spinal cord	146
Figure 14 High-dose biotin rescues TAG levels in <i>Abcd1</i> ⁻ mice spinal cord	149
Figure 15 High-dose biotin normalizes excess lipid droplet accumulation in <i>Abcd1</i> ⁻ / <i>Abcd2</i> ^{-/-} mice	151
Figure 16 High-dose biotin inhibits lipogenesis through mTOR in <i>Abcd1</i> ⁻ mice	152
Figure 17 Lipid metabolism in 3-month-old X-ALD mouse models	154
Figure 18 High-dose biotin halts axonal degeneration and locomotor disability in <i>Abcd1</i> ⁻ / <i>Abcd2</i> ^{-/-} mice	157
Figure 19 Model recapitulating high-dose biotin’s mode of action in X-ALD.....	159
Figure 20 E2F1 induction in X-ALD	162
Figure 21 E2F1 deletion rescues mitochondrial biogenesis and prevents energetic failure in <i>Abcd1</i> ⁻ mice spinal cord	165
Figure 22 E2F1 deletion normalizes inflammatory genes expression in X-ALD mouse spinal cord	167

Figure 23 E2F1 deletion inhibits lipogenesis, induces β -oxidation and normalizes excess of lipid droplet accumulation in <i>Abcd1</i> ⁻ mice	168-169
Figure 24 Loss of E2F1 reactivates NRF2-antioxidant pathway in <i>Abcd1</i> ⁻ mice	171
Figure 25 Loss of E2F1 halts axonal degeneration and locomotor disability in <i>Abcd1</i> ⁻ / <i>Abcd2</i> ^{-/-} mice	173
Figure 26 Model illustrating E2F1-dependent effects in X-ALD	175
Figure 27 Chimerism determination at 4 months post-transplantation	177
Figure 28 Evaluation of hair depigmentation in irradiated mice	178
Figure 29 Survival rate after transplantation with BM-derived cells	179
Figure 30 Chimerism determination at 4 months post-transplantation	180
Figure 31 Chimerism determination at the end of procedure	181
Figure 32 BMT with <i>Abcd1</i> ⁻ / <i>Abcd2</i> ^{-/-} / <i>E2f1</i> ^{-/-} cells halts locomotor disability and axonal degeneration in <i>Abcd1</i> ⁻ / <i>Abcd2</i> ^{-/-} mice	183-184
Figure 33 Model illustrating the role of mTOR in the etiopathogenesis of axonal degeneration in X-linked adrenoleukodystrophy	205

LIST OF ABBREVIATIONS

AASA	Aminoadipic semialdehyde
ABC	ATP-binding cassette
ABCD1	ATP-binding cassette, sub-family D, member 1
ABCD2	ATP-binding cassette, sub-family D, member 2
ABCD3	ATP-binding cassette, sub-family D, member 3
ABCD4	ATP-binding cassette, sub-family D, member 4
ACTH	Adrenocorticotrophic hormone
AD	Alzheimer's disease
ADP	Adenosine diphosphate
AKT	RAC-alpha serine/threonine-protein kinase
ALDP	Adrenoleukodystrophy protein
ALDRP	Adrenoleukodystrophy-related protein
ALS	Amyotrophic lateral sclerosis
AMN	Adrenomyeloneuropathy
AMP	Adenosine monophosphate
AMPK	Adenosine monophosphate (AMP)-activated protein kinase
ATP	Adenosine triphosphate
A β	Amyloid- β
BBB	Brain blood barrier
BM	Bone marrow
C16:0	Palmitic acid
C18:0	Stearic acid
C22:0	Docosanoic acid
C24:0	Tetracosanoic acid
C26:0	Hexacosanoic acid
C26:0-LPC	C26:0 lysophosphatidylcholine
cAMN	Cerebral adrenomyeloneuropathy
ccALD	Childhood cerebral adrenoleukodystrophy

CD34 ⁺	Cluster of differentiation 34
CDKs	Cyclin-dependent kinases
CDK1	Cyclin-dependent kinase 1
CDK4	Cyclin-dependent kinase 4
CDK5	Cyclin-dependent kinase 5
cDNA	Complementary deoxyribonucleic acid
CEL	Carboxyethyl lysine
CML	Carboxymethyl lysine
CNS	Central nervous system
CO ₂	Carbon dioxide
CoA	Coenzyme A
CTL	Control
DAG	Diacylglycerols
DKO	<i>Abcd1</i> ^{-/-} / <i>Abcd2</i> ^{-/-} double knockout
DNA	Deoxyribonucleic acid
DS	Down syndrome
E2F	E2 promoter binding factor
E2F1	E2 promoter binding factor 1
E2F2	E2 promoter binding factor 2
E2F3	E2 promoter binding factor 3
E2F4	E2 promoter binding factor 4
E2F5	E2 promoter binding factor 5
E2F6	E2 promoter binding factor 6
E2F7	E2 promoter binding factor 7
E2F8	E2 promoter binding factor 8
ELOVL	Elongase of very long-chain fatty acids
ELOVL1	Elongase of very long-chain fatty acids 1
ELOVL6	Elongase of very long-chain fatty acids 6
ER	Endoplasmic reticulum
ERR	Estrogen-related receptors

ERR α	Estrogen-related receptors α
ERR β	Estrogen-related receptors β
ERR γ	Estrogen-related receptors γ
ETC	Electron transport chain
FAD	Flavin adenine dinucleotide
FADH ₂	Flavin adenine dinucleotide (reduced form)
FAO	Fatty acid β -oxidation
GABP	GA-binding protein
GC/MS	Gas chromatography/mass spectrometry
GSA	Glutamic semialdehyde
GSH	Reduced glutathione
GSK-3 β	Glycogen synthase kinase 3 β
H ₂ O	Water
H ₂ O ₂	Hydrogen peroxide
HD	Huntington's disease
HDACs	Histone deacetylases
HSCT	Haematopoietic stem cell transplantation
IHC	Immunohistochemistry
IL	Interleukin
iNOS	Inducible nitric oxide synthase
LD	Lipid droplet
LDL	Low-density lipoprotein
LPC	Lysophosphatidylcholine
LPS	Lipopolysaccharide
LSCS	Lumbar spinal cord slices
MDA	Malondialdehyde
MDAL	MDA-lysine
MIM	Mitochondrial inner membrane
mPTP	Mitochondrial permeability transition pore
MRI	Magnetic resonance imaging

mRNA	Messenger ribonucleic acid
MS	Multiple sclerosis
mtDNA	Mitochondrial DNA
mTOR	Mammalian target of rapamycin
NAD ⁺	Nicotinamide adenine dinucleotide
NADH	Nicotinamide adenine dinucleotide (reduced form)
NADPH	Nicotinamide adenine dinucleotide phosphate (reduced form)
NAFLD	Nonalcoholic fatty liver disease
NAWM	Normal-appearing white matter
NCOR1	Nuclear receptor co-repressor 1
NRF1	Nuclear respiratory factor 1
NRF2	Nuclear factor, erythroid 2 like 2
O ₂	Oxygen
OPC	Oligodendrocyte precursor cell
ORO	Oil red O
OXPHOS	Oxidative phosphorylation
p70 S6K	Ribosomal protein S6 kinase beta-1
PBDs	Peroxisome biogenesis disorders
PBMC	Peripheral blood mononuclear cells
PCR	Polymerase chain reaction
PD	Parkinson's disease
PDK4	Pyruvate dehydrogenase kinase 4
PEDs	Peroxisomal enzyme deficiencies
PEX	Peroxisins
PGC-1	Peroxisome proliferator-activated receptor gamma coactivator 1
PGC-1 α	Peroxisome proliferator-activated receptor gamma coactivator 1 α
PGC-1 β	Peroxisome proliferator-activated receptor gamma coactivator 1 β
PI3K	Phosphoinositol 3-kinase
POLRMT	Mitochondrial RNA polymerase
PLP	Proteolipid protein

PPAR	Peroxisome proliferator-activated receptors
PPAR α	Peroxisome proliferator-activated receptors α
PPAR β/δ	Peroxisome proliferator-activated receptors β/δ
PPAR γ	Peroxisome proliferator-activated receptors γ
PPi	Pyrophosphate
pRB	Product of retinoblastoma
PUFA	Polyunsaturated fatty acids
qRT-PCR	Quantitative real-time PCR
RB	Retinoblastoma
RCDP	Rhizomelic chondrodysplasia punctata
R.C.R	Respiratory control ratio
RIP140	Receptor-interacting protein 140
RNS	Reactive nitrogen species
ROS	Reactive oxygen species
RXR	Retinoid X receptors
SREBP	Sterol regulatory element binding-protein
TAG	Triacylglyceride
TBS-T	Tris-buffer saline-Tween 20
TCA	Tricarboxylic acid
TKO	<i>Abcd1</i> ^{-/-} / <i>Abcd2</i> ^{-/-} / <i>E2f1</i> ^{-/-} triple knockout
TFAM	Mitochondrial transcription factor A
TFB1M	Mitochondrial transcription factor B1
TFB2M	Mitochondrial transcription factor B2
UPS	Ubiquitin proteasome system
USA	United States of America
VLCFA	Very long-chain fatty acids
WT	Wild type
X-ALD	X-linked adrenoleukodystrophy

INTRODUCTION

1 Introduction

1.1 Peroxisomes: function and diseases

1.1.1 Peroxisome overview

Present in virtually all eukaryotic cells except for erythrocytes, peroxisomes are small single-bound membrane subcellular organelles that lack DNA (Schluter et al., 2010). They contain a granular matrix and a crystalline core, and their diameter ranges from 0.1 μm to 1 μm . However, their shape and size can vary in different tissues depending on their needs (Smith and Aitchison, 2013). They were first observed by Johannes Rhodin during his doctoral thesis on the ultrastructure of proximal tubule cells from mouse kidney (Rhodin, 1954) and later described by Christian de Duve and collaborators, which gave them the name of peroxisomes based on the presence of oxidases, enzymes that generate hydrogen peroxide (H_2O_2), and catalase within these organelles (De Duve and Baudhuin, 1966). In the beginning, an endosymbiotic origin like mitochondria was proposed for these organelles, as they also contain their own protein import system and share some functions as well as fission machinery. Nonetheless, the current view of peroxisomes origin points to the endoplasmic reticulum (ER) (Gabaldon et al., 2006; Schluter et al., 2006; van der Zand et al., 2012) and mitochondria (Sugiura et al., 2017) as the organelles from which peroxisomes are formed. Peroxisomes perform essential metabolic functions in the organism and are dynamic organelles able to adjust their number and protein content in response to metabolic needs and physiological conditions.

1.1.2 Peroxisome functions

Essentially all types of peroxisomes degrade toxic H_2O_2 by catalase and are involved in fatty acid β -oxidation (FAO) (Lazarow and De Duve, 1976). Additionally, peroxisomes in higher eukaryotes carry out essential functions for metabolic homeostasis (Wanders and Waterham, 2006) such as fatty acid α -oxidation, glyoxylate detoxification (Breidenbach and Beevers, 1967) and anabolic functions (Schluter et al., 2006) such as biosynthesis of bile acids or essential polyunsaturated fatty acids like docosahexaenoic acid ($\text{C}_{22:6} \omega_3$) and ether phospholipids like plasmalogens for instance (Hajra and

Bishop, 1982). Detoxification of reactive oxygen species was the first described function in peroxisomes (Schrader and Fahimi, 2004) as these organelles harbour both the oxidases that generate H_2O_2 , as well as the enzymes needed for their clearance, such as catalase (De Duve and Baudhuin, 1966), glutathione peroxidase (Singh et al., 1994) and peroxiredoxin V (PMP20) (Yamashita et al., 1999). Another reactive oxygen specie, the superoxide anion (O_2^-), can be generated in the peroxisome by xanthine oxidase (Angermuller et al., 1987), and posteriorly inactivated by superoxide dismutases (Cu/Zn-SOD and Mn-SOD), enzymes reported to be present in the peroxisome (Dhaunsi et al., 1992; Keller et al., 1991; Singh et al., 1999). In addition to reactive oxygen species, the detection of inducible nitric oxide synthase (iNOS) enzyme in this organelle suggests that peroxisomes may also be a source of nitric oxide and its subsequent toxic species, such as peroxynitrite (Stolz et al., 2002). FAO is a universal property of peroxisomes in most organisms, either as the sole site of β -oxidation, like in yeasts and plants, or as a shared function with mitochondria, in higher eukaryotes. Short- and medium-chain fatty acids are exclusively, while long-chain fatty acids are predominantly, β -oxidized in mitochondria. Meanwhile, very long-chain fatty acids (VLCFA), particularly hexacosanoic acid (C26:0), can only be oxidized by peroxisomes (Singh et al., 1984b). Mitochondrial and peroxisomal FAO share a similar mechanism but differ in their function, as suggested by the different clinical signs and symptoms observed in disorders associated with inherited defects in mitochondrial and peroxisomal β -oxidation (Wanders, 2003). The mechanism by which fatty acids are oxidized through the shortening of 2 carbons through a sequential cycle of dehydrogenation, hydration, dehydrogenation, and thiolytic cleavage that produces acetyl-coenzyme A (Acetyl-CoA) molecules, is common in both organelles. However, they differ in how the flavin adenine dinucleotide (reduced form) ($FADH_2$), produced in the first dehydrogenation step, is reoxidized. In peroxisomes, the $FADH_2$ reacts with O_2 to produce H_2O_2 , which is degraded by peroxisomal catalase into H_2O and O_2 , while in mitochondria, the reoxidation of $FADH_2$ is coupled to the electron transport chain to produce energy. Although peroxisomes contain all the necessary machinery to carry out the oxidation of fatty acids, it is not completed in the peroxisome. When fatty acids reach a certain size (C6-C8), short, medium and long-chain fatty acids, they are transported to the mitochondria to finish their oxidation. Both β -oxidation pathways have been illustrated in **Fig. 1**. Acetyl-CoA molecules, together with other products of β -oxidation in the peroxisome such as medium-chain acyl-CoA are transferred to the

mitochondria for full oxidation to CO₂ and H₂O via carnitine- and thioesterase-mediated pathways, although this process is not well known yet.

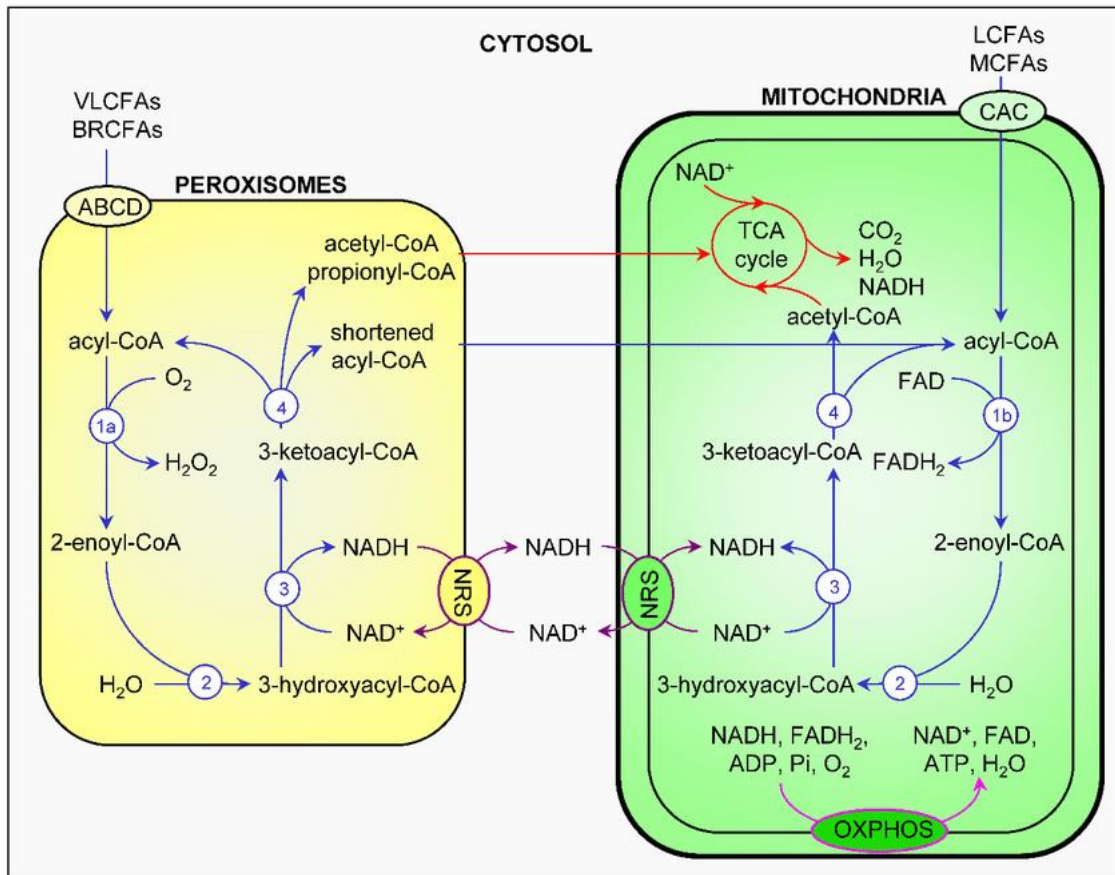


Figure 1. Comparison and interplay of peroxisomal and mitochondrial fatty acid β -oxidation in humans. Fatty acid β -oxidation, NAD(H) redox shuttles, tricarboxylic acid cycle, and the electron transfer chain are respectively depicted in blue, purple, red, and pink. 1a) acylCoA oxidase; 1b) acyl-CoA dehydrogenase; 2) enoyl-CoA hydratase; 3) 3-hydroxyacyl-CoA dehydrogenase; 4) 3-ketoacyl-CoA thiolase. ABCD: ATP-binding cassette transporters of subfamily D; ADP: adenine dinucleotide phosphate; BRCFA: branched-chain fatty acid; CAC: carnitineacylcarnitine carrier; FAD: flavin adenine dinucleotide; FADH₂: reduced FAD; LCFA: long-chain fatty acid; MCFA: medium-chain fatty acid; NAD: nicotinamide adenine dinucleotide; NADH: reduced NAD; NRS: NAD(H) redox shuttles; OXPHOS: oxidative phosphorylation; TCA: tricarboxylic acid; VLCFA: very long-chain fatty acid. From (Fransen et al., 2017).

1.1.3 Peroxisomal ABC transporters

ATP-binding cassette (ABC) transporters couple ATP hydrolysis to the transport of substrates across biological membranes. *ABCD1*, the defective gene in X-linked

adrenoleukodystrophy (X-ALD) (Mosser et al., 1993) belongs to the mammalian peroxisomal ABC subfamily D (ABCD) transporters, which also include ALD-related protein (ALDRP or ABCD2) (Lombard-Platet et al., 1996), peroxisomal membrane protein of 70 kDa (PMP70 or ABCD3) (Kamijo et al., 1990) and PMP70-related protein (PMP70R or ABCD4) (Shani et al., 1997). All the four ABCD subfamily genes are conserved in vertebrates whereas in *Drosophila* and yeasts only two members of the subfamily are present (Bossier et al., 1994; Ewart et al., 1994; Shani et al., 1995). In the brain, ABCD1 is expressed strongly in glia (astrocytes, microglia and a subpopulation of oligodendrocytes) and endothelial cells, but not in most neurons, except for a few regions: hypothalamus, basal nucleus of Meynert, periaqueductal grey matter and the locus coeruleus (Fouquet et al., 1997; Hoftberger et al., 2007; Troffer-Charlier et al., 1998). ABCD2 is the closest homolog to ABCD1 (Ferrer et al., 2005), as they share 66% of identity with overlapping functions (Pujol et al., 2004), and a mirror expression in most tissues (Troffer-Charlier et al., 1998). ABCD3 is involved in the transport of hydrophilic substrates like long-chain unsaturated-, long branched-chain- and long-chain dicarboxylic fatty acids into the peroxisome (van Roermund et al., 2014), and is also essential for bile acid biosynthesis (Ferdinandusse et al., 2015). Although ABCD4 was initially considered a peroxisomal transporter, it is no longer considered a peroxisomal protein, since it is located in lysosomes and ER (Coelho et al., 2012; Kashiwayama et al., 2009). Functional ABC transporters comprise two structurally similar halves, each containing six transmembrane alpha-helices and one hydrophilic nucleotide-binding domain (Dean and Annilo, 2005). Half transporters need to homo- or hetero-dimerize to be functional. Indeed homo-dimerization of ABCD1 and hetero-dimerization of ABCD1 with ABCD2 and ABCD3 have been described *in vitro* (Geillon et al., 2014; Genin et al., 2011; Liu et al., 1999). Conversely, *in vivo* evidence suggests that at least ABCD1 and ABCD3 function as homodimers (Guimaraes et al., 2004). Finally, a recent study has shown that ABCD1 and ABCD2 are organized in tetramers, i.e dimers of full transporters, *in vitro* (Geillon et al., 2017).

1.1.4 Peroxisomal disorders

Most of the information known about the essential functions of peroxisomes comes from the phenotype of patients with mutations in genes encoding for peroxisomal

proteins. The severity of these diseases varies from early lethality to mild neurosensory defects. These disorders can be classified into peroxisome biogenesis disorders (PBDs) and single peroxisomal enzyme deficiencies (PEDs). The majority of PBDs are autosomal recessive disorders caused by mutations in any of the 14 PEX genes encoding the peroxins, which are involved in the import of peroxisomal membrane and/or matrix proteins into the peroxisome (Smith and Aitchison, 2013). Within PBDs, there are three distinct subtypes: the Zellweger spectrum disorders; rhizomelic chondrodysplasia punctata (RCDP) type 1 and 5, and the recently described peroxisomal fission defects. Genetic causes, as well as phenotypic description of these disorders, have been reviewed in detail elsewhere (Waterham et al., 2016). On the other hand, PEDs include defects of peroxisomal matrix enzymes as well as peroxisomal membrane proteins involved in metabolite transport. The biochemical and clinical consequences of each PED thus depend on the specific function of each affected protein in the peroxisome. Among PEDs, we can find defects in peroxisomal fatty acid α - and β -oxidation, including Refsum disease and X-ALD; glyoxylate metabolism, ether-phospholipid biosynthesis (RCDP type 2, 3 and 4), bile acid synthesis, and catalase metabolism, all of them comprehensively reviewed in (Waterham et al., 2016). In summary, peroxisomes play an essential role in metabolism and are crucial for life. Peroxisomal disorders comprise a heterogeneous group of disorders that account for a substantial fraction of inborn errors of metabolism, with an estimated combined incidence of 1:5000 individuals, being X-ALD the most common among them.

1.2 General aspects of X-linked adrenoleukodystrophy (X-ALD)

1.2.1 History

The first report of X-ALD goes back to 1910, when Haberland and Spieler described the case of a six-year-old boy with visual impairment, school failure, altered gait and hyperpigmentation, symptoms that would be later described as the prototypical of the disease. The disease rapidly progressed to an inability to walk and speak, and he died 8 months later. This boy had an older brother who died at 8.5 years old due to a similar illness. The neuropathological post-mortem examination by Paul Schilder, reported diffuse involvement of the cerebral hemispheres with severe loss of myelin, relative

preservation of axons and accumulation of lymphocytes, fat-laden phagocytes and glial cells (Schilder, 1924). Siemerling and Creutzfeldt described a similar case, but with adrenal gland involvement (Siemerling and Creutzfeldt, 1923). The disease was first named Schilder's disease and later, in 1970, Blaw coined the term adrenoleukodystrophy.

Based on the pedigree analysis and the notion that all patients were boys, Fanconi proposed that X-ALD was a genetic disorder with X-linked inheritance (Fanconi et al., 1963). Key insights were achieved during the seventies. Powers and Schaumburg described characteristic lamellar inclusions in the adrenal gland and brain macrophages of X-ALD boys, which had an unusually high proportion of VLCFA (C24-30) (Powers and Schaumburg, 1974). Few years later, X-ALD research achieved a milestone when it was demonstrated that these inclusions were enriched in cholesterol esterified with saturated very long-chain fatty acids (VLCFA) (Igarashi et al., 1976). From that moment, X-ALD is classified as a lipid storage disease. In 1976, two independent groups identified adult X-ALD patients (Budka et al., 1976; Griffin et al., 1977). In the 80s, it was shown that high levels of VLCFA accumulate in cultured skin fibroblasts and plasma from X-ALD patients (Moser et al., 1981; Moser et al., 1980), thus VLCFA levels could be used for diagnosis and is still nowadays used as pathognomonic marker of the disease (Moser and Moser, 1999). Later on, it was demonstrated that white blood cells and cultured skin fibroblasts had an impaired capacity to degrade VLCFA (Singh et al., 1984b) and the gene mutated in X-ALD was mapped to Xq28 (Migeon et al., 1981), which corroborated the mode of inheritance proposed in the 60s (Fanconi et al., 1963). The inclusion of X-ALD into the group of peroxisomal disorders did not arrive until 1984, when Singh et al. proved that X-ALD patients are not able to degrade VLCFA (Singh et al., 1984b), a reaction localized in the peroxisome (Singh et al., 1984a). In 1993, Mosser et al. identified the X-ALD gene by positional cloning, coding for a peroxisomal membrane ABC transporter (Mosser et al., 1994), referred to as ALDP protein, and later, as ABCD1. This crucial discovery allowed the generation of mouse models in 1997 (Forss-Petter et al., 1997; Kobayashi et al., 1997; Lu et al., 1997) and the successful lentiviral-mediated gene therapy in 2009 (Cartier et al., 2009).

1.2.2 Clinical features

X-ALD (McKusick no. 300100) is the most common peroxisomal disease and leukodystrophy, with an incidence of 1:14700 live births (Moser and Fatemi, 2018). X-ALD affects the nervous system white matter and the adrenal cortex and, as other inborn errors of metabolism, is considered a progressive metabolic disease, as all patients are asymptomatic at birth. The major and pathognomonic biochemical alteration in X-ALD is the accumulation of VLCFA, especially C26:0 and C24:0, in target organs (central nervous system and adrenal glands), fibroblasts and plasma. X-ALD patients display a complex range of clinical phenotypes, starting from adrenal insufficiency (Addison disease) to rapidly progressive and fatal cerebral demyelination (cerebral ALD). Overall, adrenal function is abnormal in 80% of patients (Dubey et al., 2005). The two main clinical phenotypes in affected males are:

1) Adrenomyeloneuropathy (AMN): Virtually all patients who reach adulthood develop AMN, characterized by peripheral neuropathy and distal axonopathy involving corticospinal tracts of the spinal cord, but neither brain neuroinflammation nor cerebral demyelination. 60% of affected patients present AMN, manifested in the late twenties as progressive spastic paraparesis, sphincter incontinence, sexual disturbances and impaired adrenocortical function (Moser, 2001). All symptoms progress over decades, leading to the development of additional cerebral demyelination (cerebral AMN, cAMN), in a high proportion of AMN patients at later stages, between 20% (van Geel et al., 2001) and 63% (de Beer et al., 2014), depending on the study.

2) Childhood cerebral ALD (ccALD): This phenotypic presentation affects boys before the 10th year of age. It affects approximately 35% of patients. The first neurologic symptoms are in the behavioural and learning sphere and often misdiagnosed as hyperactivity or attention deficit disorder. Next, progressive impairment of cognition, behaviour, vision, hearing and motor function often leads to total disability within two years and eventual death before adolescence (Kemp et al., 2012). It is characterized by cerebral demyelination with a strong inflammatory component. Lesions show gadolinium enhancement just behind the leading edge of the lesion (**Fig. 2**). Cerebral white matter lesions in X-ALD can be scored using the Loes classification system on a

scale from 0 (normal on magnetic resonance imaging, MRI) to 34 (severely abnormal) (Loes et al., 1994).

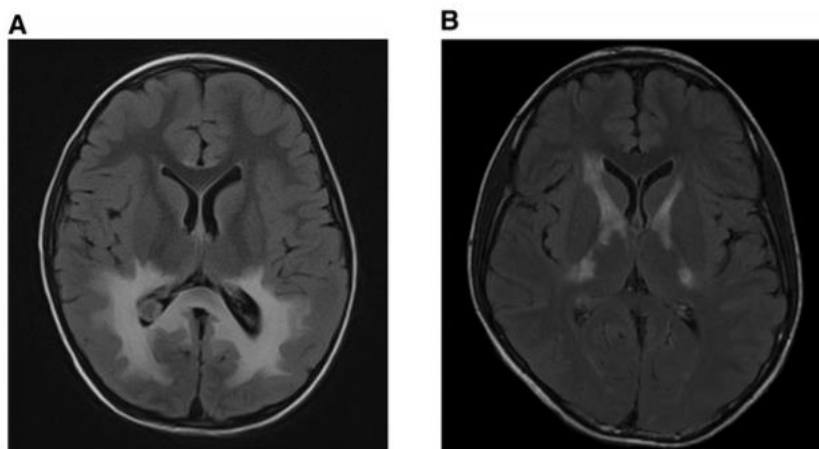


Figure 2. (A) Brain MRI (axial images; FLAIR sequence) showing abnormally increased signal in the splenium of the corpus callosum, the parieto-occipital white matter, the visual pathways (optic radiations and lateral geniculate bodies), as well as the medial geniculate bodies of auditory pathway and the posterior limbs of the internal capsules. The demyelinating lesions are extensive and correspond to an advanced disease stage. (B) Brain MRI (axial images; FLAIR sequence) showing abnormally increased signal involving the posterior and anterior limbs of the left and right internal capsule. From (Kemp et al., 2012).

Although with a lesser phenotypic manifestation, other clinical phenotypes of the disease have been described:

3) **Asymptomatic or presymptomatic**: Some asymptomatic patients have been diagnosed after family screening, either by presenting elevated levels of VLCFA or mutations in the *ABCD1* gene. This form is common in boys under 4 years of age and very rare in males after age 40 (Engelen et al., 2012a).

4) **Adolescent cerebral ALD (AdolcALD)**: This phenotype resembles ccALD but with a slower progression and a later onset, between 11 and 21 years of age. Present in 4 to 7% of patients (Engelen et al., 2012a).

5) **Adult cerebral ALD (AcALD)**: This phenotype corresponds to X-ALD patients who develop cerebral symptoms after 21 years without spinal cord involvement. These patients are often misdiagnosed as having paranoid psychosis, schizophrenia or brain

tumour. The progression parallels that of the ccALD, with a mean interval between first neurological symptoms and vegetative state or death of 3 to 4 years. This phenotype is relatively rare and affects only 2 to 5% of patients (Engelen et al., 2012a).

6) Female carriers: Approximately 80% of carrier women develop AMN-like symptoms, including myelopathy or peripheral neuropathy. The frequency of symptomatic women is directly proportional to age (from 18% in women <40 years to 88% in women >60 years of age) (Engelen et al., 2014; Engelen et al., 2012a).

7) Addison Disease Only: Adrenocortical insufficiency is present in 80% of all male X-ALD patients and may be the initial presentation years or even decades prior to the onset of neurological symptoms (Dubey et al., 2005). However, there is a small subset of X-ALD patients (10%) who suffer adrenal insufficiency without demonstrable evidence of nervous system involvement (Engelen et al., 2012a).

1.2.3 Biochemical and molecular diagnosis

VLCFA are elevated in all male X-ALD patients regardless of age, disease duration, metabolic status, or clinical symptoms. Definitive diagnosis of X-ALD is achieved by demonstration of the biochemical defect (accumulation of VLCFA in plasma and organs) and by *ABCD1* mutation analysis. If X-ALD is suspected in a male, for instance, due to neurological symptoms, family with a history of X-ALD or Addison's disease, the demonstration that VLCFA are elevated in plasma confirms the diagnosis. Plasma VLCFA assay detects abnormally high concentrations of C26:0, especially C26:0-lysophosphatidylcholine (C26:0-LPC), and abnormally high ratios of C24:0/C22:0 and C26:0/C22:0, which can be detected at the day of birth, even in most heterozygous females (Moser et al., 1999). Given that 15% of carrier women with X-ALD have normal plasma VLCFA, a mutation analysis of the *ABCD1* is needed (Engelen et al., 2012a). Prenatal diagnosis using the VLCFA assay in cultured amniocytes or cultured chorion villus cells is also available (Moser and Moser, 1999). Not long ago, direct DNA mutation analysis has also become available, being of special interest in the case of heterozygous women, where VLCFA analysis can result in false negatives (Engelen et al., 2014). Recent validation of a method for detecting C26:0-LPC

in dried blood spots from newborns (Hubbard et al., 2009) has permitted to include X-ALD in the Recommended Uniform Screening Panel (RUSP) in the United States of America (USA) (Kemper et al., 2017). Therefore, it is currently being applied in sixteen states of the USA (Lee et al., 2020) (see “NewSTEPs Newborn Screening status for all disorders” database <https://www.newsteps.org/resources/newborn-screening-status-all-disorders>) and in the Netherlands (Barendsen et al., 2020), and it is expected to be implanted in more countries in the coming years. This new screening will allow the identification of the majority of X-ALD patients presymptomatically. To identify the subset of males who will develop ccALD, all males with *ABCD1* mutations require clinical tracking and serial MRI to monitor neuroradiological changes, as well as evaluation of adrenocortical function to guide treatment. Proper genetic counsel of affected families is also of huge importance.

1.2.4 Genetics and biochemistry

1.2.4.1 X-ALD mutations and modifier genes

X-ALD patients carry a mutation in the *ABCD1* gene, located on Xq28 (Mosser et al., 1993). *ABCD1* contains 10 exons and encodes for an mRNA of 4.3 kb that translates to a protein of 745 amino acids. Up to date, over 850 different mutations in *ABCD1* have been catalogued in the X-ALD database (Kemp et al., 2001) (see www.x-ald.nl), with 4% of the patients affected by *de novo* mutations (Wang et al., 2011). Interestingly, all clinical phenotypes can occur within the same family (Berger et al., 1994; Kemp et al., 1994), indicating that there is no direct genotype-phenotype correlation. Even in monozygotic twins, different clinical phenotypes have been observed (Korenke et al., 1996). These evidences suggest that the defect in *ABCD1* and subsequent accumulation of VLCFA, results in adrenal insufficiency and myelopathy, but for the initiation of cerebral demyelination, further additional environmental triggers and/or genetic factors are required, altogether exemplified by the “three-hit” hypothesis (Singh and Pujol, 2010). This hypothesis suggests the following: the metabolic dearrangements characterized by the excess of VLCFA, low plasmalogen levels and oxidative stress (first hit), generates inflammatory disease (second hit). Subsequently, the cytokine and chemokine mediators further cause a generalized loss of peroxisomes (third hit), creating a vicious circle resulting in cell loss and progressive inflammatory

demyelinating disease (Singh and Pujol, 2010). Initially, a segregation analysis based on 3862 individuals from 89 kindreds suggested the presence of an autosomal modifier locus (Moser et al., 1992). The members of the ABCD subfamily, *ABCD2* (Holzinger et al., 1997; Holzinger et al., 1999) and to a lesser extent *ABCD3* (Braiterman et al., 1998) seemed to be suitable candidates for modifier genes, as their overexpression compensates for the lack of *ABCD1* *in vitro* and *in vivo* (Kemp et al., 1998; Netik et al., 1999; Pujol et al., 2004). However, two independent association studies comparing *ABCD2* and *ABCD3* polymorphisms within X-ALD patients with different clinical phenotypes failed to determine significant correlations (Maier et al., 2008; Matsukawa et al., 2011). Cluster of differentiation 1 (CD1), proteins are lipid-antigen presenting molecules encoded by five *CD1* genes in human. A single nucleotide polymorphism (SNP) in the *CD1* gene, rs973742, arose as another modifier candidate gene, but the association was no longer significant after Bonferroni correction for multiple testing (Barbier et al., 2012). Polymorphisms in two genes related to methionine metabolism (cystathionine beta-synthase, *CBS*, and transcobalamin 2, *TC2*), which are important for myelination, together with a polymorphism in superoxide dismutase 2 (*SOD2*), involved in the antioxidant response, were found associated with phenotypic outcome in X-ALD, although, again, the results were not conclusive (Brose et al., 2012; Linnebank et al., 2006; Semmler et al., 2009). Moreover, a recent report has found a correlation between total antioxidant capacity and SOD levels and activity in samples of monocytes and blood plasma from X-ALD patients with magnetic resonance imaging severity score (Turk et al., 2017), reinforcing the link between the response against oxidative stress and X-ALD. Additionally, none of the human leukocyte antigen (HLA) type II haplotypes, a confirmed risk factor in multiple sclerosis (MS) (International Multiple Sclerosis Genetics et al., 2011), are involved in the triggering of inflammation that leads to cerebral demyelination in cerebral ALD (Berger et al., 1995; McGuinness et al., 1997; Schmidt et al., 2003). As in other rare diseases, the relatively small number of X-ALD patients makes the extraction of definitive conclusions difficult. When comparing mRNA expression from normal-appearing white matter (NAWM) from cAMN patients versus ccALD patients, few genes have shown a differential pattern of expression. For instance, *ABCD4* and acyl-CoA synthetase bubblegum family member-1 (*ACSBG1*) were decreased only in NAWM from ccALD and cAMN patients when compared to controls (Asheuer et al., 2005), correlating with the severity of the disease. Other differentially expressed genes or molecules between AMN and ccALD are 25-

hydroxycholesterol and cytochrome P450 family 4 subfamily F member 2 (*CYP4F2*), associated with cholesterol metabolism (Jang et al., 2016; van Engen et al., 2016) and nuclear factor kappa B (NF- κ B)-dependent inflammatory components regulated by a microRNA, miR-196a (Shah and Singh, 2017). Viral infections associated with demyelination have also been investigated as a plausible environmental factor in X-ALD, even though, for the moment, this possibility has been ruled out after negative results of an immunohistochemical search for viral antigens in the white matter of cerebral ALD patients (Ito et al., 2001). Complementary to this, some studies suggest that head trauma may be a possible environmental trigger for cerebral ALD (Bouquet et al., 2015; Raymond et al., 2010; Weller et al., 1992). Chitotriosidase (CHIT) activity, an enzyme produced by activated monocytes and macrophages, showed highly significant elevations in both the plasma and spinal fluid in boys with ccALD considered for transplantation (Orchard et al., 2011). These findings suggest that these levels predict the prognosis of patients with ccALD undergoing transplantation. As recently published by our group (Schluter et al., 2018), epigenetic changes in the brains of X-ALD patients might contribute to explaining the lack of genotype-phenotype correlation. A common methylation status was uncovered in genes involved in oligodendrocyte differentiation and the immune response among ccALD and cAMN patients. More interestingly, good markers capable of discriminating childhood from adult inflammatory phenotypes were identified, such as combined methylation levels of *SPG20*, *UNC45A* and *COL9A3* or combined expression of *ID4* and *MYRF* (Schluter et al., 2018). In a recent study published last year, a multi-omic approach was carried out to identify biomarkers prognostic of the advancement to ccALD (Richmond et al., 2020). Slight hypermethylation of *UNC45A* was also identified in blood samples of ccALDs, reinforcing our previous results (Schluter et al., 2018). In addition, they corroborated previous observations about the role of immune response in the disease, as PFN1 protein, profilin 1, was found in overabundance in ccALD compared to controls. The protein encoded by PFN1 plays an important role in actin dynamics by regulating actin polymerization in response to extracellular signals, so the increased protein levels could precede or act as biomarkers of the autoimmune response within the subset of patients who exhibit this trend (Richmond et al., 2020). To finish, neurofilament light (NfL) has emerged as a potential biomarker in adrenoleukodystrophy (van Ballegoij et al., 2020; Weinhofer et al., 2021). In AMN, elevated NfL correlates with higher grading of myelopathy-related disability. Intriguingly, NfL is a significant predictor to discriminate

non-converting AMN from cohorts later developing the cerebral form of the disease. In ccALD, markedly amplified NfL levels reflect brain lesion severity, inflammatory activity and disease, thus constituting a potential surrogate biomarker that may facilitate clinical decisions and therapeutic development (Weinhofer et al., 2021).

Taken together, this evidence strongly indicates a highly unlikely existence of a single modifier gene/locus. Thus, the clinical phenotype of ALD patients will probably be defined by the intertwin of rare genetic variants and environmental factors. Further research is needed to shed light on these factors.

1.2.4.2 Origin of VLCFA

A small proportion of VLCFA is provided by the diet (Kishimoto et al., 1980). However, VLCFA mainly come from endogenous synthesis through elongation of long-chain fatty acids (LCFA) (FA with aliphatic tails of 13-21 carbons). Palmitic acid (C16:0), and stearic acid (C18:0) account for over 90% of all saturated FA in humans. The synthesis of polyunsaturated fatty acids (PUFA), monounsaturated VLCFA and saturated VLCFA takes place at the cytosolic side of the ER membrane and involves a four sequential reaction: (i) condensation of a fatty acyl-CoA with malonyl-CoA, (ii) reduction to 3-ketoacyl-CoA, (iii) dehydration to trans-2-enoyl-CoA, and (iv) reduction to fully elongated fatty acyl-CoA. The initial condensation step is carried out by one of the seven elongases (ELOVLs) of VLCFA described in mammals. The synthesis of C24:0 and C26:0 requires two ELOVLs. First, the elongation complex with ELOVL6 elongates C16:0 to C20:0/C22:0. After, ELOVL1 elongates these FAs to C24:0 and C26:0. Thus, VLCFA accumulation is caused not only by an impaired peroxisomal β -oxidation but also by the raised levels of C22:0/C24:0, which are the substrates for elongation through ELOVL1 (Ofman et al., 2010).

1.2.4.3 Biochemical aspects of X-ALD

In X-ALD, VLCFA content is increased, mainly tetracosanoic (C24:0) and hexacosanoic (C26:0) fatty acids, in cholesterol esters and complex lipids such as gangliosides, phosphatidylcholine, sphingomyelin, cerebrosides and sulfatides (Igarashi et al., 1976; Moser et al., 1981; Wiesinger et al., 2013). This accumulation is caused by an impaired capacity of peroxisomes to degrade VLCFA (Singh et al., 1984b; Wanders

et al., 1987). VLCFA are metabolically inactive and thioesterification to CoA (VLCFA-CoA) is necessary for the initiation of the peroxisomal β -degradation. Thereby, as mentioned above, until the discovery of *ABCD1* as the mutated gene in X-ALD, VLCFA oxidation defect was first misassigned to a defect in the very long-chain fatty acyl-CoA synthetase (VLCS) enzyme (Lazo et al., 1988; Wanders et al., 1988). Experimental evidence of actual ABCD1 function comes from complementation studies, in which expression of wild-type *ABCD1* cDNA in X-ALD fibroblasts restored VLCFA β -oxidation (Braiterman et al., 1998; Shinnoh et al., 1995) and reduced VLCFA levels (Cartier et al., 1995). Structural and functional features of ABCD1 were also extracted from studies with the *Saccharomyces cerevisiae* peroxisomal ABC half transporters, Pxa1p and Pxa2p, which form a heterodimer to import acyl-CoA esters into the peroxisome (Hettema et al., 1996). Because the inability of yeast mutants lacking these genes to grow in a medium with oleic acid is partially restored when ABCD1 is expressed, it was demonstrated that ABCD1 transports acyl-CoA esters across the peroxisomal membrane (van Roermund et al., 2008). In X-ALD fibroblasts, β -oxidation activity is reduced up to 75%-85% of the levels measured in normal fibroblasts (McGuinness et al., 2001). This fact is explained by the ability of ABCD3 to also transport VLCFA-CoA into the peroxisome (Wiesinger et al., 2013). The impairment in the degradation of VLCFA causes a rise in the levels of cytosolic VLCFA-CoA, and further elongation of the chain length by ELOVL1, the human VLCFA-specific elongase (Ofman et al., 2010). This elongation leads to enhanced incorporation of VLCFA into complex lipids (Kemp et al., 2005). In summary, ABCD1 is active as a homodimer, and *ABCD1* mutations impair the import of VLCFA-CoA into the peroxisome, leading to the accumulation of VLCFA.

1.2.5 Therapeutic strategies

Given the wide clinical spectrum of X-ALD patients, different therapeutic strategies must be considered for individual symptoms. Follow-up in boys and men with X-ALD is important to detect adrenocortical insufficiency and crucial to early identify first signs of cerebral demyelination to propose allogeneic hematopoietic stem cell transplantation (HSCT), the only available intervention able to arrest the progression of cerebral

demyelination. Therapies addressed to correct VLCFA accumulation and to improve neurologic symptoms are listed below:

1) **Steroid Replacement**: As 70% of X-ALD patients develop adrenal insufficiency, X-ALD diagnosed boys and men should be monitored by measuring adrenocorticotrophic hormone (ACTH) levels in plasma and with the ACTH stimulation test. Then, if necessary, they must be treated with steroid replacement, in the same way as for other forms of primary adrenal insufficiency (Moser et al., 2007).

2) **Lorenzo's oil** is a 4:1 mixture of oleic (C18:1 ω 9) and erucic (C22:1 ω 9) acids, which competes for the fatty acid elongation system, preventing the synthesis of saturated VLCFA. Oral administration of this oil, combined with moderate reduction of fat in the diet, reduces plasma levels of VLCFA within four weeks (Moser et al., 1987), so it was a promising therapeutic strategy in the 80s-90s. Nevertheless, after 15 years of clinical trials with asymptomatic and symptomatic patients, it has been concluded that Lorenzo's oil does not reduce VLCFA levels in the brain (Rasmussen et al., 1994) and further studies proved that administration of this oil does not stop the progression of X-ALD (Aubourg et al., 1993; van Geel et al., 1999).

3) **Lovastatin**, a cholesterol-lowering drug, normalizes VLCFA levels in X-ALD fibroblasts and plasma of X-ALD patients (Singh et al., 1998a; Singh et al., 1998b). However, in a placebo-controlled trial, it did not lower C26:0 levels in peripheral-blood cells, and its effect on plasma VLCFA were attributed to be a consequence of a nonspecific decrease in the level of low-density lipoprotein (LDL)-cholesterol (Engelen et al., 2010).

4) **Bezafibrate** gave hope for therapy, as it reduces *de novo* C26:0 synthesis, by competitive inhibition of ELOVL1 in X-ALD fibroblasts (Engelen et al., 2012b), but it does not lower VLCFA levels in plasma or lymphocytes of X-ALD patients (Engelen et al., 2012c).

5) **Immunomodulators or immunosuppressants drugs**: Up to now, none of the anti-inflammatory therapies used against the cerebral forms of ALD have shown any success. The agents tested so far are cyclophosphamide (Naidu et al., 1988; Stumpf et

al., 1981), INF- β (Korenke et al., 1997), intravenous immunoglobulins (Miike et al., 1989) and NatalizumAb (monoclonal antibody against integrin α -4) (Berger et al., 2010).

6) Pharmacological induction of ABCD2 gene expression: Since overexpression of *ABCD2* in X-ALD fibroblasts (Flavigny et al., 1999; Netik et al., 1999) and *Abcd1*⁻ mice (Pujol et al., 2004) prevents VLCFA accumulation, ABCD2-inducing drugs were proposed as an interesting therapeutic option for X-ALD. Histone deacetylase inhibitors (which promote the genetic transcription of ABCD2) such as 4-phenylbutyrate (Gondcaille et al., 2005; McGuinness et al., 2001), fibrates (Albet et al., 1997; Fourcade et al., 2001) and valproic acid (Fourcade et al., 2010) have been tested with limited success.

7) Antioxidant supplementation: Given the important role of oxidative stress in X-ALD, antioxidant therapies were tested in the X-ALD animal models. A combination of antioxidants (vitamin E, N-acetylcysteine and lipoic acid) halts axonal degeneration and prevents locomotor deficits in *Abcd1*⁻ mice (Lopez-Erauskin et al., 2011). These results from our group led to a phase II clinical trial in AMN patients with a cocktail of antioxidants, which reported normalization of several inflammation markers, in addition to markers of oxidative damage, indicating that redox and inflammatory homeostasis are deeply intertwined in this disease (Casasnovas et al., 2019). Moreover, oral administration of dimethyl fumarate (DMF/BG12/Tecfidera), a nuclear factor, erythroid 2 like 2 (NRF2)-antioxidant response activator in use for MS, showed beneficial effects in *Abcd1* knockout mice (Ranea-Robles et al., 2018).

8) Apart from these therapeutic strategies, the only useful therapy for cerebral X-ALD is hematopoietic stem cell transplantation (HSCT) (Miller et al., 2011). Microglia are the sensor of pathological situations in the central nervous system (CNS). In contrast to other glial cells, microglia are originated from bone marrow myelomonocytic cells. HSCT arrests neuroinflammation when performed at an early stage of the disease. Only patients with a Loes score of ≤ 9 in the X-ALD MRI Severity Scale (Loes et al., 2003) and no neurologic or neuropsychological deficits are apt. Because of this, the monitoring of X-ALD boys is so important. After transplantation, the demyelination process persists from 12 to 18 months before is permanently arrested, due to the slow

turnover of the brain microglia (Cartier and Aubourg, 2010; Cartier et al., 2009; Kennedy and Abkowitz, 1997; Lawson et al., 1992). Despite the successful results obtained so far, HSCT still presents serious limitations: (i) narrow therapeutic window, given that most of the index cases are diagnosed when cognitive deficits are too advanced for a safe intervention and (ii) HSCT remains associated with a severe graft vs. host disease and a prolonged immune deficiency (Cheng et al., 2009; Hwang et al., 2007). The absence of biomarkers that can predict the evolution of cerebral disease together with the fact that HSCT performed in childhood does not seem to prevent myelopathy and peripheral neuropathy in adulthood (van Geel et al., 2015), makes mandatory the search for new therapies for X-ALD patients. Although there are not many studies reporting HSCT in the adult form of adrenoleukodystrophy, some groups have shown positive long-term outcomes (Kuhl et al., 2017). In a recent publication, arrest of inflammatory demyelination, but no reduction of plasma VLCFA levels, was obtained in adolescent-/adult-onset cerebral form patients of adrenoleukodystrophy, posing the possibility of performing HSCT in the adult form of cerebral adrenoleukodystrophy (Matsukawa et al., 2020).

9) An alternative to allogeneic HSCT is **gene therapy**, by transplantation of genetically corrected autologous CD34⁺ cells, with encouraging results in the first two treated boys, in which this therapy has impeded the progression of the disease (Cartier et al., 2009; Eichler et al., 2017).

To sum up, given that the only available therapy (HSCT) has a narrow therapeutic window and elevated risks associated; together with the fact that most of the approaches followed until now have failed, much more research on X-ALD pathophysiology and subsequent therapies needs to be done.

1.2.6 Animal models

The identification of *ABCD1* as the gene mutated in X-ALD allowed the generation of *Abcd1*-deficient mice (*Abcd1*^{-/-}), seeking for an animal model which could be used to better understand X-ALD pathophysiology. In 1997, three different groups developed three independent X-ALD mouse models, by inactivating the *Abcd1* gene (Forss-Petter

et al., 1997; Kobayashi et al., 1997; Lu et al., 1997). The three models display the main biochemical hallmark of the disease, which is the accumulation of VLCFA. However, these mice do not develop cerebral demyelination or brain inflammation, characteristic of ccALD. At approximately 18 months of age, these mice develop a late-onset AMN-like phenotype, characterized by spastic paraparesis due to degeneration of corticospinal tracts, without signs of inflammatory demyelination in the brain. Axonal pathology is found in sciatic nerves and spinal cord, including slower sciatic nerve conduction and motor behaviour abnormalities in rotarod, bar cross and treadmill tests (Pujol et al., 2002). *Abcd1*-deficient mice have been instrumental in dissecting pathomechanisms of AMN (Fourcade et al., 2020; Fourcade et al., 2008; Galino et al., 2011; Launay et al., 2015; Launay et al., 2013; Launay et al., 2017; Lopez-Erauskin et al., 2013a; Lopez-Erauskin et al., 2013b; Morato et al., 2013; Morato et al., 2015; Ranea-Robles et al., 2018). With the aim of obtaining a more severe phenotype, *Abcd1/Abcd2* double-deficient mice (*Abcd1^{-/-}/Abcd2^{-/-}*) were generated, although they do not develop brain inflammation or demyelination either (Pujol et al., 2004). The neuropathology in these mice is also restricted mainly to the spinal cord and, due to the contribution of ABCD2, the dorsal root ganglia, resulting in sensory neuropathy. Nevertheless, these defects are more pronounced and start earlier, at 12 months of age (Pujol et al., 2004), setting up a suitable preclinical model for testing disease-modifying drugs (Fourcade et al., 2020; Launay et al., 2017; Lopez-Erauskin et al., 2011; Mastroeni et al., 2009; Morato et al., 2013; Morato et al., 2015; Ranea-Robles et al., 2018). Up to now, the cerebral phenotype has not been reproduced in mice. The lack of progression from the metabolic syndrome to cerebral demyelination and neuroinflammation in *Abcd1^{-/-}* mice reinforces the hypothesis that, in addition to the loss of ALDP function, it is likely that modifier genes, epigenetic and environmental or stochastic factors, might be determinant in the onset of the cerebral forms.

Drosophila mutants of *bubblegum* (*bbg*) and *double bubble* (*dbb*) very long-chain acyl-CoA synthetases have been also claimed as X-ALD models (Min and Benzer, 1999; Sivachenko et al., 2016), as these mutations provoke profound effects on behaviour and brain morphology, although the mouse model of the ortholog gene does not present neurodegeneration (Heinzer et al., 2003).

In a recent publication from our group (Coppa et al., 2020), we characterized a nematode model of X-ALD with loss of *pmp-4* gene, the worm orthologue of ABCD1. Despite the fact that the *C. elegans* nervous system is not myelinated (El Bejjani and Hammarlund, 2012), thus precluding the study of the physiopathology of the infantile form of X-ALD (ccALD), *pmp-4* worms may constitute a valuable model of the axonopathy occurring in the adult form of the disease, as these mutants recapitulate the hallmarks of X-ALD: (i) VLCFA accumulation and impaired mitochondrial redox homeostasis and (ii) axonal damage coupled to locomotor dysfunction.

A new tool for studies of ALD was provided through the generation of a zebrafish *abcd1* mutant model (Strachan et al., 2017). The zebrafish ALD model not only recapitulates key aspects of ALD, but also manifests a motor phenotype in the first week of life. Importantly, in zebrafish, the ABCD1 DNA and protein sequences are highly conserved, as are other key genes in lipid metabolism including SCD1 and ELOVL1 (Bhandari et al., 2016; Hsieh et al., 2003).

Collectively, several animal models have been developed to study X-ALD. The most studied one is *Abcd1*⁻ mouse, which develops an AMN-like phenotype. Further efforts are needed to obtain a model for the devastating ccALD.

1.2.7 The role of VLCFA in the pathogenesis of X-ALD

The exact mechanism that links VLCFA accumulation to axonal degeneration in AMN or cerebral inflammatory demyelination in ccALD remains elusive. Conversely, the wide clinical spectrum of X-ALD phenotypes and the lack of cerebral demyelination in *Abcd1* null mice, despite VLCFA accumulation in the brain (Pujol et al., 2002), suggests the presence of additional factors associated with VLCFA accumulation. Several mechanisms of VLCFA-induced cytotoxicity have been proposed. VLCFA are usually found as constituents of complex lipids, such as ganglioside, phosphatidylcholine and cholesterol ester fraction of brain myelin. In agreement with this, C26:0 increases the membrane microviscosity in erythrocytes of patients with cerebral ALD and AMN (Knazek et al., 1983), and adrenocortical cells from X-ALD patients, altering their capacity to secrete cortisol (Whitcomb et al., 1988). In particular, gangliosides and

phosphatidylcholine have been proposed to trigger immune response in cerebral ALD (Theda et al., 1992), whereas the accumulation of VLCFA in myelin components, such as the proteolipid protein (PLP), would destabilize myelin sheaths (Bizzozero et al., 1991). Consistently, the amounts of VLCFA were found to be higher in normal-appearing white matter and induced pluripotent stem cells (iPSCs) oligodendrocytes from ccALD patients compared with AMN patients (Asheuer et al., 2004; Jang et al., 2011). Thus, the initial phase of spontaneous onset of demyelination might be directly related to the level of VLCFA in the myelin sheath (Berger et al., 2014). VLCFA could also alter the permeability of the inner mitochondrial membrane by substituting the lateral chains of phospholipid bilayers and physically interfering with the assembly of oxidative phosphorylation (OXPHOS) system, or by increasing membrane microviscosity (Knazek et al., 1983; Whitcomb et al., 1988) and provoking its disruption (Ho et al., 1995).

Compelling evidence indicates that X-ALD recapitulates the pathological hallmarks of the main neurodegenerative disorders, exemplified by redox dyshomeostasis, mitochondrial dysfunction, proteostasis impairment, the latter being defined by proteasomal and autophagy flux dysfunction, and neuroinflammation (Fourcade et al., 2015; Pujol, 2016). The following sections explain and illustrate the different molecular pathways affected in X-ALD, as well as the plausible therapeutic targets derived from them, which would be the focus of this thesis.

1.3 Hallmarks of X-ALD

1.3.1 Redox dyshomeostasis

Oxidative stress occurs as a result of an imbalance between the excessive formation of reactive oxygen/nitrogen species (ROS/RNS) and limited antioxidant defences. A direct consequence of excessive ROS production is the interaction with cellular biomolecules, such as DNA, lipids and proteins, which are modified and may cause deregulation of cellular signalling pathways implicated in a myriad of human diseases, or even cell death. These disorders range from neurodegenerative diseases to metabolic disorders

such as obesity or type 2 diabetes (Cross et al., 1987; Halliwell, 2006). Besides exogenous sources such as ionizing radiation, diet, metals, pesticides or other toxic compounds, ROS can be generated endogenously in a variety of sites and conditions (e.g ischemia–reperfusion and enzymatic reactions). These molecules are generated in metabolic processes that consume oxygen in the mitochondria, peroxisomes and ER, although the majority of ROS is produced in mitochondria (Boveris et al., 1972; Halliwell, 2007), where superoxide anion is produced during the flow of electrons along the respiratory chain to produce ATP (Jensen, 1966; Murphy, 2009). Extra-mitochondrial sources of ROS include, for instance, the membrane nicotinamide adenine dinucleotide phosphate oxidase, lipoxygenases, cyclooxygenases, peroxidases, other heme proteins, xanthine oxidase, peroxisomal β -oxidation and hepatic P-450 microsomal detoxification. To combat ROS produced from such a vast set of sources, the cell is equipped with its own antioxidant defences.

1.3.1.1 Role of ROS in X-ALD

In the case of peroxisomal diseases, and in particular, X-ALD, it is currently well established that oxidative stress plays a key role in the pathophysiology of the disease (Galea et al., 2012; Singh and Pujol, 2010). In X-ALD, first clues were given by studies showing higher oxidability of LDL in plasma from X-ALD patients compared to that in control subjects (Di Biase et al., 2000), and the presence of iNOS in astrocytes and microglia from brain tissue of X-ALD patients but not in controls (Gilg et al., 2000). The role of oxidative damage in X-ALD was reinforced when oxidative stress was detected in plasma, erythrocytes and fibroblasts from X-ALD patients (Petrillo et al., 2013; Vargas et al., 2004), and in adrenal cortex and brain sections from child patients with cerebral phenotype (Powers et al., 2005). X-ALD derived lymphoblasts also present higher levels of oxidative stress (Uto et al., 2008). Interestingly, total antioxidant status is decreased in symptomatic but not in asymptomatic X-ALD cases (Deon et al., 2007), presuming that asymptomatic patients seem to be protected against oxidative stress and that other factors besides oxidative damage may be responsible for the severity of the symptoms in X-ALD and need to be investigated. Oxidative stress also occurs in asymptomatic female carriers as manifested by the increase of lipid peroxidation products and decreased antioxidant reactivity in plasma, whereas total antioxidant status is not altered (Deon et al., 2008). Interestingly, no correlation was

observed between oxidative stress markers and VLCFA (C26:0 and C26:0/C22:0) levels in plasma of female carriers (Deon et al., 2008). These results can be obscured since the measures were non-quantitative and subjected to technical limitations mainly due to a lack of specificity of the chemical reagents (Halliwell and Whiteman, 2004).

No direct evidence of oxidative stress or damage could be evidenced in adrenal cortex, kidney or brain in the X-ALD mouse model at 12 weeks of age, despite an increased immunohistochemical reaction against MnSod (Sod2) in adrenal cortex and kidney (Powers et al., 2005). However, later studies from our group in 3.5-month-old *Abcd1* null mice spinal cord using more sensitive methods (gas chromatography/mass spectrometry) have demonstrated that oxidative stress is an early event in X-ALD pathophysiology (Fourcade et al., 2008). Indeed, fibroblasts and peripheral blood mononuclear cells (PBMC) derived from X-ALD patients display a two-fold increase in the concentration of selected biomarkers of oxidative damage [glutamic semialdehyde (GSA) and amino adipic semialdehyde (AASA) for carbonylation; N ϵ - (carboxymethyl)-lysine (CML), N ϵ -(carboxyethyl)-lysine (CEL) for glycooxidation/lipoxidation; and N ϵ -MDA-lysine (MDAL) for lipoxidation], (Fourcade et al., 2008; Fourcade et al., 2010). At 12 months of age, *Abcd1*⁻ mice also accumulate oxidative damage products arising from metal-catalyzed oxidation and glycooxidation/lipoxidation (Fourcade et al., 2008). The degree of VLCFA accumulation parallels the level of lipoxidative damage to proteins as seen in a double knockout mouse deficient for both *Abcd1* and *Abcd2* genes (Fourcade et al., 2010; Pujol et al., 2004). These mice display an earlier disease onset with a more severe neurodegenerative phenotype, which presents axonal damage, locomotor and behavioural abnormalities and peripheral nerve conduction impairment (Ferrer et al., 2005; Pujol et al., 2004). We also unveiled an impairment of bioenergetic homeostasis in the *Abcd1*⁻ mice due to oxidation of key enzymes of the glycolytic pathway and Krebs cycle (Galino et al., 2011; Lopez-Erauskin et al., 2013b). This was associated with decreased activity of pyruvate kinase, and lowered levels of ATP and NADH, as well as reduced glutathione (GSH) pools (Galino et al., 2011). Finally, a functional genomic analysis of transcriptomic data from the spinal cord of the X-ALD mouse model and NAWM of X-ALD patients revealed a dysregulation in a wide array of mitochondrial genes related to the pyruvate and oxoglutarate dehydrogenase

complexes, tricarboxylic acid (TCA) cycle, OXPHOS system and antioxidant defences (Schluter et al., 2012).

Furthermore, VLCFA accumulation has been identified as the causative agent of redox imbalance in X-ALD. Excess of C26:0 generates ROS in human fibroblasts (Fourcade et al., 2008; Fourcade et al., 2010), immortalized neuronal and oligodendrocyte cell cultures (Baarine et al., 2012; Zarrouk et al., 2012), and mitochondria and primary astrocytes from WT and *Abcd1*⁻ mice brain (Kruska et al., 2015). In X-ALD fibroblasts, ROS generated by C26:0 oxidize mtDNA and impair the OXPHOS system, triggering mitochondrial ROS production from electron transport chain complexes (Lopez-Erauskin et al., 2013b). Collectively, all these data provide enough pieces of evidence of the key role of oxidative stress in X-ALD. Recent data from our group has reinforce the major impact of redox homeostasis in the development of the disease. From one side, it was shown that the NRF2-antioxidant response pathway is blunted in *Abcd1*⁻ mice and can be reactivated by oral administration of DMF, an NRF2 activator in use for MS (Ranea-Robles et al., 2018). On the other side, a phase II clinical trial in AMN patients with a cocktail of antioxidants reported normalization of several inflammation markers and addition to markers of oxidative damage (Casasnovas et al., 2019).

1.3.2 Mitochondrial dysfunction

1.3.2.1 Mitochondrial functions

Mitochondria are organelles that derive from an α -proteobacterial endosymbiont (Gray et al., 1999) and are comprised of two separate membranes, the mitochondrial outer membrane (MOM) and the mitochondrial inner membrane (MIM), that encapsulate the intermembrane space and matrix compartments. They contain a circular genome, mtDNA, which encodes 13 out of the 1500 mitochondrial proteins, while the rest are encoded in the nucleus. Mitochondria form a dynamic, interconnected network that is intimately integrated with other cellular compartments, like the peroxisome (Schrader et al., 2015). The main function of mitochondria is the production of energy through the OXPHOS system in the form of ATP. During these processes, NAD⁺ or FAD are reduced to form NADH and FADH₂, respectively. In the inner mitochondrial membrane, electrons are transferred from NADH/FADH₂ through the four complexes

(complex I to IV) of the electron transport chain (ETC) and finally passed to O₂ to form H₂O. This electron transport system uses the energy released from the oxidation of the reducing agents (NADH/FADH₂) to pump protons from the matrix to the mitochondrial intermembrane space, generating an electrochemical gradient across the inner membrane. The energy stored in this potential is used by the ATP-synthase (or complex V) to transform ADP into ATP. Mitochondria regulate other important functions such as the β -oxidation of fatty acids, the biosynthesis of amino acids, heme group and steroids, calcium homeostasis, cell death, thermogenesis and cellular stress responses (McBride et al., 2006). Thereby, mitochondrial dysfunction is associated with a myriad of human inherited disorders and is implicated in neurodegenerative disorders, cardiomyopathies, metabolic syndrome, cancer, and obesity (Nunnari and Suomalainen, 2012).

1.3.2.2 Mitochondria and the central nervous system

Although the brain makes up only 2% of the total body mass, it demands 20% of the oxygen and 25% of the glucose consumed by the human body. The main process contributing to this high energy need is neurotransmission (Bélanger et al., 2011). Axons are the ultra specialized structures of neurons responsible for conducting the electrical impulses away from the neuronal soma to other neurons, muscle or glands. Axons are responsible for the maintenance and restoration of the ionic gradient necessary for the impulse conduction, as well as for the synthesis, release and recycling of neurotransmitters. All these processes are ATP-dependent, and this requirement of energy is primarily met by axonal mitochondria (Court and Coleman, 2012). Other cells of the CNS also require a proper mitochondrial function. For instance, in oligodendrocytes, mitochondrial oxidation is critical to provide the necessary lipids for the myelination process (Schoenfeld et al., 2010; Silva et al., 2009; Viader et al., 2013; Ziabreva et al., 2010). Furthermore, lack of functional mitochondria in oligodendrocytes or Schwann cells in mice leads to severe neuropathy (Funfschilling et al., 2012). Essential roles of astrocytes, including support of neurotransmission (uptake of glutamate from the synaptic cleft) and supply of energetic substrates (e.g. glutamate, lactate) to neurons, requires an accurate mitochondrial function (Cambron et al., 2012). Even inflammatory responses in microglial cells are regulated by mitochondria (Bulua et al., 2011; Naik and Dixit, 2011; Park et al., 2013; Zhou et al., 2011). Thus, mitochondrial function is essential both in neurons and in glial cells.

1.3.2.3 Mitochondrial dysfunction associated to neurodegeneration

Three main homeostatic disruptions can combine to threaten mitochondria viability in axons: oxidative stress, ATP reduction and Ca^{2+} overload (Court and Coleman, 2012). First, oxidative stress occurs when there is an imbalance between the production of ROS and the antioxidant capacity (Halliwell, 2007). Mitochondria can generate ROS from different redox centres in the ETC, in particular from complex I and complex III (Murphy, 2009). Neurons are especially vulnerable to oxidative damage due to: (i) the high rate of oxidative metabolic activity, (ii) the relatively poor expression of enzymatic antioxidant defences, (iii) the high abundance of peroxidizable PUFAs in membranes, (iv) the high ratio of membrane surface to cytoplasm and (v) their non-replicative nature (Galea et al., 2012; Lee et al., 2012). Second, ATP synthesis may be compromised if the OXPHOS system is altered, as occurs when these proteins are oxidized or when the corresponding genes are mutated (Lopez-Erauskin et al., 2013b; Wallace et al., 2010). Third, impairment of the ionic pumps in the axonal plasmalemma (Na^+/K^+ -ATPases), caused by a decrease in ATP, inevitably leads to a massive Na^+ influx, membrane depolarization and opening of voltage-dependent Ca^{2+} channels. In addition, the direction of the $\text{Na}^+/\text{Ca}^{2+}$ exchanger is reversed, resulting in an extra influx of Ca^{2+} . Mitochondria play a crucial role in buffering the cytosolic Ca^{2+} when it rises over a physiological range. However, a chronic increase of cytosolic Ca^{2+} overloads the mitochondrial uptake capacity, induces mitochondrial membrane depolarization and promotes ROS production. In its turn, excessive cytosolic Ca^{2+} can activate calpains (Ca^{2+} dependent proteases), leading to axonal cytoskeleton cleavage and eventually causing axonal swelling and axonal degeneration (Mammucari et al., 2011; Wang et al., 2012).

Excessive ROS production together with an ATP drop and Ca^{2+} dysregulation induces the opening of the mitochondrial permeability transition pore (mPTP) (Lopez-Erauskin et al., 2012; Rasola and Bernardi, 2011). Opening of the mPTP abolishes the inner mitochondrial membrane potential, which negatively interferes with the OXPHOS system, exacerbating the imbalance in the triad ROS/ATP/ Ca^{2+} . Finally, the mPTP opening may trigger apoptotic cell death if sufficient ATP is available or may prime the cell to enter the necrotic process (Lopez-Erauskin et al., 2012; Stavrovskaya and Kristal, 2005). Therefore, the combination of oxidative stress, energetic failure and Ca^{2+}

dyshomeostasis endangers mitochondrial viability, eventually leading to a pathological scenario. In fact, many lines of evidence suggest that mitochondria and oxidative stress have a central role in age-related neurodegenerative diseases (Beal, 2005).

1.3.2.3.1 Mitochondrial dysfunction in X-ALD

Although from a classical point of view X-ALD cannot be considered a primary mitochondrial disease, due to its peroxisomal origin, recent evidence points at mitochondria as a central hub in the pathophysiology of the disease. Even though one study found no impairment in respiratory efficacy when working with purified mitochondria from the muscle of X-ALD mouse (Oezen et al., 2005), evidence of morphological abnormalities of mitochondria have been reported in AMN patients (Powers et al., 2001; Schroder et al., 1996) as well as in other peroxisomal disorders, like in Zellweger patients (Goldfischer et al., 1973) or *Pex5*^{-/-} mice (Baumgart et al., 2001; Peeters et al., 2015), suggesting a role for the mitochondria in the physiopathology of peroxisomal disorders. Furthermore, the results from the transcriptomic functional analysis in X-ALD mice and human patients unravelled a common metabolic abnormality signature, characterized, among other pathways, by mitochondrial dysregulation (Schluter et al., 2012). In our group, we have demonstrated that VLCFA-derived ROS are mainly originated in the mitochondria, and that oxidative stress induces mitochondrial membrane depolarization (Fourcade et al., 2008; Lopez-Erauskin et al., 2013b), as well as triggers the opening of the mitochondrial permeability transition pore due to Cyclophilin D oxidation (Lopez-Erauskin et al., 2013a). Excess of VLCFA induced mitochondrial ROS formation from complexes I and II, and impaired complex V function in human skin fibroblasts, which correlates with the oxidation of several subunits of complex III and V of OXPHOS found in *Abcd1*⁻ mice spinal cord homogenates and defective phosphorylative respiration evidenced *in vitro* in fibroblasts and *ex vivo* using spinal cord slices (Lopez-Erauskin et al., 2013b). Similar mechanisms have been observed *in vitro* using SK-NB-E neuroblastoma cell line (Zarrouk et al., 2012), B12 oligodendrocytes and U87 astrocytes (Baarine et al., 2015), and primary astrocytes from WT and *Abcd1*⁻ mice (Kruska et al., 2015). In the latter study, Kruska and collaborators also found VLCFA-dependent impairment of Ca²⁺ retention capacity in brain mitochondria from 6-month-old *Abcd1*⁻ mice (Kruska et al., 2015). These results have permitted our group to hypothesize on how VLCFA

excess triggers oxidative stress from the mitochondria in X-ALD, also based on other data which suggest that C26:0 may replace the lateral chain of phospholipids of the MIM, increasing membrane microviscosity (Whitcomb et al., 1988), together with interfering with OXPHOS system and inducing ROS production (Lopez-Erauskin et al., 2013b). The proof of concept that oxidative stress and global mitochondria dysfunction underlie axonal degeneration is provided by halting axonal damage with an antioxidant cocktail (Galino et al., 2011; Lopez-Erauskin et al., 2011) and with the mitochondrial booster pioglitazone (Morato et al., 2013). In short, these studies demonstrate the interplay between mitochondrial dysfunction and oxidative stress in the pathophysiology of X-ALD.

1.3.2.4 Mitochondrial biogenesis

The traditional paradigm of mitochondria as static organelles has dramatically changed in the past years. Mitochondria undergo an array of dynamic changes that include biogenesis and selective degradation by mitophagy, shape changes regulated by fission and fusion events, and transport along the cell structure. New mitochondria grow and divide from pre-existing mitochondria (Nisoli et al., 2004). Thus, a fine-tuned balance between the different aspects of mitochondrial dynamics determines the success of the mitochondrial biogenesis program and the overall health of mitochondria (Anne Stetler et al., 2013). Mitochondrial biogenesis is comprised of three aspects. The first includes transcription, import and assembly of nuclear-encoded proteins within the mitochondrion. The second involves replication and transcription of the mitochondrial DNA. Finally, the third aspect represents the incorporation of lipids to the pre-existing mitochondria to generate new mitochondrial membranes (Michel et al., 2012). Although the mitochondrial proteome comprises ~1500 proteins, evolution has left to the mitochondrial genome only 37 genes. Thus, nuclear genes encode most mitochondrial proteins, including those responsible for mtDNA transcription and replication. The tightly regulated network of transcription factors and coregulators necessary to coordinate both genomes is described below.

1.3.2.4.1 Upstream metabolic sensors

The cell needs to adapt to the environmental conditions required for each situation. Upstream metabolic sensors are on top of this tight regulatory system and are sensors of these variations. Mammalian target of rapamycin (mTOR), adenosine monophosphate (AMP)-activated protein kinase (AMPK) and sirtuin 1 (SIRT1) are just an example of these regulators. mTOR stimulates anabolic pathways and suppresses autophagy when energy is abundant (Saxton and Sabatini, 2017). AMPK is activated by a decrease in ATP production, which increases AMP/ATP ratio, and increased ADP concentrations (Mihaylova and Shaw, 2011). SIRT1 is a NAD⁺-dependent deacetylase (Imai et al., 2000; Vaziri et al., 2001) that together with AMPK, coordinately regulates mitochondrial mass, nutrient oxidation, and ATP production via PGC-1 α (Canto et al., 2009). In X-ALD these upstream sensors are altered, as mTOR signalling is aberrant, inhibiting autophagy (Launay et al., 2015) and AMPK levels are decreased in fibroblasts and lymphoblasts from ccALD patients compared with cells from AMN patients, as well as in NAWM from ccALD patients compared with controls (Singh and Giri, 2014; Singh et al., 2016). SIRT1 is also inhibited, and its activation by resveratrol or transgenic overexpression in *Abcd1*⁻ mice is neuroprotective (Morato et al., 2015).

1.3.2.4.2 Regulation of mtDNA transcription and replication

As previously mentioned, human mtDNA (16 kb) encodes 37 genes, including 7 of the 46 subunits of complex I (ND1, 2, 3, 4, 4L, 5, and 6), one of the 11 subunits of complex III (cytochrome *b*, CYTB), 3 of the 13 subunits of complex IV (COX I, II, and III), 2 of the 16 subunits of complex V (ATP6 and ATP8), 2 rRNAs (12S and 16S), and 22 tRNAs. All 13 proteins encoded by mtDNA are essential subunits of respiratory complexes I, III, IV and V. Mitochondrial transcription machinery consists of an RNA polymerase (POLRMT), two transcription factors including mitochondrial transcription factor A (TFAM) (Larsson et al., 1998) and one of the two transcription factor B paralogues (TFB1M and TFB2M), together with a family of termination factors (mTERFs) (Bonawitz et al., 2006). Besides, the replication machinery contains the heterotrimeric mtDNA polymerase gamma (POLG) (Lee et al., 2009), the hexameric DNA helicase TWINKLE (Milenkovic et al., 2013) and the tetrameric mitochondrial single-stranded DNA-binding protein (mtSSB) (Korhonen et al., 2004).

1.3.2.4.3 Regulation of nuclear-encoded mitochondrial genes:

- Transcription factors:

1) **Nuclear respiratory factor 1 (NRF1)**: NRF1 coordinates nuclear and mitochondrial genome transcription by regulating the expression of: (i) nuclear-encoded OXPHOS components, mitochondrial import proteins and mitochondrial ribosomal proteins (Scarpulla, 2006), and (ii) TFAM, TFB1M and TFB2M genes. NRF1 is constitutively active and thus important for the basal expression of mitochondrial genes (Dhar et al., 2008).

2) **GA-binding protein (GABP)**: GABP is a heterotetramer of GABP α (DNA-binding domain) and GABP β (transcriptional activation domain). Similar to NRF1, GABP binding sites have been reported in the proximal promoters of OXPHOS component, mitochondrial import, and also in TFAM, TFB1M and TFB2M genes (Kressler et al., 2007).

3) **E2F1, a cell cycle protein with new skills**: E2F1 protein is one out of the eight E2F proteins (E2F1-8) described up to date (Black et al., 2005). Members of the E2F family of transcription factors are downstream effectors of the tumour suppressor pRB (product of retinoblastoma) and are considered to have a pivotal role in controlling cell cycle progression. Participation of E2F1 in the regulation of oxidative metabolism is being largely studied. Researchers demonstrated that siRNAs against E2F1 in human cells prompted the induction of the TOP1MT (mitochondrial DNA Topoisomerase 1), which is encoded by the nuclear genome, as well as increased the transcription and replication of the mitochondrial genome (Goto et al., 2006). More details on the subject are collected in the section “1.5 E2F1: cycling through metabolism”.

- Nuclear receptors:

1) **Peroxisome proliferator-activated receptors (PPARs)**: PPARs (PPAR α , PPAR β/δ and PPAR γ) are three different genes encoding nuclear receptors that act as heterodimers with the retinoid X receptors (RXR). PPARs regulate the transcription of a broad set of genes involved in lipid uptake, storage and FA oxidation, thereby providing energy substrates for mitochondrial respiration. PPARs are integrated with other regulators of mitochondrial biogenesis such as NRF1 and GABP, through the

transcriptional coactivators peroxisome proliferator-activated receptor gamma coactivator 1- α (PGC-1 α) and β (PGC-1 β), which interact physically with PPARs and potentiate their transcriptional capacity (Puigserver et al., 1998; Wang et al., 2000).

2) **Estrogen-related receptors (ERR)**: Three members, ERR α , ERR β and ERR γ , each encoded by a different gene, comprise this family of nuclear receptors. ERR response elements (ERRE) are enriched in OXPHOS, TCA, mitochondrial import, FA oxidation and oxidative stress genes (Giguère, 2008) and often found in association with NRF1 and GABP sites (Mootha et al., 2003).

- Transcriptional coregulators:

Mitochondrial biogenesis is also controlled by a set of transcriptional coregulators which finely tune the network of genes involved in energetic homeostasis (Feige and Auwerx, 2007).

1) **Receptor-interacting protein 140 (RIP140)**: This transcriptional coregulator of nuclear receptors interacts with other nuclear receptors (including PPARs and ERRs) and recruits additional corepressors such as C-terminal binding protein (CtBP) and histone deacetylases (HDACs), leading to the suppression of gene transcription (White et al., 2008). Silencing of RIP140 leads to increased expression of TCA cycle enzymes, OXPHOS components and FA oxidation genes (Leonardsson et al., 2004; Powelka et al., 2006; Seth et al., 2007). In a very recent work from our lab, we show that RIP140 is induced in the spinal cord of X-ALD mice and NAWM from ccALD patients, and we uncover a new redox-dependent mechanism of RIP140 regulation. RIP140 deficiency exerts neuroprotection by inhibiting neuroinflammation and preventing mitochondrial and bioenergetic dysfunction in X-ALD mice, but more importantly, RIP140 deletion also halts axonal degeneration and improves the performance of X-ALD mice in behavioural tests. Hence, enough evidence is provided to develop RIP140-inhibiting strategies to block neurodegeneration in X-ALD and related disorders that share mitochondrial damage and neuroinflammation as common features (Ranea-Robles et al., *in press*).

2) **Nuclear receptor co-repressor 1 (NCOR1)**: Like RIP140, NCOR1 binds to PPARs and ERRs and mediates transcriptional repression. Silencing of NCOR1 leads to increased mitochondrial number and activity in muscle (Yamamoto et al., 2011).

3) Peroxisome proliferator-activated receptor-gamma coactivator-1 (PGC-1) coactivators: The PGC-1 coactivator-1 family comprises PGC-1 α , PGC-1 β and the PGC-1-related coactivator (PRC), being PGC-1 α the best studied. PGC-1 α binds to the transcription factors (e.g., NRF1, GABP, PPARs and ERRs) located at their respective response elements in the promoters. Next, the transcriptional activation domain of PGC-1 α recruits the histone acetyltransferase CBP/p300 and the Mediator complex (Wallberg et al., 2003), which enhances the transcription initiation and elongation.

1.3.2.4.4 Mitochondrial biogenesis impairment in neurodegeneration

The brain, like other organs, undergoes a gradual decline in energy metabolism and mitochondrial function during ageing. In fact, mitochondrial dysfunction is a culprit in the pathogenesis of an ever-increasing number of neurodegenerative diseases such as Alzheimer's disease (AD), Parkinson's disease (PD), Huntington's disease (HD) or amyotrophic lateral sclerosis (ALS) (Beal, 2005). The phenotype of *Pgc-1 α* null mice reflects the important functions of this coactivator in the nervous system, as these mice are hyperactive and present lesions in the striatum (Lin et al., 2004). The mRNA expression of the genes involved in mitochondrial biogenesis is decreased in most of the tissues of these mice, including the brain (Leone et al., 2005; Lin et al., 2004). Furthermore, loss of PGC-1 α leads to oxidative phosphorylation impairment and bioenergetic deficits in many tissues, being the mice intolerant to exercise (Handschin et al., 2007). Moreover, *Pgc-1 α* -deficient mice are more sensitive to chemically induced neurodegeneration of the substantia nigra and hippocampus and increasing PGC-1 α levels protects neural cells against oxidative stress (St-Pierre et al., 2006). Overall, PGC-1 α and its downstream targets are dysregulated in neurodegenerative disorders.

Besides malfunctioning of the OXPHOS, significant mitochondrial depletion is found in the spinal cord of *Abcd1*⁻ mice and the affected white matter of X-ALD patients (Morato et al., 2013). This depletion comprises reduction of mtDNA levels, concomitant with downregulation of the mitochondrial biogenesis pathway driven by PGC-1 α /PPAR γ , with diminished expression of the biogenesis factors NRF1 and TFAM, which negatively impact on the amounts of mitochondrial proteins such as cytochrome *c*, NADH:ubiquinone oxidoreductase subunit B8 (NDUFB8), complex II subunit succinate

dehydrogenase complex iron-sulfur subunit B (SDHB) and voltage-dependent anion channel (VDAC). Indeed, boosting mitochondrial generation via PPAR γ activation with pioglitazone (Morato et al., 2013) or by SIRT1 activation with resveratrol or SIRT1 overexpression (Morato et al., 2015), normalizes redox balance and prevents axonal degeneration in X-ALD mice.

1.3.3 Neuroinflammation

Inflammation is an active host defence mechanism of multi-cellular organisms against diverse insults (pathogens or injury) to inhibit and counteract the detrimental effects caused by them. Inflammation is an intriguing feature regarding X-ALD, as it is the major differentiating factor between AMN and ccALD. However, as already mentioned, the molecular mechanisms that govern disease progression, and its transformation to the cerebral inflammatory form, remain unknown. In many ways, X-ALD resembles MS, since infiltrating inflammatory cells are mainly macrophages and T cells rather than B cells (Griffin et al., 1985; Powers et al., 1992), but an autoimmune component has not been identified in X-ALD. Furthermore, while in MS lesions infiltrating cells are located in the lesion edge; inflammatory cells in X-ALD trail the demyelinating edge, suggesting that they emerge as a secondary feature after white matter degeneration (Eichler et al., 2008; Schaumburg et al., 1975). Classical pro-inflammatory cytokines, such as TNF α (Powers et al., 1992) and IL6 (McGuinness et al., 1997), among others, have been detected in inflammatory lesions in ccALD. On the other side, recent publications have opened the debate about whether AMN is actually a pure non-inflammatory disease. In a transcriptomics analysis with samples from the X-ALD mouse model and cerebral ALD patients, induction of NF- κ B-dependent pro-inflammatory response represents one of the main dysregulated pathways, together with increased expression of several pro-inflammatory cytokines (Schluter et al., 2012). Moreover, a study from our group unveiled a low-grade inflammatory induction in plasma and PBMC from AMN patients, with a mixed profile of M1 and M2 components induction (Ruiz et al., 2015). PBMC from cerebral ALD and AMN patients secrete higher amounts of TNF α than PBMC obtained from controls (Lannuzel et al., 1998). Therefore, AMN cannot be considered anymore as a non-inflammatory disease. These findings provide a basis to argue that a low-grade pro-inflammatory reaction initiated by VLCFA and present in the mouse model and AMN patients, may adopt a

more aggressive profile should a second (or third or several) hit appear (Singh and Pujol, 2010) during disease progression.

Microglia are immune-resident cells in the brain, performing countless physiological functions (Tremblay et al., 2011), but also involved in the pathogenesis of almost all CNS diseases (Cartier et al., 2014). Under physiological conditions, microglia exhibit a deactivated phenotype where they produce neurotrophic factors and maintain the CNS homeostasis. Upon insults or pathogens, microglia turn to an activated phenotype and promotes an inflammatory response to initiate the repair mechanism. This process is usually self-limiting and gets to the normal form once the damage has been repaired. If maintained during extended time, overt activation of these cells causes sustained inflammation associated with abundant production of cytotoxic factors which ultimately leads to cell death (Aldskogius et al., 1999; Wyss-Coray and Mucke, 2002). Microglia are one of the main players in the abnormal inflammatory response of X-ALD. This is evidenced by the fact that bone marrow transplantation and gene therapy can arrest demyelination (Cartier et al., 2009). As microglial cells derive from the same origin of monocytes and macrophages (Ginhoux et al., 2010), these are the only cells of the central nervous system that come from the bone marrow after transplantation. In the case of gene therapy, genetically corrected CD34⁺ cells differentiate into microglia in the brain (Asheuer et al., 2004). In addition, studies from our group using *Abcd1*⁻ and *Abcd1/Abcd2*^{-/-} mice show that microgliosis and astrogliosis are consistent features in the neuropathology of these mice (Ferrer et al., 2005; Fourcade et al., 2020; Launay et al., 2015; Launay et al., 2017; Lopez-Erauskin et al., 2011; Morato et al., 2013; Morato et al., 2015; Pujol et al., 2004; Ranea-Robles et al., 2018). Furthermore, VLCFA trigger inflammatory response mainly by abnormal activation of microglia and apoptosis in mice injected with C24:0-LPC (Eichler et al., 2008). Subsequently, activated microglia produce higher amounts of the pro-inflammatory cytokine TNF α , that together with IL1 β , induce further accumulation of VLCFA (Khan et al., 1998), creating a vicious cycle that worsens the pathology of X-ALD. The role of microglia in neurodegeneration is not limited to X-ALD, being common in other neurodegenerative disorders, such as AD, ALS and PD (Heneka et al., 2005). In the last years, microglial-like cells have been obtained from human pluripotent stem cells, expanding the therapeutic potential of targeting these cells in central nervous system disorders (Muffat et al., 2016).

1.3.3.1 Microglial dysfunction in X-ALD

Mature oligodendrocytes sustain myelin sheaths with a high lipid content, representing 70-75% of their dry weight (Nave and Werner, 2014). Accordingly, this cell type was considered central to the pathogenesis of leukodystrophies (Gieselmann, 2008). However, the fact that X-ALD cerebral patients partly respond to allogeneic or genetically modified autologous stem cell transplantation (Eichler et al., 2017) underscores the fundamental importance of cells derived from-or replaceable by- descendants of haematopoietic lineage. Besides, studies in animal models and human tissue highlight early changes of microglia in lesion development (Bergner et al., 2019; Eichler et al., 2008; Gong et al., 2017; Weber et al., 2014; Weinhofer et al., 2018) and corroborate what others previously reported (Griffin et al., 1985; Ito et al., 2001; Powers et al., 1992), which is that immune cells have indeed a major role in the pathogenesis of the X-ALD.

Phenotypic variability in X-ALD appears to be linked to brain inflammation that causes progressive neurological decline mostly in children, and sometimes adults, with X-ALD (Engelen et al., 2012a). The inflammatory nature of the demyelination sets X-ALD apart from other leukodystrophies and motivates the comparison with MS, the most common demyelinating disorder of the brain. However, in contrast to the relentless progression of ccALD, MS typically displays a relapsing-remitting course. In addition, the metabolic component of X-ALD makes it to be studied as a distinct entity. In the childhood form of X-ALD, CNS symptoms often appear abruptly, and the course is rapidly progressive, frequently accompanied by asymmetrical distribution of the lesions, and striking accumulation of lymphocytes in active brain lesions (Eichler et al., 2008; Schaumburg et al., 1975). These features prompted the possibility that some aspects of the childhood form of X-ALD may be immunologically mediated. Several groups put effort in characterizing the nature of these inflammatory cells and immunocytochemical stains were carried out in brain and cerebrospinal fluid of patients with adrenoleukodysptrophy (Eichler et al., 2008; Griffin et al., 1985). These studies showed that the primary cells involved in the inflammatory infiltrates are astrocytes, macrophages, cytokines and T lymphocytes and that most of these cells are of the T4 phenotype (“helper” cells). It must be considered that commented studies were performed almost 40 years ago with the associated technical limitations. Since then, advances in the field of immunohistological techniques and the discovery of new

markers for immune cells have allowed having a wider knowledge on the topic. The proposed hypothesis was that the initial biochemical lesion, the accumulation of VLCFA, causes an instability in myelin sheaths with spontaneous myelin break down. The liberation of these myelin components stimulates nearby astrocytes and macrophages to initiate a TNF-cytokine cascade eventuating in demyelination.

In an attempt of determining whether the main immune cell types are equally affected in X-ALD, Weber and co-workers evaluated the extent of the metabolic defect in different immune cell-types of AMN patients (Weber et al., 2014). The results showed that monocytes are the most vulnerable cell type to ABCD1 loss, compared to B and T cells, as they showed higher expression of ABCD1 (in control cells), and greater VLCFA accumulation (Weber et al., 2014). Monocytes are the progenitor cells of macrophages. The latter have the capacity of phagocytosing myelin debris in the absence of appropriate FA degradation, which are then esterified to cholesterol, as observed by lipid analysis of autopsy material from X-ALD patient's cerebral white matter lesions (Theda et al., 1992). Intracellular VLCFA-cholesterol esters deposited inside macrophages have been visualized as crystalline structures (Schaumburg et al., 1975) and are expected to promote cellular stress. It has been demonstrated that the immunoreactivity of oxidative stress markers correlates with the degree of inflammation and myelin breakdown (Powers et al., 2005). Moreover, VLCFA-enriched lipids, in particular in the lysophosphatidylcholine fraction, can lead to microglial activation and apoptosis (Eichler et al., 2008). In another study, Weinhofer et al. published that macrophages in X-linked adrenoleukodystrophy, despite showing normal differentiation and phagocytosis, are pro-inflammatory skewed, rendering them unable to acquire the anti-inflammatory polarization state necessary to dampen the destruction of myelin and initiate repair (Weinhofer et al., 2018). In post-mortem ccALD brains, a zone lacking microglia was found in perilesional white matter beyond the active demyelinating lesion edge (Eichler et al., 2008). This lack of microglia, together with the impaired lipid-laden macrophages, perpetuates the demyelinating process. Finally, alterations in the brain endothelium have also been described (Musolino et al., 2015; Musolino et al., 2012), leading to a blood-brain-barrier leakage and incremented transmigration of monocytes. Altogether, the inherent molecular defect in circulating monocytes/macrophages seems to be involved in the progression of inflammation. The metabolic defect in macrophages/microglia may explain the failure of anti-inflammatory treatment attempts for X-ALD, as they do not target the intrinsic defect of these cells. Hence, it is tempting

to speculate that the correction of the transport of VLCFA for peroxisomal β -oxidation in invading macrophages could be a promising approach for dampening the pro-inflammatory response in ccALD lesions.

1.3.4 Proteostasis impairment

The term proteostasis has been used to define protein homeostasis within the cell. This concept comprises the study of individual proteins, starting from their synthesis, localization and function, and continuing with their half lifetime and degradation. Disruption in protein homeostasis, evidenced by the presence of misfolded or aggregated proteins, is prevalent in most neurodegenerative disorders, being documented in animal models as well as in the brain of the patients (Douglas and Dillin, 2010; Selkoe, 2003). Within this hallmark, we can embody malfunction of the proteasome and alterations in the autophagic flux, pathological conditions arising from an improper response against misfolded proteins. Indeed, in our group, we have described alterations in these pathways in X-ALD (Launay et al., 2015; Launay et al., 2013; Launay et al., 2017).

1.3.4.1 Ubiquitin-proteasome system

Most soluble misfolded proteins are cleared through the ubiquitin-proteasome system (UPS), the major eukaryotic proteolytic pathway (Ciechanover, 1998). Proteins assigned to be degraded, are tagged by polyubiquitination and then sent for destruction to the 26S proteasome (Wilkinson, 2000). UPS is pivotal in the rapid clearance of damaged, misfolded or aggregated proteins in both healthy and diseased states and has been shown to play a role in the degradation of oxidized proteins (Dennissen et al., 2012; Goldberg, 2003). Alterations in this pathway are commonly found in many neurodegenerative disorders (Hyun et al., 2003; Keller et al., 2000; McNaught and Jenner, 2001). The link between the UPS and neurodegeneration is clearly exemplified by juvenile forms of PD caused by a mutation in Parkin, an ubiquitin-ligase (Kitada et al., 1998). In X-ALD, chronic and progressive malfunctioning of the UPS caused by the accumulation of oxidatively modified proteins has been detected. Notably, immunoproteasome machinery appears upregulated in response to redox imbalance.

Immunoproteasome is recruited towards mitochondria when X-ALD fibroblasts are exposed to an excess of C26:0 (Launay et al., 2013). All these events are prevented in *Abcd1* null mice by the treatment with antioxidants (Launay et al., 2013; Launay et al., 2017). The results suggested a possible role of the UPS and the immunoproteasome as the first line of defence against oxidative damage to the mitochondria by elimination of oxidized mitochondrial proteins, thereby improving mitochondrial viability and turnover.

1.3.4.2 Autophagic flux

Along with degradation by the proteasome, autophagy constitutes an alternative route for eliminating misfolded or modified intracellular proteins by their delivery to lysosomes (Martinez-Vicente and Cuervo, 2007), and is often malfunctioning in neurodegenerative diseases (Wong and Cuervo, 2010). Moreover, alterations in autophagy, as well as in mTOR, a key upstream regulator of this process, and also one of the most important nutrient sensors, as stated above, have been described elsewhere (Cuervo et al., 2004; Lee et al., 2010). Impaired autophagic flux was detected in *Abcd1* mice (Launay et al., 2015). The mechanism appeared to be an aberrant overactivation of the mammalian target of rapamycin (mTOR) pathway, mediated by VLCFA excess. The induction of autophagic flux through the rapamycin ester temsirolimus (inhibitor of mTOR) preserved autophagy, maintained the redox and metabolic homeostasis, and successfully arrested axonal degeneration in X-ALD mice.

1.3.5 ER stress

The ER is an essential organelle for the maturation and processing of proteins folded through the secretory pathway. For that purpose, ER contains a dynamic network of chaperones, foldases and co-factors in the lumen (Matus et al., 2011). When homeostasis in the ER is disrupted, abnormally folded proteins accumulate, leading to ER stress, which engages the unfolded protein response (UPR) (Ron and Walter, 2007), a physiological response addressed to restore the capacity to generate properly folded proteins and reduce the amount of misfolded proteins. Signs of ER stress have been detected in most animal models of neurodegeneration and in the brain of human patients, for example in ALS (Nassif et al., 2010; Saxena et al., 2009), PD (Hoozemans

et al., 2007), HD (Vidal et al., 2011), AD (Hoozemans et al., 2005), and in diseases associated with myelin (Lin and Popko, 2009). Unlike the mentioned cases, protein aggregation has not been described up to date in X-ALD. Instead, oxidative stress (van der Vlies et al., 2003) and lipid dyshomeostasis (Hou et al., 2014) are the culprit of ER stress activation and UPS engagement in X-ALD (Launay et al., 2017). This dysregulation was characterized by the activation of three main ER stress sensors: PERK, ATF6 and IRE1 causing an early engagement of UPR in *Abcd1*⁻ mice. Moreover, activation of PERK pathway in the affected white matter of ccALD and cAMN patients with no changes in IRE1 or ATF6 pathways was also observed. Remarkably, the bile acid tauroursodeoxycholate (TUDCA) administration abolished UPR activation in *Abcd1*⁻ mice (Launay et al., 2017).

1.3.6 Lipidic imbalance: new member in the family?

1.3.6.1 Lipids and the central nervous system

Lipid metabolism in the CNS is of particular interest as the highest concentration of lipids is concentrated in the CNS, only behind the adipose tissue. There are eight different classes of lipids that form the CNS: fatty acyls, glycerolipids, glycerophospholipids, sphingolipids, sterol lipids, prenol lipids, saccharolipids and polyketides (Fahy et al., 2005). Lipids have a variety of functions like the formation of lipid bilayers that form the structure and provide a necessary channel for protein activity, function as an energy reservoir (for example triglycerides), and serve as precursors for various secondary messengers such as arachidonic acid (AA), docosahexaenoic acid (DHA), ceramide, 1,2-diacylglycerol (DAG), phosphatidic acid (PA) and lysophosphatidic acid (Lyso-PA). Maybe one of the most important roles of lipids in the CNS (and peripheral nervous system, PNS) is the lipid synthesis required for the formation of myelin (Chrast et al., 2011). The wrapping of myelin around an axonal segment increases axonal resistance and enables the clustering of axonal ion channels at nodes of Ranvier. The myelin membrane is an extended and highly specialized plasma membrane synthesized by myelinating glial cells: oligodendrocytes in the CNS, and Schwann cells in the PNS. Major lipids in its composition include cholesterol, cerebroside (galactosylceramide, a sphingolipid found in high

concentrations only in the myelin sheath), and other sphingolipids such as sphingomyelin (Aschner and Toews, 2010). The phospholipid composition is unusual in that most of the ethanolamine phosphatides are present as plasmalogens. The particular lipid composition of myelin, the transport of lipid-associated myelin proteins, and the necessity for timely assembly of the myelin sheath all contribute to the observed vulnerability of the brain in numerous lipid metabolism disorders.

The normal functions of these lipids govern the overall normal physiology of the brain. Any abnormal deviation from the normal function of the brain, either due to any mechanical injury or due to pathological changes in neurons, leads to different types of neurodegenerative diseases, mental disorders, stroke and CNS traumas (Adibhatla and Hatcher, 2010; Shichiri, 2014). Currently, there exists no successful cure for these CNS injuries and disorders, resulting in a huge impact on quality of life, so the understanding of these alterations may help in the creation of new therapeutic approaches.

1.3.6.2 Lipid-derived neurodegeneration in the CNS

The importance of lipids in cell signalling and tissue physiology is demonstrated by many neurological disorders, including bipolar disorders and schizophrenia, and neurodegenerative diseases such as AD, PD, Niemann-Pick and HD, that involve deregulated lipid metabolism (Adibhatla and Hatcher, 2010; Wenk, 2005). Oxidative stress and lipid peroxidation are also believed to be key events that contribute to CNS injuries (Adibhatla et al., 2006). Since the discovery of oxidized phospholipids and their role in the modulation of inflammation in cardiovascular diseases, the importance of lipid oxidation products in several CNS pathologies has been identified (Adibhatla and Hatcher, 2008; Koppaka et al., 2003; Qin et al., 2007; Ross et al., 2001).

The brain is extremely sensitive to oxidative damage for several reasons. Firstly, the brain consumes an inordinate amount of oxygen (around 20%), considering the fact that the brain accounts for only 2% of body weight (Halliwell, 2006; Shichiri, 2014). A major reason for the high O₂ uptake is the vast amounts of ATP required to maintain neuronal intracellular ion homeostasis in the face of ion channels need for action potentials and neurosecretion. Additionally, several brain areas, including the substantia nigra, caudate nucleus, putamen and globus pallidus, are rich in iron content (Zecca et

al., 2004). High concentrations of reactive iron can act as catalyst for reactive species formation, increasing oxidative-stress induced neuronal vulnerability (Ward et al., 2012). The brain is a source of ROS; it generates a lot of H₂O₂, but on the other hand, has lower antioxidant defences compared to other organs. Lastly, neuronal membranes are rich in polyunsaturated fatty acids (PUFAs), particularly AA, DHA and eicosapentaenoic acid (EPA) (Chen et al., 2008). These PUFAs are particularly vulnerable to oxidative stress due to their possession of unsaturated double bonds.

Lipid peroxidation comprises three distinct mechanisms: free radical-mediated oxidation, free radical-independent nonenzymatic oxidation, and enzymatic oxidation (Niki et al., 2005). Free radical-mediated lipid peroxidation proceeds by a chain mechanism, that is, one initiating free radical can oxidize both lipid molecules in biological membranes and low-density lipoproteins. Lipid oxidation by nonradical mechanisms can be accomplished by singlet oxygen and ozone (Pryor et al., 2006). The third mechanism, enzymatic oxidation, is carried out by lipoxygenases and cyclooxygenases, which have both been reported to oxidize AA into hydroperoxyeicosatetraenoic acid (HPETE), prostaglandins, prostacyclin, thromboxane, and leukotrienes (Schneider et al., 2007). Lipid peroxidation has been shown to induce disturbance to membrane organization and functional loss/modification of proteins and DNA.

Beyond damage to membranes, lipid peroxides give rise to reactive α , β -unsaturated aldehydes including malondialdehyde (MDA), 4-hydroxynonenal (HNE) and acrolein, by far the strongest electrophile among all α , β -unsaturated aldehydes. These aldehydes covalently bind to proteins through reaction with thiol groups, altering their function, and have been widely used as markers of neurodegeneration (Reed, 2011).

The cell is provided by several mechanisms to overcome such detrimental effects such as detoxifying enzymes that scavenge ROS, which include the superoxide dismutases (SOD), glutathione peroxidases (GPX), peroxiredoxins (PRX) and catalase. However, as it has been mentioned, brain antioxidant defence is limited compared to other organs. Since oxidative stress is a shared scenario in many neurodegenerative disorders, lipid-peroxidation induced damage has been identified in many of them. For further information, we direct the reader to more detailed reviews on the topic (Adibhatla and Hatcher, 2010; Reed, 2011).

Another strategy to avoid redox damage is the formation of lipid droplets (LDs). LDs are evolutionary conserved ubiquitous organelles found in almost all organisms, from bacteria to mammals. They are composed of a hydrophobic neutral lipid core (triacylglycerols and sterol esters) surrounded by a phospholipid monolayer membrane with various decorating proteins. LDs originate from the ER and, when lipids are needed, they are broken down by cytoplasmic lipases and autophagy. For a long time, LDs were accepted as inert intracellular vesicles storing neutral lipids in all living organisms. However, thanks to advances in functional analysis techniques and imaging, it has become apparent that LDs play even broader cellular roles than previously appreciated (Onal et al., 2017; Welte, 2015). For example, they modulate the availability of proteins and signalling lipids in the nucleus, act as hubs for fatty acid trafficking, are used as assembly platforms by viruses, and their dysfunction in neurons and glia may lead to neurodegeneration (Onal et al., 2017; Welte, 2015). LDs may allow cells to safely sequester otherwise toxic lipids, particularly in cases of overabundant fatty acids, which may pose a threat to membrane integrity and peroxidability (Bailey et al., 2015).

Concerning LDs, yet until recently, there has been only sparse and unconnected information on their role in neurons and other cells of the nervous system. At the beginning of the 20th century, Alois Alzheimer noted the presence of glial lipid accumulations in the human brain after death from AD patients. In the decade of the 70-80s, several studies were published, claiming the presence of LDs in response to injury (de Estable-Puig and Estable-Puig, 1973) and the brain of aged-mice (Brawer and Walsh, 1982; Marschallinger et al., 2020; Shimabukuro et al., 2016), suggesting LD accumulation as a marker of compromised brain health. In addition, the presence of LDs was observed close to amyloid inclusions and *APOE4*-expressing cells have been found to accumulate excess cholesterol and LDs, evidencing their role in the pathophysiology of AD (Eriksson and Westermarck, 1990; Farmer et al., 2019; Lin et al., 2018). There are also links between α -synuclein and LDs: α -synuclein has been reported to bind to LDs *in vitro* (Cole et al., 2002), and overexpression in yeast promotes droplet accumulation (Outeiro and Lindquist, 2003). LDs have also been detected in brain sections of an HD mouse model (Martinez-Vicente et al., 2010). To finish, in genetic screens looking for enhancers and suppressors for the development of ALS, one of the most represented functional categories was proteins linked to LDs, including proteins involved in droplet

biogenesis and motility (Sanhueza et al., 2015). These findings are of vital importance since they indicate that excess of LDs is not only due to increased formation and/or limited degradation, but also due to aberrant droplet dynamics or malfunction of the proteins involved in their motility (Klemm et al., 2013).

It is well known that glia play key roles not only in supporting brain homeostasis but also working on essential brain functions, namely electrolyte homeostasis, inflammation, synapse formation, neurotransmission and importantly neurometabolism (Jha and Morrison, 2018). Studies focusing on lipid deposition during glial LD generation have come to the forefront of cell biology research as recent papers have identified that under certain conditions, disrupted LD function can contribute to neurodegeneration. Ageing is one of these particular conditions (Farmer et al., 2020), as LDs appear to accumulate in the brain during the normal process of ageing, as observed both in post-mortem human tissue (Marschallinger et al., 2020) and mice model of ageing (Marschallinger et al., 2020). In a recent study, researchers showed that microglia neutralize oxidized phosphatidylcholine found in MS lesions via trigger receptor expressed on myeloid cells 2 (TREM2) receptor and prevents neurodegeneration *in vitro* and in mice (Dong et al., 2021).

Inflammation is another major cause of LD formation (Farmer et al., 2020). From *in vitro* studies of LDs to *ex vivo* brain imaging, inflammation has repeatedly been associated with LD formation as both a cause and/or as a consequence (Bozza and Viola, 2010). Lipopolysaccharide (LPS) has been shown to increase the number and size of LDs in microglia (Khatchadourian et al., 2012), both *in vitro* in microglia-derived BV2 cells and in an *in vivo* mice model of LPS (Marschallinger et al., 2020).

Lastly, intracellular ROS, as well as ectopic treatment with oxidative stressors such as hydrogen peroxide, induce LD formation in various cell types (Jin et al., 2018; Lee et al., 2013). For example, neuronal hyperactivity caused by trauma or chemogenetic activation increases LD accumulation in astrocytes (Ioannou et al., 2019). Fatty acid-derived neurotoxicity is avoided thanks to the neuron-astrocyte metabolic coupling, as these LD-laden glia upregulate genes responsible for the neutralization of the peroxidated lipids generated by activated neurons (Ioannou et al., 2019).

Although studies demonstrate that oxidative damage occurs in several neurodegenerative diseases, in chronic conditions such as those, it is difficult to

determine if this damage relates directly to the underlying cause of the disease or represents secondary damage in cells with otherwise compromised function (Agar and Durham, 2003). Interpretation of data from patients is complicated by the fact that observations are usually obtained at the end stage of neurological disease and thus the time course of oxidative damage relative to the progression of the disease is not obtained. Also, these oxidative modifications are not disease-specific but occur in many neurodegenerative diseases.

1.3.6.2.1 Lipid-derived neurodegeneration in X-ALD

First evidences of lipid accumulations in X-ALD appeared in the early 1970s, when Powers and Schaumburg reported the presence of intracytoplasmic lamellae and lamellar lipid inclusions in adrenal, testicular and Schwann cells and brain macrophages from X-ALD patients (Powers and Schaumburg, 1974). Biochemical analysis of these inclusion bodies revealed that they contained cholesterol, phospholipids and gangliosides esterified with saturated VLCFA (Igarashi et al., 1976). The subsequent discovery by Moser and colleagues that these elevated VLCFA, in particular C26:0, were also detectable in fibroblasts, blood cells and especially plasma of X-ALD patients was of crucial importance as this finding allowed unequivocal identification of male patients (Moser et al., 1981). Plasma VLCFA analysis is still the best initial biomarker of X-ALD. Microglia/brain macrophages engulfing myelin debris, and occasionally containing fibrillary deposits of lipidic materials and paracrystalline, specular needle-like inclusions, were encountered in actively demyelinated lesion edge of X-ALD patients (Eichler et al., 2008) and X-ALD mice spinal cords (Pujol et al., 2002). Furthermore, *Abcd1*^{-/-}/*Abcd2*^{-/-} double knockout mice presented a dramatic accumulation of LDs across the adrenal cortex, encompassing glomerular, fascicular and reticular cell layers (Pujol et al., 2004). LDs were recently detected in an *in vitro* endothelial model mimicking the blood-brain-barrier of ccALD patients (Lee et al., 2018) and in a *Caenorhabditis elegans* model for adrenoleukodystrophy, *pmp-4* defective nematode, (Coppa et al., 2020). More importantly, treatment with mitochondria-targeted antioxidant MitoQ normalized LD accumulation in mutant larvae and prevented axonal degeneration and locomotor disability (Coppa et al., 2020), evidencing the importance of redox status in the formation of LDs and pathophysiology of the disease.

There have been reports of oxidative modifications in post-mortem X-ALD brains, where lipid peroxidation products, especially in the form of HNE, mainly occur in the inflammatory demyelinating lesions and adrenal cortex (Powers et al., 2005). Lipid peroxidation is particularly linked to a rapidly progressive disease of myelin because, once it begins, it self-perpetuates and does not normally stop until the target substrate (i.e. lipids) is exhausted (Montine et al., 2002). As a consequence of oxidative stress, the elevated production of free radicals leads to a significant increase in plasma levels of lipid-peroxidation markers such as thiobarbituric acid reactive substances (TBARS) and MDA in X-ALD patients (Deon et al., 2007; El-Bassyouni et al., 2012; Petrillo et al., 2013; Vargas et al., 2004). In addition, the oxysterols 7-ketocholesterol (7KC) and 7 β -hydroxycholesterol (7 β -OHC) are also associated with demyelinating neurodegenerative diseases such as X-ALD and MS (Nury et al., 2017). Oxysterols are lipid peroxidation products formed by either spontaneous auto-oxidation of cholesterol, by enzymatic reactions involving cytochrome P450 enzymes, hydroxylases and dehydrogenases, or by both processes (Mutemberezi et al., 2016). Importantly, the brain is rich in cholesterol due to its presence not only in the plasma membrane but also as a component of myelin sheaths. Thus, several studies have highlighted the harmful effects of some oxysterols, particularly in age-related diseases (Zarrouk et al., 2014) and many neurodegenerative diseases including PD (Cheng et al., 2011), HD (Kreilaus et al., 2016) and AD (Nelson and Alkon, 2005).

This section describes what is known about the main hallmarks of X-ALD, which are oxidative stress, mitochondria and proteostasis impairment, neuroinflammation and lipidic imbalance. **Figure 3** illustrates a general scheme of the pathophysiology of X-ALD and the hallmarks of oxidative stress, mitochondria and proteostasis impairment, and neuroinflammation are represented.

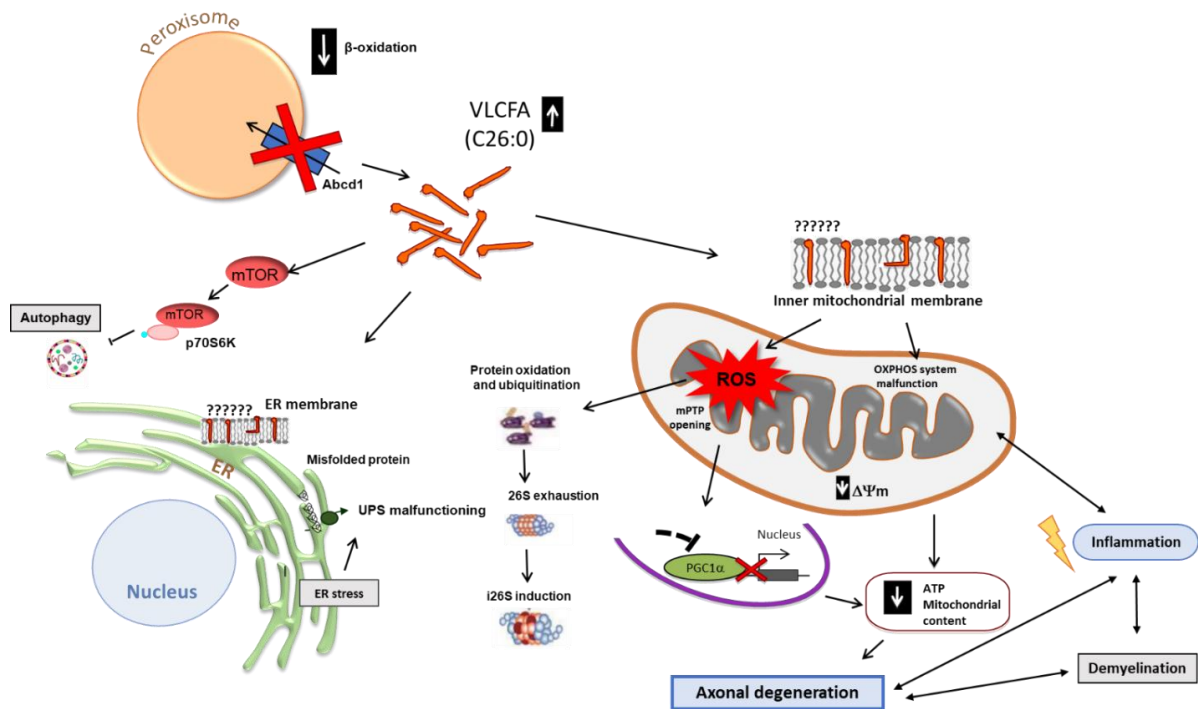


Figure 3. Model recapitulating the noxious effects of VLCFA excess on mitochondria, redox homeostasis and proteolytic machineries in X-ALD.

In X-ALD, excess of VLCFA leads to the production of intramitochondrial ROS from the electron transport chain, probably, by an unknown mechanism. The consequences are mitochondrial dysfunction resulting in loss of $\Delta\Psi_m$ and ATP production, mPTP opening, inhibition of mitochondrial biogenesis via the SIRT1/PGC-1 α /PPAR γ pathway, and ultimately axonal degeneration due to energetic failure. In addition, VLCFA-dependent ROS induce protein oxidation and ER-stress, and the accumulation of defective proteins provokes the inhibition of the proteasome machinery. Autophagy is inhibited via aberrant activation of mTOR signalling pathway. Also, the mitochondrial ROS production regulates inflammation by activating NF- κ B pathway. In turn, the production of pro-inflammatory mediators such as cytokines, alter mitochondrial function by increasing ROS production and decreasing the activity of respiratory complexes. When prolonged in time, neuroinflammation can lead to demyelination, contributing to axonal degeneration.

1.4 Biotin: physiological functions and therapeutic potential

Biotin is a water-soluble essential B-complex vitamin (B7) that serves as coenzyme for five carboxylases in humans. Biotin is also covalently attached to distinct lysine residues in histones, affecting chromatin structure and mediating gene regulation

(Camporeale et al., 2004; Chew et al., 2006; Hymes and Wolf, 1999; Kobza et al., 2008). Biotin-dependent carboxylases include acetyl-CoA carboxylase (ACC), propionyl-CoA carboxylase (PCC), 3-methylcrotonyl-CoA carboxylase (MCC), geranyl-CoA carboxylase (GCC), pyruvate carboxylase (PC), and urea carboxylase (UC). They contain biotin carboxylase (BC), carboxyltransferase (CT) and biotin-carboxyl carrier protein (BCCP) components. These enzymes are widely distributed in nature and have important functions in fatty acid, amino acid, and carbohydrate metabolism, polyketide biosynthesis, urea utilization, and other cellular processes (Tong, 2013; Zempleni et al., 2009). Biotin-dependent carboxylases have two distinct enzymatic activities and catalyze their reactions in two steps. As an example, **Fig. 4** illustrates the generation of malonyl-Coa, catalyzed by ACC.

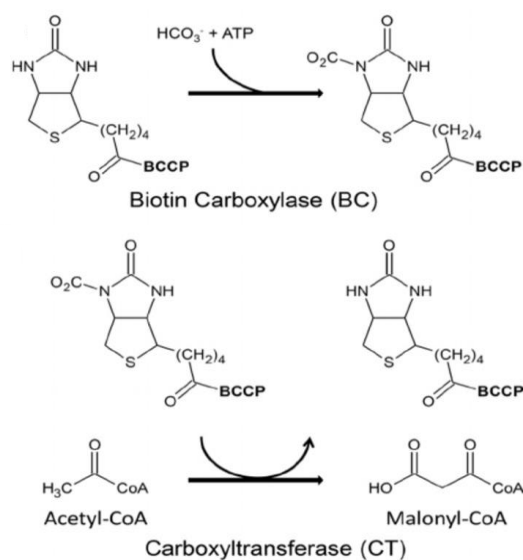


Figure 4. The acetyl-CoA carboxylase (ACC) reaction.

The synthesis of malonyl-CoA is carried out in two distinct partial reactions. First, a biotin carboxylase (BC) component catalyzes the ATP-dependent carboxylation of the biotin cofactor, using bicarbonate as CO₂ donor. Biotin is covalently linked through an amide bond to a lysine side chain in the biotin carboxyl carrier protein (BCCP) component. In the second step of the reaction, a carboxyltransferase (CT) component catalyzes the CO₂ transfer from carboxybiotin to the acceptor of the carboxyl group, acetyl-CoA here. Modified from (Smith and Cronan, 2012).

During evolution, mammals lost the ability to synthesize biotin and now satisfy their need through a delicate balance between dietary biotin and reutilization of endogenous, protein-bound biotin (Pacheco-Alvarez et al., 2002). To ensure a continuous supply of the vitamin, eukaryotic organisms have developed a biotin utilization cycle that depends on the participation of three different proteins. The first is a transporter for the uptake of biotin through the plasma membrane. The sodium-dependent multivitamin transporter (SMVT) transports biotin and pantothenic and lipoic acids (Prasad et al., 1997). The second is the holocarboxylase synthetase (HCLS). It catalyzes the biotinylation of carboxylases in a two-step ATP-dependent reaction in which biotin is first activated to biotinyl-5-AMP and then transferred to the apocarboxylase substrate (Chapman-Smith and Cronan, 1999; León-Del-Río et al., 1995). The third enzyme of the biotin cycle is biotinidase. It is responsible for releasing biotin from protein-bound biotin by hydrolysis (Hymes and Wolf, 1996). In humans, the balance between the utilization of exogenous and recycled biotin can be disrupted by genetic abnormalities with devastating consequences for metabolic homeostasis.

In vitro and *in vivo* studies have shown that biotin is a key transcriptional regulator of several genes involved in glucose and lipid metabolism and that elevated biotin levels can upregulate the expression of hepatic and pancreatic glucokinase, insulin and the insulin receptor, and downregulate hepatic phosphoenolpyruvate carboxykinase (Chauhan and Dakshinamurti, 1991; Dokusova and Krivoruchenko, 1972; Pacheco-Alvarez et al., 2002; Romero-Navarro et al., 1999). Interestingly, biotin also regulates the expression of two of the carboxylases for which it acts as a cofactor (PC and ACC1), and of HCLS (Pacheco-Alvarez et al., 2005). The mechanism by which biotin regulates gene expression remains elusive. Biotin was initially not thought to be a natural modifier of histones (Healy et al., 2009). However, biotinylation sites have been shown to be present on histones H2A, H3, and H4 (Zempleni et al., 2014) and several studies have demonstrated that biotinylation of histones by HCLS induces chromatin remodelling that can regulate gene expression (Filenko et al., 2011; Gralla et al., 2008; Kuroishi et al., 2011). Yet, more recent data suggests that HCLS itself may interact directly with chromatin as part of a multiprotein gene regulating complex (Liu and Zempleni, 2014; Zempleni et al., 2012).

As an essential vitamin, biotin deficiency is accompanied by several clinical manifestations. Biotin deficiency has adverse effects on cellular and humoral immune functions. For example, children with hereditary abnormalities of biotin metabolism develop *Candida* dermatitis and present absent delayed-hypersensitivity skin-tests responses, IgA deficiency, and subnormal percentages of T lymphocytes in peripheral blood (Cowan et al., 1979). In rodents, biotin deficiency decreases antibody synthesis (Kumar and Axelrod, 1978), decreases the number of spleen cells and the percentage of B lymphocytes in the spleen (Báez-Saldaña et al., 1998), and impairs thymocyte maturation (Báez-Saldaña and Ortega, 2004). Biotin deficiency is also linked to cell stress, enhancing the nuclear translocation of the transcription factor NF- κ B in human lymphoid cells (Rodriguez-Melendez et al., 2004). To finish, stress-resistant *Drosophila* can be selected by feeding biotin-deficient diets for multiple generations (Smith et al., 2007).

ACC1 is the rate-limiting enzyme that generates malonyl-CoA, the two-carbon building block for fatty acid synthesis, which is an essential component of the myelin sheath (DeWille and Horrocks, 1992; Tansey et al., 1988). PC, PCC and MCC generate intermediates for the TCA cycle and thus, increase the levels of cellular ATP at the rate of one molecule of acetyl-CoA used by the TCA cycle, producing one molecule of ATP. Malonyl-CoA is also a well-known inhibitor of carnitine palmitoyltransferase I (CPT1) (McGarry and Brown, 1997), the first enzyme required in the process of mitochondrial FAO. CPT1 inhibition is mainly due to ACC2-derived malonyl-CoA, as ACC2 (Abu-Elheiga et al., 2001) is bound to the mitochondrial outer membrane, where CPT1 acts.

Consistent with the roles of biotin-dependent ACC1 and 2, and propionyl-CoA carboxylase in lipid metabolism, biotin deficiency causes alterations of the fatty acid profile in liver, skin, and serum of several animal species (Zempleni and Mock, 2000). Biotin deficiency is associated with an increased abundance of odd-chain fatty acids, suggesting that odd-chain fatty acid accumulation may be a marker for reduced propionyl-CoA carboxylase activity in biotin deficiency (Zempleni and Mock, 2000). Nevertheless, biotin deficiency does not affect the fatty acid composition in brain tissue to the same extent as in the liver (Pacheco-Alvarez et al., 2005; Zempleni and Mock, 2000), probably due to a mechanism aimed to preserve the essential function of biotin in the brain at the expense of organs such as liver and kidney during biotin deprivation.

The importance of biotin in the brain is best manifested in the inherited errors of biotin metabolism, including biotinidase, and holocarboxylase deficiencies (Dabbagh et al., 1994; Ozand et al., 1998), and perhaps biotin transporter deficiency (Ozand et al., 1998; Zempleni et al., 2002), which might cause encephalopathies. These disorders are reversible to some extent with biotin treatment (Bousounis et al., 1993; Grunewald et al., 2004; Wolf, 2011), in the same manner as biotin-thiamine responsive basal ganglia disease (BTBGD) (Bindu et al., 2009; Ozand et al., 1998). Biotin deficit is frequently associated with epileptic seizures and studies suggest that it facilitates convulsive disorders (Bregola et al., 1996). One explanation for this is that, as a cofactor of carboxylase enzymes, biotin has a central function in the metabolism of carbon dioxide, which is known to have an important influence on the seizure threshold (Jasper, 1969). Moreover, biotin-dependent carboxylases are involved in the metabolism of some neurotransmitters (Krause et al., 1985). Treatment with anticonvulsants appears to diminish plasma biotin levels, probably by increasing biotin catabolism (Mock and Dyken, 1997) or by competitive inhibition of biotin transport in the human intestine (Said et al., 1989). Over time, this can lead to reduced biotin status, so biotin supplementation should be considered as adjuvant therapy in the treatment of epileptic patients. To finish, in the only study published to date examining the impact of pharmacological doses of biotin on stroke, stroke-prone spontaneously hypertensive rats receiving biotin administration had a modest but significant impact on blood pressure on the wall-to-lumen ratio of cerebral arterioles, and reduced mortality overall (Watanabe-Kamiyama et al., 2008).

Regarding other peripheral tissues, nutritional biotin deficiency and biotin deficiency induced by the loss of the recycling enzyme biotinidase causes severe ATP depletion with resulting AMPK activation, and changes in carbon metabolism gene expression in the mouse liver, such as inhibition of lipogenesis and activation of FAO, adaptations that mitigate energy shortage (Hernandez-Vazquez et al., 2012; Hernandez-Vazquez et al., 2013; Velazquez-Arellano et al., 2011). Comparable results were observed in other living organisms, *Saccharomyces cerevisiae*, *Caenorhabditis elegans* and in rats, unveiling the importance of this molecule in the general energetic status of the cells (Ortega-Cuellar et al., 2010). These studies provide new and important information that may be relevant to human disorders like hypertriglyceridemias and diabetes.

Treatment with a high-dose pharmaceutical-grade biotin (MD1003; 10,000 times the recommended daily intake), showed clinical improvement in patients suffering progressive MS (Tourbah et al., 2016). These beneficial effects have been hypothesized to target two key pathophysiological mechanisms in progressive MS: (1) activating carboxylases to support myelin synthesis by oligodendrocytes by enhancing fatty acid synthesis and (2) protecting against hypoxia-driven axonal degeneration by replenishing ATP in neurons (Lazzarino et al., 2010; Trapp and Stys, 2009). Prompted by these promising outcomes, a phase III clinical trial for this condition was designed to assess the safety and efficacy of high-dose biotin in progressive forms of MS (NCT02936037). Unfortunately, the previously reported efficacy of high-dose biotin could not be replicated, and thus, high-dose biotin cannot be recommended for the treatment of progressive MS (Cree et al., 2020).

To sum up, biotin is a coenzyme with important functions in carbon metabolism and overall energetic maintenance of the cell, being a promising therapeutic candidate for those diseases presenting mitochondrial dysfunction and metabolic impairment among their hallmarks.

1.5 E2F1: cycling through metabolism

We have briefly introduced in a previous section the E2F1 protein. This section includes broader information on the structure, regulation and different functions carried out by the transcription factor. Further, examples of its role in the regulation of mitochondrial activity and its implication in the CNS are provided.

1.5.1 The E2Fs transcription factors family

The E2Fs or E2 promotor binding (Nevins et al., 1991) transcription factors were first identified as proteins that were able to bind to the promoter of the adenoviral gene E2 (Kovesdi et al., 1986). Members of the E2F family are downstream effectors of the tumour suppressor pRB and are considered to have a pivotal role in controlling cell cycle progression (Attwooll et al., 2004). Initially, it was believed that E2Fs determine

the timely expression of genes required for the entry into the S phase of the cell cycle. Later, it became clear that transcriptional activation of those genes is only one of E2F's activities, as it was discovered that it can both transactivate and repress gene expression (Polager and Ginsberg, 2008). E2F transcriptional activity is modulated by multiple mechanisms, but the best known is its interaction with the product of the retinoblastoma (RB) tumour-suppressor gene, pRB (Bagchi et al., 1991; Bandara and La Thangue, 1991; Chittenden et al., 1991). This association not only inhibits the ability of E2F to transactivate, but also represses transcription through the recruitment of various chromatin modifiers and remodelling factors to the promoters of E2F-target genes. These co-repressors include histone deacetylases (HDACs), histone methyltransferases and DNA methyltransferases (van den Heuvel and Dyson, 2008). HDACs remove acetyl groups on lysines, leading to a closed chromatin state, and thus repressing transcription (Perissi et al., 2010). In mammals, eight E2F genes (*E2F1-8*) have been discovered up to date, that give rise to nine distinct proteins. These include E2F3a and E2F3b, which are generated by the use of alternative promoters (Degregori and Johnson, 2006). These proteins can be classified either based on their protein structure, interaction partners or their transcriptional properties (Black et al., 2005). All E2F family members contain a DNA-binding domain and E2F1-5 have a transactivation domain that enables activation of gene expression (Polager and Ginsberg, 2008). A short amino acid stretch that mediates binding of pRB is inserted within the transactivation domain and, thus, this domain also functions as a repressor of gene expression. E2F1-6 contain a dimerization domain that is required for their interaction with a member of the dimerization-partner family (DP1-DP4) (Dyson, 1998; Gaubatz et al., 1998). This interaction enables them to bind DNA and exert their function as transcriptional regulators. Except for E2F7 and E2F8, all E2F members exist as a heterodimer with a DP protein, which forms functionally active E2Fs in cells. Instead, E2F7 and E2F8 bind DNA as homodimers or as E2F7-E2F8 heterodimers (Di Stefano et al., 2003; Li et al., 2008). Moreover, E2F1-3 share a canonical basic nuclear localization signal (NLS) that is absent in E2F4 and E2F5, which have nuclear export signals (NES) instead. E2F1-3 have an additional cyclin binding domain. The structure and different domains of all the family members is represented in **Fig. 5**. E2F1, E2F2 and E2F3a are often referred to as “activators”, as they are believed to function mainly in activating gene expression. On the other side, E2F3b and E2F4-8 are known as “repressor E2Fs”. This nomenclature is however controversial, and it highly depends on

the cellular process involved (DeGregori et al., 1997; Leone et al., 2000; Lukas et al., 1996; Nevins et al., 1991; Trimarchi et al., 1998).

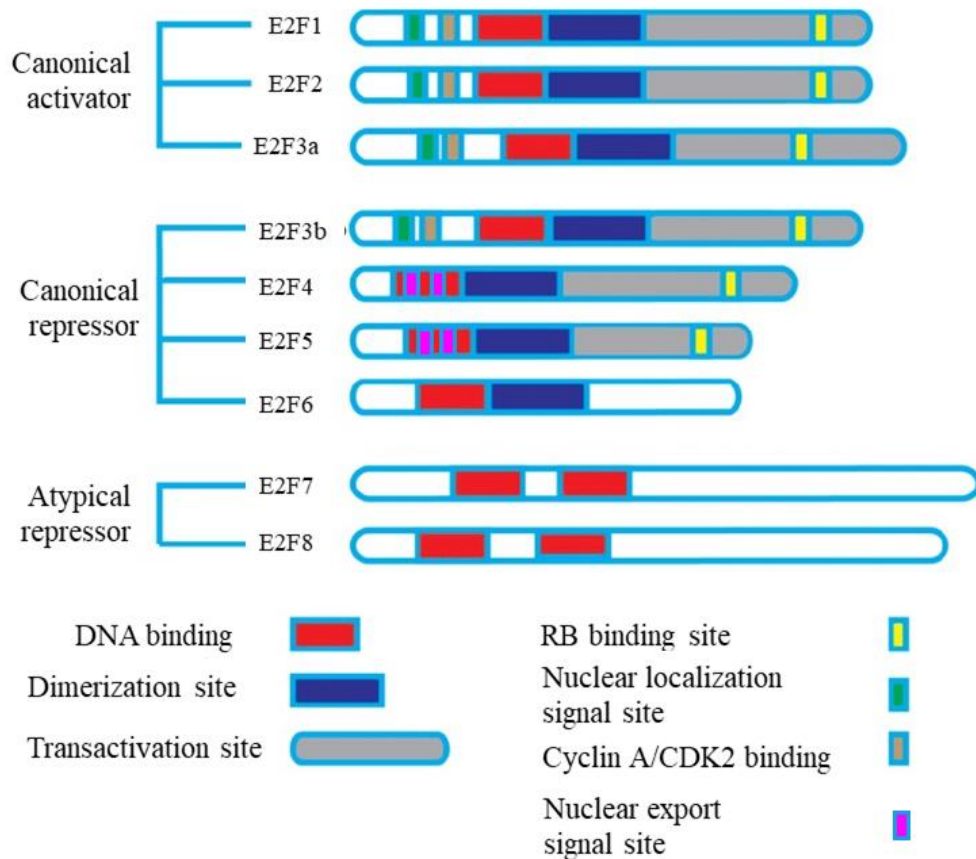


Figure 5. Structure of the E2F family members. Modified from (Lv et al., 2017).

E2F1 was the first member of the family to be identified (Bagchi et al., 1991; Dyson, 2016). Its activity depends on its binding partners, the abovementioned DP and pRB family proteins, composed by pRB or p105 (RB1), p107 (RBL1) and p130 (RBL2) (Dyson, 1998). E2F1-pRB interaction blocks the transcriptional activation domain of the E2F1-DP complex and avoids the recruitment of the transcriptional coactivators to the promoters of its target genes (Frolov and Dyson, 2004). During cell cycle progression, cyclin-dependent kinases (CDKs) phosphorylate pRB, producing E2F1-pRB disassociation. E2F1 is then released and able to bind to the promoter of its target genes (**Fig. 6**).

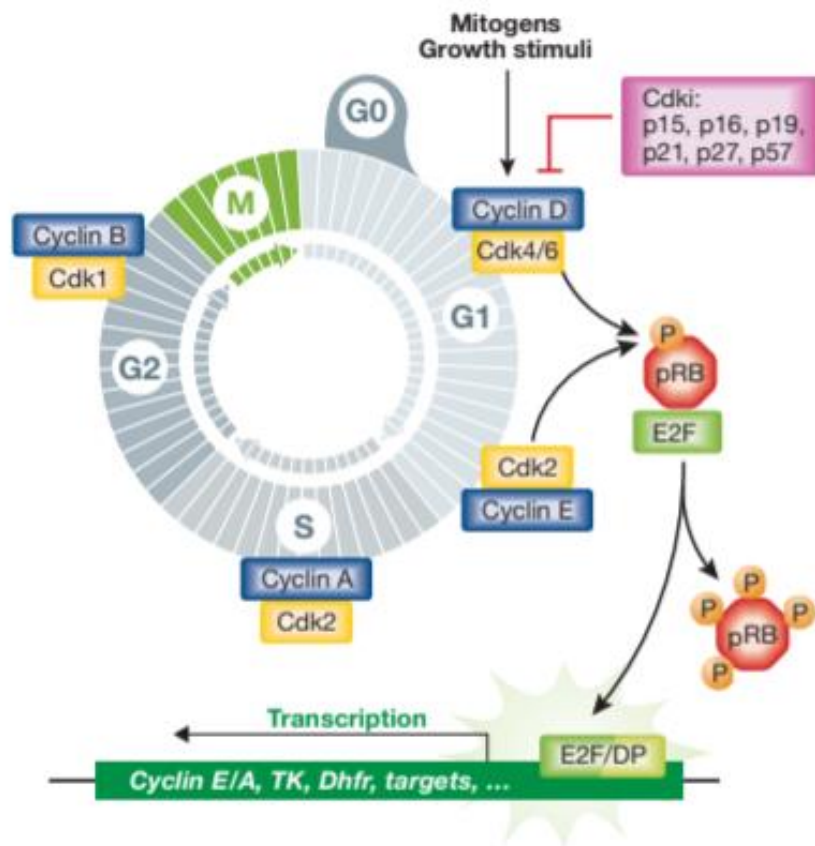


Figure 6. Molecular regulation of cell cycle. Mitogen-induced signal transduction pathways activates the cyclin D-CDK complex early in the G1 phase. Activation of these complexes leads to partial inactivation by phosphorylation of the pocket proteins, comprising Rb, p107 and p130. Inactivated pocket proteins will release E2Fs transcription factor activity and thus, allow the expression of E-type cyclins, necessary for G1/S transition. CDKs are further activated during the cell cycle by A-type cyclins to drive the transition from S phase to mitosis, a period known as the G2 phase. The activities and functions of cyclin/cdk complexes are regulated by CKIs, cyclin-dependent kinase inhibitors, both under normal as well as extreme conditions, such as stress, DNA damage and others. From (Aguilar and Fajas, 2010).

What ultimately determines E2F1's biological function is its protein levels, the combination of several post-transcriptional modifications and its interaction with different partners (Poppy Roworth et al., 2015). A plethora of post-translational modifications (PTMs) have been described among different residues of E2F1, such as phosphorylation (Stevens et al., 2003), acetylation (Galbiati et al., 2005; Nagy and Tora,

2007), methylation (Cho et al., 2012; Kontaki and Talianidis, 2010; Zheng et al., 2013) or ubiquitination (Budhavarapu et al., 2012; Galbiati et al., 2005). Also, several miRNAs have been reported to regulate E2F1 (Knoll et al., 2013; Li et al., 2009; Ofir et al., 2011; Pickering et al., 2009). Lastly, another mechanism for switching off E2F1 is through negative feedback responses from the E2F1 target genes products themselves. This lag is crucial to ensure that the cell passes into the S phase during the cell cycle. Understanding the fact that all these modifications on E2F1 and interacting partners exist, help us to assume that E2F1 activity can be controlled at different levels to facilitate its diverse and dichotomous functions.

1.5.2 Metabolic functions of E2F1

Three decades after its discovery it is now clear that E2F1 is involved in the regulation of myriad processes, such as regulation of mitosis, apoptosis, senescence and DNA-damage response (Dimri et al., 2000; Polager et al., 2002; Stevens and La Thangue, 2004). Indeed, genome-wide location studies have revealed that E2F1 binds to hundreds of promoter regions of genes of an ample range of cellular pathways (Bieda et al., 2006; Denechaud et al., 2016; Ouyang et al., 2009). In the past years, several lines of evidence have shown that cell cycle regulatory proteins can also modulate the biogenesis and metabolic activity of mitochondria (Abella et al., 2005; Fajas et al., 2002a; Fajas et al., 2002b; Sarruf et al., 2005). To proliferate, a cell must enter the cell cycle and go through interphase, which consists of G1, S and G2 phases, and then mitosis, the stage at which a cell divides into two daughter progenies. Cells must be able to assess whether there are adequate amounts of carbohydrates, nucleotides, amino acids and fatty acids to initiate and complete the replication process, and this includes DNA as well as organelles and membrane components. Several members of the cell cycle regulatory axis have been linked to mitochondrial biogenesis. For example, *cyclin D1*^{-/-} hepatocytes exhibit increased mitochondrial size, mitochondrial activity and expression of *NRF1* (Wang et al., 2006). On the other hand, overexpression of cyclin D1 led to a two-fold decrease in mitochondrial activity that was mediated by CDK4 kinase activity, independent of RB (Wang et al., 2006). Other CDK family members have also been linked to mitochondrial activity. CDK1, along with cyclin B1, was shown to couple G2>M transition with mitochondrial respiration by extensive phosphorylation of

complex I subunits (Wang et al., 2014). Furthermore, deletion of pRB resulted in decreased PGC-1 β expression in erythroid progenitors with consequent failure to induce mitochondrial biogenesis (Sankaran et al., 2008).

The first evidence of the involvement of E2F1 in metabolic control came from the observation that *E2f1*^{-/-} mice had decreased body fat mass and impaired pancreatic growth and function (Fajas et al., 2004; Fajas et al., 2002b; Nisoli et al., 2004). Later, it was demonstrated that E2F1 directly regulates the expression of Kir6.2 (Annicotte et al., 2009), a key component of the KATP channel that is involved in the regulation of glucose-induced insulin secretion in non-proliferating pancreatic β cells. E2F1 was also implicated in the regulation of adipose tissue metabolism through transcriptional regulation of the master adipogenic factor PPAR γ during the early stages of adipogenesis (Fajas et al., 2002b). In HeLa cells, silencing of *E2F1* prompted an increase in the transcription and replication of the mitochondrial genome and ATP levels (Goto et al., 2006). Of note, extensive works have demonstrated that E2F1 acts upstream of the regulation of the expression of key oxidative metabolism genes that control energy expenditure in response to exercise or thermogenesis stimulation (Blanchet et al., 2011). *E2f1*^{-/-} mice show increased expression of mitochondrial ETC, fatty acid oxidation and uncoupling genes, as well as increased expression of genes involved in mitochondrial biogenesis in muscle and brown adipose tissue (Blanchet et al., 2011). E2F1, in association with pRB, represses mitochondrial genes under basal conditions, and this negative regulation of gene expression is abrogated upon CDK4 activation. Further studies performed in a mouse model of Duchenne muscular dystrophy (DMD) confirmed these results as *E2f1* genetic inactivation demonstrated a notorious reduction of physiopathological signs of DMD, including preservation of muscle structure and function, decreased inflammatory profile, and increased oxidative metabolic gene program and mitochondrial activity (Blanchet et al., 2012).

As a transcription factor, E2F1 regulates the transcriptional activity of key metabolic genes by its intrinsic ability to bind the promoter of concrete genes depending on the energetic demands of the cell (Denechaud et al., 2016). Noteworthy, some evidence indicates that mitochondrial function, in turn, can also impact on E2F1 activity. For instance, inhibition of ATP synthase or the electron transport chain leads to the downregulation of E2F1 activity and cell cycle arrest in several cancer cell lines (Gemin

et al., 2005; Mori et al., 2016). On the other hand, mitochondrial ROS production can promote E2F1-mediated apoptosis (Espada et al., 2012; Raimundo et al., 2012), unveiling an autoregulatory loop between mitochondria and cell cycle homeostasis. For a more detailed perspective of the complex interplay between E2F transcription factors and the mitochondrial function, we address you to specific reviews about the topic (Lopez-Mejia and Fajas, 2015).

In addition to regulating oxidative metabolism in nonproliferative conditions, E2F1 also represses mitochondrial biogenesis during proliferation. In this context, elevated E2F1 expression has been found in patients suffering cancer, including hepatocellular carcinoma, non-small-cell lung carcinoma, cervical cancer, glioblastoma, pancreatic cancer, renal, breast, and ovarian cancer (Chun et al., 2020; Goto et al., 2006; Ladu et al., 2008; Mori et al., 2016; Nevins, 2001; Yu et al., 2020). The effect of knocking down *E2F1* in HeLa cells has been already mentioned above (Goto et al., 2006). Moreover, E2F1 depletion in Mesenchymal Stem Cells (MSC) also increased mitochondrial biogenesis and oxygen consumption (Tan et al., 2016). Additionally, it has been shown that E2F1-mediated repression of oxidative metabolism results in the self-renewal capacity of tumour-initiating stem-like cells and contributes to the progression of hepatocellular carcinoma (HCC) (Chen et al., 2016).

Metabolic reprogramming is considered one of the hallmarks of cancer (Pavlova and Thompson, 2016), as coupling promotion of anabolic pathways and suppression of the catabolic ones is an essential requirement for these cells to grow. Many cancer cells are characterized by increased aerobic glycolysis and a decreased glucose oxidation, which results in high rates of glucose utilization and lactate production (Liberti and Locasale, 2016; Pavlova and Thompson, 2016). It has been shown in the past years, after Otto Warburg defined this process like the “Warburg effect”, that there are some metabolic switchers that contribute to this phenomenon. E2F1 can promote this metabolic switch by both enhancing glycolysis and by repressing glucose oxidation in the mitochondria. As an example, during HCC, increased E2F1 levels recruit two DNA helicases, promoting the expression of genes involved in glycolysis and lactate export (Tarangelo et al., 2015). During cell division, E2F1 promotes the expression of the 6-phosphofructo-2-kinase/fructose-2,6-bisphosphate enzyme, the rate-determining enzyme controlling glycolysis (Darville et al., 1995; Fernández de Mattos et al., 2002).

Besides enhancing the glycolytic pathway, E2F1 also impedes glucose oxidation in the mitochondria by promoting the expression of the pyruvate dehydrogenase kinase, PDK, enzymes (Hsieh et al., 2008; Wang et al., 2016). PDKs participate in the conversion of pyruvate to acetyl-CoA, which is then oxidized in the mitochondria to produce energy in the citric acid cycle. By downregulating the activity of PDKs, the oxidation of pyruvate in mitochondria will be decreased, while enhancing the conversion of pyruvate to lactate in the cytosol. Taken together, the above studies suggest that E2F1 contributes to whole-body metabolic homeostasis via distinct roles in different metabolic tissues.

1.5.3 E2F1 in the CNS

Up to now, effects driven by E2F1 in a wide spectrum of metabolic tissues have been mentioned, evidencing the role of this transcription factor as an important regulator of the oxidative metabolism homeostasis in these organs (Blanchet et al., 2011; Blanchet et al., 2012; Denechaud et al., 2016; Fajas et al., 2004; Fajas et al., 2002b). However, little is known about this function of E2F1 regarding CNS. Expression of E2F1 has been reported in neurons, astrocytes and microglia of mouse CNS (Jordan-Sciutto et al., 2002). Nonetheless, scarce studies have been performed related to this topic, being most publications focused on the role of E2F1 as a cell cycle regulator.

Cell cycle regulation is an essential process in the development, differentiation and proliferation of mitotic cells. Albeit, it has been demonstrated in the last decade that cell cycle re-entry contributes to the death of post-mitotic cells, neurons for instance (Liu et al., 2010a). As a member of the family of E2F transcription factors, E2F1 is considered to be a pivotal node in complex pathways that control decisions of cellular life and death (Polager and Ginsberg, 2008) and several investigations have suggested a neuroprotective role of E2F1. For example, ablation of E2F1 attenuates neuronal apoptosis in several neurological disorders, such as brain and spinal cord injury, AD (Busser et al., 1998; Vincent et al., 1997), PD (Höglinger et al., 2007), ALS (Ranganathan and Bowser, 2003) and ischemia (MacManus et al., 2003; Osuga et al., 2000) by limiting activation of caspases and thus promoting tissue recovery. Further, E2F1 up-regulation was observed in Down's syndrome patients' neurons exhibiting AD-like neuropathological features, (i.e., A β depositions) (Motonaga et al., 2001). A β

depositions may trigger E2F1-mediated neuronal apoptosis in DS brains (Motonaga et al., 2001). To finish, loss of both E2F1 and E2F2 transcription factors halts neuroinflammation and associated neurological deficits after contusive spinal cord injury (Wu et al., 2015).

Overall, there is enough evidence reinforcing that E2F1's activity is not only limited to the correct functioning of the cell cycle, but it is also responsible for metabolic adaptations to satisfy the energetic demands of the cell or give a response to threatening stimuli. A better understanding of the mechanism underlying such processes will help researchers in the development of new therapeutic strategies. Likewise, therapies addressed to silence E2F1, have been proved to be neuroprotective.

1.5.4 The role of E2F1 in BM-derived cells

Previous in this section the importance of microglia in the pathogenesis of X-ALD has been reported. X-ALD displays microglial dysfunction, characterized by cytokine-induced inflammation, lipid-laden glial cells and microgliosis, eventuating in demyelination. Evidence pointing to microglia as an important contributor in the physiopathogenesis of the disease came from the observations that bone marrow transplantation and gene therapy are able to arrest demyelination (Cartier et al., 2009), probably through an improvement in microglial functions, as these cells derive from bone marrow progenitors (Eglitis and Mezey, 1997). This section is focused to describe the origin of microglia and reviews the research and discoveries that preceded and allowed the development of HSCT as a therapy for the cerebral form of X-ALD. Finally, the role of cell cycle regulators, and more specifically of E2F1, in BM-derived cells will be briefly discussed. The importance of this protein in the hematopoietic system apparently goes beyond its function as a cell cycle regulator and can be attributed to its effects as a metabolic modulator.

1.5.4.1 The origin of microglia

Microglia and brain macrophages are myeloid lineage cells strategically located throughout the brain parenchyma and barrier regions where they ingest and degrade dead cells, debris and foreign material and orchestrate inflammatory processes

(Ransohoff and Cardona, 2010) (**Fig. 7**). The origin of microglia remained debated for an extended period of time. It was commonly held that all glial cells were of neuroectodermal origin. Río-Hortega was the first to introduce the term “microglia” to discriminate true mesodermal elements from oligodendrocytes, which were previously considered a component of the mesoglia (Penfield, 1932). His conviction of the mesodermal origin of microglia was supported both by studies coupling light/electron microscopy and immunohistochemistry, which recognized typical morphological features of macrophages in the various stages of microglial development (Murabe and Sano, 1982), and by the demonstration that microglial cells reacted positively to antisera recognizing monocyte/macrophage antigens (Ginhoux et al., 2013; Murabe and Sano, 1983). Finally, a pivotal genetic study revealed that mice lacking PU.1, a crucial transcription factor for myeloid cells, were also devoid of microglia (Beers et al., 2006; McKercher et al., 1996). This unequivocally established the myeloid nature of microglia and simultaneously suggested that these cells might be ontogenetically related to macrophages. Thus, bone marrow–derived myeloid cells might reflect microglial precursors and may serve as a natural vehicle for CNS cell and gene therapy (Asheuer et al., 2004; Eglitis and Mezey, 1997).

In contrast to the established origin of microglial cells, the ontogeny of non-parenchymal macrophages has remained less clear. Since the 1980s, it was assumed, based on BM chimera data using whole-body irradiation, that macrophages at CNS interfaces were blood-derived (Hickey and Kimura, 1988). The involvement of the CNS during the irradiation procedure leads to substantial local priming with concomitant induction of myelo-attracting and myelopromoting factors and damage of BBB (Kierdorf and Prinz, 2013; Mildner et al., 2007). Consequently, all previous studies on brain macrophages using these techniques to establish BM chimeras have to be interpreted with caution. Thanks to new evidence using powerful genetic fate-mapping approaches and single-cell transcriptomic profiling, it is now accepted that non-parenchymal macrophages share a common ontogenetic origin with microglia but still represent a distinct specialized population of macrophages (Goldmann et al., 2016).

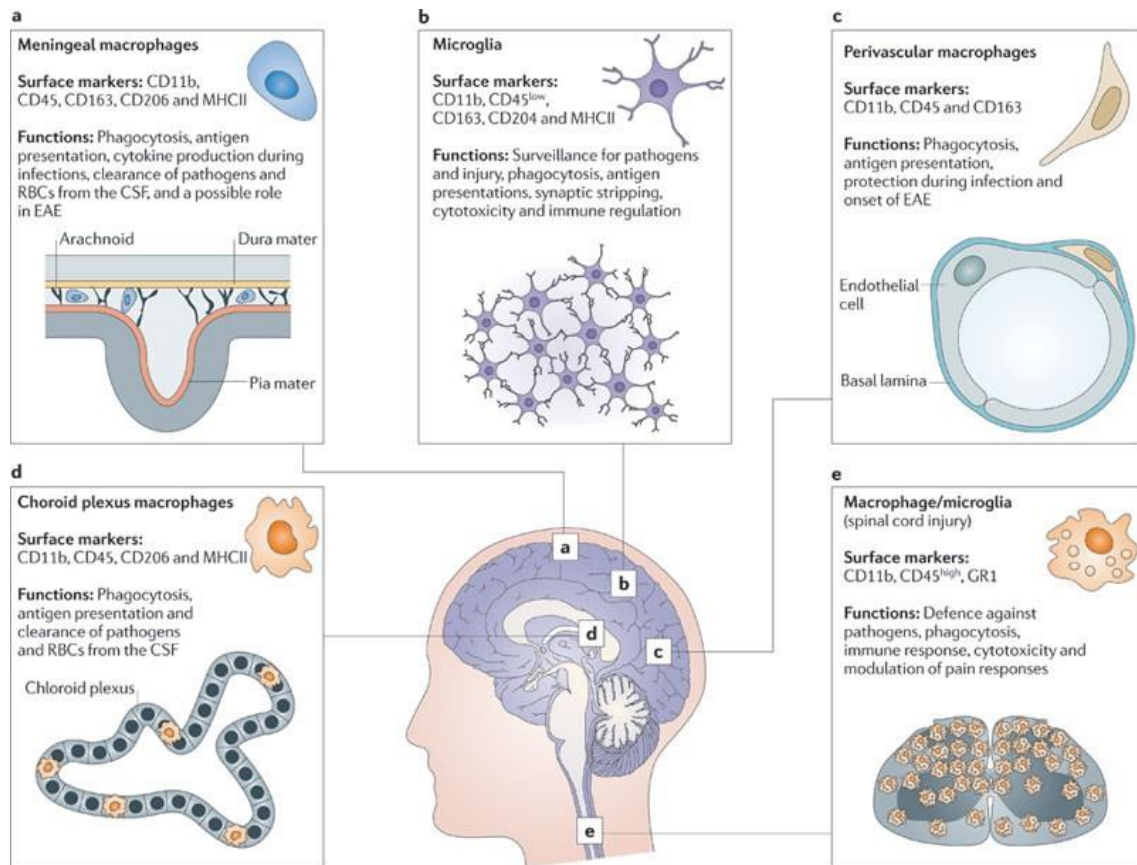


Figure 7. Macrophages and microglia in the CNS. (a–d) Macrophages (a, c, d) and microglia (b) in different regions of the uninjured CNS show differences in morphology and surface markers. (e) In the injured CNS (the spinal cord is shown) macrophages and microglia have a different morphology from those seen in the uninjured CNS, and as they cannot be distinguished from each other, they are referred to as macrophages/microglia. The common markers expressed by these cells are shown, whereas other markers on these cells are variably expressed in M1 and M2 subpopulations. CSF, cerebrospinal fluid; EAE, experimental autoimmune encephalomyelitis; RBCs, red blood cells. From (David and Kroner, 2011).

Microglia and brain macrophages originate during primitive haematopoiesis from prenatal erythromyeloid precursors (EMPs) found in the yolk sac (Goldmann et al., 2016; Hashimoto et al., 2013; Kierdorf and Prinz, 2013; Lopez-Atalaya et al., 2018; Schulz et al., 2012). Once established in the CNS, all brain macrophages, except for choroid plexus macrophages, are maintained locally throughout adulthood by self-renewal (Goldmann et al., 2016). Choroid plexus macrophages own exceptional turnover capacity due to their dual origin, yolk sac or foetal liver, another source of

macrophage progenitor. Although discrepancies among different groups produced different estimations (Askew et al., 2017; Fügler et al., 2017; Kee et al., 2002; Tay et al., 2017), microglial self-renewal rates under physiological conditions are extremely low. This concept is of important relevance in the field of HSCT as the efficiency of the transplant will depend on the replacement of the defective microglia by normal-haematopoietic donor-derived cells (Krivit et al., 1995). Interestingly, in ALD patients that underwent HSCT (Cartier et al., 2009), clinical benefit was observed despite the bone marrow engraftment of the genetically corrected cells was less than 15%.

1.5.4.1.1 CD34⁺ cells

CD34 is a transmembrane phosphoglycoprotein, first identified in 1984 on haematopoietic stem and progenitor cells (Civin et al., 1984). Clinically, it is associated with the selection and enrichment of haematopoietic stem cells for bone marrow transplants. Due to these historical and clinical associations, CD34 expression is almost ubiquitously related to haematopoietic cells. However, CD34 is now also established as a marker of several other non-haematopoietic cell types, including vascular endothelial progenitors (Fina et al., 1990) and embryonic fibroblasts (Brown et al., 1991). It has a molecular weight of approximately 115 kDa and possesses an extracellular domain that is heavily sialylated, O-linked glycosylated, and contains some N-linked glycosylation sites. There is a single transmembrane helix and a cytoplasmic tail that contains PDZ (PSD-95-Dlg-ZO-1)-domain binding motifs (Krause et al., 1996; Nielsen and McNagny, 2008). Although the structure of CD34 is well investigated, there is still relatively little known about its function. Early studies in human and animal models showed that autologous and allogeneic transplantation of selected CD34⁺ cells could reconstitute haematopoiesis (Andrews et al., 1992; Berenson et al., 1988). Since then, many groups have reported sustained engraftment using bone marrow or peripheral blood CD34⁺ cells from HLA-matched donors, and from related or unrelated donors. Although the exact mechanism exerted by these cells remains uncovered, studies in haematopoietic cells suggest roles in cytoadhesion and regulation of cell differentiation and proliferation (Healy et al., 1995; Nielsen and McNagny, 2009).

1.5.4.2 Bone Marrow Transplantation in X-ALD

As it has already been mentioned, therapeutic options for ccALD patients are restricted to bone marrow transplantation (Miller et al., 2011) and haematopoietic stem cell gene therapy (Cartier et al., 2009; Eichler et al., 2017), both limited by a narrow therapeutic window.

Although the origin of microglia was a matter of controversy, it is now clear that microglial cells derive from haematopoietic precursors (Ginhoux et al., 2013; Goldmann et al., 2016; Lopez-Atalaya et al., 2018). Therefore, the rationale for attempting to use bone marrow transplantation in X-ALD relies on the hypothesis that functional bone marrow cells from the donor could cross the blood-brain barrier and replace abnormal microglia in the recipient and exert favourable effects on the mechanism leading to demyelination (Aubourg et al., 1990; Krivit et al., 1995).

The first attempt to perform haematopoietic stem cell transplantation was not successful (Moser et al., 1984). Although before transplant the 13-year-old boy had normal examination, except for a slight spasticity in the right leg, and normal cognitive functions, he experienced continuous neurological deterioration after HSCT. This patient had a classical parieto-occipital form of cerebral ALD, and retrospectively, the extent of demyelinating lesions could be scored between 10 and 12 in the Loes score. Thus, this failure could be attributed to a late transplantation, given the evident brain lesions and their rapid extension. For the relief of researchers and clinicians, the second attempt to perform HSCT in ALD was successful (Aubourg et al., 1990). Of note, this patient, an eight-year-old boy, was transplanted at a much early stage of cerebral demyelination. In this patient, evident correction of excess of VLCFA in plasma was obtained. Cerebral demyelination progressed after HSCT but eventually completely reversed 18 months after transplant. Two decades after, this patient presented still normal brain MRI and a normal life. At the age of 30 years, he had still not developed clinical and electrophysiological signs of adrenomyeloneuropathy.

In 1995, Cartier et al. demonstrated that retroviral transfer of ABCD1 cDNA is followed by appropriate targeting of the vector-encoded ALDP in peroxisome and restores VLCFA oxidation in X-ALD fibroblasts (Cartier et al., 1995). Soon after, the same investigators reported the retroviral transfer of ABCD1 cDNA to peripheral blood and bone marrow CD34⁺ cells from control donor and X-ALD patients (Doerflinger et al., 1998). Transplantation of transduced ALD CD34⁺ cells into non-obese diabetic/severe

combined immunodeficient (NOD/SCID) mice resulted in long-term expression of ALD protein in monocytes/macrophages derived from engrafted human stem cells. (Benhamida et al., 2003). More importantly, human bone marrow-derived cells were shown to migrate into the brain of recipient mice and then differentiate into microglia expressing the human ALD protein (Asheuer et al., 2004). Further, the transplantation of lentivirally transduced murine ALD Sca-1⁺ cells (a functional equivalent of CD34⁺ cells in humans) into X-ALD mice resulted in the replacement of 20-25% of brain microglial cells expressing the ALD protein 12 months after transplantation (Cartier et al., 2009). Unfortunately, because the X-ALD mouse does not develop cerebral demyelination (Pujol et al., 2002), the neuropathological and clinical effects of lentiviral gene transfer could not be assessed in this model. Finally, researchers observed that transplantation of murine HSCs from wildtype donor into *Abcd1*⁻ and *Abcd1*⁻/*Abcd2*^{-/-} mice is able to improve locomotor performance (rotarod test) and decrease oxidative stress markers and microgliosis and astrogliosis 15 months post-graft (Ruffert, 2012; P026). Based on these promising preclinical data, lentiviral-mediated HSC gene therapy was carried out in two ALD boys who had progressive cerebral demyelination and adrenal insufficiency and who had no human leukocyte antigen (HLA)-matched donor or cord blood for allogeneic HCT (Cartier et al., 2009). Neurologic benefits of HSC gene therapy were comparable to those seen in HCT, so these results positioned HSC-based gene therapy as a preferable treatment option for X-ALD, as it abrogates the morbidity associated with the allogeneic source of HSCs in conventional transplantation. Further studies have been carried out involving more patients (Eichler et al., 2017), showing that lentivirus-mediated HSC gene-therapy may be a safe and effective therapeutic strategy for patients with this otherwise rapidly fatal childhood neurodegenerative disease.

1.5.4.3 The role of E2F1 in BM-derived HSCs

Haematopoietic stem cells are highly quiescent and can occasionally enter the cell cycle to either self-renew or differentiate into intermediary progenitor cells (Morrison and Scadden, 2014). Under homeostatic conditions, the adult haematopoietic system is maintained by a small number of stem cells that reside in the bone marrow in a specialized microenvironment, termed the niche (Adams and Scadden, 2006).

Evidence shows that many cell-cycle regulators, such as cyclins, cyclin-dependent kinases or E2F transcriptions factors, are important determinants of stem cell self-

renewal (Hao et al., 2016; Tesio and Trumpp, 2011; Viatour, 2012), and defects in their functions are linked to several defects in haematopoiesis and a wide range of haematopoietic cancers (Bilousova et al., 2005; Li et al., 2003; Pulikkan et al., 2010; Trikha et al., 2011). However, the exact contribution of each regulator, more in particular the E2F transcription factors, is still not well defined. Interestingly, transplantation with murine E2F1 KO BM progenitor cells showed enhanced vascular growth, reduced infarct size and improved cardiac function in WT mice after surgically induced myocardial infarction (Xu et al., 2018). Beneficial effects come from E2F1-mediated metabolic control, as deletion of E2F1 in BM progenitor cells augments oxidative metabolism. Undifferentiated progenitor cells are relatively quiescent, relying primarily on anaerobic glycolysis for energy production (Simsek et al., 2010). In contrast, in order to differentiate, progenitors need to switch to mitochondrial oxidative metabolism, as higher energetic demands are required for differentiation (Chung et al., 2007). Thus, inhibition of the E2F1-PDK4 axis and subsequent enhancement of oxidative phosphorylation favours BM progenitor cells differentiation into endothelial cells.

The development of therapeutic strategies to combat X-ALD is limited to the available knowledge regarding molecular drivers of neurodegeneration. Our efforts have been always focused on the molecular dissection of the neuropathogenesis of the disease to contribute to the generation of new interventional strategies. In this regard, E2F1 might be considered as a potential driver of axonal degeneration in X-ALD. From one side, as already mentioned before, the transcriptomics analysis carried out in X-ALD mice and human patients unravelled that oxidative metabolism has an important role in the pathophysiology of X-ALD (Schluter et al., 2012), and E2F1 is nowadays considered as a metabolic modulator (Denechaud et al., 2017). Moreover, therapies focused to inhibit E2F1 have shown neuroprotection (Busser et al., 1998; Vincent et al., 1997). On the other side, E2F1 is highly expressed in the bone marrow and lymphoid tissues (see <https://www.proteinatlas.org/ENSG00000101412-E2F1/tissue>), and it is known that the success of HSCT in X-ALD relies on the effective replacement of the defective microglia by functional haematopoietic donor-derived cells that cross the blood-brain barrier (Aubourg et al., 1990; Krivit et al., 1995). Hence, given the abundant expression of the transcription factor in the bone marrow, E2F1 could provide a plausible link between metabolic impairment and neurodegeneration in X-ALD.

AIM AND OBJECTIVES

2 Aim and objectives

The main aim of this study is to identify new therapeutic targets for X-ALD that will also contribute to the understanding of the pathophysiology of this disease, based on the existing knowledge on the hallmarks of X-ALD that are also shared with other neurodegenerative disorders. This aim was accomplished by fulfilling the following objectives:

- 1) To investigate the efficacy of **high-dose biotin** in the pathophysiology of X-ALD and its applicability as a pharmacologic strategy in X-ALD. To accomplish this objective, we:
 - a) Investigated the **mode of action of high-dose biotin** by assessing its effect on the established biochemical hallmark of redox dyshomeostasis in X-ALD patient's derived fibroblasts.
 - b) Evaluated the **therapeutic potential of high-dose biotin** for X-ALD. For this purpose, we tested the effect of treatment with high-dose biotin on the classical biochemical defects found in *Abcd1*⁻ mice, as well as on axonal degeneration and behavioural abnormalities present in *Abcd1*⁻/*Abcd2*^{-/-} mice.
- 2) To explore the **role of E2F1** in the pathophysiology of X-ALD, and its possible application as a therapeutic target for X-ALD. To address this objective, we:
 - a) Quantified **E2F1 expression** in WT and *Abcd1*⁻ mice.
 - b) Assessed whether the loss of **E2F1 can exert neuroprotection** in X-ALD mice, by crossing E2F1-deficient mice with *Abcd1*⁻ and *Abcd1*⁻/*Abcd2*^{-/-} mice. We therefore determined the effect of E2F1 loss on the classical biochemical defects found in *Abcd1*⁻ mice, but also on axonal degeneration and locomotor impairment in *Abcd1*⁻/*Abcd2*^{-/-} mice.

- c) Determined the importance of **E2F1 in cells derived from the BM that will repopulate the CNS**, and expect to **identify the responsible cell-type(s) for the beneficial effects of BMT in X-ALD**.

MATERIALS AND METHODS

3 Materials and Methods

3.1 Human samples

All procedures involving human samples were approved by local ethics committees from IDIBELL. Primary human fibroblasts were prepared from skin biopsies collected from healthy individuals and X-ALD patients according to the IDIBELL guidelines for sampling, including informed consent from the persons involved or their representatives. Control and X-ALD cells were grown in Dulbecco's Modified Eagle's Medium (DMEM) containing 1g/L glucose, pyruvate, L-glutamine, 10% foetal calf serum (FCS), 100U/ml penicillin and 100 µg/ml streptomycin and maintained at 37°C in humidified 95% air/5% CO₂ incubator (Lopez-Erauskin et al., 2012). Tested compounds were added to 80-90% confluent cells in medium containing 10% FCS at the following concentrations: 50 µM C26:0 and 0.25 to 10 µM pharmaceutical-grade biotin.

3.1.1 Evaluation of intracellular ROS

Intracellular H₂O₂ levels were estimated using the ROS-sensitive probe H₂DCFDA (DCF) as previously described (Fourcade et al., 2008). Following incubation with 10 µM DCF for 30 min, cells were washed twice with PBS and scraped into water. Intracellular and mitochondrial superoxide anion levels were estimated using DHE probes and MitoSOXTM Red (Molecular Probes), respectively (Lopez-Erauskin et al., 2013b). Following incubation with 5 µM DHE for 10 min or 5 µM MitoSox for 10 min, cells were washed twice with PBS and scraped into water. The homogenate was transferred to a 96-well plate for fluorescence detection with a spectrofluorimeter. The fluorescence of DCF-, DHE- and MitoSOX-stained cells was measured with a spectrofluorimeter (excitation wavelength of 493 nm and emission wavelength of 527 nm for DCF; excitation wavelength of 530 nm and emission wavelength of 590 nm for DHE and MitoSOX). Fluorescence values were corrected to protein content. Fatty acids were dissolved in ethanol and added to the medium for 24 h, and biotin was dissolved in DMSO. Antimycin A (Ant A; 200 µM for 1 h) was used as positive control.

3.1.2 Evaluation of reduced glutathione

The intracellular content of GSH was determined using monochlorobimane, a thiol-reactive probe. Following incubation for 30 min with 100 μ M monochlorobimane, cells were washed twice with PBS and scraped into water. The fluorescence of monochlorobimane-stained cells was measured with a spectrofluorimeter (excitation wavelength of 380 nm and emission wavelength of 460 nm). L-Buthionine sulfoximine (BSO) (500 μ M) was used as positive control.

3.1.3 Inner mitochondrial membrane potential quantification by flow cytometry

Treated cells were washed with PBS and incubated with 50 nM TMRE (Molecular Probes) in pre-warmed PBS for 30 min at 37°C. Cells were trypsinized, centrifuged at 1000 x g for 5 min and resuspended in pre-warmed PBS. All samples were captured by a FACSCanto™ flow cytometer, which recorded 20,000 cells for each condition and genotype tested. FCCP (200 μ M for 10 min) was used as positive control. Histograms showing the inner mitochondrial membrane potential levels ($\Delta\psi_m$) were obtained after gating live cells. The data were analyzed with FlowJo Tree Star software.

3.2 Mouse experiments

3.2.1 Mouse strains

The methods for generating and genotyping of *Abcd1*⁻ (*Abcd1*^{Tm1Kds}) and *Abcd2*^{-/-} (*Abcd2*^{Tm1Apuj}) mice were previously described (Ferrer et al., 2005; Lu et al., 1997; Pujol et al., 2004; Pujol et al., 2002). The mice used for the study were male of a pure C57BL/6J background. All the methods employed in this study were in accordance with the Guide for the Care and Use of Laboratory Animals published by the U.S. National Institutes of Health (NIH Publications No. 85-23, revised 1996), European (2010/63/UE) and Spanish (RD 53/2013) legislation. The IDIBELL animal facility is accredited by The Association for Assessment and Accreditation of Laboratory Animal Care (AAALAC, Unit 1155). Animals were housed at 22°C under specific-pathogen-

free conditions on a 12-hour light/dark cycle and *ad libitum* access to food and water. Cages contained three to four animals.

3.2.1.1 X-ALD mice

Two X-ALD mouse models were employed in this study: *Abcd1*⁻ and *Abcd1*⁻/*Abcd2*⁻ mice. The *Abcd1* and *Abcd2* gene inactivation has been described before (Ferrer et al., 2005; Lu et al., 1997; Pujol et al., 2004; Pujol et al., 2002).

We evaluated the effect of biotin administration or E2F1 deletion on the biochemical signs of adult X-ALD in *Abcd1*⁻ mice at 12 months of age. These mice present oxidative stress (Fourcade et al., 2008) and energetic homeostasis impairment (Galino et al., 2011) before the first clinical signs of adrenomyeloneuropathy-like pathology (axonopathy and locomotor impairment) emerge at 20 months of age (Pujol et al., 2002).

To evaluate the therapeutic effect of biotin administration or E2F1 ablation, we studied the clinical signs of the disease in the *Abcd1*⁻/*Abcd2*⁻ mice at 18 months of age. These mice display increased VLCFA accumulation in the spinal cord (Pujol et al., 2004), higher levels of oxidative damage to lipids and proteins (Fourcade et al., 2008; Galino et al., 2011), and a more severe adrenomyeloneuropathy-like pathology with an earlier onset at 12 months of age (Pujol et al., 2004), which makes them more suitable for therapeutic assays.

To perform biochemical analysis, we euthanized the mice and quickly froze their tissues in liquid nitrogen and stored them at -80°C, except for mitochondrial respiration, in which the tissue was used fresh. For histological analysis, spinal cords were harvested after the mice were perfused with 4% paraformaldehyde (PFA; Sigma-Aldrich, Ref. 441244) in 0.1 M phosphate buffer, pH 7.4.

3.2.1.2 Generation of *Abcd1*⁻/*E2f1*⁻ and *Abcd1*⁻/*Abcd2*⁻/*E2f1*⁻ mice

Abcd1⁻ and *Abcd1*⁻/*Abcd2*⁻ mice were crossbred with *E2f1*⁻ mice (Fajas et al., 2004) to obtain double knockout *Abcd1*⁻/*E2f1*⁻ and triple knockout *Abcd1*⁻/*Abcd2*⁻/*E2f1*⁻ mice. The specific primers of *E2f1* gene used for genotyping genomic DNA from mouse tail tips were as follows: a common forward primer (5'-

CTAAATCTGACCACCAAACGC-3') used together with specific reverse primers for the WT (5'-GGATATGATTCTTGGACTTCTTGG-3') or KO allele (5'-CAAGTGCCAGCGGGGCTGCTAAAG-3'). These combinations of primers amplified a 172 bp segment for the WT allele and a 227 bp segment for the KO allele (**Fig. 8A**), under the following PCR conditions: 35 cycles of 94°C for 20 s, 55°C for 30 s, 72°C for 30s. We confirmed that E2F1 protein was not expressed in *E2f1*^{-/-} mice tissues by western blot using an anti-E2F1 antibody (**Fig. 8B**).

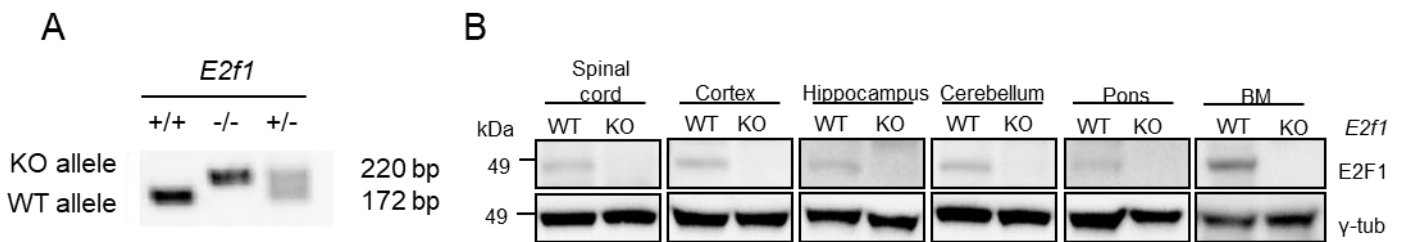


Figure 8. Characterization of E2F1 knockout mice

(A) PCR bands obtained after genotyping wild-type (*E2f1*^{+/+}), heterozygous (*E2f1*^{+/-}) and knockout (*E2f1*^{-/-}) mice tails. (B) Characterization of *E2f1* knockout mice. E2F1 protein expression in spinal cord, cortex, hippocampus, cerebellum, pons and bone marrow from 12-month-old wild-type (WT) (n=3) and *E2f1*^{-/-} (KO) (n=3) mice.

Morbidity and mortality

Each animal was checked for mortality and morbidity once every 3 days during the acclimation period and treatment period, including on weekends and public holidays.

Body weight

The body weight of the animals was recorded at the moment of performing locomotor tests and at the time of sacrifice.

3.2.2 Biotin administration

The dose selected for use in mice (60 mg/kg/day) is equivalent to the human therapeutic dose used in clinical trials (300 mg/day) (Sedel et al., 2015). Biotin was mixed into AIN-76A chow to provide a dose of 60 mg/kg/day. Treated animals had free access to AIN-76A chow + 0.06% high-dose pharmaceutical-grade biotin, which was distributed twice a week so that a dose of 60 mg/kg/day was reached. To measure biochemical

alterations, animals were treated for 3.5 months and sacrificed at 13 months of age. In this first cohort, the animals were randomly assigned to one of the following dietary groups: group I, WT mice that received normal AIN-76A chow (n=18); group II, *Abcd1*⁻ mice that received normal AIN-76A chow (n=18); or group III, *Abcd1*⁻ mice that received AIN-76A chow containing high-dose biotin (n=18). To measure the clinical signs of the disease (locomotor dysfunction and axonal degeneration), a second cohort of 12-month-old animals were treated for 6 months. The animals were randomly assigned to one of the following dietary groups: group I, WT mice that received normal AIN-76A chow (n=14); group II, *Abcd1*⁻/*Abcd2*^{-/-} mice that received normal AIN-76A chow (n=15); or group III, *Abcd1*⁻/*Abcd2*^{-/-} mice that received AIN-76A chow containing high-dose biotin (n=16).

3.2.3 Bone marrow transplantation

To determine the importance of E2F1 in BM-derived cells in X-ALD, *Abcd1*⁻/*Abcd2*^{-/-} mice were transplanted with *Abcd1*⁻/*Abcd2*^{-/-}/*E2f1*^{-/-} bone marrow cells. To avoid any bias coming from the transplantation itself, WT and *Abcd1*⁻/*Abcd2*^{-/-} mice were transplanted with bone marrow from their same genotype. These mice were used as the control group (WT + BM_{wt}) or affected group (*Abcd1*⁻/*Abcd2*^{-/-} + BM_{dko}), correspondingly.

3.2.3.1 Bone marrow extraction, processing and injection

WT, *Abcd1*⁻/*Abcd2*^{-/-}, *Abcd1*⁻/*Abcd2*^{-/-}/*E2f1*^{-/-} mice between 1.5-3 months were employed as bone marrow donors. Bone marrow was extracted from femurs and tibias. Briefly, mice were sacrificed by cervical dislocation and tibias and femurs were extracted. Bones were cut at both ends with sharp sterile scissors and, using a 23-gauge needle and a 1mL syringe filled with ice-cold DMEM, bone marrow was flushed out onto a 100 μm nylon cell strainer placed in a 50 ml Falcon conical tube. The procedure was performed under the hood. Next, bone marrow was centrifuged for 4 min at 450g and resuspended in PBS. To avoid cell-clumps, cells were incubated with DNase, 10 minutes at 25°C, 10UI/10⁶ cells. Suspension was washed with PBS and centrifuged again for 4 min at 450g. Supernatant was discarded, and cells were resuspended in PBS. Cell counting was performed in a Neubauer chamber, using Türk solution for assaying cell viability. Finally, necessary PBS volume was added to reach the desired cell

concentration to be injected in recipient mice. Total bone marrow cells were intravenously (i.v.) injected through the lateral tail vein at desired cellular dose (10^6 cells/mouse) in a volume of 200 μ l per mouse and under sterile conditions. An infrared bulb lamp was employed during injections to induce vasodilatation and facilitate injections.

3.2.3.2 Irradiation

Prior to bone marrow transplantation, recipient mice were irradiated in order to suppress their immune system and deplete the bone marrow niche of host progenitor cells, thereby allowing space for the engraftment of donor stem cells. Recipient mice were 2-3 months old WT and *Abcd1*^{-/-}/*Abcd2*^{-/-} mice. First, mice were anaesthetized using a combination of ketamine (75 mg/kg) and medetomidine (1 mg/kg). Then, mice were myeloablated with total body irradiation (9 Gy, in two doses of 4.5Gy of 2', with an interval of 1h between both administrations) using a gamma-irradiator. Heat was provided during the resting time to avoid cooling of animals. Also, physiological serum was injected (100 μ L/mice) to avoid vasoconstriction due to anaesthesia. Once mice were irradiated, anaesthesia was reversed with atipamezole (5 mg/kg). All drugs were diluted in saline and administered in a final volume of 100 μ L. Mice were allowed to fully get over from anaesthesia and recover normal blood circulation for 2h approximately before bone marrow injection.

3.2.3.3 Recipient mice follow up

After irradiation, animals were kept in quarantine, as the irradiation procedure was performed outside animal house facilities. Specific-pathogen-free (SPF) condition was checked after 5 months by performing PCRs for specific pathogens (IDEXX BioAnalytics). Results confirmed that SPF conditions were maintained, so animals could return to their original SPF area.

After bone marrow transplantation, daily follow up of the recipient mice was performed by visual analysis, and body weight was weekly recorded. Food and water intake was also recorded until 4 months post-transplantation once successful bone marrow transplantation was determined.

3.2.3.4 Chimerism determination

For determining chimerism percentage of the recipient mice, E2F1 genotyping PCR was performed at 4 months post-transplantation, the time from which long-term repopulation is considered, and at the end of the procedure. At 4 months post-transplantation, DNA extracted from the submandibular vein was employed for the PCR. At the end of the procedure, DNA was extracted from peripheral blood and bone marrow obtained from tibias and femurs. Bone marrow was extracted as previously described. For DNA extraction, a protocol for DNA purification from whole blood or bone marrow samples from Gentra Puregene Blood Kit (Qiagen) was followed. For the extraction of some of the blood samples obtained at the end of the treatment (Mice n° 12-15, 19-20 and 22-24), some additional steps were included in the protocol. These mice were subjected to perfusion for obtaining samples for histological analysis, so, to improve the low quality and quantity of the extracted DNA due to PFA contamination, samples were incubated in a thermoblock for 1h at 90°C, alternating cycles of 5'' of shaking at 1200 rpm and 15'' of resting after protein precipitation solution addition. Then, after keeping samples on ice for 20 min, proteins were precipitated by centrifugation. For the nucleic acid precipitation, absolute ethanol was employed instead of isopropanol, as it shows higher efficiency when working with small volume samples and avoids salt precipitation.

Prior to performing the genotyping PCR, an "E2F1 KO" gradient, ranging from 0% of E2F1 KO allele presence (what is equal to WT mice) to 100% presence of E2F1 KO allele (what is equal to *E2f1*^{-/-} mice) was manually generated by combining different volumes of DNA samples from WT and *E2f1*^{+/-} mice (**Fig. 9**). For setting up the specific conditions of the PCR, DNA from heterozygous (*E2f1*^{+/-}) mice was employed and E2F1 genotyping PCR was run out at different amplification cycles, ranging from 27 to 40 cycles. At cycle 33, both bands, corresponding to the E2F1 WT allele (172 bp) and the E2F1 KO allele (220 bp), showed the same intensity (**Fig. 10**). From 33 cycle on, the band for the E2F1 KO allele started to saturate. Thus, these conditions, E2F1 genotyping PCR run at 33 cycles, were chosen to carry out the E2F1 specific PCR for chimerism determination of the transplanted mice. Following the presence of the KO allele and evaluating the proportion of intensity between the WT and KO allele, the percentage of E2F1 KO allele presence in the transplanted mice was inferred.

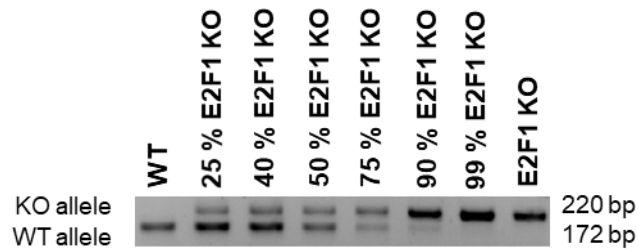


Figure 9. “E2F1 KO” gradient

PCR bands reflecting different E2F1 KO allele percentage, ranging from 0% of E2F1 KO allele presence (what is equal to WT mice) to 100% presence of E2F1 KO allele (what is equal to *E2f1*^{-/-} mice). E2F1 KO gradient was manually generated by combining different volumes of DNA samples from WT and *E2f1*^{+/-} mice.

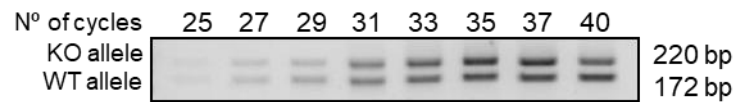


Figure 10. E2F1 PCR amplification cycle determination

PCR bands obtained after running an E2F1 specific PCR with a heterozygous (*E2f1*^{+/-}) DNA sample (50ng DNA) at different amplification cycles.

3.3 Quantitative real-time PCR

Total RNA was extracted from mouse and human tissues using RNeasy Kit (Qiagen, Hilden, Germany). Total DNA was extracted from mouse spinal cord using Genra Puregene Tissue Kit (Qiagen, Hilden, Germany). To quantify mRNA levels, 1µg of RNA was transcribed into cDNA using Superscript IV reverse transcription reagents (Invitrogen, Thermo Fisher Scientific Inc.) in a final volume of 25 µL. Dilutions ranging from 1/75 to 1/5 of cDNA or 100 ng of DNA were used to measure mRNA or mtDNA levels, respectively. The expression of the genes of interest was analyzed by RT-PCR using TaqMan[®] Gene Expression Assays (Thermo Fisher Scientific Inc.) and standardized TaqMan[®] probes (**Table 1**) or Sybr Green specific primers (**Table 2**) on a LightCycler[®] 480 Real-Time PCR System (Roche Diagnostics GmbH). Relative quantification was carried out using the ‘Delta-Delta Ct’ ($\Delta\Delta Ct$) method with mouse

Rplp0 or human *RPLP0* as an endogenous control. To quantify mouse mtDNA content, primers for mouse cytochrome b (*Cytb*) were designed (Custom TaqMan Gene Expression Assays; Thermo Fisher Scientific Inc.). The sequences for *Cytb* primers were: ATGACCCCAATACGCAAAATTA (forward) and GGAGGACATAGCCTATGAAGG (reverse) and the FAM-labeled probe sequence was TTGCAACTATAGCAACAG. Quantification of mtDNA level relative to nDNA level was determined by amplification of the intron-less mouse nuclear gene *Cebpa* (Morato et al., 2013). Transcripts were quantified in triplicate for each sample.

Table 1 List of quantitative RT-PCR probes used in this thesis

Gene	Species	Taqman ref.
<i>Acaa2</i>	Mouse	Mm00624282
<i>Acadl</i>	Mouse	Mm00599660
<i>Acadm</i>	Mouse	Mm00431611
<i>Acadvl</i>	Mouse	Mm00444293
<i>Acox1</i>	Mouse	Mm01246834
<i>Arg1</i>	Mouse	Mm00475991
<i>Cebpa</i>	Mouse	Mm00514283
<i>Cpt1a</i>	Mouse	Mm01231183
<i>Cpt2</i>	Mouse	Mm00487205
<i>Cxcl12</i>	Mouse	Mm00457276
<i>Echs1</i>	Mouse	Mm01276347
<i>Ehhdah</i>	Mouse	Mm00619685
<i>Gclc</i>	Mouse	Mm00802655
<i>Gsta3</i>	Mouse	Mm01233706
<i>Hdaha</i>	Mouse	Mm00805228
<i>Hmox1</i>	Mouse	Mm00516005
<i>Igf1</i>	Mouse	Mm00439560
<i>Il1b</i>	Mouse	Mm01336189
<i>Il6</i>	Mouse	Mm00446190
<i>Mif</i>	Mouse	Mm01611157
<i>Nfkb2</i>	Mouse	Mm00479807
<i>Nqo1</i>	Mouse	Mm01253561
<i>Nrf1</i>	Mouse	Mm00447996
<i>Pgc-1a</i>	Mouse	Mm00447183
<i>Pgc-1b</i>	Mouse	Mm01258518
<i>Pparg</i>	Mouse	Mm01184322
<i>Rplp0</i>	Mouse	Mm01974474
<i>Sirt1</i>	Mouse	Mm00490758
<i>Tfam</i>	Mouse	Mm00447485
<i>Tgfb1</i>	Mouse	Mm01178820
<i>Tnfa</i>	Mouse	Mm00443258
<i>Tnfrsf1a</i>	Mouse	Mm01182929
<i>GCLC</i>	Human	Hs00155249
<i>GCLM</i>	Human	Hs00978073
<i>GSR1</i>	Human	Hs00901986
<i>RPLP0</i>	Human	Hs99999902

Table 2 List of Sybr Green primers used in this thesis

<i>Gene</i>	<i>Species</i>	<i>Syber Green primer sequences</i>	
		<i>Sense</i>	<i>Antisense</i>
<i>36b4</i>	Mouse	ATGGGTACAAGCGCGTCCTG	GCCTTGACCTTTTCAGTAAG
<i>Acc</i>	Mouse	ACATCCCGCACCTTCTTCTACTGG	CCTTCACTGCGCCTTCAACTTCTA
<i>Acs11</i>	Mouse	CAGAACATGTGGGTGTCCAG	GTTACCAACATGGGCTGCTT
<i>Acs13</i>	Mouse	AACCTGTCAGTTCCAAACCG	GCCAATTATAGTGCCCCAGA
<i>Acs14</i>	Mouse	CTGGAAAGCAAAGTGAAGGC	AGGGATACGTTCACTGGC
<i>Acs15</i>	Mouse	GGCCAAACAGAATGCACAG	GGAGTCCCAACATGACCTG
<i>Acs16</i>	Mouse	TGAATGCACAGCTGGGTGTA	ATGTGGTTGCAGGGCAGAG
<i>E2f1</i>	Mouse	ACAGCTGCAACTGCTTTCGGAG	AGCTTGTAGTTGGGTCTCAGGAGG
<i>Fas</i>	Mouse	TGCTCCCAGCTGCAGGC	GCCCGGTAGCTCTGGGTGTA
<i>Scd1</i>	Mouse	AAAGAGAAGGGCGGAAACT	GCGTTGAGCACCAGAGTGTA
<i>Scd2</i>	Mouse	CTGGGGCGAGACTTTTGTA	GAAGGCGTGGTGGTAGTTGT
<i>Scd3</i>	Mouse	CTGCGGATCTTCCTCATCAT	AGTTTTCCGCCCTTCTCTT
<i>Srebp1c</i>	Mouse	GGAGCCATGGATTGCACATT	GCTTCCAGAGAGGAGGCCAG

3.4 Immunoblotting

Mouse tissues were homogenized in radioimmunoprecipitation assay (RIPA) buffer, sonicated, centrifuged and heated for 10 min at 70°C after the addition of 4X NuPAGE® LDS Sample Buffer (Invitrogen, Thermo Fisher Scientific Inc.). In the case of bone marrow, samples were treated with red blood cell lysis buffer in order to discard red blood cells, which impeded the correct migration of the sample. A total of 25 to 80µg of protein was loaded onto 10% Novex NuPAGE® SDS-PAGE gels (Invitrogen, Thermo Fisher Scientific Inc.) and run for 90 min at 120 V in NuPAGE® MOPS SDS Running Buffer (Invitrogen, Thermo Fisher Scientific Inc.) supplemented with 5 mM sodium bisulfite (Ref. 243973, Sigma-Aldrich). SeeBlue® Plus2 pre-stained (Invitrogen, Thermo Fisher Scientific Inc.) was used as a ladder.

The resolved proteins were then transferred onto PVDF membranes. After blocking in 5% BSA (milk in the case of anti-E2F1) in 0.05% TBS-Tween (TBS-T) for 1 h at room temperature, the membranes were incubated with appropriate diluted primary antibodies in 1% BSA in 0.05% TBS-T overnight at 4°C. Following incubation with diluted secondary antibody in 0.01% TBS-T for 1 hour at room temperature, the proteins were detected with an ECL western blotting analysis system (GE Healthcare, Buckinghamshire, UK), followed by exposure in ChemiDoc™ Touch Imaging system software v 2.3.0.07 (BioRad). A list of primary and secondary antibodies used in this study can be found in **Table 3 and 4**. Immunoblots were quantified by densitometry using Imagemag v 5.2.1 software (BioRad).

Table 3 List of primary antibodies used in this thesis

Antibody	Source	Reference	Dilution
β -actin	Sigma-Aldrich	A2228	1:10000
AMPK α	Cell Signalling	2532	1:1000
Phospho-AMPK α (Thr132)	Cell Signalling	2531	1:1000
APP	AbD Serotec	AHP538	1:100
Cytochrome c	BD Biosciences Pharmigen	55643	1:100
E2F1	Cell Signalling	3742	1:1000
GFAP	Dako	Z0334	1:500
GSK-3 β	Cell Signalling	9315	1:1000
Phospho-GSK-3 β (Ser9)	Cell Signalling	9331	1:1000
IBA1	Wako	019-19741	1:1000
MDA	-	Hall et al. 2007 ¹	1:1000
Neurifilament H non- phosphorylated (SMI- 32)	Covance Antibody- Biolegend	801701	1:3000
Phospho-mTOR (Ser2448)	Cell signaling	5536S	1:1000
phospho-p70S6 kinase (Thr389)	Cell signaling	9205	1:1000
Synaptophysin	Leica Biosystems	299-L-CE	1:500
γ -Tubulin	Sigma-Aldrich	T6557	1:10000

¹Hall, E. D., Oostveen, J. A., Andrus, P. K., Anderson, D. K., & Thomas, C. E. (1997). Immunocytochemical method for investigating in vivo neuronal oxygen radical-induced lipid peroxidation. *J Neurosci Methods*, 76(2), 115-122.

Table 4 List of secondary antibodies used in this thesis

Antibody	Source	Reference	Dilution
Goat anti-rabbit HRP	Dako	P0448	1:10000
Goat anti-mouse HRP	Dako	P0447	1:30000

3.5 High-resolution respirometry

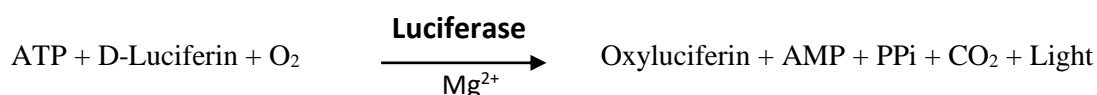
O₂ consumption in sets of 5 permeabilized lumbar spinal cord slices (LSCS) was measured at 37°C in MiR05 medium, pH 7.4, by high-resolution respirometry using an Oxygraph-2k (Oroboros Instruments, Innsbruck, Austria) as previously described (Lopez-Erauskin et al., 2013b; Morato et al., 2015).

In detail, fresh spinal cords were rinsed in ice-cold normal saline and cut into slices with a tissue chopper adjusted to a cut width of 300 µm. O₂ consumption was measured in sets of 5 LSCS at 37°C with high-resolution respirometry in permeabilized conditions (including substrates and inhibitors of specific respiratory complexes) using an Oxygraph-2k (Oroboros Instruments, Innsbruck, Austria) with chamber volumes set at 2 mL. Spinal cord permeabilization was a modification of a previously published method (Safiulina et al., 2004). Slices of the lumbar region were collected and transferred quickly into an individual well of a 6-well tissue culture plate with 2 mL of ice-cold permeabilization medium (7.23 mM potassium ethylene glycol-bis{b aminoethyl ether}N,N,N',N'-tetraacetate [K2-EGTA]; 2.77 mM CaK2-EGTA; 60 mM N,N-bis{2-hydroxyethyl}-2-aminoethanesulfonic acid [BES]; 5.69 mM MgATP, 20 mM taurine; 3 mM K₂HPO₄; 0.5 mM dithiothreitol [DTT] and 81 mM potassium methanesulfonate, pH 7.1 at 25°C), rinsed and immediately transferred into another well with the same medium containing 20 µL of saponin stock solution (5 mg/mL; final concentration 50 µg/mL). LSCS were then shaken by gentle agitation at 4°C for 30 min. Afterwards, all samples were quickly transferred from the saponin permeabilization medium into 2 mL of respiration medium (7.23 mM K2-EGTA; 2.77 mM CaK2-EGTA; 100 mM potassium salt of 2-{N-morpholino}ethanesulfonic acid [K-MES], 1.38 mM MgCl₂; 20 mM taurine; 3 mM K₂HPO₄; 0.5 mM DTT; 20 mM imidazole and 5 mg/mL BSA, pH 7.1 at 25°C), then shaken by gentle agitation for 10 min in the cold room (on ice) before performing respirometry. In order to avoid tissue disaggregation, LSCS required setting a slow bar stirring speed (150 rpm), but not too low to compromise homogeneity of substrate and oxygen concentrations in the measuring chambers, and, therefore, signal stability. DatLab software (Oroboros Instruments, Innsbruck, Austria) was used for data acquisition (2 s time intervals) and analysis, which includes calculation of the time derivative of oxygen concentration and correction for instrumental background oxygen flux (Gnaiger, 2001). Respiration of LSCS required tissue or cell permeabilization before placing the sample in the measurement chamber. Initially, we measured

endogenous respiration in the absence of additional substrates. For evaluation of relative contributions of mitochondrial complexes to oxygen consumption, several specific mitochondrial inhibitors and substrates were added sequentially and calculated as steady-state respiratory flux in the time interval between 5 and 10 min after their addition. First, we added glutamate (10 mM) and malate (5 mM) to increase NADH levels in order to measure the complex I non-phosphorylative activity, or state 2. ADP (10 mM) was added to quantify the complex I-dependent phosphorylative activity, or state 3. Immediately afterwards, we added succinate (10mM), which is the substrate for complex II. At this point, the level of oxygen consumption corresponded to complex I and II-dependent phosphorylative activity. The addition of rotenone (0.5 μ M; SigmaAldrich) inhibits complex I; therefore, oxygen consumption measured after the addition of rotenone only reflects complex II-dependent phosphorylative activity (in the absence of electron back flux to complex I). Then, complex III activity was inhibited with antimycin A (2.5 μ M; Sigma-Aldrich) to obtain residual oxygen consumption. To avoid oxygen limitations, all the experiments were performed above 50% oxygen saturation. Oxygen consumption was normalized for actual protein content in the respirometer chambers.

3.6 ATP measurement

ATP content was measured by a chemiluminescence system using ATPlite 1step (PerkinElmer, Inc., Waltham, MA, USA). Mice were sacrificed by cervical dislocation, and spinal cords were immediately frozen in liquid nitrogen and stored at -80°C . ATP was extracted with cold perchloric acid (10%) from 10 mg of spinal cord, neutralized with KOH, and centrifuged. Then, measurement of ATP was performed according to the manufacturer's instructions, and relative ATP levels were calculated by normalizing the luminescence obtained to the total protein concentration of the sample measured by BCA (bicinchoninic acid assay). All assays were performed in triplicate. The ATPlite 1step assay system is based on the production of light caused by the reaction of ATP with added luciferase and D-luciferin, as depicted in the following reaction:



3.7 Lipidomic analysis

Lipidomic analysis of the mouse spinal cord were performed according to the modified Folch method (Folch et al., 1957). For each sample, the solvent volume was adjusted to the weight of the fresh tissue. In brief, 190 μL of $\text{CHCl}_3/\text{MeOH}$ 2:1 (v/v) and 10 μL of internal standard mixture were added to 10 mg of spinal cord. The samples were vortexed for 60 s and then sonicated for 30 s using a sonication probe. Extraction was performed after incubation for 2 h at 4°C and centrifugation at $15,000 \times g$ for 10 min at 4°C. The upper phase (aqueous phase), which contained ganglioside species and several lysophospholipids, was transferred and dried under a stream of nitrogen. The protein interphase was discarded, and the lower lipid-rich phase (organic phase) was pooled with the dried upper phase. The samples were then reconstituted in 200 μL of $\text{CHCl}_3/\text{MeOH}$ 2:1, vortexed for 30 s, and sonicated for 60 s, and these total lipid extracts (TLEs) were then stored at -80°C until analysis. Samples were diluted 100 times in $\text{MeOH}/\text{IPA}/\text{H}_2\text{O}$ 65:35:5 (v/v/v) before injection.

The samples were separated on an HTC PAL system (CTC Analytics AG) coupled with a Transcend 1250 liquid chromatographic system (Thermo Fisher Scientific, Inc.) using a Kinetex C8 2.6 μm 2.1 \times 150 mm column (Phenomenex, Sydney, NSW, Australia). High-resolution mass spectrometry using a Q-Exactive mass spectrometer (Thermo Fisher Scientific, Inc.) was performed as previously described (Seyer et al., 2016). The relative amount of each lipid was semi-quantified as the area of its corresponding chromatographic peak.

3.8 LPC 26:0 absolute quantification

A total of 400 μL of $\text{CHCl}_3/\text{MeOH}$ 2:1 followed by 75 μL of pure water was added to 100 μL of total lipid extract. The samples were then centrifuged at $15,000 \times g$ for 10 min. The lower phase, which contained phospholipids, was transferred, dried under a stream of nitrogen and reconstituted in 200 μL of CHCl_3 .

Glycerophospholipids were further purified by solid-phase extraction (SPE) using Supelclean™ LC-NH2 cartridges (Sigma-Aldrich; ref: 57014) (Bodenec et al., 2000). The cartridges were first conditioned in 2 mL of hexane and loaded with 200 μL of

samples reconstituted in CHCl_3 . Four different washing steps with 2 mL of diethylether, 1.6 mL of $\text{CHCl}_3/\text{MeOH}$ 23:1 (v/v), 1.8 mL of diisopropyl ether/acetic acid 98:4 (v/v) and 2 mL of acetone/MeOH 9:1.2 (v/v) were then performed. Finally, 2 mL of $\text{CHCl}_3/\text{MeOH}$ 2:1 (v/v) was added, and the corresponding eluent was dried under a stream of nitrogen and reconstituted in $\text{MeOH}/\text{IPA}/\text{H}_2\text{O}$ 65:35:5 (v/v/v) before injection. LC-HRMS experiments were performed in positive ionization mode using the same system as that used for the lipidomic method described above.

Absolute quantification of LPC 26:0 in the mouse spinal cord was performed using the standard addition method. A calibration curve was obtained by adding increasing quantities (0 ng/mg, 10 ng/mg, 40 ng/mg and 100 ng/mg of tissue in triplicate) of pure LPC 26:0 standard (Avanti Polar Lipids; ref: 855810P) to pooled of mouse spinal cord tissues. The calibration curves were analysed in duplicate, i.e., at the beginning of the analytical batch containing the mouse spinal cord samples and at the end. The endogenous concentration of LPC 26:0 in the mouse spinal cord samples was then evaluated by measuring the area under the curve of the protonated $[\text{M}+\text{H}]^+$ ion and calculated according to calibration curves and the standard addition procedure.

3.9 Triglyceride level measurement

Spinal cords (~10 mg) were homogenized in 100 ml of solution containing 5% NP-40 in water, and then the samples were slowly heated to 80-100°C in a water bath for 2-5 min or until the NP-40 became cloudy and cooled to room temperature. The heating was repeated one more time to solubilize all TAGs. The samples were centrifuged for 2 min (top speed in a microcentrifuge) to remove any insoluble material. The TAG levels were quantified with a triglyceride quantification kit according to the manufacturer's protocol (BioVision, ref: K622-100). The absorbance was measured at 570 nm. All assays were performed in duplicate.

3.10 Oil red O staining and quantification of lipid droplets (LD)

Spinal cords were harvested from mice after perfusion with 4% PFA and embedded in Tissue-Tek® OCT (optimum cutting temperature). Serial sections (12- μ m thick) were then cut in the transverse plane at -20°C using a cryostat. Oil red O (ORO) staining was used to measure lipid accumulation. A stock ORO solution was generated by diluting 0.35 g ORO (Sigma-Aldrich; ref: 000625) in 100 ml of isopropanol. To prepare the staining solution, the ORO stock solution was filtered, mixed with dH₂O at 6:4 ratio and then filtered using a 0.2-micron syringe filter. Spinal cord sections were incubated in ORO staining solution for 15 min at room temperature, washed in tap water and immediately covered with Fluoromount™ Aqueous mounting medium (Sigma-Aldrich; ref: F4680). Brightfield microscopy images were acquired using a *Nikon Eclipse 80I* microscope equipped with a Nikon DS-Ri1 camera operated by NIS-Elements BR software. An average of 6 images per animal was acquired. To assess LDs, images were edited using Adobe Photoshop CS5 software. The area corresponding to the neuronal soma were selected and saved as the region of interest (an average of 14 selections/animal). Then, the total area of lipid droplets accumulated in each neuronal soma was analyzed using ImageJ software. For each measurement, the data were normalized to the tissue area to exclude unwanted biases and to determine the ratio of LD area to tissue area. The researcher was blinded to the genotype and condition of the sample when analyzing the images.

3.11 Immunohistochemistry (IHC)

Mice were anaesthetized by intraperitoneal injection of sodium pentobarbital (Dolethal®; Vetoniqual, Alcobendas, Spain) diluted 1:10 in physiological serum (Braun, Rubí, Spain). Spinal cords were harvested after mice were perfused with 4% paraformaldehyde (PFA; Sigma-Aldrich, Ref. 441244) in 0.1 M phosphate buffer, pH 7.4.

To study axonal degeneration, spinal cords were embedded in paraffin, and serial sections (4 μ m thick) were cut along the transverse or longitudinal (1-cm long) plane with a microtome (Microm HM 340E, Thermo Fisher Scientific). At least three sections

of the spinal cord were analysed per animal and per stain. The sections were stained with haematoxylin and eosin and 3% Sudan black or processed for immunohistochemistry with a rabbit anti-Iba1 antibody (diluted 1/1000; Wako; 019-19741); a rabbit anti-glial fibrillary acidic protein (GFAP) antibody (diluted 1/500; Dako; Z-0334); a mouse anti-synaptophysin antibody (diluted 1/500; Leica; SYNAP-299-L-CE); a rabbit anti-amyloid precursor protein (APP) antibody (diluted 1/100; Serotec; AHP538); a mouse anti-cytochrome c antibody (diluted 1/100; BD Pharmigen; 55643); a mouse anti-non-phosphorylated neurofilament H (SMI32) antibody (diluted 1/3000; Covance Inc.; SMI-32P); and a rabbit anti-malondialdehyde (MDA) antibody (diluted 1/1000; (Ferrer et al., 2005; Lopez-Erauskin et al., 2011; Morato et al., 2013). After primary antibody incubation, the sections were incubated with the Labelled Streptavidin-Biotin2 System (LSAB2, Ref. K0675, Dako). Staining was visualized after incubation with 3,30 -diaminobenzidine (DAB) substrate chromogen (Ref. D5637, Sigma-Aldrich), which results in a brown-coloured precipitate at the antigen site. After dehydrating the sections, slides were mounted with DPX (Ref. 06522, Sigma-Aldrich).

Microscopic examination

Images were acquired using an Olympus BX51 conventional light microscope coupled to an Olympus DP71 colour digital camera. The software used to analyze the photos was Cell[^]B from Olympus. APP and synaptophysin were quantified as previously described (Ferrer et al., 2005; Launay et al., 2015; Launay et al., 2017; Lopez-Erauskin et al., 2011; Morato et al., 2013; Morato et al., 2015; Pujol et al., 2004). The number of GFAP⁺ cells (astrocytes) and Iba1⁺ positive cells (microglia) per mm² in the spinal cord ventral horn was determined. The number of positive cells was counted with the Cell Counter ImageJ plugin. The researcher was blinded to genotype and condition when analysing the images. The data are presented as the average of the data obtained from two 20x images per animal for each group.

3.12 Behavioural tests

3.12.1 Horizontal bar cross test

Bar cross test uses a wooden bar of 100 cm in length and 2 cm in width (diameter). This bar is just wide enough for mice to stand on with their hind feet hanging over the edge

such that any slight lateral misstep will result in a slip. The bar was elevated 50 cm from the bench surface, so that animals did not jump off, yet were not injured upon falling from the bar. The mice were put on one end of the bar and expected to cross to the other end. To eliminate the novelty of the task as a source of slips, all animals were given two trials on the bar the day before the testing session. In the experimental session, the numbers of hindlimbs lateral slips and the time to cross the bar were counted on three consecutive trials. The researcher was blinded to the genotype and condition of the mice while performing these behavioural tests.

3.12.2 Treadmill test

Treadmill apparatus (Panlab, Barcelona, Spain) consist of a belt (50 cm long and 20 cm wide) varying in terms of speed (5–30 cm/s) and slope (0–25°) enclosed in a plexiglass chamber. An electrified grid is located to the rear of the belt on which foot shocks (0.2 mA) were administered whenever the mice fell down the belt. The mice were placed on the top of the belt in the opposite direction to the movement of the belt. Thus, to avoid the foot shocks, the mice had to move forward. The latency to falling off the belt (time of shocks in seconds) and the number of shocks received were measured. The mice were evaluated in five trials in a single-day session, always between 2 p.m. and 6 p.m. In the first trial, the belt speed was set at 20 cm/s and the inclination at 5°. In the second and third trial, the belt speed was 10 cm/s, and the slope was increased to 10° and 20°, respectively. Then, for the fourth and the fifth trials, the slope was maintained at 20° and the belt speed was increased to 20 and 30 cm/s, respectively. For the three first trials, mice ran for 1 min. For the fourth and fifth tests, the times of the experiment were 3 minutes, and 7 minutes and 30 seconds, respectively. Intervals between each test were 1, 1, 5 and 20 minutes, respectively. When the mice were subjected to consecutive trials at increasing speeds of up to 20 cm/s and a 20° slope, no differences were detected from one session to another between the WT and *Abcd1⁻/Abcd2⁻* mice. However, when the belt speed was increased up to 30 cm/s and the slope was 20°, differences were detected between the *Abcd1⁻/Abcd2⁻* mice and the controls because this task requires greater coordination. These conditions were therefore chosen to assess the effects of the genotype.

3.12.3 Hindlimbs clasping test

Assessment of hindlimbs clasping was done by suspending mice from their tails until they reached a vertical position. The hindlimbs extension reflex was analysed for 10 seconds in three consecutive trials separated by 5 min rest. The hindlimbs extension reflex was scored as described in **Table 5**, adapted from Dumser et al. (Dumser et al., 2007). The researcher was blinded for the genotype of the mice while performing these behavioural tests.

3.13 Statistical analysis

The values are expressed as the means \pm standard deviations (SD). Significant differences (*/# $p < 0.05$, **/## $p < 0.01$ and ***/### $p < 0.001$) between two groups were determined by a two-tailed unpaired Student's t-test. When comparing more than two groups, significant differences were determined by one-way ANOVA followed by Fisher's *post hoc* test or Kruskal Wallis non-parametric test followed by Dunn's *post hoc* test, or by two-way ANOVA followed by pairwise comparisons on the estimated marginal means *post hoc* test or Kruskal Wallis non-parametric test after verifying normality (Shapiro-Wilk test). Statistical analyses were performed using Graphpad version 6.01 for Windows (GraphPad Software, La Jolla, California, USA).

Table 5 Scoring system for the hindlimbs clasping test

SCORE	PHENOTYPE
0	Total paralysis of the hindlimbs
0.5	Both hindlimbs are entirely retracted and touching the abdomen during 100% of the time suspended
0.75	Both hindlimbs are entirely retracted toward the abdomen during 100% of the time suspended
1	Both hindlimbs are partially retracted toward the abdomen during 100% of the time suspended
1.25	Alternating clasping and flexion of hindlimbs, although clasping occurs for more than 50% of the time suspended
1.5	Alternating clasping and flexion, equally occurring during 100% of the time suspended
1.75	Alternating clasping and flexion of hindlimbs, although flexion occurs for more than 50% of the time suspended
2	Flexion of hindlimbs during 100% of the time suspended
2.25	Alternating flexion and extension of hindlimbs, although flexion occurs for more than 50% of the time suspended
2.5	Alternating flexion and extension, equally occurring during 100% of the time suspended
2.75	Alternating flexion and extension of hindlimbs, although extension occurs for more than 50% of the time suspended
3	Extension of hindlimbs in an angle $<90^\circ$ during 100% of the time suspended
3.5	Alternating extension of hindlimbs in an angle $<90^\circ$ and $\geq 90^\circ$ during 100% of the time suspended
4	Extension of hindlimbs in an angle $\geq 90^\circ$ during 100% of the time suspended

RESULTS

4 Results

4.1 Chapter I: high-dose biotin restores redox balance, energy and lipid homeostasis, and axonal health in a model of adrenoleukodystrophy

4.1.1 Biotin counteracts redox imbalance in human fibroblasts

The fibroblasts of X-ALD patients are a good surrogate cell model for dissecting disease mechanisms, as they recapitulate the main X-ALD hallmarks. We previously showed that excess C26:0 triggers mitochondrial ROS production by electron transport chain (ETC) complexes while depleting the reduced glutathione (GSH) pool and decreasing membrane potential ($\Delta\Psi_m$) (Lopez-Erauskin et al., 2013b). Using this cell system, we sought to determine whether biotin is efficient in addressing a core problem of X-ALD, the increased ROS production generated by an excess of hexacosanoic acid C26:0.

At doses of 0.5 to 5 μM , biotin successfully prevented ROS production induced by the excess of C26:0, as visualized using the dichlorodihydrofluorescein diacetate (DCF) and dihydroethidium (DHE) fluorescent probes, to assess total intracellular H_2O_2 and superoxide anion respectively (**Fig. 11A-B**). The same doses of biotin were efficacious at preventing mitochondrial ROS production assessed by MitoSOX (**Fig. 11C**). Moreover, biotin treatment also reduced the mitochondrial ROS produced by the complex III inhibitor antimycin A, indicating that the precise mechanism of protection against ROS may not be restricted to the protection against an excess of VLCFA (**Fig. 11D**). The mechanism might be indirect, as incubation with biotin for a short period of time (1 h) was not sufficient to abolish the increase in ROS levels (**Fig. 11E**), ruling out a possible scavenger role of the vitamin.

Further, incubation for 24h with biotin at 0.5 to 5 μM prevented the reduction of the reduced form of GSH in fibroblasts challenged with C26:0 excess, in both X-ALD and control fibroblasts (**Fig. 12A**). In contrast, incubation of 1h was insufficient (**Fig. 12B**). Regarding inner mitochondrial membrane potential, biotin did not exert any effect on the decrease provoked by excess C26:0 (**Fig. 12C**).

We next explored whether biotin would influence the transcription of genes governing glutathione biosynthesis. Indeed, upon biotin treatment, the expression of the first rate-limiting enzyme in glutathione biosynthesis, glutamate-cysteine ligase (GCL), was increased. This was true for both subunits, namely, the catalytic subunit (*GCLC*) and the modifier subunit (*GCLM*). Additionally, the expression of glutathione reductase (*GSRI*), the enzyme that catalyses the reduction of glutathione disulphide (GSSG) to GSH, was increased in X-ALD fibroblasts only (**Fig. 12D**). These transcriptional events may indicate a possible pathway through which GSH is replenished and ROS levels are compensated in human skin fibroblasts.

4.1.2 High-dose biotin rescues mitochondrial biogenesis and energy failure in *Abcd1*⁻ mice

Based on these positive results, we felt prompted to treat *Abcd1*⁻ mice (Pujol et al., 2002) with a dose of biotin equivalent to the dose administered to MS patients, in which clinical improvement was observed after high-dose pharmaceutical-grade biotin treatment (Tourbah et al., 2016). Mice were fed 60 mg/kg/day biotin for 3.5 months, from the age of 9.5 months to 13 months.

We then evaluated the following parameters of altered pathways in X-ALD: i) target genes of NRF2, nuclear factor, erythroid 2 like 2, a transcription factor that governs the endogenous antioxidant response and shows a blunted response in X-ALD (Kansanen et al., 2012; Ranea-Robles et al., 2018); ii) mtDNA copy number and the master regulators of mitochondrial biogenesis, which are reduced in X-ALD (Fourcade et al., 2015; Morato et al., 2013); and iii) ATP levels, which are also reduced in X-ALD (Lopez-Erauskin et al., 2013b) (**Fig. 13A-D**). Treatment with high-dose biotin normalized the expression of NRF2 targets (*Hmox1*, *Nqo1*, *Gsta3* and *Gclc*) (**Fig. 13A**). In agreement with previous data in fibroblasts, the enzymes GSTA3 and GCLC may have directly contributed to the preservation of the redox homeostasis (**Fig. 12D**). Next, we examined the effect of biotin on mitochondrial dysfunction in *Abcd1*⁻ mouse spinal cord (Morato et al., 2013). mtDNA levels and mitochondrial biogenesis were normalized by the treatment based on the mitochondrial DNA/nuclear DNA (mtDNA/nDNA) ratio (**Fig. 13B**) and the induction of *Pgc-1 α* and *Tfam* mRNA in *Abcd1*⁻ mice (**Fig. 13C**). We also observed that high-dose biotin reversed the drop in ATP content (**Fig. 13D**). Effects of

biotin on ATP generation have been documented in different scenarios (Lazzarino et al., 2010; Trapp and Stys, 2009), and have been attributed to the activation of AMPK α in a model of biotin deficiency (Hernandez-Vazquez et al., 2012; Hernandez-Vazquez et al., 2013). In our case, the maintenance of ATP appears independent of the activation of AMPK α , since the P-AMPK α /AMPK α ratio was not altered by high-dose biotin (**Fig. 13E**). The increase in the number of mitochondria could be a possible mechanism for the replenishment of ATP pools.

4.1.3 Increased triglyceride levels in the spinal cord of *Abcd1*⁻ mice and restoration by high-dose biotin

Knowing the effects of biotin on fatty acid synthesis as a cofactor of the enzymes ACC1 and ACC2, we generated an untargeted lipidomic profile of the spinal cord of 13-month-old WT, *Abcd1*⁻ and *Abcd1*⁻ + High-dose biotin mice to evaluate the possible global effects of the treatment. We identified and annotated 747 unique lipid species belonging to different lipid classes: free fatty acids (FA), fatty acylcarnitines (FA-Carn), cholesteryl esters (CE), diacylglycerols (DAG), triacylglycerols (TAG), lysoglycerophosphocholines (LPC), lyso-glycerophosphoethanolamines (LPE), lysoglycerophosphoinositols (LPI), lyso-glycerophosphoserines (LPS), glycerophosphocholines (PC), glycerophosphoethanolamines (PE), glycerophosphoglycerols (PG), glycerophosphoinositols (PI), glycerophosphoserines (PS), ceramides (Cer), hexosylceramides (HexCer), dihexosylceramides (DiHexCer), sphingomyelins (SM), sulfoglycosphingolipids (Su) and gangliosides (GSL). The only significantly altered class in *Abcd1*⁻ mice were TAGs (**Fig. 14A**). This is in line with the increased TAGs detected in peripheral blood mononuclear cells (PBMC) of a cohort of patients with AMN (Ruiz et al., 2015) and more recently in fibroblasts of ccALD patients (Lee et al., 2019). Seventy-nine different TAG species, ranging from TAGs with 42 carbons and 0 double bonds (TAG 42:0) to TAGs with 75 carbons and 4 double bonds (TAG 75:4), were annotated. Out of these 79 species, 61 accumulated over 1.3-fold, with 36 of these 61 species reaching statistical significance. Strikingly, the levels of all of these different species of TAG were normalized by treatment with high-dose biotin (**Fig. 14B-D**).

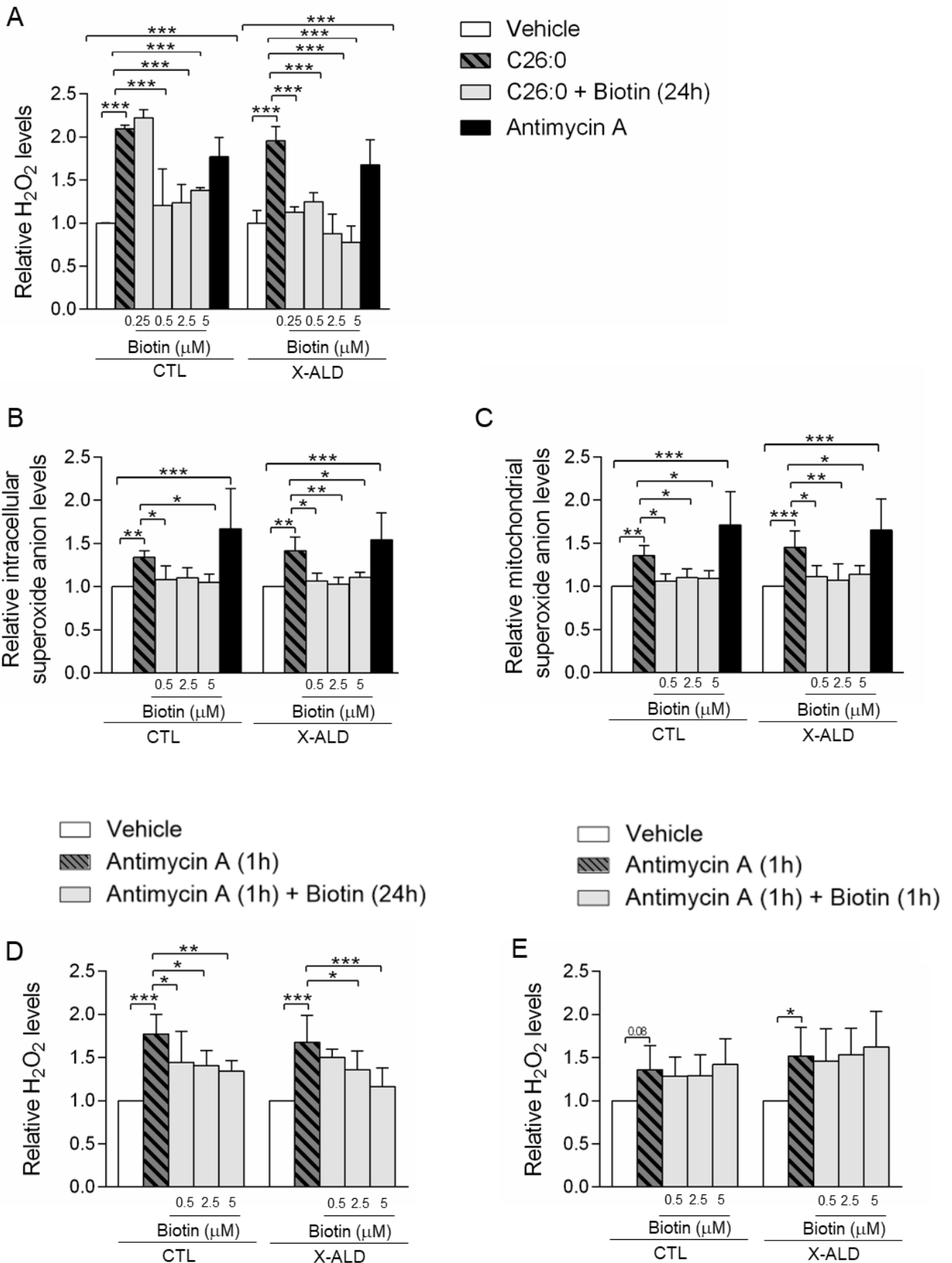


Figure 11. Biotin prevents ROS production of mitochondrial origin in X-ALD patients' fibroblasts

(A) Intracellular H₂O₂ (DCF probe) was quantified in CTL (n=3) and X-ALD human fibroblasts (n=3) after 24h with vehicle as control, C26:0 or biotin (0.25, 0.5, 2.5 or 5uM) with C26:0 in medium containing 10% FCS. For this and next experiments in B and C, C26:0 was used at 50uM. Antimycin (200uM for 1h) was used as positive control. (B) Intracellular superoxide anion (DHE probe) was quantified in CTL (n=5) and X-ALD human fibroblasts (n=5) after 24h with vehicle as control, C26:0 or biotin (0.5, 2.5 or 5uM) with C26:0 in medium containing 10% FCS. Antimycin (200uM for 1h) was used as positive control. (C) Mitochondrial superoxide anion (MitoSOX probe) was quantified in CTL (n=5) and X-ALD human fibroblasts (n=5) after 24h with vehicle as control, C26:0 or biotin (0.5, 2.5 or 5uM) with C26:0 in medium containing 10% FCS. Antimycin (200uM for 1h) was used as positive control. (D) CTL (n=4) and X-ALD human fibroblasts (n=5) were pretreated with biotin (0.5, 2.5 or 5uM) for 24h and then Antimycin A was added in the medium containing 10% FCS for 1h. Next, H₂O₂ (DCF probe) was quantified in CTL (n=4) and X-ALD human fibroblasts (n=5). (E) Intracellular H₂O₂ (DCF probe) was quantified in CTL (n=4) and X-ALD human fibroblasts (n=5) after 1h with vehicle as control, Antimycin A or biotin (0.5, 2.5 or 5uM) with Antimycin A in medium containing 10% FCS. Quantification depicted as fold change to vehicle-treated fibroblasts. Values are expressed as mean ± SD. (A-E) * $p < 0.05$; ** $p < 0.01$; *** $p < 0.001$; one-way ANOVA followed by Fisher's *post hoc* test.

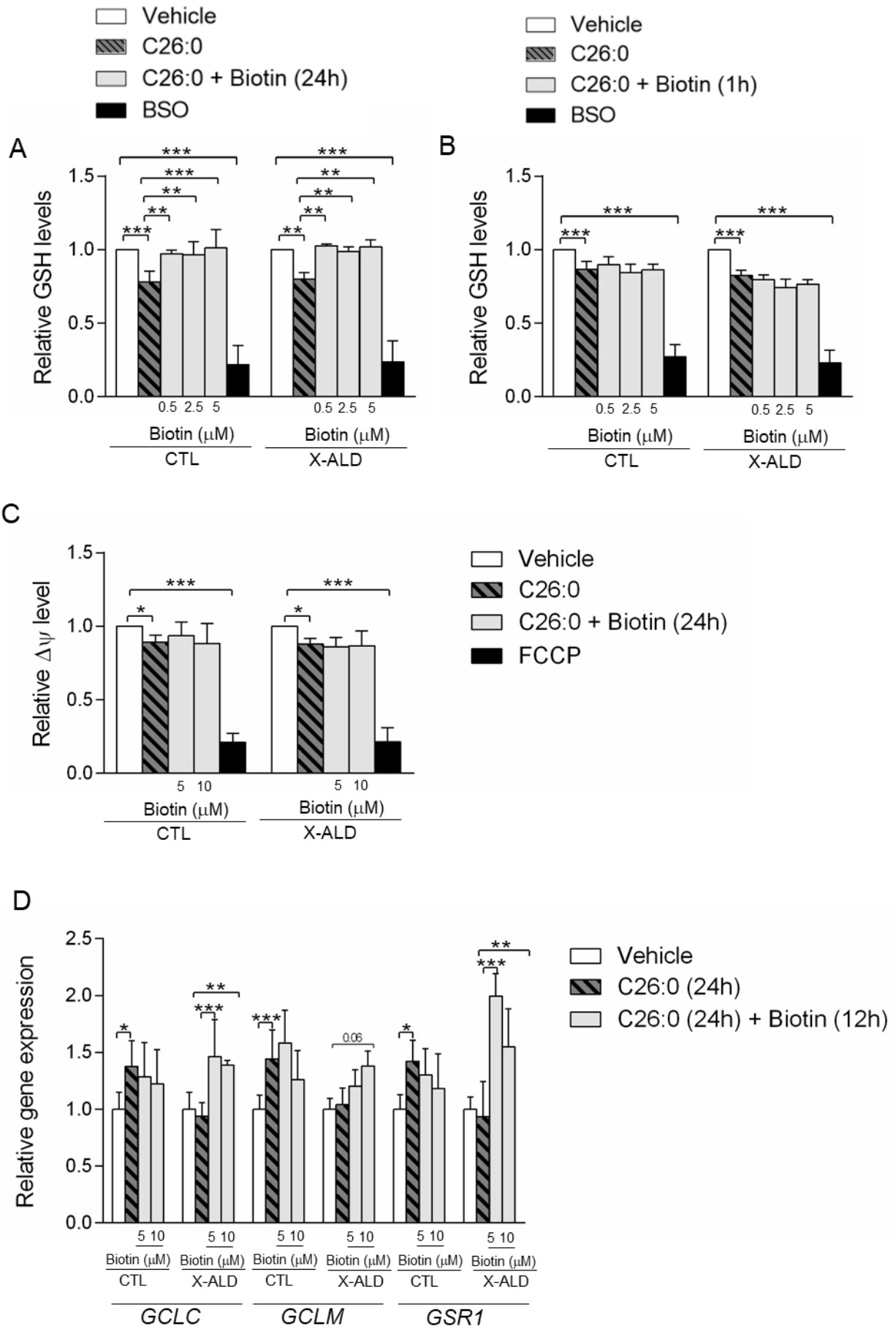


Figure 12. Biotin normalizes GSH levels in X-ALD patients' fibroblasts

(A) Relative GSH level was quantified in CTL (n=4) and X-ALD human fibroblasts (n=3) after 24h with vehicle as control, C26:0 or biotin (0.5, 2.5 or 5uM) with C26:0 in medium containing 10% FCS. For this and next experiments, C26:0 was used at 50uM. Buthionine sulfoximine (BSO; 500uM for 24h) has been used as positive control. **(B)** Relative GSH level was quantified in CTL (n=5) and X-ALD human fibroblasts (n=3) after 24h with vehicle as control, C26:0 or C26:0 with biotin (0.5, 2.5 or 5uM) where biotin was incubated the last hour in medium containing 10% FCS. **(C)** Relative inner mitochondrial potential ($\Delta\psi_m$) was measured in CTL (n=5) and X-ALD human fibroblasts (n=4) after 24h with vehicle as control, C26:0 or biotin (5 or 10uM) with C26:0 in medium containing 10% FCS. FCCP (200uM for 10min) has been used as positive control. **(D)** Relative *GCLC*, *GCLM* and *GSRI* gene expression was measured in CTL (n=5) and X-ALD human fibroblasts (n=5) after 24h with vehicle as control, C26:0 or biotin (5 or 10uM) with C26:0 in medium containing 10% FCS. Biotin was added 12h after C26:0 treatment for 12h. Gene expression normalized relative to *RPLP0*. Quantification depicted as fold change to vehicle-treated fibroblasts. Values are expressed as mean \pm SD. **(A-D)** * $p < 0.05$; ** $p < 0.01$; *** $p < 0.001$; one-way ANOVA followed by Fisher's *post hoc* test.

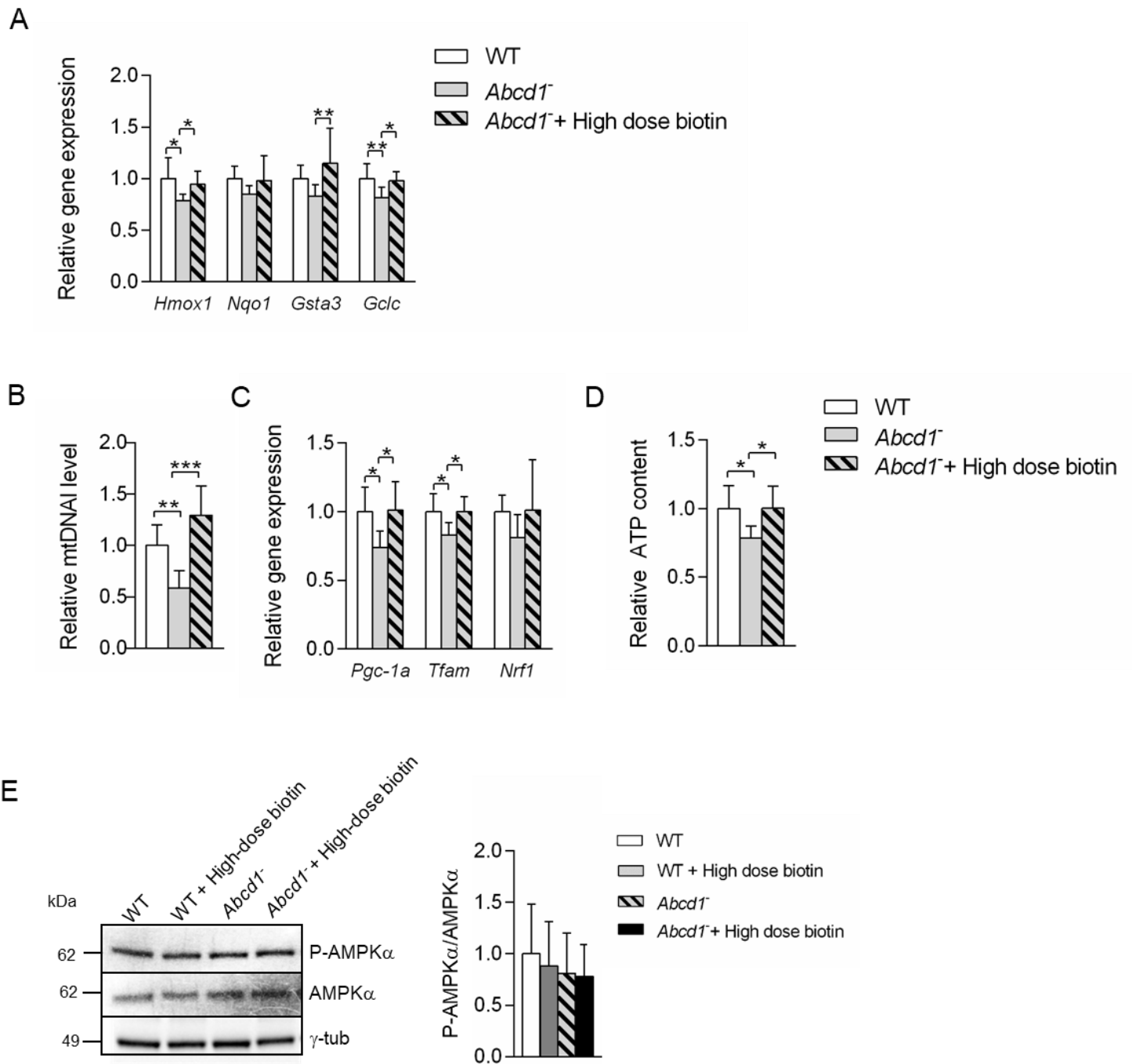


Figure 13. High-dose biotin rescues mitochondrial biogenesis and prevents energetic failure in *Abcd1*^{-/-} mice spinal cord

(A) Relative gene expression of NRF2 target genes (*Hmox1*, *Nqo1*, *Gsta3*, *Gclc*) has been analyzed by quantitative RT-PCR in WT (n=5-11), *Abcd1*^{-/-} (n=8-11) and *Abcd1*^{-/-} + High-dose biotin (n=5-7) mice. Gene expression normalized relative to mouse *Rplp0* and depicted as fold change to WT mice. (B) mtDNA content analyzed by quantitative RT-PCR and expressed as the ratio of mtDNA to nuclear DNA (mtDNA/nDNA) (n= 6-7 per genotype/ condition). (C) *Pgc-1a*, *Tfam* and *Nrf1* relative gene expression analyzed by quantitative RT-PCR (n=6-8 per

genotype/condition). Gene expression normalized relative to mouse *Rplp0* and depicted as fold change to WT mice. **(D)** ATP content in spinal cord of 13-month-old mice (n=7 per genotype/condition). **(E)** P-AMPK α /AMPK α protein level (n=5 per condition). Protein content was normalized relative to γ -tub in each case and then represented relative to non-phosphorylated form. Quantification depicted as fold change to WT mice. Values are expressed as mean \pm SD. **(A-D)** * $p < 0.05$; ** $p < 0.01$; *** $p < 0.001$; one-way ANOVA followed by Fisher's *post hoc* test.

We also detected a tendency for cholesteryl esters (CE) to be increased in the *Abcd1*⁻ mice, albeit non-significantly (**Fig. 14A**). Both, CE and TAG alterations were normalized by high-dose biotin (**Fig. 14A**). However, when we specifically investigated the effects of high-dose biotin on lysophosphatidylcholine C26:0, a phospholipid species widely used as a pathognomonic marker for the diagnosis of X-ALD (Turgeon et al., 2015), we found no amelioration of the profile (**Fig. 14E**).

4.1.4 Increased size and number of LDs accumulated in motor neurons of *Abcd1*⁻/*Abcd2*⁻ mice and restoration by high-dose biotin

TAG and sterol esters are mostly stored in cells as LDs, which serve as reservoirs to be used in case of insufficient energy sources (Walther et al., 2017). We therefore decided to visualize possible LD accumulation at the cellular level in the spinal cord of X-ALD mice by performing classical Oil red O (ORO) staining on spinal cord sections. This histological stain is specific for neutral lipids and does not stain the polarized phospholipids of the cell membrane (Mehlem et al., 2013), enabling clear visualization of LDs by bright-field microscopy (Melo et al., 2011). ORO staining revealed an increase in LDs in neuronal somas in the ventral horn of *Abcd1*⁻ and *Abcd1*⁻/*Abcd2*⁻ (DKO) mice, with no differential staining in glial cells (**Fig. 15A-D, F, G, I, J**). Quantitative analysis to assess the area occupied by LDs relative to the area of the motoneuronal soma indicated an augmented surface in mutant animals, in *Abcd1*⁻ mice at 12 months of age (**Fig. 15A-E**), and in *Abcd1*⁻/*Abcd2*⁻ mice at 18 months of age (**Fig. 15F, G, I, J, L**). This accumulation of LDs was normalized in *Abcd1*⁻/*Abcd2*⁻ mice after 6 months of treatment with high-dose biotin (**Fig. 15F-L**).

4.1.5 Transcriptional dysregulation of lipid homeostasis in *Abcd1*⁻ mice spinal cord and restoration by high-dose biotin

We set out to gain insight into the origin of the increased TAG levels in X-ALD and the mechanisms of normalization by high-dose biotin to determine whether the effects were due to an increased biosynthesis or a decreased degradation of TAGs. Accordingly, the expression of a set of genes involved in the main lipid homeostatic pathways were measured: i) the synthesis of fatty acids (**Fig. 16A**) and ii) the degradation of fatty acids via β -oxidation (FAO) in mitochondria and peroxisomes (**Fig. 16B**). At baseline, an induction of lipogenesis in the *Abcd1*⁻ spinal cord was observed, which is characterized by an upregulation of sterol regulatory element binding protein 1c (SREBP-1c) and its targets *Fas*, *Scd1*, *Scd2*, *Scd3*, *Acs11*, *Acs13*, *Acs14*, *Acs15*, and *Acs16* (**Fig. 16A**). SREBP-1c belongs to the basic-helix-loop-helix-leucine zipper (bHLH-LZ) family of transcription factors and controls lipogenesis (Shimano and Sato, 2017). On the other hand, the FAO genes, in particular *Cpt2*, *Acadm*, *Acadl*, *Acadvl*, *Echs1*, *Hadha*, *Acaa2*, *Acox1* and *Ehhadh*, showed decreased expression in *Abcd1*⁻ mice spinal cord (**Fig. 16B**).

High-dose biotin exerted a striking effect in modulating the transcription of core lipid homeostatic pathways; the treatment repressed SREBP-1c and thus reduced lipogenesis gene expression (**Fig. 16A**), while induced FAO by normalizing the levels of enzymes in both peroxisomes and mitochondria (**Fig. 16B**), which may explain the correction of total TAG levels in the treated X-ALD mice (**Fig. 14A-D**). Intrigued by this concerted dysregulation of both anabolic and catabolic lipid pathways, we investigated mTOR, the mammalian target of rapamycin and nutrient sensor. This kinase is activated by anabolic signals and governs global lipid metabolism, including SREBP-1c, in response to nutrition (Bakan and Laplante, 2012; Owen et al., 2012; Porstmann et al., 2008). When induced, mTOR facilitates the accumulation of TAGs by promoting lipogenesis and inhibits β -oxidation of fatty acids and lipolysis (Caron et al., 2015; Soliman, 2011). Here we detected increased levels of P-mTOR, the active form of mTOR. Importantly, treatment with high-dose biotin restored the levels of activated mTOR (**Fig. 16C**). Similarly, we analyzed p70 S6K (ribosomal protein S6 kinase beta-1), a well-known mTOR target, and observed increased p70 S6K phosphorylation in the spinal cords of *Abcd1*⁻ mice, which was reduced with high-dose biotin treatment (**Fig. 16D**), confirming that biotin modulates mTOR activation state in the X-ALD mice.

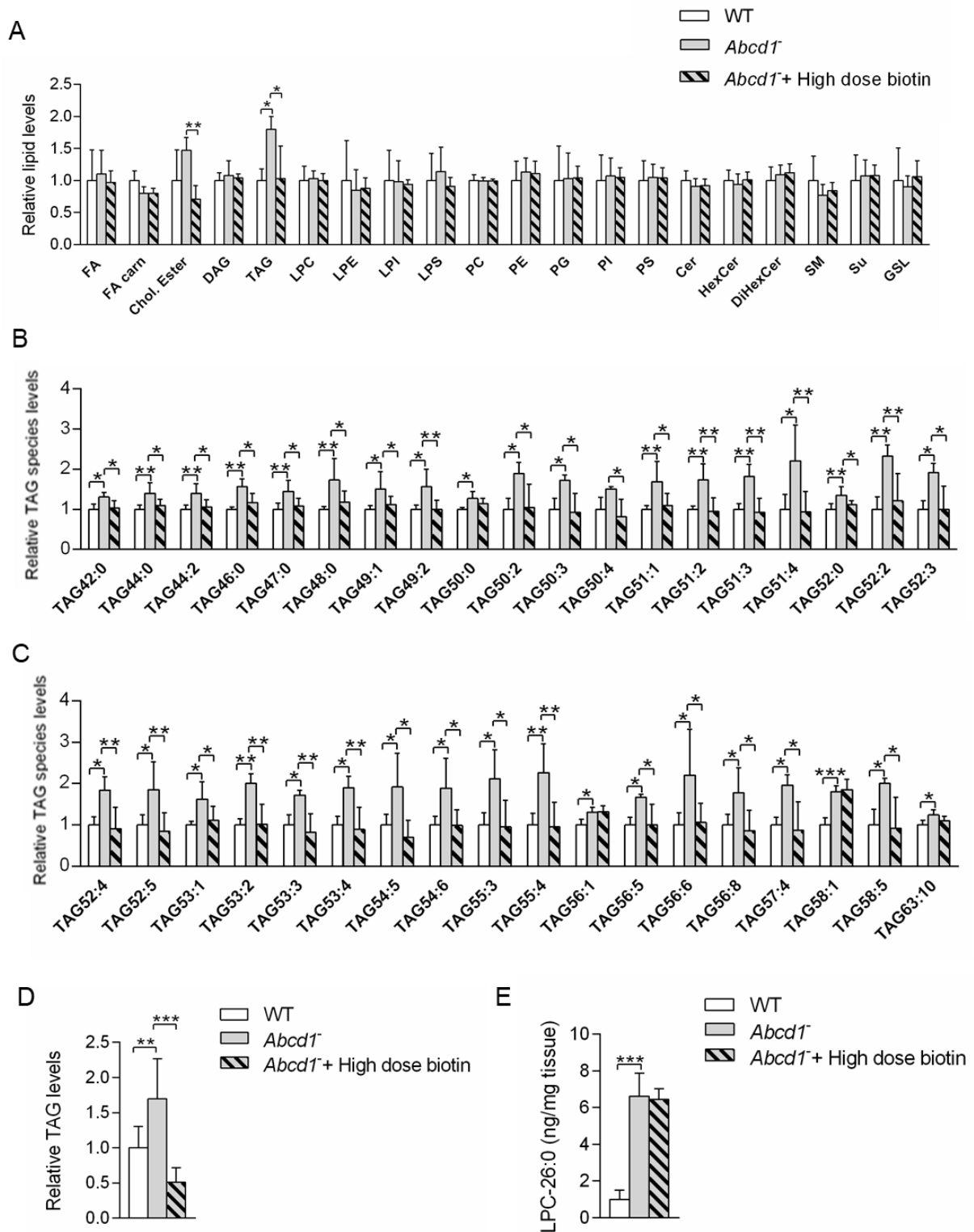


Figure 14. High-dose biotin rescues TAG levels in *Abcd1*⁻ mice

(A) Lipidomic experiments have been performed in spinal cord of 13-month-old WT (n=5), *Abcd1*⁻ (n=3) and *Abcd1*⁻ + High-dose biotin (n=6) mice and all lipid species identified are

represented (FA= Free fatty acids, FA-Carn= Fatty acyl carnitines, CE= Cholesteryl esters, DAG= Diacylglycerols, TAG= Triacylglycerols, LPC= Lyso-Glycerophosphocholines, LPE= Lyso-Glycerophosphoethanolamines, LPI= Lyso-Glycerophosphoinositols, LPS= Lyso-Glycerophosphoserines, PC= Glycerophosphocholines, PE= Glycerophosphoethanolamines, PG= Glycerophosphoglycerols, PI= Glycerophosphoinositols, PS= Glycerophosphoserines, Cer= Ceramides, HexCer= Hexosylceramides, DiHexCer= Dihexosylceramides, SM= Sphingomyelins, Su= Sulfoglycosphingolipids and GSL=gangliosides). **(B-C)** Species of TAG identified by lipidomics which are significantly altered in *Abcd1^{-/-}* or *Abcd1^{-/-}* + High-dose biotin mice. They are represented in function of the number of both total carbons and double bonds. Relative lipid levels were normalized to WT mice. **(D)** TAG levels in spinal cord of 13-month-old mice (n=5-6 per genotype/condition). **(E)** LPC-26:0 levels (ng/mg of tissue) in WT (n=5), *Abcd1^{-/-}* (n=3) and *Abcd1^{-/-}* + High-dose biotin (n=6) mice. Quantifications depicted as fold change to WT mice. Values are expressed as mean \pm SD. **(A-D)** * $p < 0.05$; ** $p < 0.01$; *** $p < 0.001$; one-way ANOVA followed by Fisher's *post hoc* test. **(E)** ### $p < 0.001$; non-parametric Kruskal–Wallis' test followed by Dunn's *post hoc* test.

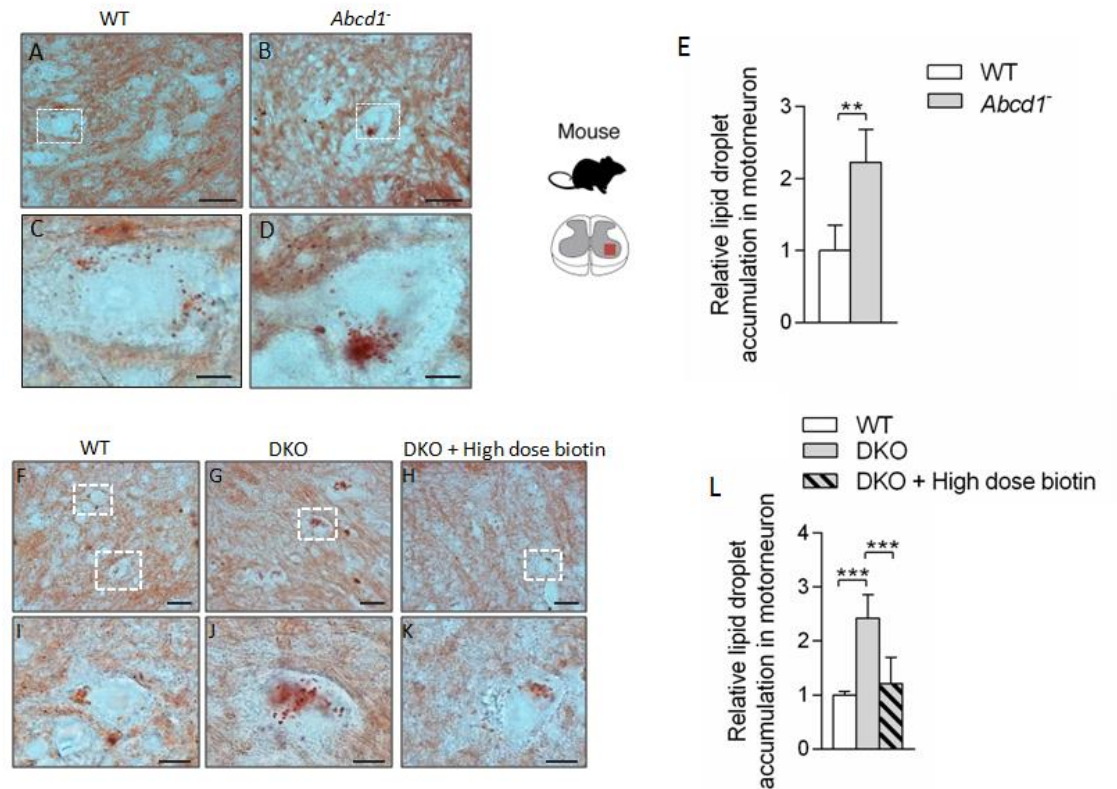


Figure 15. High-dose biotin normalizes excess lipid droplet accumulation in *Abcd1*^{-/-}/*Abcd2*^{-/-} mice

(A-D) Histological analysis performed in 13-month-old (A, C) WT and (B, D) *Abcd1*^{-/-} mice. Spinal cord histological sections were processed for ORO (n=5/genotype and condition). (E) Quantification of lipid droplet accumulation in spinal cord histological sections in 13-month-old WT and *Abcd1*^{-/-} mice. (F-K) Histological analysis performed in 18-month-old (F, I) WT, (G, J) *Abcd1*^{-/-}/*Abcd2*^{-/-} (DKO) and (H, K) *Abcd1*^{-/-}/*Abcd2*^{-/-} mice treated with high-dose biotin (DKO + High-dose biotin). Spinal cord histological sections were processed for Oil Red O (ORO) (n=4-5 per genotype/condition). (L) Quantification of lipid droplet accumulation in spinal cord histological sections in 18-month-old WT, DKO and DKO + High-dose biotin mice by ImageJ. Scale bar 25µm (A-B, F-H); scale bar 8.3 µm (C-D, I-K). Quantifications depicted as fold change to WT mice. Values are expressed as mean ± SD. (E) ** *p*<0.01; unpaired Student's *t*-test. (L) *** *p*<0.001; one-way ANOVA followed by Fisher's *post hoc* test.

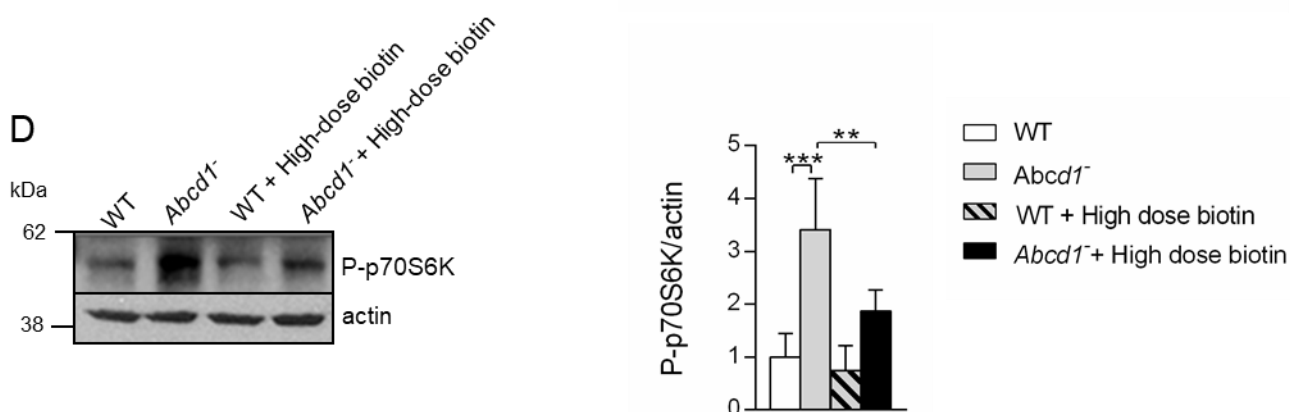
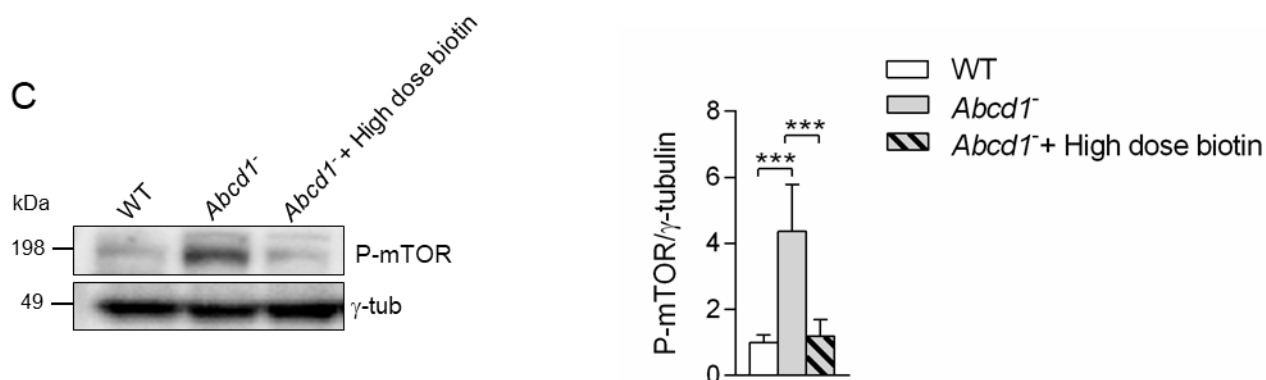
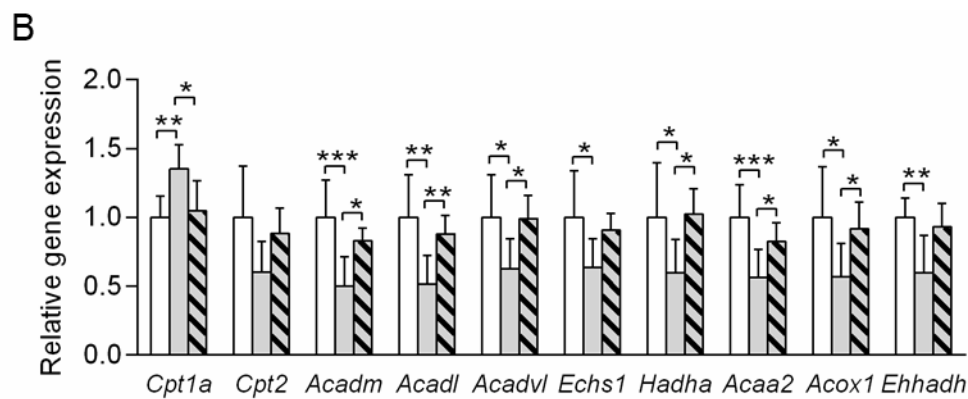
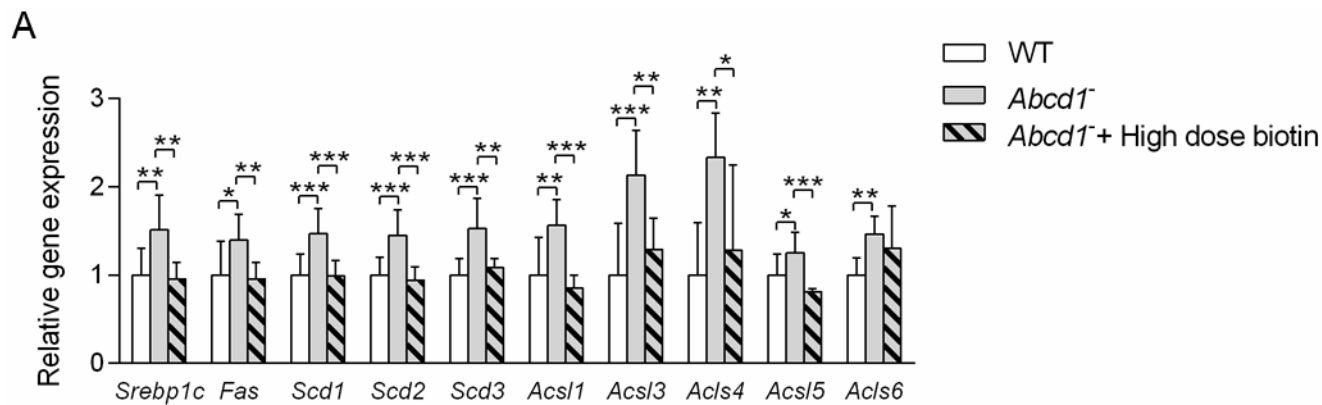


Figure 16. High-dose biotin inhibits lipogenesis through mTOR in *Abcd1*^{-/-} mice

(A) Lipogenesis (*Srebp1c*, *Fas*, *Scd1*, *Scd2*, *Scd3*, *Acsl1*, *Acsl3*, *Acsl4*, *Acsl5*, *Acsl6*) in WT (n=9-11), *Abcd1*^{-/-} (n=7-8) and *Abcd1*^{-/-} + High-dose biotin (n=7-8) mice and (B) mitochondrial and peroxisomal FAO (*Cpt1a*, *Cpt2*, *Acadm*, *Acadl*, *Acadvl*, *Echs1*, *Hadha*, *Acaa2*, *Acox1*, *Ehhadh*) in WT (n=6-7), *Abcd1*^{-/-} (n=6-8) and *Abcd1*^{-/-} + High-dose biotin (n=6-8) mice. Gene expression normalized relative to mouse *Rplp0* and depicted as fold change to WT mice. (C) P-mTOR protein level (n=4 per genotype/condition). Protein content was normalized relative to γ -tubulin and quantification depicted as fold change to WT mice. (D) P-p70S6K protein level (n=5 per condition). Protein content was normalized relative to β -actin and quantification depicted as fold change to WT mice. Values are expressed as mean \pm SD. (A-C) * $p < 0.05$; ** $p < 0.01$; *** $p < 0.001$; one-way ANOVA followed by Fisher's *post hoc* test. (D) ** $p < 0.01$; *** $p < 0.001$; two-way ANOVA followed by pairwise comparisons on the estimated marginal means *post hoc* test.

4.1.6 Lipidic imbalance is not an early event in X-ALD mice

In order to establish the grade of contribution of lipid homeostasis in the development of the disease, expression of enzymes involved in lipid synthesis and degradation, and LD accumulation were analyzed in 3-month-old mice spinal cord. However, there were no appreciable differences in 3-month-old X-ALD mice compared to wild-type mice (Fig. 17A-H). Besides, no changes in the expression of NRF2-target genes were observed when analyzed by RT-PCR (Fig. 17I). These results, together with the previous knowledge that oxidative stress is an early event in X-ALD pathophysiology that occurs at 3.5-months of age (Fourcade et al., 2008), reinforce the role of oxidative stress as a major and earlier contributor to the development of the disease and are indicative of an accumulative phenotype over time.

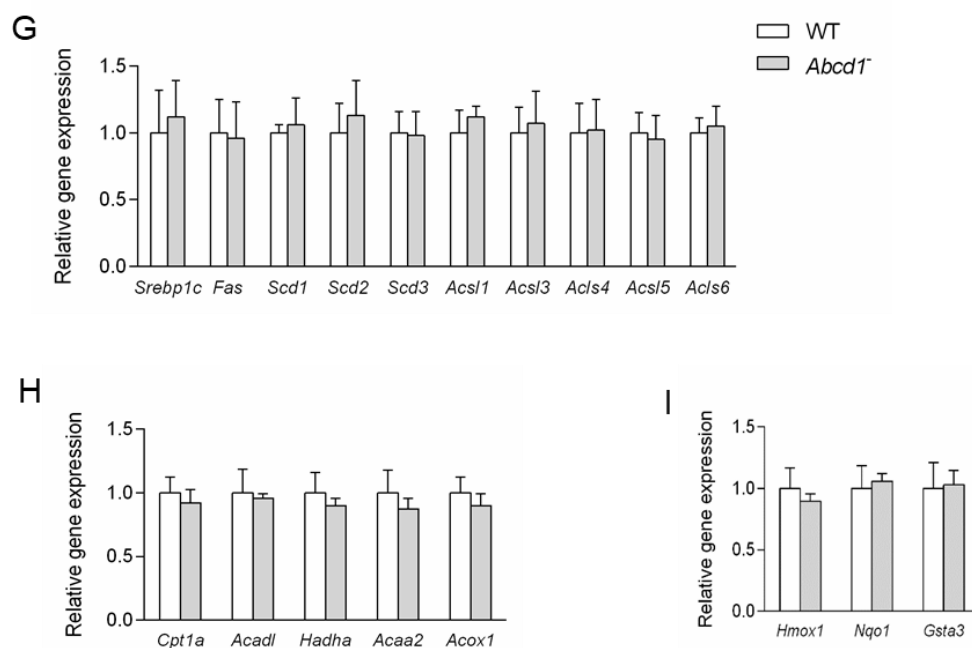
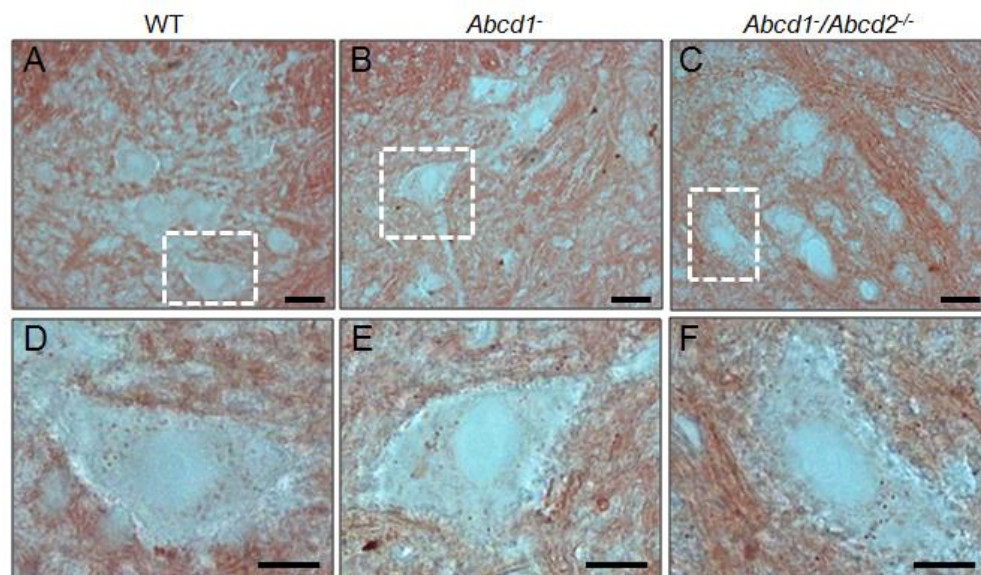


Figure 17. Lipid metabolism in 3-month-old X-ALD mouse model

(A-F) Histological analysis performed in 3-month-old (A, D) WT, (B, E) *Abcd1*^{-/-} and (C, F) *Abcd1*^{-/-}/*Abcd2*^{-/-} mice shows no accumulation of LDs. Spinal cord histological sections were processed for ORO (n=4-6/genotype and condition). Scale bar 25µm (A-C); scale bar 8.3 µm (D-F). (G) Lipogenesis (*Srebp1c*, *Fas*, *Scd1*, *Scd2*, *Scd3*, *Acs11*, *Acs13*, *Acs14*, *Acs15*, *Acs16*) in WT (n=7) and *Abcd1*^{-/-} (n=8) mice and (H) mitochondrial and peroxisomal FAO (*Cpt1a*, *Acadl*, *Hadha*, *Acaa2*, *Acox1*) in WT (n=6) and *Abcd1*^{-/-} (n=6) mice. (I) Relative gene expression of NRF2 target genes (*Hmox1*, *Nqo1*, *Gsta3*) has been analyzed by quantitative RT-PCR in WT (n=6) and *Abcd1*^{-/-} (n=6) mice. Gene expression normalized relative to mouse *Rplp0* and depicted as fold change to WT mice. Values are expressed as mean ± SD.

4.1.7 High-dose biotin prevents locomotor deficits in *Abcd1*⁻/*Abcd2*⁻ mice

Our next step was to evaluate the preclinical efficacy of high-dose biotin in alleviating axonopathy and the associated locomotor dysfunction exhibited by the X-ALD mouse model (Pujol et al., 2004). We used mice with complete loss of *Abcd1* and its closest homologue, *Abcd2* (*Abcd1*⁻/*Abcd2*⁻), which show an AMN-like phenotype at approximately 12 months of age, making them more suitable for therapeutic testing. The *Abcd1*⁻/*Abcd2*⁻ mice were treated for 6 months with high-dose biotin and then challenged with three locomotor tests. In the treadmill test, the total number and duration of shocks received by the *Abcd1*⁻/*Abcd2*⁻ mice were higher than those received by the WT mice under conditions of high speed and high slope, indicating that the mutants reached exhaustion earlier than WT. Remarkably, the animals fed with high-dose biotin performed equal to control mice (**Fig. 18A**). In the bar cross experiment, while the double knockout mice slipped off the bar more frequently and needed a longer time to reach the opposite platform, the *Abcd1*⁻/*Abcd2*⁻ + High-dose biotin mice performed the task in the same manner as their WT littermates (**Fig. 18B**). To finish, we also investigated the hindlimb clasping phenotype, which consists in the scoring of the extension reflex of the hindlimbs when suspending the mouse by its tail for ten seconds. When gently lifted by the tail, a wild type mouse typically extends its hind limbs outwards at a steady 90–120° angle. Upon impairment of the motor system, mice tend to retract their hindlimbs, holding them close to the body, often with inversion and flexion of paws. Here the *Abcd1*⁻/*Abcd2*⁻ mice presented a lower score than WT mice, demonstrating a locomotor impairment. In this test, high-dose biotin treatment also significantly improved the score obtained by the mice (**Fig. 18C**). In conclusion, high-dose biotin rescued all the locomotor parameters analysed.

4.1.8 High-dose biotin prevents axonal degeneration in *Abcd1*⁻/*Abcd2*⁻ mice

To evaluate the effect of high-dose biotin on axonal degeneration, immunohistochemical signs of neuropathology present in *Abcd1*⁻/*Abcd2*⁻ mice were studied. This neuropathological phenotype is characterized by the following features: i) microgliosis (**Fig. 18D-E, 18B'**) and astrocytosis (**Fig. 18G-H, 18C'**), as detected by Iba1 and GFAP staining, respectively; ii) axonal damage suggested by the accumulation of synaptophysin (**Fig. 18J-K, 18D'**) and amyloid precursor protein (APP) in axonal

swellings (**Fig. 18M-N, 18E'**); iii) scattered myelin debris around the axonal ovoids, probably secondary to axonal degeneration, as detected by Sudan black staining (**Fig. 18P-Q**); iv) reduced SMI-32 staining in motor neurons, an indicator of disturbed neurofilament status (**Fig. 18S-T**); v) diminished amount of cytochrome c (**Fig. 18V-W**), which is a marker of mitochondrial depletion; and vi) increased signal for MDA, a marker of lipoxidation (**Fig. 18Y-Z**) (Ferrer et al., 2005; Launay et al., 2015; Launay et al., 2017; Lopez-Erauskin et al., 2011; Morato et al., 2013; Morato et al., 2015; Pujol et al., 2004; Ranea-Robles et al., 2018). We found that treatment with high-dose biotin in *Abcd1/Abcd2*^{-/-} mice efficaciously suppressed microgliosis (**Fig. 18D-F, 18B'**) and astrocytosis (**Fig. 18G-I, 18C'**). Moreover, synaptophysin (**Fig. 18J-L, 18D'**) and APP accumulation (**Fig. 18M-O, 18E'**), and myelin debris were prevented (**Fig. 18P-R**), demonstrating that high-dose biotin halted axonal degeneration in this X-ALD mouse model. Moreover, the treated cohort presented healthier motor neurons (**Fig. 18S-U**), normalized mitochondrial content (**Fig. 18V-X**) and reduced signs of lipoperoxidation (**Fig. 18Y-A'**), confirming the role of high-dose biotin in maintaining redox and metabolic homeostasis in the nervous system in this model.

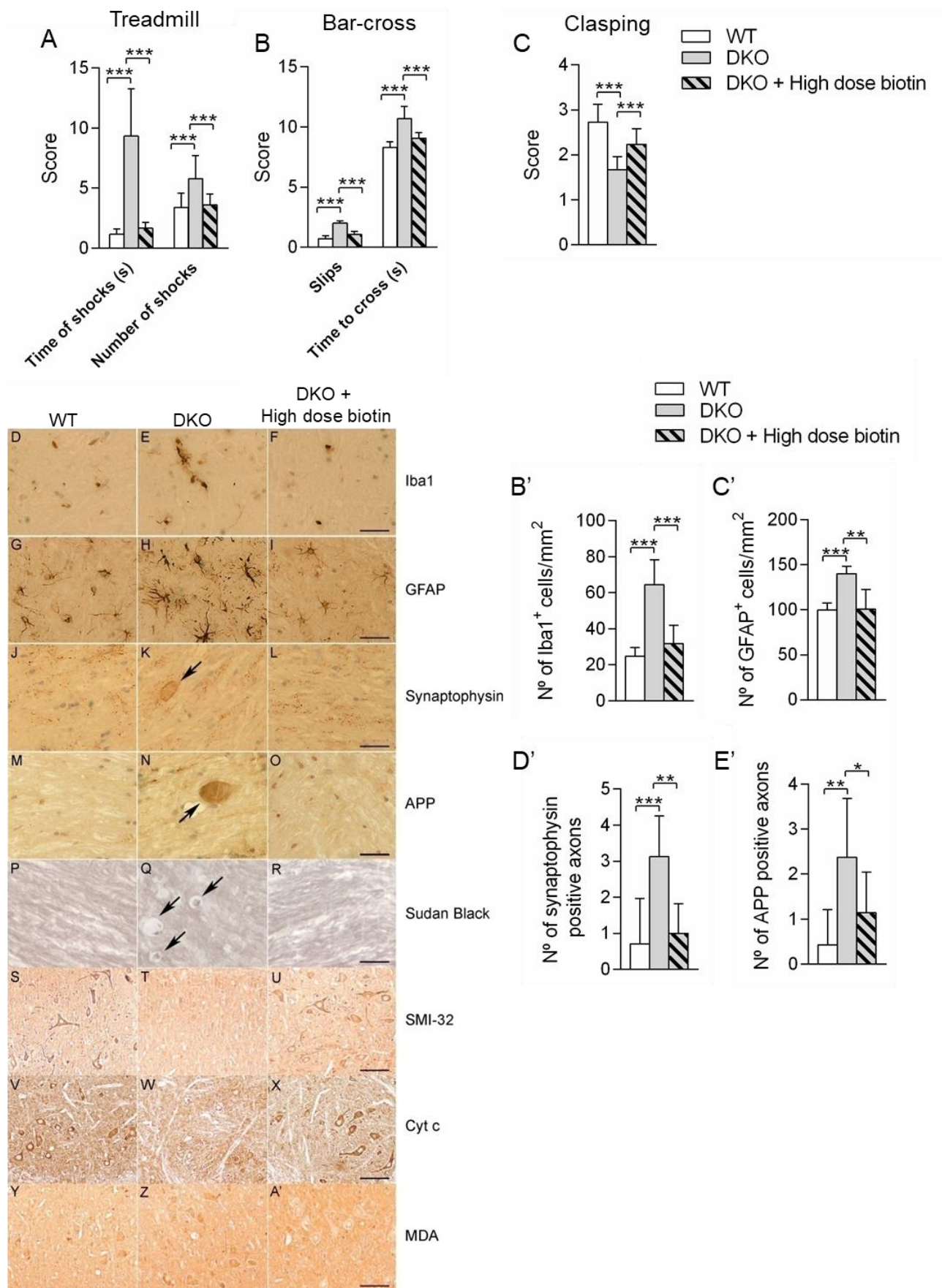


Figure 18. High-dose biotin halts axonal degeneration and locomotor disability in *Abcd1*^{-/-}/*Abcd2*^{-/-} mice

(A) Treadmill test (B) Bar cross test and (C) Clasping test have been carried out in 18-month-old WT (n=13-14), DKO (n=14-16) and DKO + High-dose biotin (n=15-16) mice. (A) The latency to falling off the belt (time of shocks) and the number of shocks received were computed after 5 minutes. (B) The time spent to cross the bar and the numbers of slips were quantified. (C) The best performance score of each animal was taken to quantify (Dumser et al., 2007). Immunohistological analysis of axonal pathologies performed in 18-month-old WT, *Abcd1^{-/-}/Abcd2^{-/-}* (DKO) and *Abcd1^{-/-}/Abcd2^{-/-}* mice treated with high-dose biotin (DKO + High-dose biotin) (n=5/genotype and condition). Spinal cord sections were processed for (D-F) Iba1, (G-I) GFAP, (J-L) synaptophysin, (M-O) APP, (P-R) Sudan black, (S-U) SMI-32, (V-X) cytochrome c and (Y-A') MDA. Representative images (D, G, J, M, P, S, V and Y) for WT, (E, H, K, N, Q, T, W and Z) for DKO and (F, I, L, O, R, U, X and A') for DKO + High-dose biotin mice are shown. Scale bar=25um. Quantification of (B') Iba1⁺ density (cells/mm²), (C') GFAP⁺ density (cells/mm²) and (D') synaptophysin and (E') APP accumulation in spinal cord sections of WT, DKO and DKO + High-dose biotin mice. For (B') and (C') WT (n=5), DKO (n=5) and DKO + High-dose biotin (n=4). For (D') and (E') WT (n=7), DKO (n=8) and DKO + High-dose biotin (n=7). Values are expressed as mean ± SD. (A-E') * *p*<0.05; ** *p*<0.01; *** *p*<0.001; one-way ANOVA followed by Fisher's *post hoc* test.

In summary, in X-ALD, high-dose biotin is efficacious in correcting the molecular drivers of disrupted lipid homeostasis in the nervous system, which may eventually lead to axonal demise (**Fig. 19**).

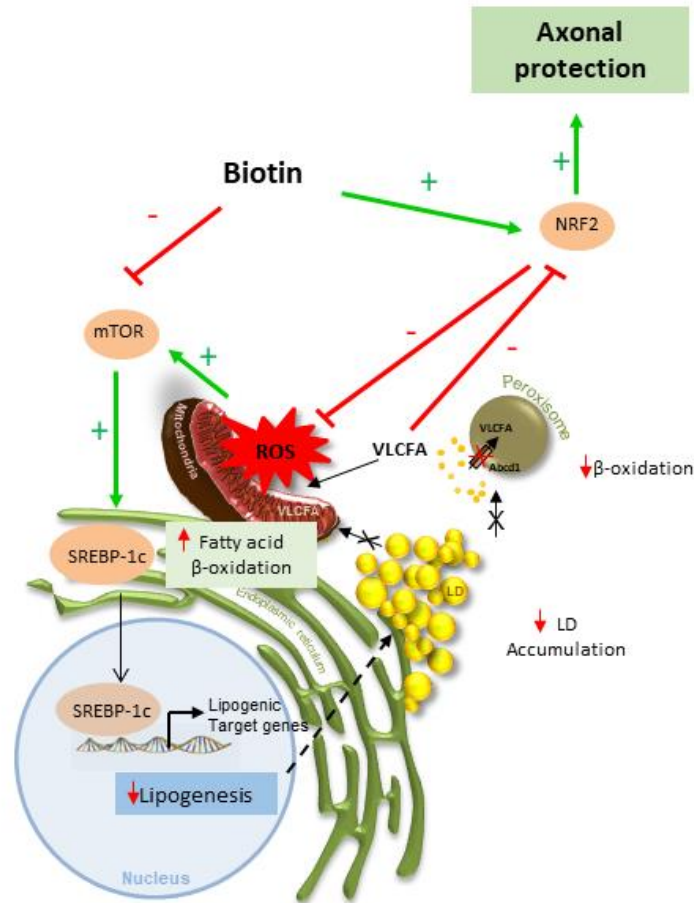


Figure 19. Model recapitulating high-dose biotin’s mode of action in X-ALD

The lipid droplet accumulation in X-ALD may obey to a combination of different factors: i) increase of the formation of lipid droplets by increased lipid synthesis driven by mTOR/SREBP-1c; ii) decrease of the lipid droplet degradation capacity by the mitochondria, due to fewer mitochondria number and lower FAO, the later driven by mTOR/SREBP-1c, and iii) the impossibility of the peroxisome to degrade some of the TAG due to the loss of ABCD1, shown to be a key element in the tethering of LDs to the peroxisomes (Chang et al., 2019). High-dose biotin restores redox imbalance through reactivation of the NRF2 response and normalizes the mTOR/SREBP-1c transcriptional program, thus reestablishing lipid homeostasis.

4.2 Chapter II: study of the role of transcription factor E2F1 in X-ALD pathophysiology: neuroprotective effect of E2F1 deletion in X-ALD mouse models

4.2.1 E2F1 expression is elevated in *Abcd1*⁻ mice spinal cord

A transcriptomic functional analysis carried out in X-ALD mice and human patients unravelled a common metabolic abnormality signature, characterized, among other pathways, by mitochondrial dysregulation (Schluter et al., 2012). As the transcription factor E2F1 regulates the expression of oxidative metabolism genes and mitochondrial activity (Blanchet et al., 2011), we decided to explore the role of E2F1 in X-ALD. We found out increase of both *E2f1* mRNA and protein levels in 12-month-old *Abcd1*⁻ mice spinal cord (**Fig. 20A-B**) as well as in 12-month-old *Abcd1*⁻/*Abcd2*^{-/-} mice (**Fig. 20C**). The overexpression of E2F1 is organ-specific as we did not observe any change in non-affected tissues in this mouse model, such as cerebellum, cortex, hippocampus, pons and liver (**Fig. 20D**). To finish, we obtained results suggesting that E2F1 is induced in a redox-dependent mechanism in X-ALD as: i) its expression was increased in human skin-derived fibroblasts upon C26:0 addition (**Fig. 20E**), and ii) *Abcd1*⁻ mice treated with a combination of antioxidants, a treatment that halts axonal degeneration and prevents locomotor deficits (Lopez-Erauskin et al., 2011), showed normalization of the increased E2F1 expression in the spinal cord (**Fig. 20F**).

4.2.2 E2F1 deletion prevents mitochondrial depletion and bioenergetic failure in X-ALD mice

Since E2F1 is a master regulator of mitochondrial biogenesis, we sought to determine the effect of this transcription factor deletion on mitochondrial dysfunction present in *Abcd1*⁻ mouse spinal cord at 12 months of age. Loss of E2F1 normalized mtDNA levels (**Fig. 21A**), and mitochondrial biogenesis associated-genes mRNA expression (*Nrf1*, *Pgc-1a*, *Pgc-1b*, *Pparg*, *Sirt1* and *Tfam*) (**Fig. 21B**). To determine whether E2F1 affects mitochondrial function in the spinal cord, we carried out high-resolution respirometry using Oroboros technology. Loss of E2F1 normalized oxygen consumption after the addition of ADP and ADP + succinate (C. I state 3 and C. I + II state 3) and normalized the respiratory control ratio (R.C.R) (**Fig. 21C**), which is associated to the

normalization of ATP levels (**Fig. 21D**) in the spinal cord of 12-month-old *Abcd1*⁻ mice. Altogether, these findings illustrate that loss of E2F1 prevented mitochondrial depletion and malfunction and ameliorated the bioenergetic deficits present in *Abcd1*⁻ mice spinal cord.

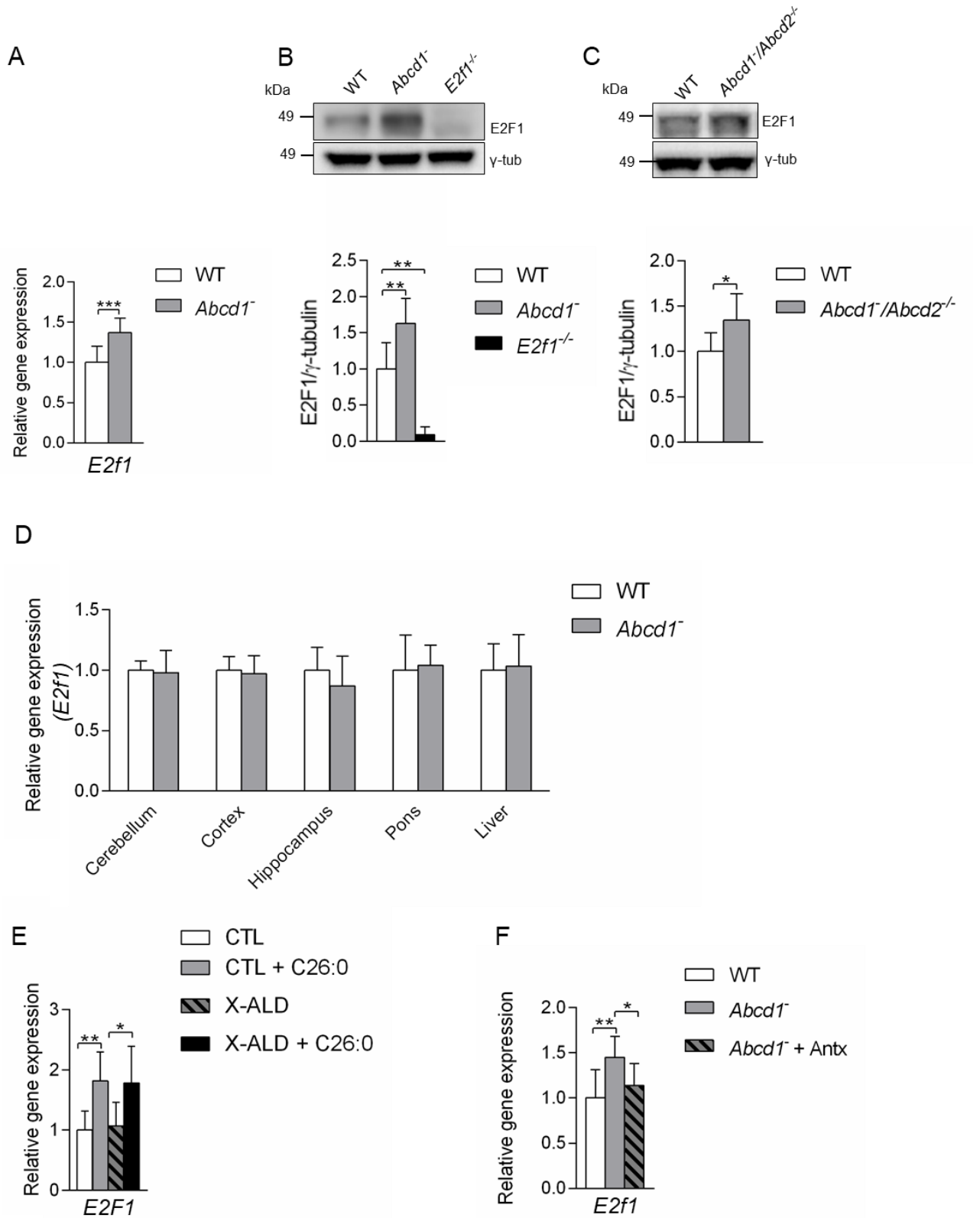


Figure 20. E2F1 induction in X-ALD

(A) *E2f1* mRNA expression was measured by quantitative RT-PCR in WT (n=11) and *Abcd1*⁻ (n=10) mice spinal cord at 12 months of age. Gene expression was normalized relative to *Rplp0*. (B) Representative immunoblot showing E2F1 protein levels in WT (n=5), *Abcd1*⁻ (n=5) and *E2f1*^{-/-} (n=4) mice spinal cord at 12 months of age. Protein levels were normalized relative to γ -tubulin (γ -tub). (C) Representative immunoblot showing E2F1 protein levels in WT (n=6) and *Abcd1*⁻/*Abcd2*^{-/-} (n=6) mice spinal cord at 12 months of age. Protein levels were normalized relative to γ -tubulin (γ -tub). (D) *E2f1* mRNA expression was measured by quantitative RT-PCR in cerebellum, cortex, hippocampus, pons and liver of 12-month-old WT (n=8) and *Abcd1*⁻ (n=8) mice. Gene expression was normalized relative to *Rplp0*. Values are expressed as mean \pm SD and quantifications depicted as fold change to WT mice. (E) *E2f1* mRNA expression was measured by quantitative RT-PCR in CTL (n=7) and X-ALD human fibroblasts (n=6) after 24h with vehicle as control or C26:0 in medium containing 10% FCS. Gene expression was normalized relative to *RPLP0*. Quantification depicted as fold change to vehicle-treated fibroblasts. Values are expressed as mean \pm SD. (F) *E2f1* mRNA expression was measured by quantitative RT-PCR in WT (n=7), *Abcd1*⁻ (n=7) and *Abcd1*⁻ + Antx (n=6) mice spinal cord at 12 months of age. Gene expression was normalized relative to *Rplp0*. Values are expressed as mean \pm SD and quantifications depicted as fold change to WT mice. (A, C) * $p < 0.05$; *** $p < 0.001$; unpaired Student's t-test. (B) ** $p < 0.01$; one-way ANOVA followed by Fisher's *post hoc* test. (E) * $p < 0.05$; ** $p < 0.01$; two-way ANOVA followed by pairwise comparisons on the estimated marginal means *post hoc*.

4.2.3 Loss of E2F1 prevents inflammatory imbalance in *Abcd1*⁻ mice spinal cord

Abcd1⁻ mice and AMN patients present a low-grade inflammatory dysregulation associated with NF- κ B pathway activation (Ranea-Robles et al., 2018; Ruiz et al., 2015; Schluter et al., 2012). Thereby, we decided to examine the effects of the lack of E2F1 on the mRNA expression of several inflammation-related genes in the *Abcd1*⁻ mice spinal cord at 12 months of age. We revealed that the lack of E2F1 normalized mRNA levels of some pro-inflammatory chemokines such as *Il1b*, *Il6*, *Nfkb2*, *Tnfa* and *Tnfrsf1a* (Fig. 22A). Moreover, E2F1 deletion in *Abcd1*⁻ mice restored the mRNA expression of anti-inflammatory genes like *Arg1*, *Cxcl12* and *Tgfb1* (Fig. 22B). Collectively, these data demonstrate that lack of E2F1 ceased NF- κ B pathway-mediated inflammatory profile in *Abcd1*⁻ mice.

4.2.4 E2F1 deletion restores lipid homeostasis in *Abcd1* null mice

We earlier showed a disrupted lipid homeostasis defined as an augmented expression of genes of the lipid synthesis pathway and a dampened expression of the FAO pathway genes, all driven by an impaired SREBP-1c signalling, in 12-month-old *Abcd1*⁻ mice spinal cord. As a consequence, excess of lipids such as TAGs, accumulate in the form of LDs in motor neurons (Fourcade et al., 2020). This metabolic dysfunction is suggested to contribute to the chronic axonal degeneration in X-ALD as shown in recent publications from our group (Coppa et al., 2020; Fourcade et al., 2020). In this study, we revealed that the deletion of E2F1 resulted in the i) repression of the lipogenesis pathway (**Fig. 23A**) and ii) upregulation of the FAO pathway (**Fig. 23B**) in mitochondria and peroxisomes in *Abcd1*⁻ mice spinal cords. Staining of LDs by ORO is reduced in neuronal somas in the ventral horn of *Abcd1*⁻/*E2f1*^{-/-} mice spinal cord (**Fig. 23C-O**), which correlates with the normalization of the total level of TAGs (**Fig. 23P**). Moreover, increased levels of the active form of mTOR, P-mTOR, present in the *Abcd1*⁻ mice were normalized in the *Abcd1*⁻/*E2f1*^{-/-} double knockout mice (**Fig. 23Q**).

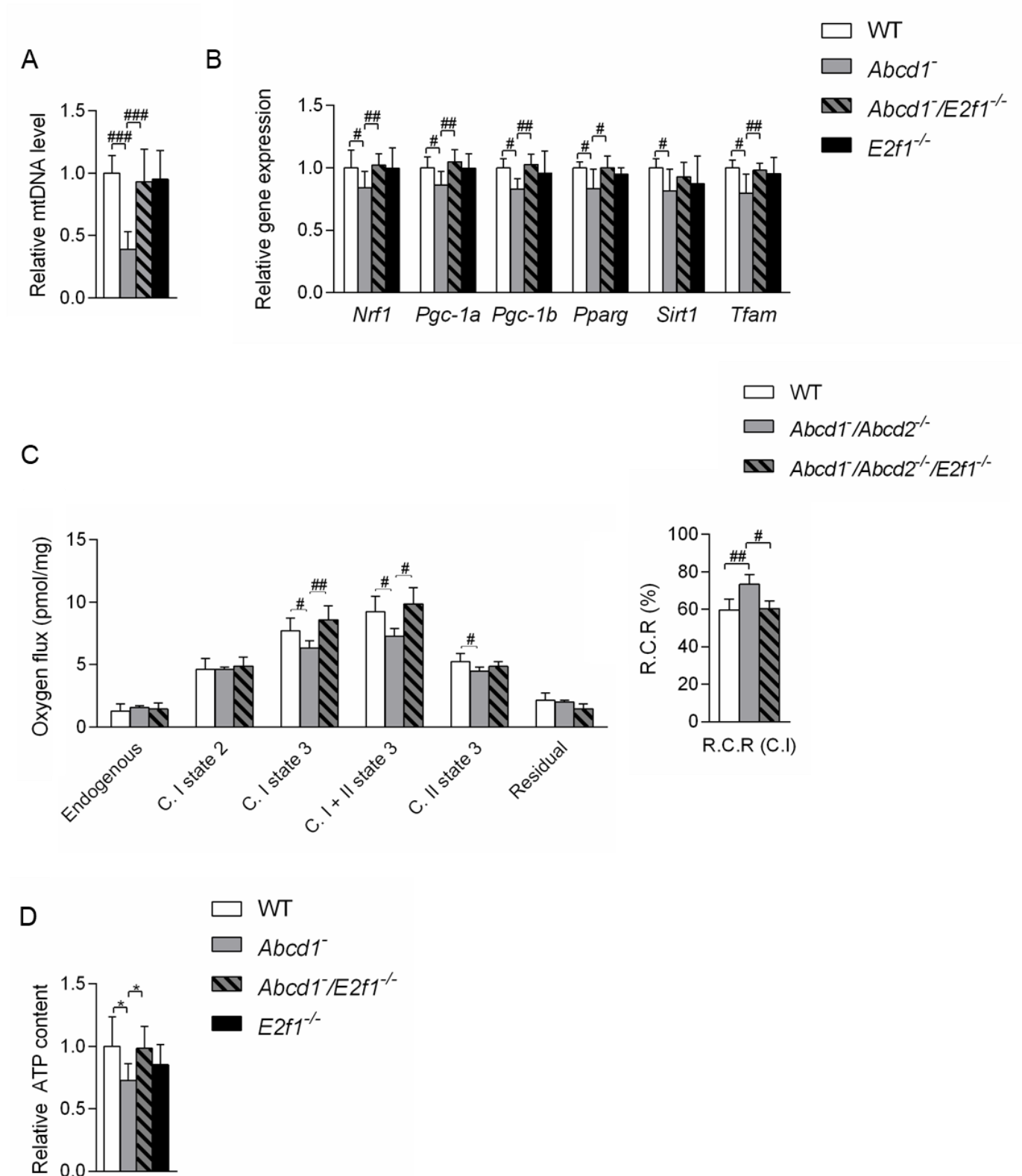


Figure 21. E2F1 deletion rescues mitochondrial biogenesis and prevents energetic failure in *Abcd1* mice spinal cord

(A) mtDNA content analyzed by quantitative RT-PCR in WT (n=10), *Abcd1*^{-/-} (n=10), *Abcd1*^{-/-}/*E2f1*^{-/-} (n=12) and *E2f1*^{-/-} (n=10) mice and expressed as the ratio of mtDNA to nuclear DNA (mtDNA/nDNA). (B) *Nrf1*, *Pgc-1a*, *Pgc-1b*, *Pparg*, *Sirt1* and *Tfam* relative gene expression analyzed by quantitative RT-PCR in WT (n=9), *Abcd1*^{-/-} (n=9), *Abcd1*^{-/-}/*E2f1*^{-/-} (n=10) and *E2f1*^{-/-} (n=7) mice. Gene expression was normalized relative to mouse *Rplp0*. Quantification depicted as fold change to WT mice. (C) *Ex vivo* mitochondrial respiration analysis performed on permeabilized spinal cord sections of 12-month-old WT (n=11), *Abcd1*^{-/-}/*Abcd2*^{-/-} (n=5) and *Abcd1*^{-/-}/*Abcd2*^{-/-}/*E2f1*^{-/-} (n=6) mice. (C. I = complex I. C. II = complex II. RCR = respiratory control ratio). (D) ATP content in WT (n=7), *Abcd1*^{-/-} (n=7), *Abcd1*^{-/-}/*E2f1*^{-/-} (n=7) and *E2f1*^{-/-} (n=6) mice. Data shown as fold change respect to WT mice. Values are expressed as mean ± SD. (A-C) # *p*<0.05; ## *p*<0.01; ### *p*<0.001; non-parametric Kruskal–Wallis’ test followed by Dunn’s *post hoc* test. (D) * *p*<0.05; two-way ANOVA followed by pairwise comparisons on the estimated marginal means *post hoc* test.

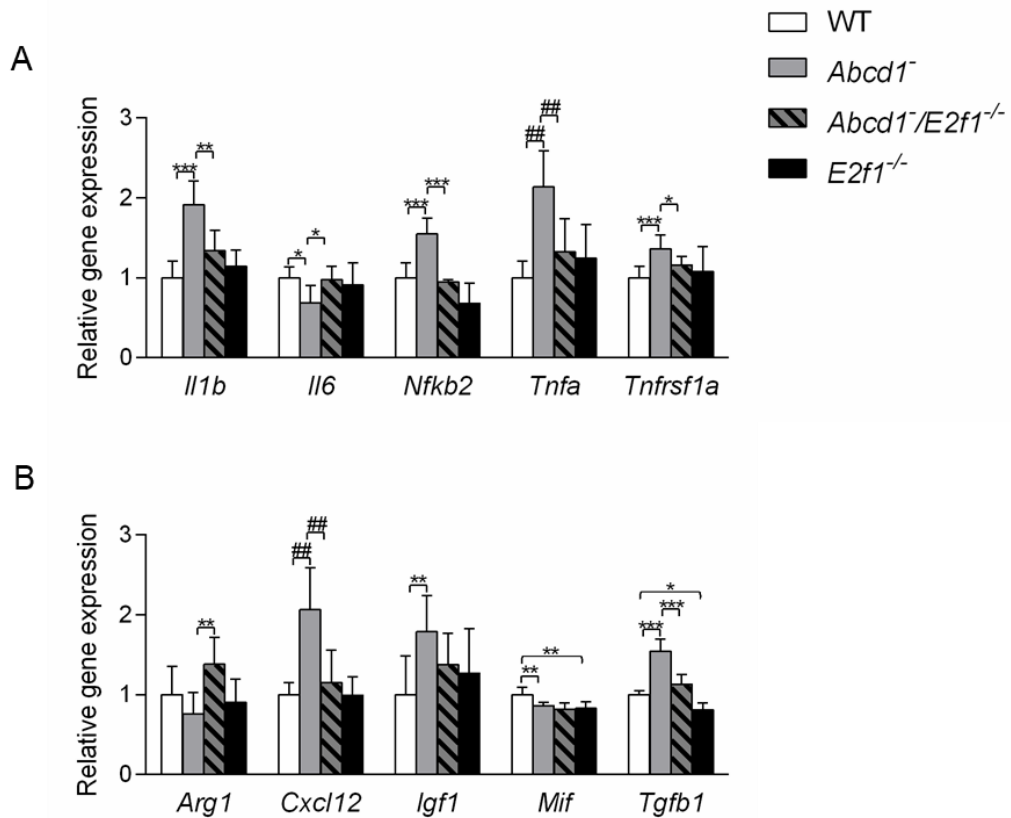


Figure 22. E2F1 deletion normalizes inflammatory genes expression in X-ALD mouse spinal cord

(A) Pro-inflammatory (*Il1b*, *Il6*, *Nfkb2*, *Tnfa* and *Tnfrsf1a*) and (B) anti-inflammatory (*Arg1*, *Cxcl12*, *Igf1*, *Mif* and *Tgfb1*) gene expression in WT (n=8), *Abcd1*⁻ (n=7), *Abcd1*⁻/*E2f1*^{-/-} (n=7) and *E2f1*^{-/-} (n=7) mice spinal cord at 12 months of age. mRNA expression was measured by quantitative RT-PCR. Gene expression was normalized relative to *Rplp0*. Quantification depicted as fold change to WT mice. Data are shown as mean ± SD. (A-B) * $p < 0.05$; ** $p < 0.01$; *** $p < 0.001$; two-way ANOVA followed by pairwise comparisons on the estimated marginal means *post hoc* test or ^{##} $p < 0.01$; non-parametric Kruskal-Wallis test followed by Dunn's *post hoc* test.

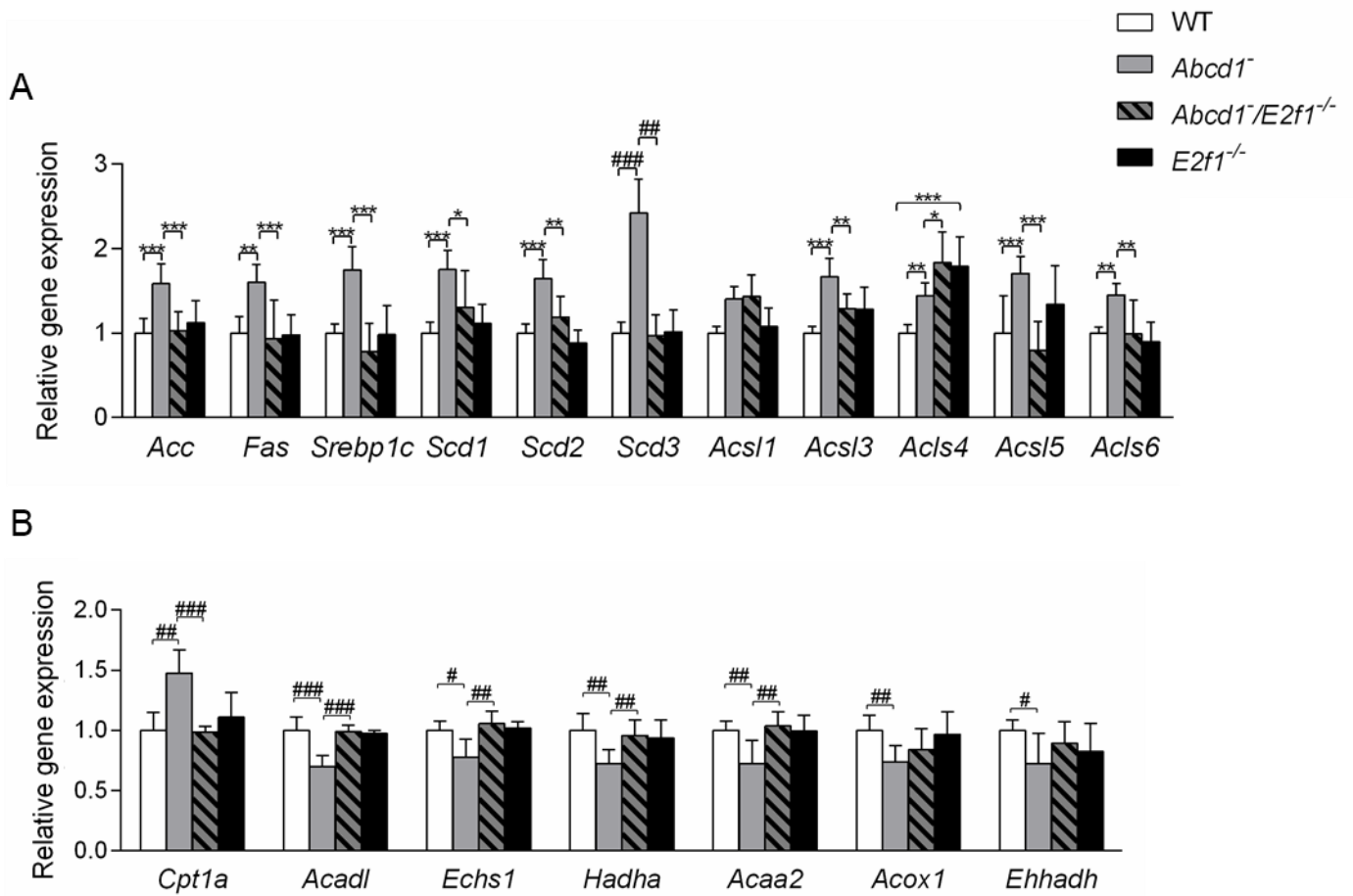


Figure 23. E2F1 deletion inhibits lipogenesis, induces β -oxidation and normalizes excess of lipid droplet accumulation in *Abcd1*⁻ mice

Relative gene expression of enzymes involved in (A) lipogenesis (*Acc*, *Fas*, *Srebp1c*, *Scd1*, *Scd2*, *Scd3*, *Acsl1*, *Acsl3*, *Acsl4*, *Acsl5* and *Acsl6*) in WT (n=8), *Abcd1*⁻ (n=8), *Abcd1*⁻/*E2f1*^{-/-} (n=5) and *E2f1*^{-/-} (n=6) mice and (B) mitochondrial and peroxisomal FAO (*Acaa2*, *Acadl*, *Cpt1a*, *Echs1*, *Hadha*, *Acox1* and *Ehhadh*) in WT (n=7), *Abcd1*⁻ (n=7), *Abcd1*⁻/*E2f1*^{-/-} (n=7) and *E2f1*^{-/-} (n=7) mice. Gene expression was normalized relative to mouse *Rplp0*. Quantification depicted as fold change to WT mice.

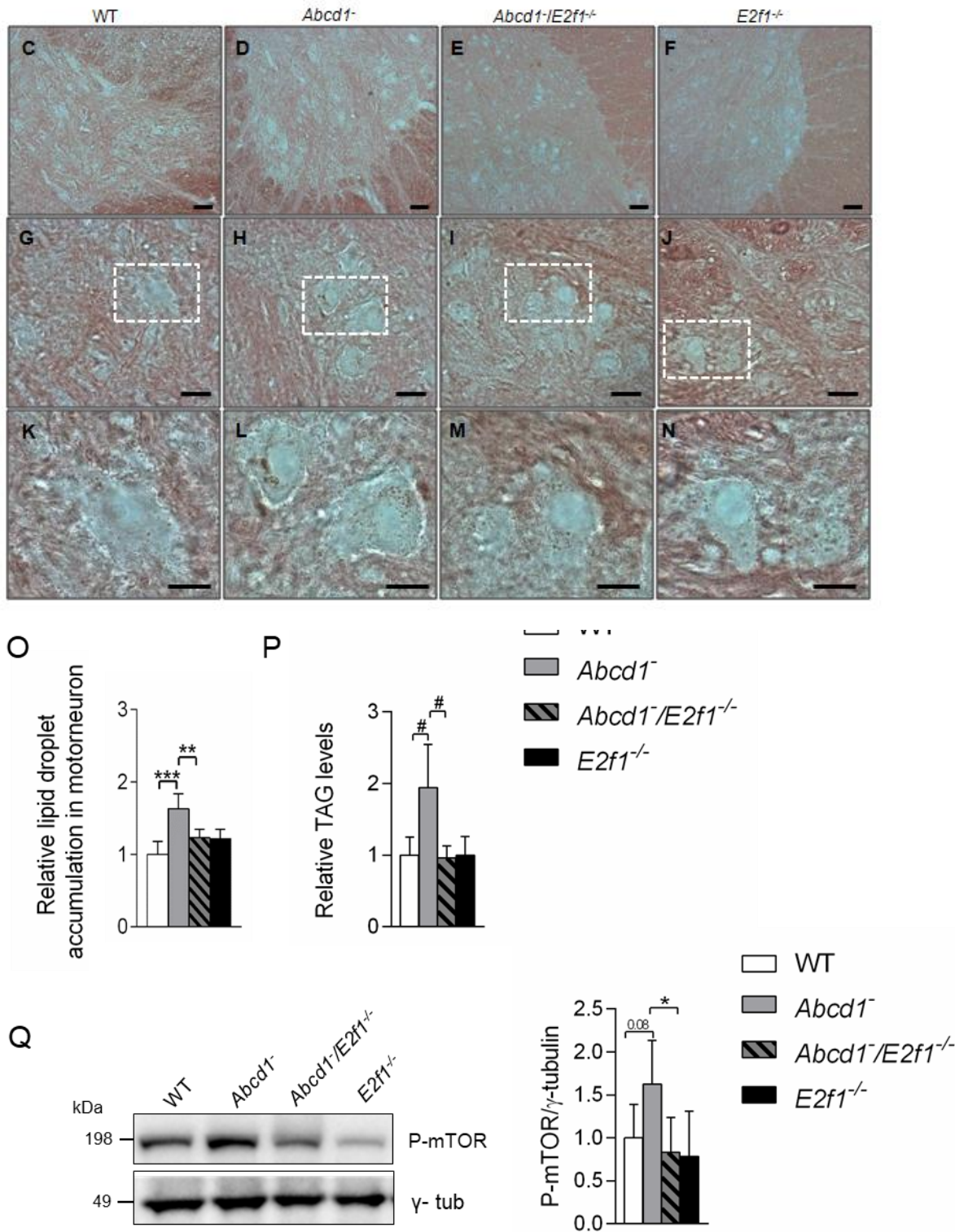


Figure 23. Continued

(C-N) Histological analysis performed in 18-month-old WT (C, G, K), *Abcd1*^{-/-} (D, H, L), *Abcd1*^{-/-}/*E2f1*^{-/-} (E, I, M), and *E2f1*^{-/-} (F, J, N) mice. Spinal cord histological sections were processed for Oil Red O (ORO) (n=4 to 5 per genotype). (O) Quantification of lipid droplet accumulation in spinal cord histological sections in 18-month-old WT, *Abcd1*^{-/-}, *Abcd1*^{-/-}/*E2f1*^{-/-} and *E2f1*^{-/-} mice by ImageJ. Scale bar 50 μm (C-F), scale bar 25 μm (G-J), scale bar 12.5 μm (K-N)

N). Quantification depicted as fold change to WT mice. **(P)** TAG levels in spinal cord of 12-month-old in WT (n=6), *Abcd1*^{-/-} (n=6), *Abcd1*^{-/-}/*E2f1*^{-/-} (n=6) and *E2f1*^{-/-} (n=5) mice. **(Q)** Representative immunoblot showing P-mTOR protein levels in WT (n=4), *Abcd1*^{-/-} (n=5), *Abcd1*^{-/-}/*E2f1*^{-/-} (n=6) and *E2f1*^{-/-} (n=6) mice spinal cord at 12 months of age. Protein content was normalized relative to γ -tubulin and quantification depicted as fold change to WT mice. Values are expressed as mean \pm SD. **(A, O, Q)** * $p < 0.05$; ** $p < 0.01$; *** $p < 0.001$; two-way ANOVA followed by pairwise comparisons on the estimated marginal means *post hoc*. **(A, B, P)** # $p < 0.05$; ## $p < 0.01$; ### $p < 0.001$; non-parametric Kruskal-Wallis test followed by Dunn's *post hoc* test.

4.2.5 E2F1 deletion restores redox homeostasis in *Abcd1* null mice

Dysregulated AKT/GSK-3 β /NRF2 axis is characterized by defective AKT phosphorylation that results in aberrant overactivation of GSK-3 β in the *Abcd1*^{-/-} mice (Ranea-Robles et al., 2018), indicated by reduced pSer9 GSK-3 β compared with total GSK-3 β levels. As a consequence, NRF2-dependent antioxidant response is impaired, allowing extensive oxidative damage. Our experiments demonstrate that the ablation of E2F1 reactivates NRF2 antioxidant pathway in the *Abcd1*^{-/-} mice (**Fig. 24A**) and inhibits GSK-3 β activity (**Fig. 24B**).

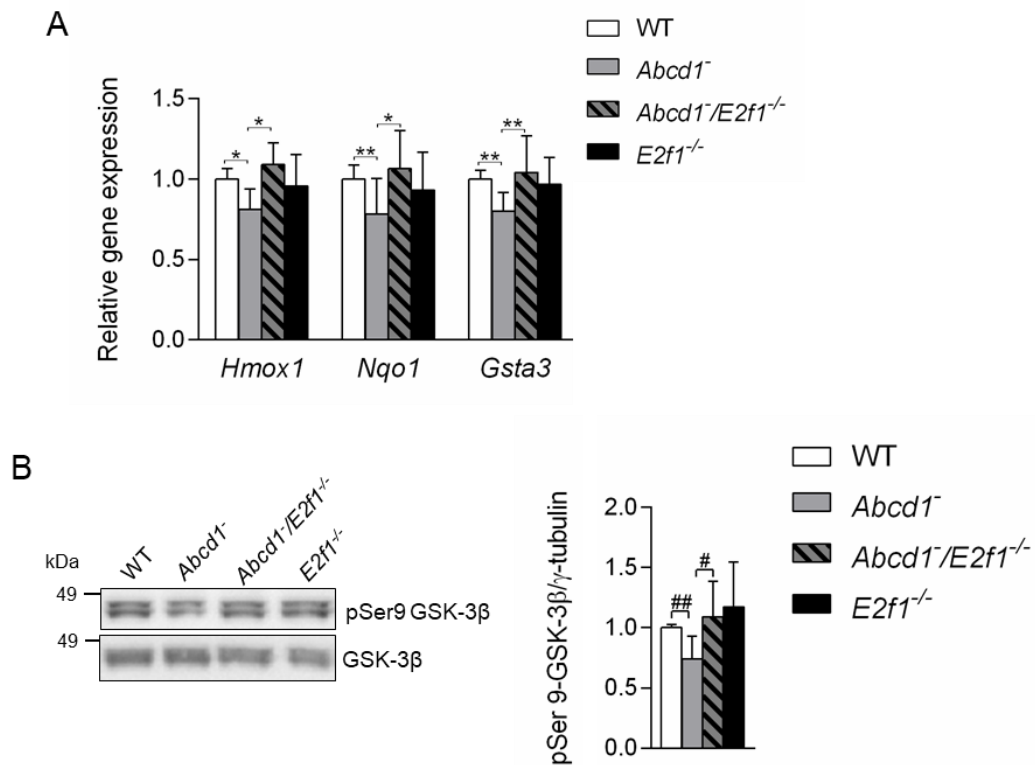


Figure 24. Loss of E2F1 reactivates NRF2-antioxidant pathway in *Abcd1*⁻ mice

(A) *Hmox1*, *Nqo1* and *Gsta3* relative gene expression analyzed by quantitative RT-PCR in WT (n=7), *Abcd1*⁻ (n=7), *Abcd1*⁻/*E2f1*^{-/-} (n=6) and *E2f1*^{-/-} (n=6) mice. Gene expression was normalized relative to mouse *Rplp0*. Quantification depicted as fold change to WT mice. (B) Representative immunoblot showing pSer9 GSK-3β and GSK-3β protein levels in WT (n=5), *Abcd1*⁻ (n=5), *Abcd1*⁻/*E2f1*^{-/-} (n=6) and *E2f1*^{-/-} (n=5) mice spinal cord at 12 months of age. Protein levels were normalized relative to non-phosphorylated form and quantification depicted as fold change to WT mice. Values are expressed as mean ± SD. (A) * $p < 0.05$; ** $p < 0.01$; two-way ANOVA followed by pairwise comparisons on the estimated marginal means *post hoc*. (B) # $p < 0.05$; ## $p < 0.01$; non-parametric Kruskal-Wallis test followed by Dunn's *post hoc* test.

4.2.6 E2F1 deficiency halts axonal degeneration and neurological symptoms of *Abcd1*⁻/*Abcd2*^{-/-} mice

With the aim of evaluating the therapeutic potential of E2F1 inhibition, we studied the effect of E2F1 deletion on axonal degeneration and associated locomotor deficits exhibited by the X-ALD mouse (Pujol et al., 2004). We used double mutants of *Abcd1* and its closest homolog gene *Abcd2*, the *Abcd1*⁻/*Abcd2*^{-/-} mouse model, as they present a more severe and earlier AMN-like phenotype, what makes them more suitable for therapeutic assays. Triple mutants, *Abcd1*⁻/*Abcd2*^{-/-}/*E2f1*^{-/-}, were generated and animals

were challenged with two locomotor tests. As previously reported (Ferrer et al., 2005; Launay et al., 2015; Launay et al., 2017; Lopez-Erauskin et al., 2011; Morato et al., 2013; Morato et al., 2015; Pujol et al., 2004), DKO mice performed worse than WT in the treadmill test (**Fig. 25A**), as the total number and duration of shocks were higher than in WT under conditions of high speed and high slope. When subjected to the test, *Abcd1⁻/Abcd2⁻/E2f1⁻* mice performed similar to WT mice (**Fig. 25A**). Regarding bar cross test, while DKO mice took a longer time to cross the bar and slipped off more times, triple knockout executed the test identical to control mice (**Fig. 25B**). In conclusion, deletion of E2F1 halted locomotor impairment observed in *Abcd1⁻/Abcd2⁻* mice.

Finally, to assess the effects of E2F1 deletion on axonal degeneration, we examined the signs of X-ALD neuropathology present in *Abcd1⁻/Abcd2⁻* mice by immunohistochemical techniques. These features include i) microgliosis (Iba1); ii) astrocytosis (GFAP); iii) axonal degeneration, determined by the accumulation of amyloid precursor protein (APP) and synaptophysin in axons; iv) lipidic myelin debris, depicted by Sudan Black staining (Pujol et al., 2004); v) oxidative damage to lipids indicated by MDA staining (Lopez-Erauskin et al., 2011); vi) damage to motor neurons, reflected by reduced SMI-32 signal, an indicator of disturbed neurofilament in motor neurons; and vii) mitochondrial depletion, featured by decreased cytochrome c (cyt c) staining in motor neurons (Morato et al., 2013).

Lack of E2F1 in *Abcd1⁻/Abcd2⁻* mice reversed microgliosis (**Fig. 25C-E, A'**), and astrocytosis (**Fig. 25F-H, B'**), prevented the accumulation of synaptophysin (**Fig. 25I-K, C'**) and APP in axons (**Fig. 25L-N, D'**), blocked the appearance of myelin debris along the spinal cord (**Fig. 25O-Q**), ameliorated mitochondrial content (**Fig. 25R-T**), attenuated oxidative damage (**Fig. 25U-W**) and improved motor neuron health (**Fig. 25X-Z**). Overall, the absence of E2F1 halted axonal degeneration and prevented the onset of neurological symptoms in *Abcd1⁻/Abcd2⁻* mice.

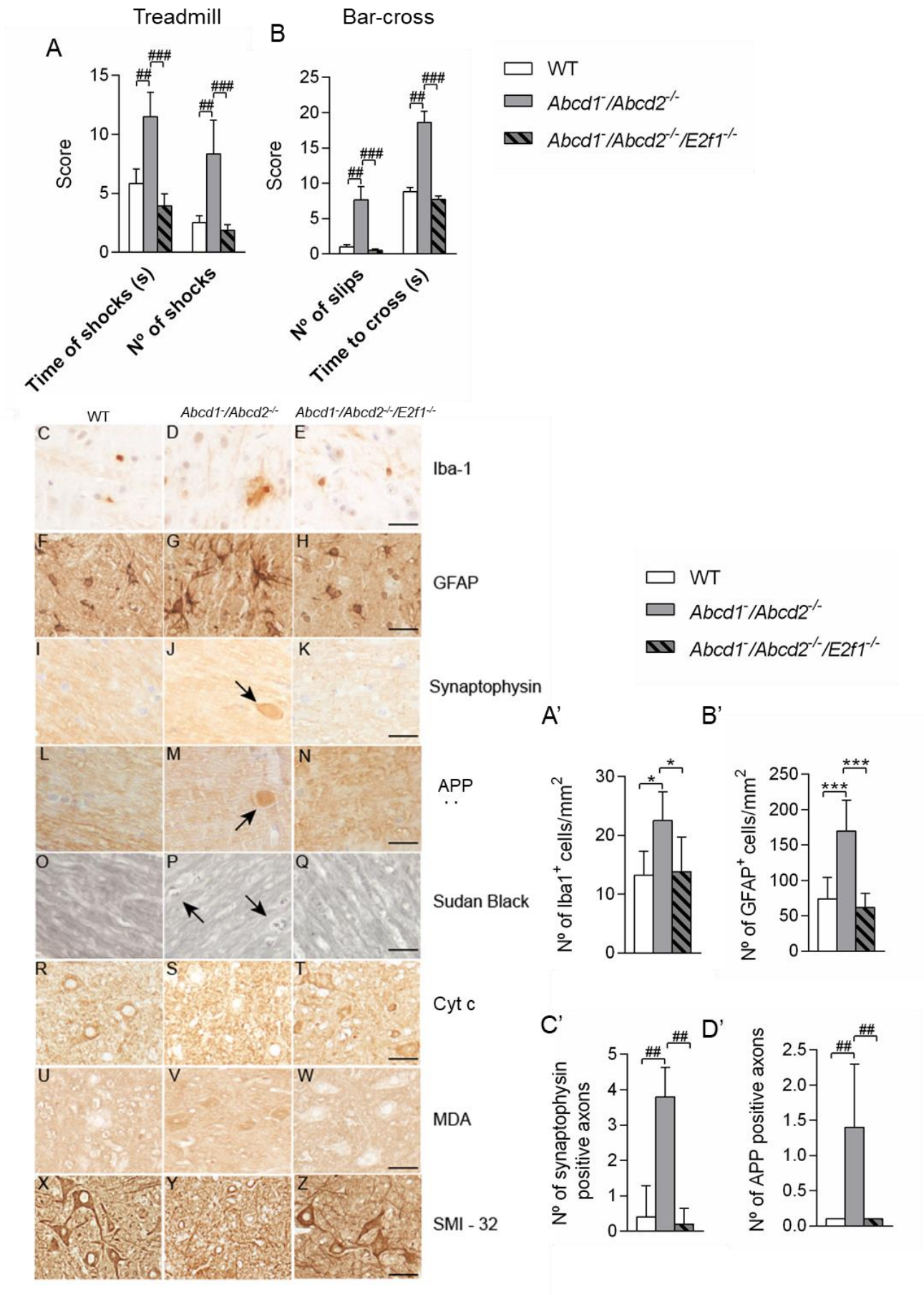


Figure 25. Loss of E2F1 halts axonal degeneration and locomotor disability in *Abcd1*/*Abcd2*⁻ mice

(A) Treadmill and (B) Bar cross tests have been carried out at in 18-month-old WT, *Abcd1*⁻/*Abcd2*⁻ and *Abcd1*⁻/*Abcd2*⁻/*E2f1*⁻ mice (n=10 to 14 per genotype). (A) The latency to falling off the belt (time of shocks) and the number of shocks received were computed after 5 minutes. (B) The time spent to cross the bar and the numbers of slips were quantified. (C-Z) Immunohistological analysis of axonal pathologies performed in 18-month-old WT, *Abcd1*⁻/*Abcd2*⁻ and *Abcd1*⁻/*Abcd2*⁻/*E2f1*⁻ mice (n=5 per genotype). Spinal cord sections were processed for (C-E) Iba1, (F-H) GFAP, (I-K) synaptophysin, (L-N) APP, (O-Q) Sudan black, (R-T) cytochrome c, (U-W) MDA and (X-Z) SMI-32. Representative images (C, F, I, L, O, R, U and X) for WT, (D, G, J, M, P, S, V and Y) for *Abcd1*⁻/*Abcd2*⁻ and (E, H, K, N, Q, T, W and Z) for *Abcd1*⁻/*Abcd2*⁻/*E2f1*⁻ mice are shown. Scale bar=25um. Quantification of (A') Iba1⁺ density (cells/mm²) (n=4 to 5 per genotype), (B') GFAP⁺ density (cells/mm²) (n=4 to 5 per genotype), (C') synaptophysin and (D') APP accumulation (n=7 to 8 per genotype) in spinal cord sections of 18-month-old WT, *Abcd1*⁻/*Abcd2*⁻ and *Abcd1*⁻/*Abcd2*⁻/*E2f1*⁻ mice. Values are expressed as mean ± SD. (A-B) ^{##} *p*<0.01; ^{###} *p*<0.001; non-parametric Kruskal-Wallis test followed by Dunn's *post hoc* test. (A'-D') * *p*<0.05; ** *p*<0.01; *** *p*<0.001; one-way ANOVA followed by Fisher's *post hoc* test.

In summary, with this work, we describe that the lack of E2F1 exerts neuroprotection in X-ALD. Impaired lipid metabolism and redox homeostasis are reestablished as the NRF2 endogenous antioxidant pathway is reactivated and the overactivated mTOR/SREBP-1c transcriptional program is normalized preventing lipid-driven axonal demise in X-ALD (Fig. 26).

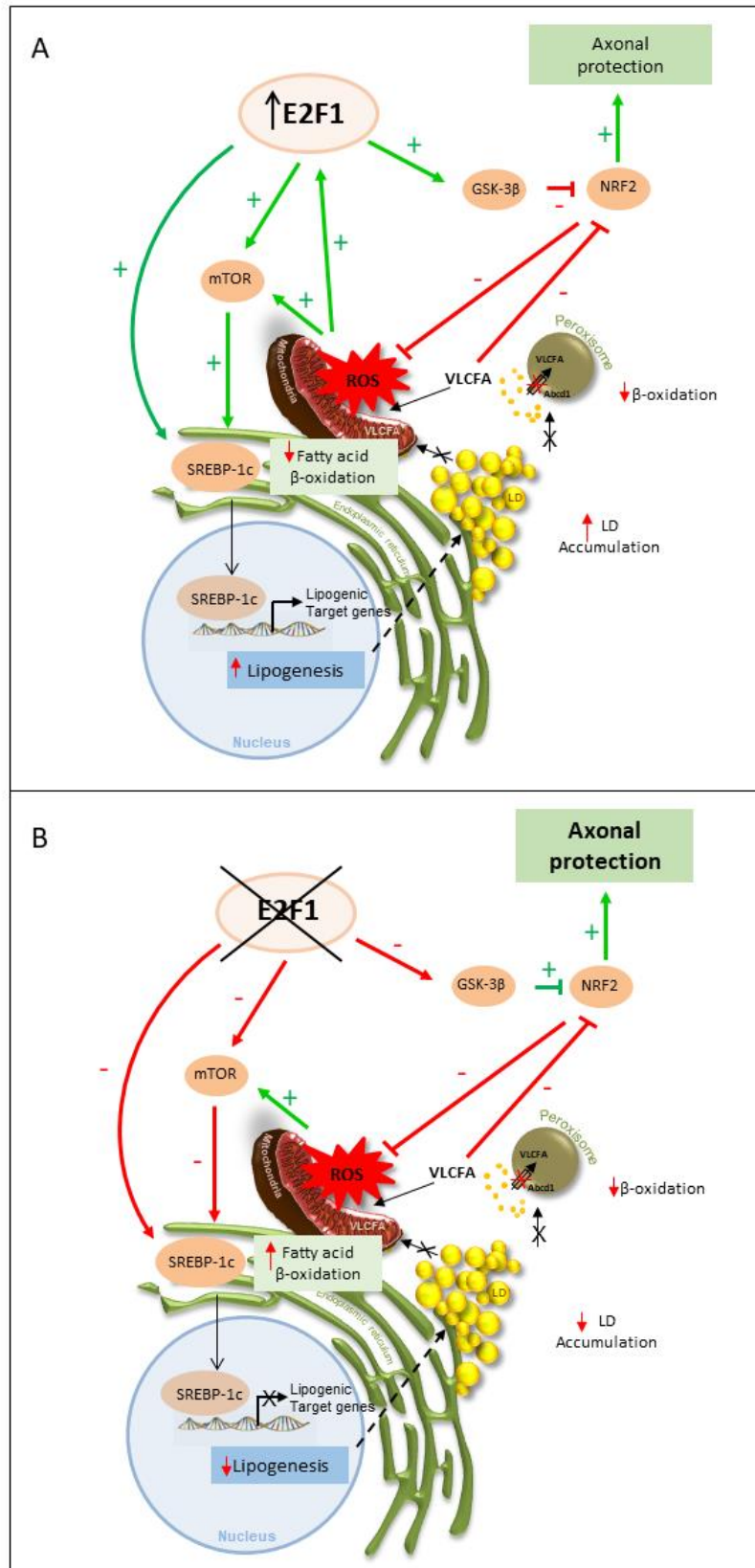


Figure 26. Model illustrating E2F1-dependent effects in X-ALD

(A) In X-ALD, VLCFA-dependent ROS induces E2F1 expression. LDs are accumulated most probably by a combination of different factors: i) increased lipid synthesis driven by upregulation of mTOR/SREBP-1c axis; ii) decrease of the LD degradation capacity by the mitochondria, due to fewer mitochondria number and lower FAO, the later driven by impaired mTOR/SREBP-1c axis, and iii) the impossibility of the peroxisome to degrade some of the TAGs due to the loss of ABCD1, shown to be a key element in the tethering of LDs to the peroxisomes (Chang et al., 2019). (B) Inhibition of E2F1 restores redox imbalance by reactivating NRF2-antioxidant response, through inactivation of GSK-3 β , and normalizes the mTOR/SREBP-1c transcriptional program by i) reducing mTOR activity and ii) inhibiting transcription of SREBP-1c, thus reestablishing lipid homeostasis.

4.2.7 *Abcd1*/*Abcd2*^{-/-}/*E2f1*^{-/-} bone marrow-derived cells are equally engrafted in WT and *Abcd1*/*Abcd2*^{-/-} mice

Bone marrow transplantation with HSCs is able to arrest demyelination in ccALD patients (Cartier et al., 2009) and prevents signs of neurodegeneration in X-ALD mouse models (Ruffert, 2012; P026). In this study, we have observed that the elimination of E2F1 normalizes the phenotype and prevents neurodegeneration in the X-ALD mouse. Moreover, E2F1 has a high expression in the bone marrow. To assess the impact of E2F1 in the CNS, *Abcd1*/*Abcd2*^{-/-} (DKO) mice were transplanted with bone marrow cells extracted from *Abcd1*/*Abcd2*^{-/-}/*E2f1*^{-/-} (TKO) mice (*Abcd1*/*Abcd2*^{-/-} + *BMtko*). By following the repopulation of the CNS by BM-derived cells, this approach will permit us to determine the role of E2F1 in BM-derived cells and to identify which cells are involved in the neurodegenerative cascade in X-ALD. First of all, for setting up the conditions (dose of the administered irradiation, injected cell concentration, evaluation of engraftment capacity, etc.) both WT and DKO mice were transplanted with TKO mice bone marrow cells. At the same time, these experiments were crucial to verify whether DKO mice present a lower repopulation capacity, compared to wildtype littermates, for the fact of being defective for ABCD1 and ABCD2.

To assess the degree of engraftment in these mice, we performed chimerism determination analysis at 2 and 4 months post-transplantation, the time from which long-term repopulation is considered. To do so, DNA from the submandibular vein blood was extracted and *E2f1*-specific PCR was performed. Results demonstrate that DKO mice (DKO #1 + *BMtko* and DKO #2 + *BMtko*) have equal capacity of engraftment (Fig. 27) to WT counterparts (WT #3 + *BMtko*), meaning that loss of

ABCD1 and ABCD2 does not impair repopulation capacity of the bone marrow. In these mice, the percentage of the E2F1 KO allele determined by the chimerism analysis is around 90%, reflecting that engraftment was successfully obtained. In the case of mice WT #1-2 + *BMtko*, engraftment efficacy was very low or even null. This was associated with some difficulties at the time of injection of the donor bone marrow. We think that the tail vein was obstructed, impeding the correct diffusion of the donor cells, so probably the low degree of engraftment could be due to regeneration of the recipient's bone marrow.

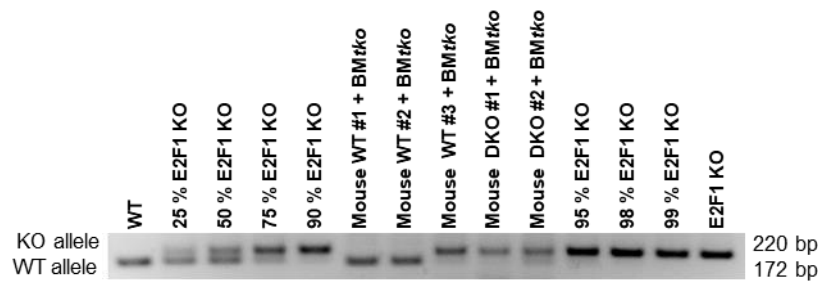


Figure 27. Chimerism determination at 4 months post-transplantation

PCR bands reflecting E2F1 KO allele presence in the transplanted mice. PCR was performed with DNA extracted from submandibular vein blood. Lane 1: reference PCR band from a WT mouse. Lane 2-5: PCR bands of 25%, 50%, 75% and 90% E2F1 KO reference samples correspondingly. Lanes 6-8: PCR bands corresponding to WT mice transplanted with *BMtko*. Lanes 9-10: PCR bands corresponding to *Abcd1*^{-/-}/*Abcd2*^{-/-} mice transplanted with *BMtko*. Lanes 11-13: PCR bands of 95%, 98% and 99% E2F1 KO reference samples correspondingly. Lane 14: reference PCR band from an E2F1 KO mouse.

Follow up of these mice was performed to evaluate any secondary effect of the procedure on their survival. Except for the death of two DKO mice due to an attack coming from one of their siblings and a sudden death of a WT mice, neither reduction in life span nor major health alterations were observed in the transplanted mice, as they were able to reach 18 months of age. The only meaningful observation was the depigmentation of the hair (**Fig. 28B-D**), which appeared in all the mice that underwent irradiation after one month approximately, regardless of their genotype. This effect is associated with the irradiation conditioning, as it has been described that radiation

affects the growth and cycle of hair follicles and melanocytes (McCart et al., 2017; Potten, 1970).

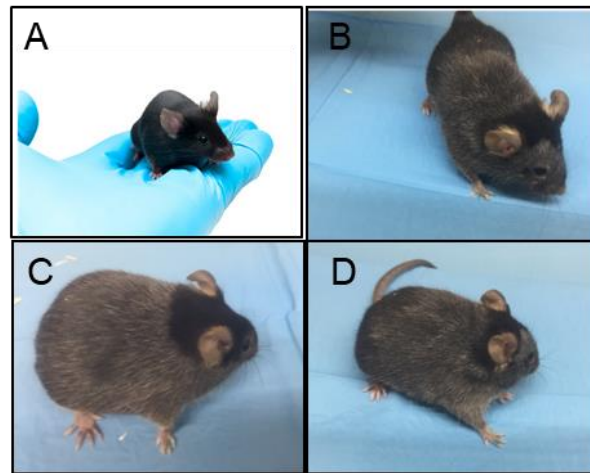


Figure 28. Evaluation of hair depigmentation in irradiated mice

(A) WT C57BL/6J mice. (B-D) WT C57BL/6J mice that underwent irradiation before bone marrow transplantation.

4.2.8 Bone marrow transplantation with *Abcd1*⁻/*Abcd2*⁻/*E2f1*⁻ bone marrow cells in *Abcd1*⁻/*Abcd2*⁻ mice

Once we demonstrated that loss of ABCD1 and ABCD2 does not affect the repopulation capacity of the mice and that bone marrow-derived *Abcd1*⁻/*Abcd2*⁻/*E2f1*⁻ cells can repopulate *Abcd1*⁻/*Abcd2*⁻ mice's bone marrow, we proceeded with the experiment. Hence, *Abcd1*⁻/*Abcd2*⁻ mice were transplanted with bone marrow cells extracted from *Abcd1*⁻/*Abcd2*⁻/*E2f1*⁻ mice (*Abcd1*⁻/*Abcd2*⁻ + BM tko , n=21). To avoid any bias coming from the transplantation itself, WT and *Abcd1*⁻/*Abcd2*⁻ mice were transplanted with bone marrow with the same genotype and these mice were used as the control group (WT + BM wt , n=13) or affected group (*Abcd1*⁻/*Abcd2*⁻ + BM dko , n=20), correspondingly.

Of all the transplanted mice, 88.9% of them survived until the end of the procedure, 18-months of age; meaning that, although the procedure itself is risky and associated with an increased mortality, the transplantation protocol used in these animals does not have profound effects on survival. The results show that the genotype of the injected BM cells does not influence lifespan, as the survival rates were similar among groups:

95.2% in the *Abcd1*⁻/*Abcd2*⁻ + *BMtko* group, 75% in the *Abcd1*⁻/*Abcd2*⁻ + *BMdko* group, and 84.6% in the WT + *BMwt* group (**Fig. 29**).

To detect any undesired effect due to the transplantation procedure in the well-being and global health status of the mice, animals were daily checked by visual observation and body weight was weekly recorded. Food and water intake was also recorded until 4 months post-transplantation, once successful bone marrow transplantation was determined. Despite a slight decrease in the body weight during the first weeks following transplantation, animals maintained a healthy status and showed no major changes by the end of the treatment.

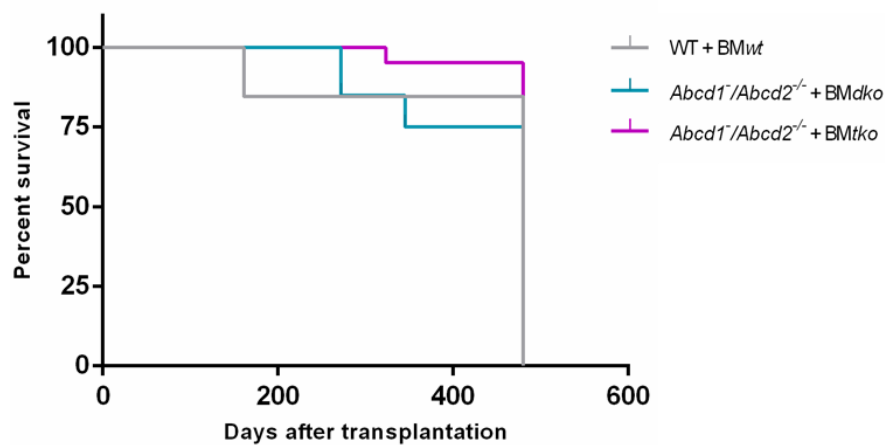


Figure 29. Survival rate after transplantation with BM-derived cells

Kaplan-Meier graph showing the survival rate of mice transplanted with BM-derived cells. WT + *BMwt* mice, blue *Abcd1*⁻/*Abcd2*⁻ + *BMdko* and purple *Abcd1*⁻/*Abcd2*⁻ + *BMtko* mice.

4.2.9 *Abcd1*⁻/*Abcd2*⁻/*E2f1*⁻ bone marrow-derived cells are successfully engrafted in *Abcd1*⁻/*Abcd2*⁻ mice

So far, we can say that bone marrow transplantation was successfully performed and that donor cells were able to repopulate the recipient's bone marrow. Engraftment was assessed by semiquantitative *E2F1* genotyping PCR. Following the presence of the KO allele and evaluating the proportion of intensity between the WT and KO allele, the percentage of *E2F1* KO allele presence in the transplanted mice was inferred. Analysis revealed that in 76% of the transplanted mice, the intensity of the *E2F1* KO allele was

above from the observed in E2F1 heterozygous mice (around 90-95% E2F1 KO), which means that engraftment of the donor bone marrow was efficacious (**Fig. 30A, B**). 19% of the transplanted mice showed a moderate repopulation of the donor BM cells, as equal intensity of the E2F1 WT and KO allele was observed (Mice n° 8, 9, 19 and 21; **Fig. 30A, B**); and only one mouse showed limited engraftment, with less than 50% presence of the E2F1 KO allele (Mouse n° 7, **Fig. 30A**).

Chimerism analysis was performed at 4 months post-transplantation and at the end of the procedure, when transplanted mice reached 18 months of age (**Fig. 31**). Results were very similar at both time points, indicating that long-term repopulation was obtained at 4 months post-transplantation and maintained for other 12 months (**Figs. 30-31**). At the end of treatment, PCR was performed with DNA obtained from peripheral blood (**Fig. 31A-B**) and also from bone marrow (**Fig. 31C-D**), which gave comparable results.

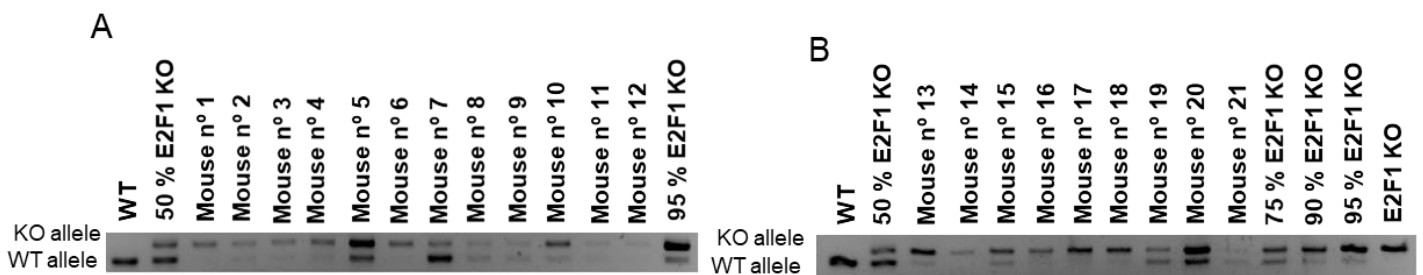


Figure 30. Chimerism determination at 4 months post-transplantation

PCR bands reflecting E2F1 KO allele presence in the transplanted mice. PCR was performed with DNA extracted from submandibular vein blood. **(A)** Lane 1: reference PCR band from a WT mouse. Lane 2: PCR bands of a 50% E2F1 KO reference sample. Lanes 3-14: PCR bands corresponding to $Abcd1^{-}/Abcd2^{-/-}$ mice transplanted with *BMtko*. Lane 15: PCR bands corresponding to a 95% E2F1 KO reference sample. **(B)** Lane 1: reference PCR band from a WT mouse. Lane 2: PCR bands of a 50% E2F1 KO reference sample. Lanes 3-11: PCR bands corresponding to $Abcd1^{-}/Abcd2^{-/-}$ mice transplanted with *BMtko*. Lanes 12-14: PCR bands of 75%, 90% and 95% E2F1 KO reference samples. Lane 15: reference PCR band from an E2F1 KO mouse.

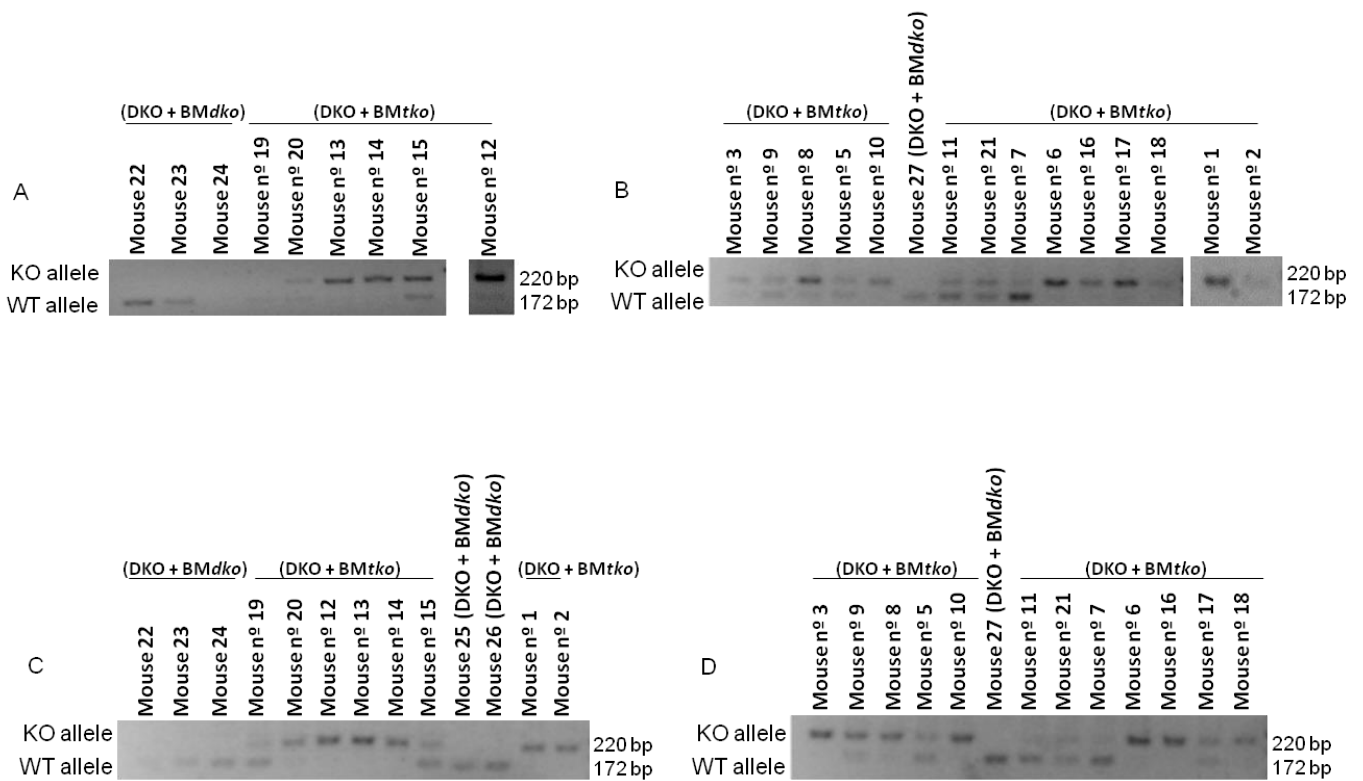


Figure 31. Chimerism determination at the end of procedure

PCR bands reflecting E2F1 KO allele presence in the transplanted mice. PCR was performed with DNA extracted from blood (**A-B**) and bone marrow (**C-D**). (**A**) Lanes 1-3: PCR bands corresponding to $Abcd1^{-}/Abcd2^{-/-}$ mice transplanted with BMdko (Lane 3: NA). Lanes 4-9: PCR bands corresponding to $Abcd1^{-}/Abcd2^{-/-}$ mice transplanted with BMtko (Lane 4: NA). (**B**) Lanes 1-5 and 7-15: PCR bands corresponding to $Abcd1^{-}/Abcd2^{-/-}$ mice transplanted with BMtko. Lane 6: PCR band corresponding to $Abcd1^{-}/Abcd2^{-/-}$ mice transplanted with BMdko. (**C**) Lanes 1-3 and 10-11: PCR bands corresponding to $Abcd1^{-}/Abcd2^{-/-}$ mice transplanted with BMdko. Lanes 4-9 and 12-13: PCR bands corresponding to $Abcd1^{-}/Abcd2^{-/-}$ mice transplanted with BMtko. (**D**) Lanes 1-5 and 7-13: PCR bands corresponding to $Abcd1^{-}/Abcd2^{-/-}$ mice transplanted with BMtko. Lane 6: PCR band corresponding to $Abcd1^{-}/Abcd2^{-/-}$ mice transplanted with BMdko. NA: No amplification.

4.2.10 Bone marrow transplantation with *Abcd1*^{-/-}/*Abcd2*^{-/-}/*E2f1*^{-/-} bone marrow cells prevents locomotor disability in *Abcd1*^{-/-}/*Abcd2*^{-/-} mice

With the aim of evaluating the preclinical efficacy of inhibition of E2F1 in BM-derived cells in X-ALD, we studied the effect of BMT with *Abcd1*^{-/-}/*Abcd2*^{-/-}/*E2f1*^{-/-} cells on locomotor dysfunction exhibited by the X-ALD mouse (Pujol et al., 2004).

In the treadmill test, at a belt speed of 20cm/sec and 20° slope, the number of mice that remained on the platform was recorded every 30 seconds in a period of 3 minutes. At already 1.5 minutes, only around 80% of *Abcd1*^{-/-}/*Abcd2*^{-/-} + *BMdko* mice were able to continue running, compared to WT mice (**Fig. 32A**). At the end of the test, only 75% remained on the platform. In contrast, 95% of the *Abcd1*^{-/-}/*Abcd2*^{-/-} + *BMtko* mice were able to perform the test until the end, meaning they overcome exhaustion (**Fig. 32A**). Regarding bar cross test, *Abcd1*^{-/-}/*Abcd2*^{-/-} + *BMdko* mice took a longer time to cross the bar and slipped off more times compared to wildtype littermates, whereas *Abcd1*^{-/-}/*Abcd2*^{-/-} mice transplanted with *BMtko* cells did not show any amelioration in their performance (**Fig. 32B**).

In the hindlimbs clasping phenotype, the *Abcd1*^{-/-}/*Abcd2*^{-/-} + *BMdko* mice presented a lower score than WT mice, demonstrating a locomotor impairment. When subjected to the test, *Abcd1*^{-/-}/*Abcd2*^{-/-} + *BMtko* mice performed similar to WT + *BMwt* mice (**Fig. 32C**). In order to detect any negative contribution in locomotion coming from the transplantation procedure, scores of transplanted WTs (WT + *BMwt*) and *Abcd1*^{-/-}/*Abcd2*^{-/-} (*Abcd1*^{-/-}/*Abcd2*^{-/-} + *BMdko*), and non-transplanted WT, *Abcd1*^{-/-}/*Abcd2*^{-/-} (provided by historical data from our group) were compared. This possibility was discarded, as obtained results were comparable between both groups (data not shown). These results possess into evidence that BMT with *Abcd1*^{-/-}/*Abcd2*^{-/-}/*E2f1*^{-/-} cells is able to prevent locomotor impairment presented by X-ALD mouse.

4.2.11 Bone marrow transplantation with *Abcd1*^{-/-}/*Abcd2*^{-/-}/*E2f1*^{-/-} cells halts axonal degeneration in *Abcd1*^{-/-}/*Abcd2*^{-/-} mice

Finally, to determine the effects of bone marrow transplantation with *Abcd1*^{-/-}/*Abcd2*^{-/-}/*E2f1*^{-/-} bone marrow cells on axonal degeneration, signs of neuropathology present in *Abcd1*^{-/-}/*Abcd2*^{-/-} mice were assessed by immunohistochemical techniques.

Mice transplanted with *Abcd1*⁻/*Abcd2*⁻/*E2f1*⁻ BM cells displayed reversed microgliosis (**Fig. 32D-F, S**), and astrocytosis (**Fig. 32G-I, T**), prevented the accumulation of synaptophysin (**Fig. 32J-L, U**) and APP in axons (**Fig. 32M-O, V**) and blocked the appearance of myelin debris along the spinal cord (**Fig. 32P-R**). Overall, the absence of E2F1 in BM-derived cells in the CNS halted axonal degeneration and arrested the onset of neurological symptoms in *Abcd1*⁻/*Abcd2*⁻ mice.

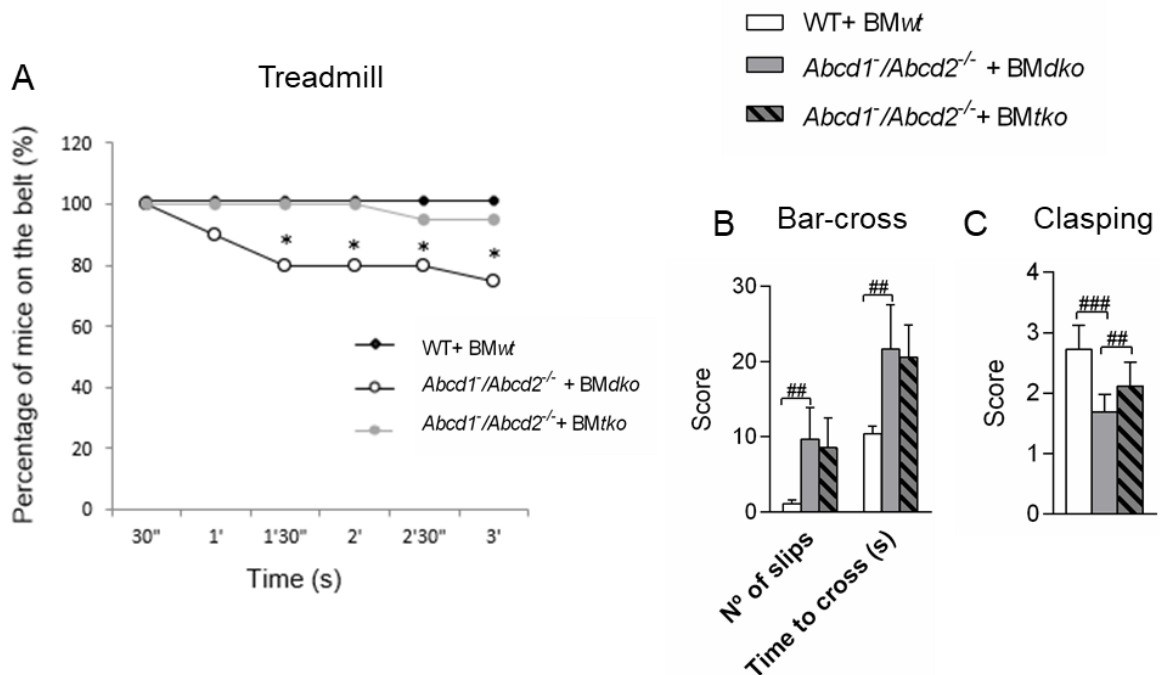


Figure 32. BMT with *Abcd1*⁻/*Abcd2*⁻/*E2f1*⁻ cells halts locomotor disability and axonal degeneration in *Abcd1*⁻/*Abcd2*⁻ mice

(A) Treadmill (B) Barcross and (C) Clasping tests have been carried out in 18-months-old WT + BMwt (n=13), *Abcd1*⁻/*Abcd2*⁻ + BMdko (n=21) and *Abcd1*⁻/*Abcd2*⁻ + BMtko (n=20) mice. (A) The number of mice that remained on the platform was recorded every 30 seconds in a period of 3 minutes. Each point represents the mean ± SD of each group. * *p*<0.05; one-way ANOVA followed by Fisher's *post hoc* test. (B) The time spent to cross the bar and the numbers of slips were quantified. (C) The best performance score of each animal was taken to quantify (Dumser et al., 2007). (B-C) Values are expressed as mean ± SD. ## *p*<0.01; ### *p*<0.001; non-parametric Kruskal-Wallis test followed by Dunn's *post hoc* test.

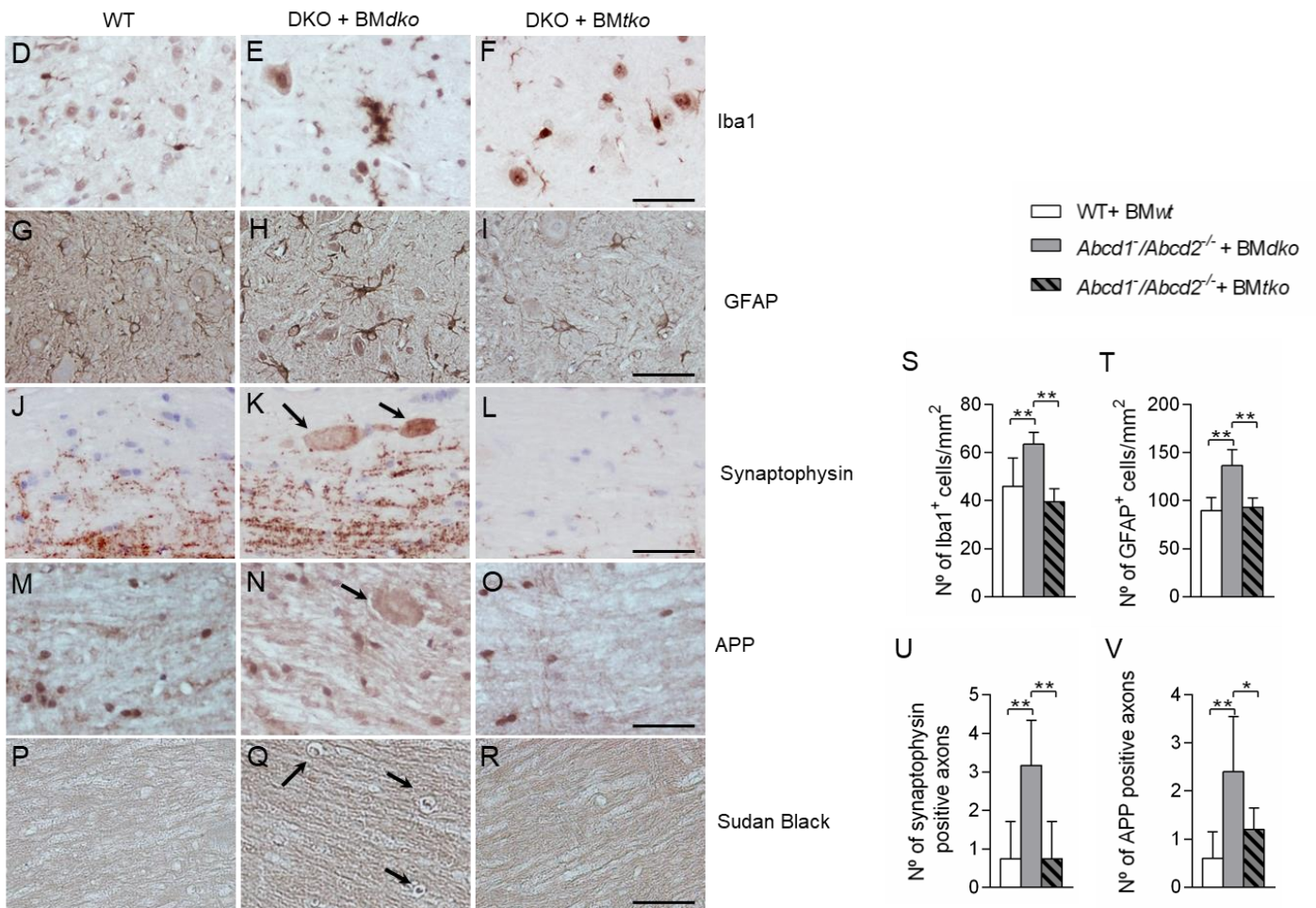


Figure 32. Continued

Spinal cord sections were processed for (D-F) Iba1, (G-I) GFAP, (J-L) synaptophysin, (M-O) APP and (P-R) Sudan black staining. Representative images (D, G, J, M and P) for WT, (E, H, K, N and Q) for *Abcd1*⁻/*Abcd2*^{-/-} + *BMdko* and (F, I, L, O and R) for *Abcd1*⁻/*Abcd2*^{-/-} + *BMtko* mice are shown. Scale bar=50um. Quantification of (S) Iba1⁺ density (cells/mm²), (T) GFAP⁺ density (cells/mm²), (U) synaptophysin and (V) APP accumulation (n=5 per genotype) in spinal cord immunohistological sections of 18-month-old WT + *BMwt*, *Abcd1*⁻/*Abcd2*^{-/-} + *BMdko*, and *Abcd1*⁻/*Abcd2*^{-/-} + *BMtko* mice. Values are expressed as mean ± SD. (S-V) **p*<0.05; ***p*<0.01; ****p*<0.001; one-way ANOVA followed by Fisher's *post hoc* test.

DISCUSSION

5 Discussion

5.1 Chapter I

This study provides novel insights into the mode of action of high-dose biotin on redox homeostasis and energy metabolism at multiple levels. Our data show that treatment with high-dose biotin halts axonal degeneration and locomotor dysfunction while preventing a decrease in ATP content, mitochondrial DNA depletion, and oxidative damage in the spinal cord of X-ALD mice. Moreover, we unveil a general dysregulation of lipid metabolism as a novel culprit that drives axonal demise in a model of X-ALD, restored upon high-dose biotin treatment. This has direct implications for X-ALD as well as MS and other metabolic axonopathies since mitochondrial dysfunction has been reported in the chronically demyelinated axons of MS patients (Dutta et al., 2006) and acute MS lesions (Mahad et al., 2008).

Biotin prevented total ROS and mitochondrial ROS production *in vitro*. To the best of our knowledge, this is the first time that biotin or high-dose biotin is shown to induce the endogenous antioxidant response of NRF2. Other authors proposed a different mechanism of action for the antioxidant role of biotin, based on the biotinylation of lysines in close proximity to sulfoxidation sites in the mitochondrial heat-shock protein HSP60, which contributes toward the elimination of ROS (Li et al., 2014).

Treatment of *Abcd1*⁻ mice with high-dose biotin decreased TAG accumulation, with a concomitant upregulation of the FAO pathway and repression of the lipogenesis pathway. These results suggest that the observed effects go beyond the actions of biotin on ACC1/ACC2 carboxylases in favour of a general effect on lipid homeostasis. In addition, the recovery of ATP content may also theorize that high-dose biotin enhanced FAO in *Abcd1*⁻ mice. To enter the TCA cycle, fatty acid-derived acetyl-CoAs are bound to oxaloacetate by citrate synthase. Additional oxaloacetate may be directly provided by other biotin-dependent carboxylases, such as pyruvate carboxylase (PC) (Jitrapakdee et al., 2008) or indirectly provided by refurbishing TCA cycle intermediates through the action of propionyl-CoA carboxylase (PCC) (Wongkittichote et al., 2017), thereby boosting the efficiency of FAO in producing ATP. Thus, the effects of biotin on PC and

PCC rather than the enzymes ACC1/ACC2 could contribute to the restoration of metabolic homeostasis we see in this model. In a very recent publication from our group, we found out a redox-dependent increase of RIP140 in the spinal cord and organotypic spinal cord slice cultures (OSCSC) from *Abcd1*⁻ mice, as well as an increase in the NAWM of ccALD patients (Ranea-Robles et al., *in press*). RIP140 is considered a master regulator of metabolic homeostasis and inhibits genes related to fatty acid oxidation, mitochondrial biogenesis and oxidative phosphorylation in adipocytes (Powelka et al., 2006). Of note, RIP140 deficiency halts axonal degeneration and improves the performance of X-ALD mice, suggesting that boosting of FAO pathway provide neuroprotective effects.

Besides the possible impact of biotin on its well-known carboxylase targets, the effect of high-dose biotin on the mTOR/SREBP-1c axis is intriguing, as it may have broad implications beyond the field of neurodegenerative diseases given its role as a master regulator of metabolism, cell growth, autophagy and innate immunity (Jones and Pearce, 2017; Perluigi et al., 2015; Shen and Shi, 2019). We propose that mTOR overactivity in the nervous system of X-ALD mice, which was already described in a previous work from our lab (Launay et al., 2015), is neutralized by high-dose biotin, igniting a cascade of compensatory effects that lead to the reestablishment of the lipid homeostasis, improved metabolic function and the axonal maintenance. Restoring the expression of SREBP-1c and its targets, the lipogenic enzymes FAS, Δ 9-desaturases, acyl-CoA synthetases and the genes involved in mitochondrial fatty acid oxidation, may have direct consequences on axonal function. Indeed, the knockout of SREBP-1c in the mouse induces the development of peripheral neuropathy and a decrease in myelin synthesis, along with a blunted fatty acid synthesis and increased fatty acid oxidation, establishing a direct link between SREBP-1c function and axonal health (Cermenati et al., 2015).

Normalization of the mTOR/SREBP-1c axis by high-dose biotin was followed by a reduction in total TAG levels in *Abcd1*⁻ spinal cords, but not the levels of LPC C26:0, indicating that there was no direct action on ABCD1 or that other peroxisomal transporter might be potentially bypassing loss of ABCD1. In this context, reduction of serum TAG level by high-dose biotin was seen in a study with WT mice fed with pharmacological doses of biotin (Larrieta et al., 2010). Authors hypothesized that the hypotriglyceridemic effects of biotin could involve increased cGMP and activation of

AMPK (Aguilera-Méndez and Fernández-Mejía, 2012; Boone-Villa et al., 2015). Nevertheless, we saw no differences in the activation of AMPK in our model (**Fig. 13E**). Compared to our study, the experimental setting in that work was shorter (8 weeks), the mice were younger (3 months) and of a different genetic background (Balbc), and lower doses of biotin were employed (13.5 mg/kg/day versus 60 mg/kg/day in our study), which underscores the effect of biotin in different organs and treatment conditions. High-dose biotin has also shown favourable effects in diabetic rodents and humans (Fernandez-Mejia, 2005; Furukawa, 1999; Zhang et al., 1996). There are studies supporting the view that biotin reduces total plasma cholesterol and triglyceride levels in diabetic rats treated with biotin (Sahin et al., 2013), in addition to lowering hepatic gene expression of SREBP-1c, ACC and FASN, compared to the control group (Sugita et al., 2008). Moreover, daily 40 microgram/kg biotin administration showed efficacy in decreasing total plasma cholesterol, low-density lipoprotein cholesterol and triglycerides levels in type 1 diabetic subjects (Hemmati et al., 2013). It is suggested that a deficiency, inactivity or unavailability of biotin may exist in diabetes (Coggeshall, 1985), resulting in a disordered activity of the biotin-dependent enzyme pyruvate carboxylase. This leads to an accumulation of pyruvate and/or depletion of aspartate, both of which play a significant role in nervous system metabolism (Patel, 1974). In patients with diabetic neuropathy, a type of nerve damage associated with diabetes mellitus, high-dose biotin treatment seems to have a therapeutic effect as patients under treatment showed improvement of clinical symptoms 4-8 weeks following biotin administration (Koutsikos et al., 1990). Although the exact mechanism of action of biotin on lipid metabolism in diabetes has not been definitively established, data from *in vivo* studies suggest that pharmacological doses of biotin decrease the expression of lipogenic genes.

We have described an altered lipid metabolism in *Abcd1* knockout mice (Fourcade et al., 2020), characterized by an increase in the biogenesis of LDs. The accumulation of LDs in the spinal motor neurons of the X-ALD mouse models may have detrimental consequences (Fourcade et al., 2020). This appears to be an undescribed pathogenic factor inherent to X-ALD underappreciated to date, although LDs were recently detected in an *in vitro* endothelial model mimicking the blood-brain-barrier (Lee et al., 2018). Likewise, in an untargeted lipidomic analysis, TAGs were found to be augmented in the spinal cord of *Abcd1*⁻ mice (Fourcade et al., 2020). This is in line with

the increased TAG levels detected in peripheral blood mononuclear cells (PBMC) of a cohort of patients with AMN (Ruiz et al., 2015) and more recently in fibroblasts of ccALD patients (Lee et al., 2019).

There is a long-held view of LDs as inert intracellular storages for neutral lipids in all living organisms and cells. However, early indications of the accumulation of TAGs and sterol esters as a consequence of membrane remodelling in neurodegenerative disorders and neural injury also exist, suggesting that LDs would merely be transient indicators of disease states (Johnson et al., 1950; Wood and Dawson, 1974). More recently, the direct impact of impaired LD dynamics on energy homeostasis and the overall physiology of organisms have begun to emerge (Greenberg et al., 2011; Lee et al., 2013; Welte, 2015). Later advances have argued for a driving role of LDs in the protection against oxidative stress. LDs may allow cells to safely sequester otherwise toxic lipids, in particular in cases of overabundant fatty acids, which may pose a threat to membrane integrity and peroxidability (Bailey et al., 2015). Once these fatty acids become TAGs, they are incorporated into LDs and become relatively harmless (Welte, 2015). Indeed, in *Drosophila* larvae, LDs are substantially increased in the CNS as a result of oxidative stress originating from either hypoxic conditions or excess free radicals. By abolishing droplets specifically in glia, the capacity of neuronal stem cells to proliferate under oxidative stress *milieu* is arrested. The role played by these glial LDs is thought to be protective and has been attributed to the sequestration of vulnerable membrane fatty acids away from free radicals, thus avoiding the vicious cycle of lipid peroxidation (Bailey et al., 2015). This view is further supported by work in flies, as elevated mitochondrial ROS in neurons induce lipid synthesis via JNK/SREBP in these cells (Liu et al., 2015). Neuronal fatty acids are then transferred to astrocytes to form LDs, where they are oxidized in mitochondria (Ioannou et al., 2019). On the other hand, the accumulation of peroxidized lipids induces neurodegeneration, supporting the role of LDs as both markers and protective agents rather than causes of neuronal demise. Furthermore, antioxidants reduced LD accumulation, thereby delaying neurodegeneration in mice (Liu et al., 2015). Besides, a primary causative role of disrupted LD dynamics in neuronal dysfunction was underscored by examining the consequence of loss of function of genes that are responsible for a number of hereditary cortical motoneuron diseases (the hereditary spastic paraplegias), such as atlastin, REEP1, seipin, spartin, and kinesin-1. These proteins play crucial roles in LD biology,

such as mediating the fusion of ER tubules or controlling the size of LDs (Klemm et al., 2013; Onal et al., 2017; Pennetta and Welte, 2018). The dysfunction of these genes might therefore alter the supply or composition of the lipids stored in LDs. More precise insights are derived from the study of DDHD2, the principal brain TAG lipase, which is defective in patients with spastic paraplegia 54 (SPG54) (Schuurs-Hoeijmakers et al., 2012). DDHD2 patients exhibit a thin corpus callosum and periventricular myelin abnormalities in MRI, features reminiscent of other leukodystrophies, including X-ALD. In *Ddhd2*^{-/-} mice, a similar untargeted lipidomic study to ours demonstrated that a great amount of TAGs in the form of LDs accumulates in the brain and spinal cord (Inloes et al., 2014), being TAGs ranging from 48:0 to 66:18. The disruption of TAG hydrolase activity impairs the capacity to protect cells from LD accumulation following free fatty acid exposure (Inloes et al., 2018). While the mechanisms that link droplet accumulation and neuronal impairment remain obscure, one intriguing observation is that in the DDHD2 knockout mice some of the large droplets observed were associated with noticeable swellings of the neuronal processes and, thus, might present obstacles to intracellular trafficking in the relatively thin axons and dendrites. These results converge into a strong body of evidence directly connecting the dysfunction of LDs to decreased protection from lipid-caused oxidative stress, leading to motoneuron disease.

In sum, we believe the LD accumulation in X-ALD may constitute a protective mechanism against excess VLCFAs, which does not rule out a direct contribution of the increased LDs to axonal demise when the situation becomes chronic. The increased size of the LD compartment is most likely caused by multifactorial mechanisms: i) an increase in the biogenesis of LDs through increased lipid synthesis driven by mTOR/SREBP-1c and oxidative stress; ii) a decrease in LD degradation capacity through impaired mitochondrial function due to lower mitochondrial mass and lower FAO expression, the latter driven by mTOR/SREBP-1c; and iii) the incapacity of peroxisomes to degrade at least some of the TAG fatty acids caused by the loss of ABCD1, which was shown very recently to be a key element in the tethering of LDs to the peroxisomes (Chang et al., 2019) (**Fig. 19**).

Taken together, our findings strongly suggest that interventional treatment using high-dose biotin may be an attractive therapeutic option for patients with X-adrenomyeloneuropathy. Indeed, a Phase III clinical trial (NCT02961803) was

conducted in AMN patients, in which despite high-dose biotin (300 mg/day) was well tolerated up to 24 months, but favourable demonstrated results could not be attributed to the whole treated group. Yet, AMN is a slowly developing disease, which makes it difficult to see improvements, if any, with such a short period of treatment. We consider that additional and larger studies are warranted to establish the efficacy of high-dose biotin in the treatment of neurodegenerative disorders.

5.2 Chapter II

This study provides novel insights into the role of E2F1 in the central nervous system. Our data show that genetic deletion of E2F1 halts axonal degeneration and locomotor dysfunction while prevents mitochondrial dysfunction, inflammation, and normalizes redox and lipid homeostasis in the spinal cord of X-ALD mice, which is associated to the reactivation of the NRF2 endogenous antioxidant pathway.

These findings further confirm the role of E2F1 as a metabolic switcher, from glycolysis to oxidative phosphorylation, as previously shown by the group of L. Fajas. They demonstrated that E2F1 deletion leads to increased mitochondria number and function, oxygen consumption and oxidative metabolic gene expression, such as *Pgc1a*, *Tfam*, *Cpt1a*, and *Acadl*, in brown adipose and gastrocnemius tissues, indicating that E2F1 negatively regulates oxidative metabolism (Blanchet et al., 2011). In addition, a mouse model of Duchenne muscular dystrophy in which E2F1 was ablated exhibited a strong reduction of physiopathological signs of the disease including increased oxidative metabolic gene program (induction of *Pgc1a* and *Tfam* gene expression), mitochondrial activity (increased respiratory capacity) and improved muscle functions, assessed by treadmill test (Blanchet et al., 2012).

Lipid synthesis and LD accumulation were restored after E2F1 ablation in *Abcd1*⁻ mice spinal cord. This is supported by the fact that overexpression of E2F1 in mice results in a strong alteration of lipid metabolism characterized by increased expression of lipogenic genes such as the transcription factor SREBP-1c and fatty acid synthase (FASN) to cite a few (Coulouarn et al., 2006). Further, deletion of E2F1 in a mouse model of obesity results in a reduction of LD accumulation in the liver (Denechaud et al., 2016). In a very recent publication, researchers have shown that *E2f1*^{-/-} and *E2f2*^{-/-} mice were resistant to high-fat diet (HFD) and diethylnitrosamine (DEN)-induced hepatocarcinogenesis and associated lipid accumulation and showed enhanced fatty-acid oxidation (FAO) and increased expression of *Cpt2*, an enzyme essential for fatty-acid oxidation (FAO) whose downregulation is linked to NAFLD-related hepatocarcinogenesis (Gonzalez-Romero et al., 2021). As a transcription factor, E2F1 regulates the transcriptional activity of key lipogenic genes by its inherent ability to

bind the promoter of specific genes depending on the energetic demand of the cell (Denechaud et al., 2016). By ChIP high-throughput DNA sequencing (ChIP-seq) in primary cultures of mouse hepatocytes, Fajas and colleagues showed that E2F1 binds the promoters of FASN and the transcription factor SREBP-1c, suggesting that these genes are *bona fide* E2F1 targets. This was not, however, the first evidence of E2Fs showing lipogenic effects. *E2F1*^{-/-} MEFs showed reduced capacity to differentiate into adipocytes compared to wild-type MEFs (Fajas et al., 2002b). Adipocyte formation was scored using ORO staining for LD detection. The same result was obtained when *E2F3*^{-/-} MEFs were challenged with the same approach. Noteworthy, when performing the experiment in *E2F4*^{-/-} MEFs, a significant increase in ORO-positive cells was observed. Overall, these data provide evidence that E2Fs regulate lipogenic metabolism. Likewise, in a murine Shh-induced medulloblastoma model, RB inactivation and E2F1 induction led to an exaggerated lipogenesis and reduced mitochondrial β -oxidation, characterized by increased TAGs level and induction of FASN expression (Bhatia et al., 2011). Pharmacological inhibition of lipogenesis and/or inactivation of E2F1 reduced tumour growth and improved survival of Shh-driven medulloblastoma-bearing mice.

Here we show that the lack of E2F1 is neuroprotective in X-ALD, which is defined by normalization of microgliosis and astrogliosis, markers of neurodegeneration, as well as the reduction of NF κ B-dependent pro-inflammatory response in *Abcd1*^{-/-}/*E2f1*^{-/-} mice. This is in line with the fact that E2F1 is a transcriptional partner of NF- κ B and activates its target genes (Lim et al., 2007). Accordingly, E2F1-deficient mice have increased sensitivity to systemic LPS (Warg et al., 2012) due to a reduced inflammatory response characterized by lower serum levels of *Il1b*, *Il6*, and *Tnfa* (Warg et al., 2012; Yang et al., 2011). Of note, ablation of both E2F1 and E2F2 transcription factors limits neuroinflammation and associated neurological deficits after contusive spinal cord injury (Wu et al., 2015).

In this study, we show that the ablation of E2F1 halts neurodegeneration by preventing axonal degeneration associated with locomotor disability in *Abcd1*^{-/-}/*Abcd2*^{-/-} mice. This is in accordance with previous data in the literature. Thereby, inhibition of the E2F1 pathway attenuates neuronal apoptosis *in vitro* and confers neuroprotection after spinal cord injury *in vivo* (Wu et al., 2012). E2F1 induction was observed in dopaminergic neurons of post-mortem brain tissue of PD patients, as well as *in vivo* and *in vitro* models after exposure to MPTP toxin (Höglinger et al., 2007). Interestingly, blocking

E2F1 expression mitigates MPTP-induced neurotoxicity in dopaminergic neurons both in animal and *in vitro* models. Moreover, *E2f1*^{-/-} neurons are resistant to death (Giovanni et al., 2000; Zyskind et al., 2015) and have reduced caspase 3-like activity when exposed to β -amyloid in a model of AD. However, this particular pro-apoptotic effect of E2F1 is discarded in our model because, despite presenting an overt oxidative damage (Galino et al., 2011), no activation of caspase-3 is detected in *Abcd1* knockout mice spinal cord (Lopez-Erauskin et al., 2012; Pujol et al., 2004). MacManus et al. showed that *E2f1*^{-/-} mice had improved behaviour in motor function compared to their control littermates after cerebral ischemia and presented decreased neuronal damage (MacManus et al., 2003). Moreover, the increase of E2F1 expression was shown to be age-dependent in the mouse brain and correlates with the age of onset of synaptic and behavioural perturbations in E2F1 mutant mice (Ting et al., 2014). Surprisingly, we did not detect any performance disturbance in the locomotor tests conducted in the *E2f1* null mice employed in our studies. Since E2F1, 2, and 3 (the three members in the activating E2F subgroup) share overlapping functions and similar physical interactions with pRb, it is plausible that E2F2 and E2F3 could compensate for the defects caused by E2F1 deletion. Besides, the differences observed by the researchers might be distinctive to the specific tests carried out.

In the present work, we identify for the first time an impairment of the RB-E2F1 axis in X-ALD. We provide data that indicate that the induction of E2F1 in our model is redox-dependent (**Fig. 20E-F**), which is supported by a study showing that H₂O₂ induced E2F1 in primary cortical neuron cultures (Boutahar et al., 2010). *In vivo*, in a rotenone-based PD mouse model, E2F1 was also induced in tyrosine hydroxylase-positive neurons after chronic exposure to rotenone, a mitochondrial complex I inhibitor known to produce ROS (Chen et al., 2018). Besides, Raimundo et al. proposed that increased mitochondrial ROS induces E2F1 expression, via AMPK, in a tissue-specific manner in the stria vascularis and spiral ganglion neurons of mice carrying a mitochondrial mutation that causes deafness (Raimundo et al., 2012).

In the last decade, re-entry into the cell cycle by neurons has been associated with many diseases (Liu et al., 2010a; Liu et al., 2010b; Wang et al., 2009). For reasons not completely understood, a mature neuron that re-enters the cell cycle is neither able to advance to a new G₀ quiescent state nor revert to its earlier G₀ state. Researcher defined

this event as “expanded cell cycle” and they proposed a “two-hit hypothesis” to explain the process (Yang and Herrup, 2007; Zhu et al., 2007). The hypothesis states that two conditions must be met so as aberrant cell cycle re-entry occurs in neurons: (i) an elevation in cell cycle proteins and (ii) an increase in promitogenic signals. Thus, even though mature neurons may express some cell cycle proteins, the amount produced is not sufficient on its own to drive the mature neuron to re-enter the cell cycle. The stimulus of additional promitogenic molecules, such as thrombin, A β , reactive oxygen species (ROS), nitric oxide (NO), and others, provoke the final death of the neuron. Here, albeit X-ALD mice present overt oxidative damage, it does not show caspase-3 activation-mediated apoptosis (Lopez-Erauskin et al., 2012; Pujol et al., 2004).

In a recent publication from our group, increased RIP140 mRNA and protein levels in 12-month-old *Abcd1*⁻ mice spinal cord were uncovered (Ranea-Robles et al., *in press*). RIP140 modulates energy metabolism homeostasis, by regulating glucose and lipid metabolism in skeletal muscle, liver, heart and adipose tissue (Augereau et al., 2006). RIP140 deficiency exerts neuroprotection by inhibiting neuroinflammation and preventing mitochondrial and bioenergetic dysfunction in X-ALD mice, but more importantly, RIP140 deletion halts axonal degeneration and improves the performance of X-ALD mice in behavioural tests (Ranea-Robles et al., *in press*). It was described that RIP140 is a transcriptional repressor of E2F1 activity and inhibits the expression of several E2F1 target genes (Docquier et al., 2010). Interestingly, it was later demonstrated that RIP140 is a novel target gene of E2F1 and that E2F1 participates in the induction of RIP140 expression during adipocyte differentiation (Docquier et al., 2012). These findings evidence the existence of a fine-tuned regulatory loop between these two transcription factors, in which RIP140 could in turn control its own activation by E2F1. Collectively, given that elevated expression and protein levels of both transcription factors have been found in our mice model, it is not strange that the results presented herein are similar to those obtained in (Ranea-Robles et al., *in press*).

Taken all these together, we believe that the increased E2F1 gene expression is the reflection of the defective oxidative metabolism present in X-ALD. Moreover, we propose E2F1 as a regulator of lipid-driven axonal demise in X-ALD. Since the loss of E2F1 halted axonal degeneration and improved locomotor performance of X-ALD mice, this study provides enough evidence to develop E2F1-inhibiting therapeutic

strategies to block neurodegeneration in X-ALD and similar neurological disorders with mitochondrial damage and metabolic imbalance as common features. We believe these investigations may have broad implications for therapies targeting neurodegenerative disorders where lipid signalling and axonal health are disrupted.

The role of E2F1 in BM-derived cells in X-ALD

It is difficult to develop therapies against X-ALD if the mediators of neurodegeneration are not well understood. In the first part of this chapter, we demonstrated that the elimination of E2F1 normalized the phenotype and prevented neurodegeneration in the X-ALD mouse. Tempted by these rewarding results and given that E2F1 has a high expression in the bone marrow; we speculated that E2F1 could have a central role in the CNS of the X-ALD mice. The transplantation of DKO mice with bone marrow cells extracted from TKO mice has allowed us to determine the role of E2F1 in BM-derived cells that will repopulate the CNS.

We have demonstrated that *Abcd1^{-/-}/Abcd2^{-/-}/E2f1^{-/-}* BM-derived cells are successfully engrafted and are able to repopulate *Abcd1^{-/-}/Abcd2^{-/-}* mice bone marrow. Overall, the absence of E2F1 in BM-derived cells in the CNS prevented axonal degeneration and the onset of neurological symptoms in *Abcd1^{-/-}/Abcd2^{-/-}* mice. Amelioration of the X-ALD phenotype was observed in two of the conducted behavioural tests, treadmill and hindlimbs claspings tests. On this occasion, no differences were observed between groups when mice were challenged to the bar cross test. This test assesses the motor coordination of the animals, which is governed by the cerebellum. Motor commands are not initiated in the cerebellum, but this structure modifies the motor instructions of the descending pathways to make movements more adaptive and accurate. On the other hand, in the hindlimbs claspings and treadmill tests, the reaction capacity of the mice towards a reflex is measured: i) hindlimbs reflex extension when mice are gently lifted by the tail (Dumser et al., 2007) and ii) the ability to detect and avoid shocks coming from the electrified grid located to the rear of the belt on which they are running. In vertebrates, reflexes do not pass directly into the brain, but synapse through sensory neurons in the spinal cord. We hypothesize that lack of improvement in the locomotor performance in the bar cross test could be associated with a lower engraftment of the donor BM cells in the cerebellar region compared to the spinal cord. However, we do

not have data to demonstrate this as we only determined the global repopulation at the peripheral level and not the specific engraftment of each region in the CNS. Additional experiments should be done to validate this hypothesis.

Bone marrow transplantation and gene therapy can arrest demyelination (Cartier et al., 2009), most probably by turnover of the microglia, as they are the only cells of the central nervous system that come from the bone marrow after transplantation. Noteworthy, even that X-ALD mouse does not show demyelination, we see an amelioration of the phenotype of the transplanted mice in our study. In a recent publication, a reduction in serum VLCFA levels was observed when GFP-expressing WT BM cells were transplanted into *Abcd1*-deficient mice (Morita et al., 2020). However, the accumulation of VLCFA in the brain remained unchanged. A preliminary study carried out by P. Aubourg and our laboratory showed that transplantation of murine HSCs from wildtype donor is able to prevent locomotor dysfunction and reduces markers of oxidation and microgliosis/astrocytosis in *Abcd1*⁻ and *Abcd1*/*Abcd2*^{-/-} mice (Ruffert, 2012; P026). Unlike in the aforementioned studies, in our experimental approach, we did not directly target the original defect in X-ALD, the loss of ABCD1, but, instead, we silenced the expression of E2F1 in CNS cells derived from the BM. We believe that results coming from our work have major implications as it discloses some novel concepts, which deserve further investigations.

We provide evidence demonstrating that E2F1 has an important role in the pathophysiology of the disease, as its inactivation in CNS cells derived from the BM exert neuroprotection in X-ALD mice. This is to our knowledge, the first time in which targeting a gene with metabolic implications by HSCT restores clinical signs of X-ALD. Moreover, amelioration of the phenotype was observed even that the defect underlying the disease, dysfunctional ABCD1 transporter, was still present. These results suggest that, in addition to the accumulation of VLCFA, E2F1 contributes in a considerable way to the correct functioning of the CNS in X-ALD mice and that the metabolic imbalance induced by its overexpression plays a relevant role in the triggering of axonal degeneration. The identification of the specific cell-type(s) exerting the observed favourable effects will extend previous knowledge by providing information about important cell-type(s) in the pathogenesis of the disease, as well as the function of E2F1 in these cells. Single-nuclei RNAseq analysis will allow the transcriptomic profiling of the transplanted mice spinal cord and the identification of

these cells. Considering previous findings in the literature (Morita et al., 2020), we expect to find *Abcd1*⁻/*Abcd2*⁻/*E2f1*⁻ microglia-like cells involved in these processes. However, microglial turnover is slow (Kennedy and Abkowitz, 1997; Lawson et al., 1992). In addition, the association between ABCD1 deficiency and vascular moiety disruption has already been described (Lee et al., 2018), suggesting a possible contribution of *Abcd1*⁻/*Abcd2*⁻/*E2f1*⁻ endothelial cells in the neuroprotection. Indeed, it has been reported that bone marrow is a source of endothelial cells and provide neuroprotection after BMT (Garbuzova-Davis et al., 2017; Hess et al., 2002; Schatteman et al., 2007).

In conclusion, E2F1 emerges as a major contributor to the development of axonal degeneration in X-ALD. The finding that clinical features are reversed by *Abcd1*⁻/*Abcd2*⁻/*E2f1*⁻ BM-derived cells in *Abcd1*⁻/*Abcd2*⁻ mice provides engaging evidence supporting that impaired metabolism in HSC-derived cells, independent of that produced by ABCD1 loss, could be an underlying mechanism of this devastating disease. Results obtained so far are promising and we are certain it is worthy to address further research in the identification of the cell-type(s) responsible for the beneficial effects of BMT in the X-ALD mice. Future investigations into how to overcome metabolic and redox disturbance may reveal novel approaches to prevent neurodegeneration in X-ALD.

5.3 Global discussion

In this work, we provide new insights into the physiopathology of X-ALD. In the first chapter of this thesis, a generalized disturbed lipid signature was identified in 12-month-old *Abcd1*⁻ knockout mice, uncovered to date, and characterized by extended lipid accumulation in the spinal cord. At 3 months of age *Abcd1*⁻ mice did not present alterations in the lipidic pattern, suggesting an accumulative phenotype over time and reinforcing the role of oxidative stress as a major and earlier contributor to the development of the disease (Fourcade et al., 2008). In a previous publication from our lab, it was demonstrated that oral administration of DMF, an NRF2 activator in use for MS, reactivated the NRF2-antioxidant response pathway, and molecular pathogenesis factors such as mitochondrial depletion, bioenergetic failure, oxidative damage and inflammation, as well as clinical signs of neurodegeneration manifested by the X-ALD mice, were overcome (Ranea-Robles et al., 2018), unveiling the major impact of redox homeostasis in the development of the disease. Impairment of the mTOR/SREBP-1c axis was defined as the major triggering factor of this lipidic imbalance. Lack of antioxidant response due to blunted GSK-3 β /NRF2 pathway in X-ALD mice further contributes to the formation of lipid droplets, which leads to neurodegeneration (Coppa et al., 2020; Fourcade et al., 2020). In a previous publication from our lab, mTOR inhibition by a rapamycin derivative (temsirolimus) restored autophagic flux and halted the axonal degenerative process (Launay et al., 2015). The effect was mediated through the normalization of the autophagy as well as redox and metabolic homeostasis.

In this thesis, we identified two potential upstream modulators of mTOR, the B-complex vitamin biotin and the E2F1 transcription factor, providing new knowledge towards the discovery of therapeutic targets in the field of neurodegeneration. It is tempting to speculate that protection against axonal degeneration in the X-ALD mouse model was obtained by interfering in the mTOR activation state, pharmacologically with high-dose biotin administration, or genetically by inhibiting E2F1 expression. Therapeutic effects of these strategies can be attributed, from one side, to the reduction of lipid accumulation due to the normalization of mTOR/SREBP-1c axis and, on the other side, to the reactivation of the NRF2-dependent antioxidant response, which

would restore redox balance. In the case of genetic inactivation of E2F1 in *Abcd1*⁻ mice, we consider this latter event might occur through the inactivation of GSK-3 β , as it is an upstream regulator of the NRF2-dependent antioxidant axis. Meanwhile, in the set of *Abcd1*⁻ mice treated with high-dose biotin determining GSK-3 β 's activity is a pending task for the future. All in all, the combination of both actions prevented axonal degeneration and associated locomotor disability in the *Abcd1*⁻/*Abcd2*^{-/-} mouse model. A schematic overview of the effects of the two interventional strategies performed in the X-ALD mice is represented in **Figure 33**.

Interaction between E2F1 and mTOR has already been studied, mostly in the field of cancer, as they share many functions like growth, metabolic regulation and cellular fate. Thereby, v-ATPase proton pump activity is a key step for the activation of mTOR by E2F1 and provides a potential mechanism by which E2F1 drives invasiveness and metastasis in cancer (Meo-Evoli et al., 2015). Based on the metabolic function of E2F1, Almacellas et al. demonstrated that, upon E2F1 induction, E2F1-driven glucose catabolism increases mTOR activity, conferring proliferating capacities to tumour cells (Almacellas et al., 2019). To finish, Ladu et al. showed that E2F1 activates PI3K/AKT/mTOR pathway in an HCC mouse model and in patients, and that, by exerting anti-apoptotic signals, this oncogenic event is essential for the survival of cancerous cells. In contrast, E2F1 suppression caused a dramatic reduction in PIK3, AKT, and mTOR proteins (Ladu et al., 2008). As far as we are concerned, there is no data available addressing the regulatory effect of biotin on the mTOR axis or GSK-3 β .

Regardless, we do not discard the possibility that the normalization of mTOR could be mediated by GSK-3 β . On one hand, excessive GSK-3 β activation has been identified as an important factor in the onset of numerous diseases, including diabetes, bipolar disorder, cancer and neurodegenerative disorders (Giese, 2009), which also show an activation of mTOR signalling. In addition, there is evidence demonstrating that GSK-3 β acts as either a negative or positive regulator of mTOR signalling, depending on the experimental conditions (Avrahami et al., 2013; Azoulay-Alfaguter et al., 2015; Inoki et al., 2006; Ka et al., 2014; Ma et al., 2011). In the CNS, GSK-3 β regulates neural progenitor homeostasis during brain development by limiting mTOR activity (Ka et al., 2014). In mature neurons, GSK-3 β is needed for proper mTOR signalling and is a positive regulator of prosurvival signalling (Urbanska et al., 2018). Meanwhile, GSK-3 deficiency in astrocytes results in an enlarged brain, astrocyte overproliferation and

hypertrophy and is associated with increased AKT/mTOR activity (Jung et al., 2016). Besides, GSK-3 β inhibitors have shown neuroprotective effects in several neurological disorders such as AD, hypoxic-ischemic brain injury and spinocerebellar ataxia, mediated by the activation of the mTOR signalling pathway (Ma et al., 2010; Sánchez et al., 2016; Xiong et al., 2018). In the field of cancer, GSK-3 β inhibitors represent a new opportunity for antitumoural therapies, as positive regulation of mTOR activity mediated by GSK-3 β suppresses autophagy and contributes to cancerous cell proliferation and tumour growth (Azoulay-Alfaguter et al., 2015; Shin et al., 2014; Shin et al., 2011).

Notwithstanding, mTOR can control GSK-3 β nuclear localization and function, suggesting a link between metabolic conditions sensed by mTOR and GSK-3 β -dependent regulation of transcriptional networks controlling cellular biomass production (Bautista et al., 2018). Therefore, a feedback regulation between mTOR and GSK-3 β must exist, likely to act in specific cell types and under certain conditions, as might be the case of X-ALD (Carracedo and Pandolfi, 2008; Copps and White, 2012).

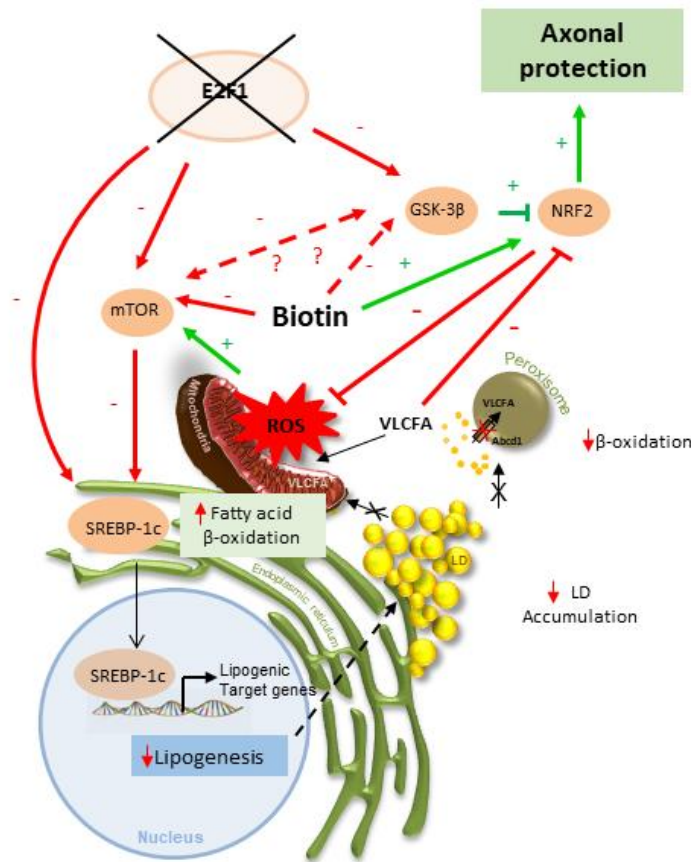


Figure 33. Model illustrating the role of mTOR in the etiopathogenesis of axonal degeneration in X-linked adrenoleukodystrophy

In X-ALD, VLCFA-dependent ROS induces overactivation of mTOR signalling, triggering a series of fatal events with axonal degeneration as the ultimate consequence. Lipid droplet accumulation in X-ALD may obey to a combination of different factors: i) increased lipid synthesis driven by aberrant mTOR/SREBP-1c axis; ii) decrease of the lipid droplets degradation capacity by the mitochondria, due to fewer mitochondria number and lower FAO, the later driven by impaired mTOR/SREBP-1c axis, and iii) the impossibility of the peroxisome to degrade some of the TAGs due to the loss of ABCD1, shown to be a key element in the tethering of LD to the peroxisomes (Chang et al., 2019). By interfering in the mTOR activation state, pharmacologically with high-dose biotin administration, and genetically by inhibiting E2F1 expression, protection against axonal degeneration was obtained in the X-ALD mice model. Therapeutic effects of the strategies are attributed, from one side to the reduction of lipid accumulation due to the normalization of mTOR/SREBP-1c axis. On the other hand, redox imbalance was restored by reactivating NRF2-dependent antioxidant response, through

inactivation of GSK-3 β . The combination of both actions prevented axonal degeneration and associated locomotor disability in the *Abcd1*⁻/*Abcd2*^{-/-} mouse model.

Initially, our hypothesis was that genetic inactivation of E2F1 and pharmacological doses of biotin normalize mTOR activity and reactivate the NRF2-antioxidant pathway in our mouse model. However, during the course of this thesis, other scenarios were contemplated, which deserve further research. From one side, we wonder whether E2F1 inactivation/high-dose biotin treatment in *Abcd1*-deficient mice inhibit mTOR directly or through GSK-3 β . On the other side, if mTOR inhibition occurs in a direct manner, inhibition of mTOR could in turn inhibit GSK-3 β and reactivate the NRF2-antioxidant pathway (**Figure 33**). To address this question and taking advantage of previous knowledge in our system, we consider it would be worth looking if the GSK-3 β /NRF2 pathway is restored in X-ALD mice treated with temsirolimus, an mTOR inhibitor with neuroprotective effects in X-ALD (Launay et al., 2015). This information would not only expand our knowledge but would also help to better understand the underlying mechanism behind the normalization of redox and lipid imbalance in our system.

Summarizing, even if lipolytic activity of E2F1 has been previously linked to its ability to bind promoters of key genes regulating lipid synthesis, such as SREBP-1c or FASN (Denechaud et al., 2016), analysis of the mTOR activation shows that a possible regulation above the E2F1/SREBP-1c axis involving mTOR cannot be ruled out. In parallel, it has been described that GSK-3 β is able to regulate the transcription of SREBP-1c by inducing its degradation in a phosphorylation-dependent manner (Kim et al., 2004; Sundqvist et al., 2005). Altogether, it cannot be excluded that the normalization of lipid accumulation observed in *Abcd1*⁻/*E2f1*^{-/-} mice is due to a synergistic effect of the impeded transcription of SREBP-1c governed by the lack of E2F1 and restoration of the mTOR/SREBP-1c axis. In the case of the pharmacological approach with high-dose biotin, reduction of mTOR activity was also achieved, as observed by the decrease of its phosphorylated form and its downstream substrate p70 S6K.

Overall, we identified a generalized metabolic disturbance present in the X-ALD mouse model. We provide insights that neuroprotective effects of high-dose biotin treatment and E2F1 deficiency are due to the refurbishing of the NRF2-antioxidant signalling pathway and that the main mechanism behind is the restoration of the aberrant

mTOR/SREBP-1c axis. This thesis also provides enough evidence to consider oxidative stress, mitochondrial dysfunction, neuroinflammation and metabolic imbalance as a central core in the pathophysiology of X-ALD, underlying axonal degeneration. Thereby, these results lay the basis for new endeavours in developing therapies for X-ALD. Furthermore, given that these pathways are commonly altered in other neurodegenerative and metabolic disorders, these findings, obtained by studying a rare disease, can be expanded to millions of patients suffering from these disorders, underscoring the applicability of rare disease's research in the biomedical field.

CONCLUSIONS

6 Conclusions

Based on the aims established for this thesis, the conclusions of the present dissertation can be formulated as follows:

1. High-dose biotin treatment prevents C26:0-induced ROS generation and reactivates NRF2-dependent antioxidant response in X-ALD patient's derived skin fibroblasts.
2. High-dose biotin treatment restores mitochondrial dysfunction, bioenergetic deficits and oxidative damage in *Abcd1*⁻ mouse model.
3. High-dose biotin treatment normalizes the hyperactivation of mTOR, decreases gene expression of lipid synthesis pathway and increases fatty acid β -oxidation pathway, contributing to the reduction of lipid accumulation in X-ALD mice spinal cord.
4. High-dose biotin treatment halts axonal degeneration and prevents locomotor disability present in *Abcd1*⁻/*Abcd2*^{-/-} mice.
5. Expression of E2F1 transcription factor is increased in the spinal cord of X-ALD mice.
6. Loss of E2F1 exerts neuroprotective effects in X-ALD mice. E2F1 ablation restores mitochondrial function, bioenergetic deficits, inflammatory dysregulation, and lipid and redox homeostasis.
7. E2F1 deletion halts axonal degeneration and prevents locomotor disability present in *Abcd1*⁻/*Abcd2*^{-/-} mice.
8. Aberrant mTOR signalling pathway is a contributing factor in the physiopathology of X-ALD as therapeutic strategies that normalize its

hyperactivation, reestablish the different hallmarks and prevent axonal degeneration in the X-ALD mouse model.

9. *Abcd1*⁻/*Abcd2*⁻/*E2f1*⁻ bone marrow cells are successfully engrafted and are able to repopulate *Abcd1*⁻/*Abcd2*⁻ mice's bone marrow.
10. Transplantation with bone marrow-derived *Abcd1*⁻/*Abcd2*⁻/*E2f1*⁻ cells halts axonal degeneration and prevents locomotor disability in *Abcd1*⁻/*Abcd2*⁻ mice.

BIBLIOGRAPHY

Biotin. In *Present Knowledge in Nutrition*, pp. 359-374.

Abella, A., Dubus, P., Malumbres, M., Rane, S.G., Kiyokawa, H., Sicard, A., Vignon, F., Langin, D., Barbacid, M., and Fajas, L. (2005). Cdk4 promotes adipogenesis through PPARgamma activation. *Cell Metab.* *2*, 239-249.

Abu-Elheiga, L., Matzuk, M.M., Abo-Hashema, K.A., and Wakil, S.J. (2001). Continuous fatty acid oxidation and reduced fat storage in mice lacking acetyl-CoA carboxylase 2. *Science* *291*, 2613-2616.

Adams, G.B., and Scadden, D.T. (2006). The hematopoietic stem cell in its place. *Nat. Immunol.* *7*, 333-337.

Adibhatla, R.M., and Hatcher, J.F. (2008). Phospholipase A(2), reactive oxygen species, and lipid peroxidation in CNS pathologies. *BMB reports* *41*, 560-567.

Adibhatla, R.M., and Hatcher, J.F. (2010). Lipid oxidation and peroxidation in CNS health and disease: from molecular mechanisms to therapeutic opportunities. *Antioxid Redox Signal* *12*, 125-169.

Adibhatla, R.M., Hatcher, J.F., and Dempsey, R.J. (2006). Lipids and lipidomics in brain injury and diseases. *The AAPS journal* *8*, E314-321.

Agar, J., and Durham, H. (2003). Relevance of oxidative injury in the pathogenesis of motor neuron diseases. *Amyotroph. Lateral Scler. Other Motor Neuron Disord.* *4*, 232-242.

Aguilar, V., and Fajas, L. (2010). Cycling through metabolism. *EMBO Mol. Med.* *2*, 338-348.

Aguilera-Méndez, A., and Fernández-Mejía, C. (2012). The hypotriglyceridemic effect of biotin supplementation involves increased levels of cGMP and AMPK activation. *Biofactors* *38*, 387-394.

Albet, S., Causeret, C., Bentejac, M., Mandel, J.L., Aubourg, P., and Maurice, B. (1997). Fenofibrate differently alters expression of genes encoding ATP-binding transporter proteins of the peroxisomal membrane. *FEBS Lett.* *405*, 394-397.

Aldskogius, H., Liu, L., and Svensson, M. (1999). Glial responses to synaptic damage and plasticity. *J. Neurosci. Res.* *58*, 33-41.

Almacellas, E., Pelletier, J., Manzano, A., Gentilella, A., Ambrosio, S., Mauvezin, C., and Tauler, A. (2019). Phosphofructokinases Axis Controls Glucose-Dependent mTORC1 Activation Driven by E2F1. *iScience* *20*, 434-448.

Andrews, R.G., Bryant, E.M., Bartelmez, S.H., Muirhead, D.Y., Knitter, G.H., Bensinger, W., Strong, D.M., and Bernstein, I.D. (1992). CD34+ marrow cells, devoid of T and B lymphocytes, reconstitute stable lymphopoiesis and myelopoiesis in lethally irradiated allogeneic baboons. *Blood* *80*, 1693-1701.

Angermuller, S., Bruder, G., Volkl, A., Wesch, H., and Fahimi, H.D. (1987). Localization of xanthine oxidase in crystalline cores of peroxisomes. A cytochemical and biochemical study. *Eur. J. Cell Biol.* *45*, 137-144.

Anne Stetler, R., Leak, R.K., Gao, Y., and Chen, J. (2013). The dynamics of the mitochondrial organelle as a potential therapeutic target. *Journal of cerebral blood flow and metabolism : official journal of the International Society of Cerebral Blood Flow and Metabolism* *33*, 22-32.

Annicotte, J.S., Blanchet, E., Chavey, C., Iankova, I., Costes, S., Assou, S., Teyssier, J., Dalle, S., Sardet, C., and Fajas, L. (2009). The CDK4-pRB-E2F1 pathway controls insulin secretion. *Nat. Cell Biol.* *11*, 1017-1023.

Aschner, M., and Toews, A.D. (2010). 13.11 - Myelin and Myelination*. In *Comprehensive Toxicology (Second Edition)*. C.A. McQueen, ed. (Oxford: Elsevier), pp. 181-198.

Asheuer, M., Bieche, I., Laurendeau, I., Moser, A., Hainque, B., Vidaud, M., and Aubourg, P. (2005). Decreased expression of ABCD4 and BG1 genes early in the pathogenesis of X-linked adrenoleukodystrophy. *Hum. Mol. Genet.* *14*, 1293-1303.

Asheuer, M., Pflumio, F., Benhamida, S., Dubart-Kupperschmitt, A., Fouquet, F., Imai, Y., Aubourg, P., and Cartier, N. (2004). Human CD34+ cells differentiate into microglia and express recombinant therapeutic protein. *Proc. Natl. Acad. Sci. U. S. A.* *101*, 3557-3562.

Askew, K., Li, K., Olmos-Alonso, A., Garcia-Moreno, F., Liang, Y., Richardson, P., Tipton, T., Chapman, M.A., Riecken, K., Beccari, S., et al. (2017). Coupled Proliferation and Apoptosis Maintain the Rapid Turnover of Microglia in the Adult Brain. *Cell Rep.* **18**, 391-405.

Attwooll, C., Lazzerini Denchi, E., and Helin, K. (2004). The E2F family: specific functions and overlapping interests. *EMBO J.* **23**, 4709-4716.

Aubourg, P., Adamsbaum, C., Lavallard-Rousseau, M.C., Rocchiccioli, F., Cartier, N., Jambaque, I., Jakobezak, C., Lemaitre, A., Boureau, F., Wolf, C., et al. (1993). A two-year trial of oleic and erucic acids ("Lorenzo's oil") as treatment for adrenomyeloneuropathy. *N. Engl. J. Med.* **329**, 745-752.

Aubourg, P., Blanche, S., Jambaque, I., Rocchiccioli, F., Kalifa, G., Naud-Saudreau, C., Rolland, M.O., Debre, M., Chaussain, J.L., Griscelli, C., et al. (1990). Reversal of early neurologic and neuroradiologic manifestations of X-linked adrenoleukodystrophy by bone marrow transplantation. *N. Engl. J. Med.* **322**, 1860-1866.

Augereau, P., Badia, E., Fuentes, M., Rabenoelina, F., Corniou, M., Derocq, D., Balaguer, P., and Cavailles, V. (2006). Transcriptional regulation of the human NRIP1/RIP140 gene by estrogen is modulated by dioxin signalling. *Mol. Pharmacol.* **69**, 1338-1346.

Avrahami, L., Farfara, D., Shaham-Kol, M., Vassar, R., Frenkel, D., and Eldar-Finkelman, H. (2013). Inhibition of Glycogen Synthase Kinase-3 Ameliorates β -Amyloid Pathology and Restores Lysosomal Acidification and Mammalian Target of Rapamycin Activity in the Alzheimer Disease Mouse Model: IN VIVO AND IN VITRO STUDIES *. *J. Biol. Chem.* **288**, 1295-1306.

Azoulay-Alfaguter, I., Elya, R., Avrahami, L., Katz, A., and Eldar-Finkelman, H. (2015). Combined regulation of mTORC1 and lysosomal acidification by GSK-3 suppresses autophagy and contributes to cancer cell growth. *Oncogene* **34**, 4613-4623.

Baarine, M., Andreoletti, P., Athias, A., Nury, T., Zarrouk, A., Ragot, K., Vejux, A., Riedinger, J.M., Kattan, Z., Bessede, G., et al. (2012). Evidence of oxidative stress in very long chain fatty acid - Treated oligodendrocytes and potentialization of ROS production using RNA interference-directed knockdown of ABCD1 and ACOX1 peroxisomal proteins. *Neuroscience* **213**, 1-18.

Baarine, M., Beeson, C., Singh, A., and Singh, I. (2015). ABCD1 deletion-induced mitochondrial dysfunction is corrected by SAHA: implication for adrenoleukodystrophy. *J. Neurochem.* **133**, 380-396.

Báez-Saldaña, A., Díaz, G., Espinoza, B., and Ortega, E. (1998). Biotin deficiency induces changes in subpopulations of spleen lymphocytes in mice. *The American Journal of Clinical Nutrition* **67**, 431-437.

Báez-Saldaña, A., and Ortega, E. (2004). Biotin Deficiency Blocks Thymocyte Maturation, Accelerates Thymus Involution, and Decreases Nose-Rump Length in Mice. *The Journal of Nutrition* **134**, 1970-1977.

Bagchi, S., Weinmann, R., and Raychaudhuri, P. (1991). The retinoblastoma protein copurifies with E2F-I, an E1A-regulated inhibitor of the transcription factor E2F. *Cell* **65**, 1063-1072.

Bailey, A.P., Koster, G., Guillermier, C., Hirst, E.M., MacRae, J.I., Lechene, C.P., Postle, A.D., and Gould, A.P. (2015). Antioxidant Role for Lipid Droplets in a Stem Cell Niche of *Drosophila*. *Cell* **163**, 340-353.

Bakan, I., and Laplante, M. (2012). Connecting mTORC1 signaling to SREBP-1 activation. *Curr. Opin. Lipidol.* **23**, 226-234.

Bandara, L.R., and La Thangue, N.B. (1991). Adenovirus E1a prevents the retinoblastoma gene product from complexing with a cellular transcription factor. *Nature* **351**, 494-497.

Barbier, M., Sabbagh, A., Kasper, E., Asheuer, M., Ahouansou, O., Pribill, I., Forss-Petter, S., Vidaud, M., Berger, J., and Aubourg, P. (2012). CD1 gene polymorphisms and phenotypic variability in X-linked adrenoleukodystrophy. *PLoS One* **7**, e29872.

Barendsen, R.W., Dijkstra, I.M.E., Visser, W.F., Alders, M., Blik, J., Boelen, A., Bouva, M.J., van der Crabben, S.N., Elsinghorst, E., van Gorp, A.G.M., et al. (2020). Adrenoleukodystrophy

Newborn Screening in the Netherlands (SCAN Study): The X-Factor. *Frontiers in cell and developmental biology* 8, 499.

Baumgart, E., Vanhorebeek, I., Grabenbauer, M., Borgers, M., Declercq, P.E., Fahimi, H.D., and Baes, M. (2001). Mitochondrial alterations caused by defective peroxisomal biogenesis in a mouse model for Zellweger syndrome (PEX5 knockout mouse). *Am. J. Pathol.* 159, 1477-1494.

Bautista, S.J., Boras, I., Vissa, A., Mecica, N., Yip, C.M., Kim, P.K., and Antonescu, C.N. (2018). mTOR complex 1 controls the nuclear localization and function of glycogen synthase kinase 3 β . *The Journal of biological chemistry* 293, 14723-14739.

Beal, M.F. (2005). Mitochondria take center stage in aging and neurodegeneration. *Ann. Neurol.* 58, 495-505.

Beers, D.R., Henkel, J.S., Xiao, Q., Zhao, W., Wang, J., Yen, A.A., Siklos, L., McKercher, S.R., and Appel, S.H. (2006). Wild-type microglia extend survival in PU.1 knockout mice with familial amyotrophic lateral sclerosis. *Proc. Natl. Acad. Sci. U. S. A.* 103, 16021-16026.

Bélanger, M., Allaman, I., and Magistretti, Pierre J. (2011). Brain Energy Metabolism: Focus on Astrocyte-Neuron Metabolic Cooperation. *Cell Metab.* 14, 724-738.

Benhamida, S., Pflumio, F., Dubart-Kupperschmitt, A., Zhao-Emonet, J.C., Cavazzana-Calvo, M., Rocchiccioli, F., Fichelson, S., Aubourg, P., Charneau, P., and Cartier, N. (2003). Transduced CD34+ cells from adrenoleukodystrophy patients with HIV-derived vector mediate long-term engraftment of NOD/SCID mice. *Mol. Ther.* 7, 317-324.

Berenson, R.J., Andrews, R.G., Bensinger, W.I., Kalamasz, D., Knitter, G., Buckner, C.D., and Bernstein, I.D. (1988). Antigen CD34+ marrow cells engraft lethally irradiated baboons. *J. Clin. Invest.* 81, 951-955.

Berger, J., Bernheimer, H., Fae, I., Braun, A., Roscher, A., Molzer, B., and Fischer, G. (1995). Association of X-linked adrenoleukodystrophy with HLA DRB1 alleles. *Biochem. Biophys. Res. Commun.* 216, 447-451.

Berger, J., Forss-Petter, S., and Eichler, F.S. (2014). Pathophysiology of X-linked adrenoleukodystrophy. *Biochimie* 98, 135-142.

Berger, J., Molzer, B., Fae, I., and Bernheimer, H. (1994). X-linked adrenoleukodystrophy (ALD): a novel mutation of the ALD gene in 6 members of a family presenting with 5 different phenotypes. *Biochem. Biophys. Res. Commun.* 205, 1638-1643.

Berger, J., Pujol, A., Aubourg, P., and Forss-Petter, S. (2010). Current and future pharmacological treatment strategies in X-linked adrenoleukodystrophy. *Brain Pathol.* 20, 845-856.

Bergner, C.G., van der Meer, F., Winkler, A., Wrzos, C., Türkmen, M., Valizada, E., Fitzner, D., Hametner, S., Hartmann, C., Pfeifenbring, S., et al. (2019). Microglia damage precedes major myelin breakdown in X-linked adrenoleukodystrophy and metachromatic leukodystrophy. *Glia* 67, 1196-1209.

Bhandari, S., Lee, J.N., Kim, Y.I., Nam, I.K., Kim, S.J., Kim, S.J., Kwak, S., Oh, G.S., Kim, H.J., Yoo, H.J., et al. (2016). The fatty acid chain elongase, Elovl1, is required for kidney and swim bladder development during zebrafish embryogenesis. *Organogenesis* 12, 78-93.

Bhatia, B., Hsieh, M., Kenney, A.M., and Nahlé, Z. (2011). Mitogenic Sonic hedgehog signaling drives E2F1-dependent lipogenesis in progenitor cells and medulloblastoma. *Oncogene* 30, 410-422.

Bieda, M., Xu, X., Singer, M.A., Green, R., and Farnham, P.J. (2006). Unbiased location analysis of E2F1-binding sites suggests a widespread role for E2F1 in the human genome. *Genome Res.* 16, 595-605.

Bilousova, G., Marusyk, A., Porter, C.C., Cardiff, R.D., and DeGregori, J. (2005). Impaired DNA Replication within Progenitor Cell Pools Promotes Leukemogenesis. *PLoS Biol.* 3, e401.

Bindu, P.S., Noone, M.L., Nalini, A., Muthane, U.B., and Kovoov, J.M. (2009). Biotin-responsive basal ganglia disease: a treatable and reversible neurological disorder of childhood. *J. Child Neurol.* 24, 750-752.

Bizzozero, O.A., Zuniga, G., and Lees, M.B. (1991). Fatty acid composition of human myelin proteolipid protein in peroxisomal disorders. *J. Neurochem.* *56*, 872-878.

Black, E., Hallstrom, T., Dressman, H., West, M., and Nevins, J. (2005). Distinctions in the specificity of E2F function revealed by gene expression signatures. *Proc. Natl. Acad. Sci. U. S. A.* *102*, 15948-15953.

Blanchet, E., Annicotte, J.S., Lagarrigue, S., Aguilar, V., Clape, C., Chavey, C., Fritz, V., Casas, F., Apparailly, F., Auwerx, J., et al. (2011). E2F transcription factor-1 regulates oxidative metabolism. *Nat. Cell Biol.* *13*, 1146-1152.

Blanchet, E., Annicotte, J.S., Pradelli, L.A., Hugon, G., Matecki, S., Mornet, D., Rivier, F., and Fajas, L. (2012). E2F transcription factor-1 deficiency reduces pathophysiology in the mouse model of Duchenne muscular dystrophy through increased muscle oxidative metabolism. *Hum. Mol. Genet.* *21*, 3910-3917.

Bodennec, J., Koul, O., Aguado, I., Brichon, G., Zwingelstein, G., and Portoukalian, J. (2000). A procedure for fractionation of sphingolipid classes by solid-phase extraction on aminopropyl cartridges. *J. Lipid Res.* *41*, 1524-1531.

Bonawitz, N.D., Clayton, D.A., and Shadel, G.S. (2006). Initiation and beyond: multiple functions of the human mitochondrial transcription machinery. *Mol. Cell* *24*, 813-825.

Boone-Villa, D., Aguilera, A., Miranda-Cervantes, A., and Fernandez-Mejia, C. (2015). Effects of Biotin Supplementation in the Diet on Adipose Tissue cGMP Concentrations, AMPK Activation, Lipolysis, and Serum-Free Fatty Acid Levels. *J. Med. Food* *18*.

Bossier, P., Fernandes, L., Vilela, C., and Rodrigues-Pousada, C. (1994). The yeast YKL741 gene situated on the left arm of chromosome XI codes for a homologue of the human ALD protein. *Yeast* *10*, 681-686.

Bouquet, F., Dehais, C., Sanson, M., Lubetzki, C., and Louapre, C. (2015). Dramatic worsening of adult-onset X-linked adrenoleukodystrophy after head trauma. *Neurology* *85*, 1991-1993.

Bousounis, D.P., Camfield, P.R., and Wolf, B. (1993). Reversal of brain atrophy with biotin treatment in biotinidase deficiency. *Neuropediatrics* *24*, 214-217.

Boutahar, N., Reynaud, E., Lassabliere, F., and Borg, J. (2010). Brain-derived neurotrophic factor inhibits cell cycle reentry but not endoplasmic reticulum stress in cultured neurons following oxidative or excitotoxic stress. *J. Neurosci. Res.* *88*, 2263-2271.

Boveris, A., Oshino, N., and Chance, B. (1972). The cellular production of hydrogen peroxide. *Biochem. J.* *128*, 617-630.

Bozza, P.T., and Viola, J.P.B. (2010). Lipid droplets in inflammation and cancer. *Prostaglandins, Leukotrienes and Essential Fatty Acids* *82*, 243-250.

Braiterman, L.T., Zheng, S., Watkins, P.A., Geraghty, M.T., Johnson, G., McGuinness, M.C., Moser, A.B., and Smith, K.D. (1998). Suppression of peroxisomal membrane protein defects by peroxisomal ATP binding cassette (ABC) proteins. *Hum. Mol. Genet.* *7*, 239-247.

Brawer, J.R., and Walsh, R.J. (1982). Response of tanycytes to aging in the median eminence of the rat. *Am. J. Anat.* *163*, 247-256.

Bregola, G., Muzzolini, A., Mazzari, S., Leon, A., Skaper, S.D., Beani, L., Bianchi, C., and Simonato, M. (1996). Biotin deficiency facilitates kindling hyperexcitability in rats. *Neuroreport* *7*, 1745-1748.

Breidenbach, R.W., and Beevers, H. (1967). Association of the glyoxylate cycle enzymes in a novel subcellular particle from castor bean endosperm. *Biochem. Biophys. Res. Commun.* *27*, 462-469.

Brose, R.D., Avramopoulos, D., and Smith, K.D. (2012). SOD2 as a potential modifier of X-linked adrenoleukodystrophy clinical phenotypes. *J. Neurol.* *259*, 1440-1447.

Brown, J., Greaves, M.F., and Molgaard, H.V. (1991). The gene encoding the stem cell antigen, CD34, is conserved in mouse and expressed in haemopoietic progenitor cell lines, brain, and embryonic fibroblasts. *Int. Immunol.* *3*, 175-184.

Budhavarapu, V.N., White, E.D., Mahanic, C.S., Chen, L., Lin, F.T., and Lin, W.C. (2012). Regulation of E2F1 by APC/C Cdh1 via K11 linkage-specific ubiquitin chain formation. *Cell Cycle* **11**, 2030-2038.

Budka, H., Sluga, E., and Heiss, W.D. (1976). Spastic paraplegia associated with Addison's disease: adult variant of adreno-leukodystrophy. *J. Neurol.* **213**, 237-250.

Bulua, A.C., Simon, A., Maddipati, R., Pelletier, M., Park, H., Kim, K.Y., Sack, M.N., Kastner, D.L., and Siegel, R.M. (2011). Mitochondrial reactive oxygen species promote production of proinflammatory cytokines and are elevated in TNFR1-associated periodic syndrome (TRAPS). *J. Exp. Med.* **208**, 519-533.

Busser, J., Geldmacher, D.S., and Herrup, K. (1998). Ectopic cell cycle proteins predict the sites of neuronal cell death in Alzheimer's disease brain. *J. Neurosci.* **18**, 2801-2807.

Cambron, M., D'Haeseleer, M., Laureys, G., Clinckers, R., Debruyne, J., and De Keyser, J. (2012). White-matter astrocytes, axonal energy metabolism, and axonal degeneration in multiple sclerosis. *J. Cereb. Blood Flow Metab.* **32**, 413-424.

Camporeale, G., Shubert, E.E., Sarath, G., Cerny, R., and Zemleni, J. (2004). K8 and K12 are biotinylated in human histone H4. *Eur. J. Biochem.* **271**, 2257-2263.

Canto, C., Gerhart-Hines, Z., Feige, J.N., Lagouge, M., Noriega, L., Milne, J.C., Elliott, P.J., Puigserver, P., and Auwerx, J. (2009). AMPK regulates energy expenditure by modulating NAD⁺ metabolism and SIRT1 activity. *Nature* **458**, 1056-1060.

Caron, A., Richard, D., and Laplante, M. (2015). The Roles of mTOR Complexes in Lipid Metabolism. *Annu. Rev. Nutr.* **35**, 321-348.

Carracedo, A., and Pandolfi, P.P. (2008). The PTEN–PI3K pathway: of feedbacks and cross-talks. *Oncogene* **27**, 5527-5541.

Cartier, N., and Aubourg, P. (2010). Hematopoietic stem cell transplantation and hematopoietic stem cell gene therapy in X-linked adrenoleukodystrophy. *Brain Pathol.* **20**, 857-862.

Cartier, N., Hacein-Bey-Abina, S., Bartholomae, C.C., Veres, G., Schmidt, M., Kutschera, I., Vidaud, M., Abel, U., Dal-Cortivo, L., Caccavelli, L., et al. (2009). Hematopoietic stem cell gene therapy with a lentiviral vector in X-linked adrenoleukodystrophy. *Science* **326**, 818-823.

Cartier, N., Lewis, C.A., Zhang, R., and Rossi, F.M. (2014). The role of microglia in human disease: therapeutic tool or target? *Acta Neuropathol.* **128**, 363-380.

Cartier, N., Lopez, J., Moullier, P., Rocchiccioli, F., Rolland, M.O., Jorge, P., Mosser, J., Mandel, J.L., Bougneres, P.F., Danos, O., et al. (1995). Retroviral-mediated gene transfer corrects very-long-chain fatty acid metabolism in adrenoleukodystrophy fibroblasts. *Proc. Natl. Acad. Sci. U. S. A.* **92**, 1674-1678.

Casasnovas, C., Ruiz, M., Schluter, A., Naudi, A., Fourcade, S., Veciana, M., Castaner, S., Alberti, A., Bargallo, N., Johnson, M., et al. (2019). Biomarker Identification, Safety, and Efficacy of High-Dose Antioxidants for Adrenomyeloneuropathy: a Phase II Pilot Study. *Neurotherapeutics*.

Cermenati, G., Audano, M., Giatti, S., Carozzi, V., Porretta-Serapiglia, C., Pettinato, E., Ferri, C., D'Antonio, M., De Fabiani, E., Crestani, M., et al. (2015). Lack of sterol regulatory element binding factor-1c imposes glial Fatty Acid utilization leading to peripheral neuropathy. *Cell Metab.* **21**, 571-583.

Chang, C.L., Weigel, A.V., Ioannou, M.S., Pasolli, H.A., Xu, C.S., Peale, D.R., Shtengel, G., Freeman, M., Hess, H.F., Blackstone, C., et al. (2019). Spastin tethers lipid droplets to peroxisomes and directs fatty acid trafficking through ESCRT-III. *J. Cell Biol.*

Chapman-Smith, A., and Cronan, J.E., Jr. (1999). In vivo enzymatic protein biotinylation. *Biomol. Eng.* **16**, 119-125.

Chauhan, J., and Dakshinamurti, K. (1991). Transcriptional regulation of the glucokinase gene by biotin in starved rats. *J. Biol. Chem.* **266**, 10035-10038.

Chen, C.-L., Uthaya Kumar, Dinesh B., Punj, V., Xu, J., Sher, L., Tahara, Stanley M., Hess, S., and Machida, K. (2016). NANOG Metabolically Reprograms Tumor-Initiating Stem-like Cells through

Tumorigenic Changes in Oxidative Phosphorylation and Fatty Acid Metabolism. *Cell Metab.* 23, 206-219.

Chen, C.T., Green, J.T., Orr, S.K., and Bazinet, R.P. (2008). Regulation of brain polyunsaturated fatty acid uptake and turnover. *Prostaglandins Leukot. Essent. Fatty Acids* 79, 85-91.

Chen, Y., Hou, Y., Ge, R., Han, J., Xu, J., Chen, J., and Wang, H. (2018). Protective effect of roscovitine against rotenone-induced parkinsonism. *Restor. Neurol. Neurosci.* 36, 629-638.

Cheng, D., Jenner, A.M., Shui, G., Cheong, W.F., Mitchell, T.W., Nealon, J.R., Kim, W.S., McCann, H., Wenk, M.R., Halliday, G.M., et al. (2011). Lipid pathway alterations in Parkinson's disease primary visual cortex. *PLoS One* 6, e17299.

Cheng, F.W., Lee, V., To, K.F., Chan, K.C., Shing, M.K., and Li, C.K. (2009). Post-transplant EBV-related lymphoproliferative disorder complicating umbilical cord blood transplantation in patients of adrenoleukodystrophy. *Pediatr. Blood Cancer* 53, 1329-1331.

Chew, Y.C., Camporeale, G., Kothapalli, N., Sarath, G., and Zemleni, J. (2006). Lysine residues in N-terminal and C-terminal regions of human histone H2A are targets for biotinylation by biotinidase. *J. Nutr. Biochem.* 17, 225-233.

Chittenden, T., Livingston, D.M., and Kaelin, W.G., Jr. (1991). RB associates with an E2F-like, sequence-specific DNA-binding protein. *Cold Spring Harb. Symp. Quant. Biol.* 56, 187-195.

Cho, E.C., Zheng, S., Munro, S., Liu, G., Carr, S.M., Moehlenbrink, J., Lu, Y.C., Stimson, L., Khan, O., Konietzny, R., et al. (2012). Arginine methylation controls growth regulation by E2F-1. *EMBO J.* 31, 1785-1797.

Chrast, R., Saher, G., Nave, K.A., and Verheijen, M.H. (2011). Lipid metabolism in myelinating glial cells: lessons from human inherited disorders and mouse models. *J. Lipid Res.* 52, 419-434.

Chun, J.N., Cho, M., Park, S., So, I., and Jeon, J.-H. (2020). The conflicting role of E2F1 in prostate cancer: A matter of cell context or interpretational flexibility? *Biochimica et Biophysica Acta (BBA) - Reviews on Cancer* 1873, 188336.

Chung, S., Dzeja, P.P., Faustino, R.S., Perez-Terzic, C., Behfar, A., and Terzic, A. (2007). Mitochondrial oxidative metabolism is required for the cardiac differentiation of stem cells. *Nature clinical practice. Cardiovascular medicine* 4 Suppl 1, S60-S67.

Ciechanover, A. (1998). The ubiquitin-proteasome pathway: on protein death and cell life. *EMBO J.* 17, 7151-7160.

Civin, C.I., Strauss, L.C., Brovall, C., Fackler, M.J., Schwartz, J.F., and Shaper, J.H. (1984). Antigenic analysis of hematopoiesis. III. A hematopoietic progenitor cell surface antigen defined by a monoclonal antibody raised against KG-1a cells. *J. Immunol.* 133, 157-165.

Coelho, D., Kim, J.C., Miousse, I.R., Fung, S., du Moulin, M., Buers, I., Suormala, T., Burda, P., Frapolli, M., Stucki, M., et al. (2012). Mutations in ABCD4 cause a new inborn error of vitamin B12 metabolism. *Nat. Genet.* 44, 1152-1155.

Coggeshall, J.C.H., John P. Robson, Martic C. Baker, Herman (1985). Biotin Status and Plasma Glucose in Diabetics. In *Ann. N. Y. Acad. Sci.*, pp. 389-392.

Cole, N.B., Murphy, D.D., Grider, T., Rueter, S., Brasaemle, D., and Nussbaum, R.L. (2002). Lipid Droplet Binding and Oligomerization Properties of the Parkinson's Disease Protein α -Synuclein. *J. Biol. Chem.* 277, 6344-6352.

Coppa, A., Guha, S., Fourcade, S., Parameswaran, J., Ruiz, M., Moser, A.B., Schlüter, A., Murphy, M.P., Lizcano, J.M., Miranda-Vizueté, A., et al. (2020). The peroxisomal fatty acid transporter ABCD1/PMP-4 is required in the *C. elegans* hypodermis for axonal maintenance: A worm model for adrenoleukodystrophy. *Free Radic. Biol. Med.* 152, 797-809.

Copps, K.D., and White, M.F. (2012). Regulation of insulin sensitivity by serine/threonine phosphorylation of insulin receptor substrate proteins IRS1 and IRS2. *Diabetologia* 55, 2565-2582.

Coulouarn, C., Gomez-Quiroz, L.E., Lee, J.S., Kaposi-Novak, P., Conner, E.A., Goldina, T.A., Onishchenko, G.E., Factor, V.M., and Thorgerisson, S.S. (2006). Oncogene-specific gene

expression signatures at preneoplastic stage in mice define distinct mechanisms of hepatocarcinogenesis. *Hepatology* 44, 1003-1011.

Court, F.A., and Coleman, M.P. (2012). Mitochondria as a central sensor for axonal degenerative stimuli. *Trends Neurosci.* 35, 364-372.

Cowan, M.J., Wara, D.W., Packman, S., Ammann, A.J., Yoshino, M., Sweetman, L., and Nyhan, W. (1979). Multiple biotin-dependent carboxylase deficiencies associated with defects in T-cell and B-cell immunity. *Lancet* 2, 115-118.

Cree, B.A.C., Cutter, G., Wolinsky, J.S., Freedman, M.S., Comi, G., Giovannoni, G., Hartung, H.-P., Arnold, D., Kuhle, J., Block, V., et al. (2020). Safety and efficacy of MD1003 (high-dose biotin) in patients with progressive multiple sclerosis (SPI2): a randomised, double-blind, placebo-controlled, phase 3 trial. *The Lancet Neurology* 19, 988-997.

Cross, C.E., Halliwell, B., Borish, E.T., Pryor, W.A., Ames, B.N., Saul, R.L., McCord, J.M., and Harman, D. (1987). Oxygen radicals and human disease. *Ann. Intern. Med.* 107, 526-545.

Cuervo, A.M., Stefanis, L., Fredenburg, R., Lansbury, P.T., and Sulzer, D. (2004). Impaired degradation of mutant alpha-synuclein by chaperone-mediated autophagy. *Science* 305, 1292-1295.

Dabbagh, O., Brismar, J., Gascon, G.G., and Ozand, P.T. (1994). The clinical spectrum of biotin-treatable encephalopathies in Saudi Arabia. *Brain Dev.* 16 Suppl, 72-80.

Darville, M.I., Antoine, I.V., Mertens-Strijthagen, J.R., Dupriez, V.J., and Rousseau, G.G. (1995). An E2F-dependent late-serum-response promoter in a gene that controls glycolysis. *Oncogene* 11, 1509-1517.

David, S., and Kroner, A. (2011). Repertoire of microglial and macrophage responses after spinal cord injury. *Nature Reviews Neuroscience* 12, 388-399.

de Beer, M., Engelen, M., and van Geel, B.M. (2014). Frequent occurrence of cerebral demyelination in adrenomyeloneuropathy. *Neurology* 83, 2227-2231.

De Duve, C., and Baudhuin, P. (1966). Peroxisomes (microbodies and related particles). *Physiol. Rev.* 46, 323-357.

de Estable-Puig, R.F., and Estable-Puig, J.F. (1973). Intraneuronal lipid droplets in irradiated nervous tissue. *Virchows Archiv B* 14, 117-125.

Dean, M., and Annilo, T. (2005). Evolution of the ATP-binding cassette (ABC) transporter superfamily in vertebrates. *Annu Rev Genomics Hum Genet* 6, 123-142.

Degregori, J., and Johnson, D. (2006). Distinct and Overlapping Roles for E2F Family Members in Transcription, Proliferation and Apoptosis. *Curr. Mol. Med.* 6, 739-748.

DeGregori, J., Leone, G., Miron, A., Jakoi, L., and Nevins, J.R. (1997). Distinct roles for E2F proteins in cell growth control and apoptosis. *Proc. Natl. Acad. Sci. U. S. A.* 94, 7245-7250.

Denechaud, P.-D., Fajas, L., and Giral, A. (2017). E2F1, a Novel Regulator of Metabolism. *Front. Endocrinol. (Lausanne)* 8.

Denechaud, P.D., Lopez-Mejia, I.C., Giral, A., Lai, Q., Blanchet, E., Delacuisine, B., Nicolay, B.N., Dyson, N.J., Bonner, C., Pattou, F., et al. (2016). E2F1 mediates sustained lipogenesis and contributes to hepatic steatosis. *J. Clin. Invest.* 126, 137-150.

Dennissen, F.J., Kholod, N., and van Leeuwen, F.W. (2012). The ubiquitin proteasome system in neurodegenerative diseases: culprit, accomplice or victim? *Prog. Neurobiol.* 96, 190-207.

Deon, M., Sitta, A., Barschak, A.G., Coelho, D.M., Pigatto, M., Schmitt, G.O., Jardim, L.B., Giugliani, R., Wajner, M., and Vargas, C.R. (2007). Induction of lipid peroxidation and decrease of antioxidant defenses in symptomatic and asymptomatic patients with X-linked adrenoleukodystrophy. *Int. J. Dev. Neurosci.* 25, 441-444.

Deon, M., Sitta, A., Barschak, A.G., Coelho, D.M., Terroso, T., Schmitt, G.O., Wanderley, H.Y., Jardim, L.B., Giugliani, R., Wajner, M., et al. (2008). Oxidative stress is induced in female carriers of X-linked adrenoleukodystrophy. *J. Neurol. Sci.* 266, 79-83.

DeWille, J.E., and Horrocks, L.A. (1992). Synthesis and turnover of myelin phospholipids and cholesterol.

Dhar, S.S., Ongwijitwat, S., and Wong-Riley, M.T.T. (2008). Nuclear respiratory factor 1 regulates all ten nuclear-encoded subunits of cytochrome c oxidase in neurons. *The Journal of biological chemistry* 283, 3120-3129.

Dhaunsi, G.S., Gulati, S., Singh, A.K., Orak, J.K., Asayama, K., and Singh, I. (1992). Demonstration of Cu-Zn superoxide dismutase in rat liver peroxisomes. Biochemical and immunochemical evidence. *J. Biol. Chem.* 267, 6870-6873.

Di Biase, A., Salvati, S., VarÀ, R., Avellino, C., Sforza, F., Cappa, M., and Masella, R. (2000). Susceptibility to oxidation of plasma low-density lipoprotein in X-linked adrenoleukodystrophy: effects of simvastatin treatment. *Mol. Genet. Metab.* 71, 651-655.

Di Stefano, L., Jensen, M.R., and Helin, K. (2003). E2F7, a novel E2F featuring DP-independent repression of a subset of E2F-regulated genes. *The EMBO journal* 22, 6289-6298.

Dimri, G., Itahana, K., Acosta, M., and Campisi, J. (2000). Regulation of a Senescence Checkpoint Response by the E2F1 Transcription Factor and p14ARF Tumor Suppressor. *Mol. Cell. Biol.* 20, 273-285.

Docquier, A., Augereau, P., Lapierre, M., Harmand, P.O., Badia, E., Annicotte, J.S., Fajas, L., and Cavailles, V. (2012). The RIP140 gene is a transcriptional target of E2F1. *PLoS One* 7, e35839.

Docquier, A., Harmand, P.O., Fritsch, S., Chanrion, M., Darbon, J.M., and Cavailles, V. (2010). The transcriptional coregulator RIP140 represses E2F1 activity and discriminates breast cancer subtypes. *Clin. Cancer Res.* 16, 2959-2970.

Doerflinger, N., Miclea, J.M., Lopez, J., Chomienne, C., Bougnères, P., Aubourg, P., and Cartier, N. (1998). Retroviral transfer and long-term expression of the adrenoleukodystrophy gene in human CD34+ cells. *Hum. Gene Ther.* 9, 1025-1036.

Dokusova, O.K., and Krivoruchenko, I.V. (1972). [The effect of biotin on the level of cholesterol in the blood of patients with atherosclerosis and essential hyperlipidemia]. *Kardiologiya* 12, 113.

Dong, Y., D’Mello, C., Pinsky, W., Lozinski, B.M., Kaushik, D.K., Ghorbani, S., Moezzi, D., Brown, D., Melo, F.C., Zandee, S., et al. (2021). Oxidized phosphatidylcholines found in multiple sclerosis lesions mediate neurodegeneration and are neutralized by microglia. *Nat. Neurosci.* 24, 489-503.

Douglas, P.M., and Dillin, A. (2010). Protein homeostasis and aging in neurodegeneration. *J. Cell Biol.* 190, 719-729.

Dubey, P., Raymond, G.V., Moser, A.B., Kharkar, S., Bezman, L., and Moser, H.W. (2005). Adrenal insufficiency in asymptomatic adrenoleukodystrophy patients identified by very long-chain fatty acid screening. *J. Pediatr.* 146, 528-532.

Dumser, M., Bauer, J., Lassmann, H., Berger, J., and Forss-Petter, S. (2007). Lack of adrenoleukodystrophy protein enhances oligodendrocyte disturbance and microglia activation in mice with combined Abcd1/Mag deficiency. *Acta Neuropathol.* 114, 573-586.

Dutta, R., McDonough, J., Yin, X., Peterson, J., Chang, A., Torres, T., Gudz, T., Macklin, W.B., Lewis, D.A., Fox, R.J., et al. (2006). Mitochondrial dysfunction as a cause of axonal degeneration in multiple sclerosis patients. *Ann. Neurol.* 59, 478-489.

Dyson, N. (1998). The regulation of E2F by pRB-family proteins. *Genes Dev.* 12, 2245-2262.

Dyson, N.J. (2016). RB1: a prototype tumor suppressor and an enigma. *Genes Dev.* 30, 1492-1502.

Eglitis, M.A., and Mezey, E. (1997). Hematopoietic cells differentiate into both microglia and macroglia in the brains of adult mice. *Proc. Natl. Acad. Sci. U. S. A.* 94, 4080-4085.

Eichler, F., Duncan, C., Musolino, P.L., Orchard, P.J., De Oliveira, S., Thrasher, A.J., Armant, M., Dansereau, C., Lund, T.C., Miller, W.P., et al. (2017). Hematopoietic Stem-Cell Gene Therapy for Cerebral Adrenoleukodystrophy. *N. Engl. J. Med.* 377, 1630-1638.

Eichler, F.S., Ren, J.Q., Cossoy, M., Rietsch, A.M., Nagpal, S., Moser, A.B., Frosch, M.P., and Ransohoff, R.M. (2008). Is microglial apoptosis an early pathogenic change in cerebral X-linked adrenoleukodystrophy? *Ann. Neurol.* 63, 729-742.

El-Bassyouni, H.T., Abdel Maksoud, S.A., Salem, F.A., Badr El-Deen, R., Abdel Aziz, H., and Thomas, M.M. (2012). Evidence of oxidative stress in peroxisomal disorders. *Singapore Med. J.* *53*, 608-614.

El Bejjani, R., and Hammarlund, M. (2012). Neural regeneration in *Caenorhabditis elegans*. *Annu. Rev. Genet.* *46*, 499-513.

Engelen, M., Barbier, M., Dijkstra, I.M., Schur, R., de Bie, R.M., Verhamme, C., Dijkgraaf, M.G., Aubourg, P.A., Wanders, R.J., van Geel, B.M., et al. (2014). X-linked adrenoleukodystrophy in women: a cross-sectional cohort study. *Brain* *137*, 693-706.

Engelen, M., Kemp, S., de Visser, M., van Geel, B.M., Wanders, R.J., Aubourg, P., and Poll-The, B.T. (2012a). X-linked adrenoleukodystrophy (X-ALD): clinical presentation and guidelines for diagnosis, follow-up and management. *Orphanet J. Rare Dis.* *7*, 51.

Engelen, M., Ofman, R., Dijkgraaf, M.G., Hijzen, M., van der Wardt, L.A., van Geel, B.M., de Visser, M., Wanders, R.J., Poll-The, B.T., and Kemp, S. (2010). Lovastatin in X-linked adrenoleukodystrophy. *N. Engl. J. Med.* *362*, 276-277.

Engelen, M., Schackmann, M.J., Ofman, R., Sanders, R.J., Dijkstra, I.M., Houten, S.M., Fourcade, S., Pujol, A., Poll-The, B.T., Wanders, R.J., et al. (2012b). Bezafibrate lowers very long-chain fatty acids in X-linked adrenoleukodystrophy fibroblasts by inhibiting fatty acid elongation. *J. Inherit. Metab. Dis.* *35*, 1137-1145.

Engelen, M., Tran, L., Ofman, R., Brennecke, J., Moser, A.B., Dijkstra, I.M., Wanders, R.J., Poll-The, B.T., and Kemp, S. (2012c). Bezafibrate for X-linked adrenoleukodystrophy. *PLoS One* *7*, e41013.

Eriksson, L., and Westermarck, P. (1990). Age-related accumulation of amyloid inclusions in adrenal cortical cells. *Am. J. Pathol.* *136*, 461-466.

Espada, L., Meo-Evoli, N., Sancho, P., Real, S., Fabregat, I., Ambrosio, S., and Tauler, A. (2012). ROS production is essential for the apoptotic function of E2F1 in pheochromocytoma and neuroblastoma cell lines. *PLoS One* *7*, e51544-e51544.

Ewart, G.D., Cannell, D., Cox, G.B., and Howells, A.J. (1994). Mutational analysis of the traffic ATPase (ABC) transporters involved in uptake of eye pigment precursors in *Drosophila melanogaster*. Implications for structure-function relationships. *J. Biol. Chem.* *269*, 10370-10377.

Fahy, E., Subramaniam, S., Brown, H.A., Glass, C.K., Merrill, A.H., Jr., Murphy, R.C., Raetz, C.R., Russell, D.W., Seyama, Y., Shaw, W., et al. (2005). A comprehensive classification system for lipids. *J. Lipid Res.* *46*, 839-861.

Fajas, L., Annicotte, J.-S., Miard, S., Sarruf, D., Watanabe, M., and Auwerx, J. (2004). Impaired pancreatic growth, beta cell mass, and beta cell function in E2F1 (-/-) mice. *The Journal of clinical investigation* *113*, 1288-1295.

Fajas, L., Egler, V., Reiter, R., Hansen, J., Kristiansen, K., Debril, M.B., Miard, S., and Auwerx, J. (2002a). The retinoblastoma-histone deacetylase 3 complex inhibits PPARgamma and adipocyte differentiation. *Dev. Cell* *3*, 903-910.

Fajas, L., Landsberg, R.L., Huss-Garcia, Y., Sardet, C., Lees, J.A., and Auwerx, J. (2002b). E2Fs Regulate Adipocyte Differentiation. *Dev. Cell* *3*, 39-49.

Fanconi, A., Prader, A., Isler, W., Luethy, F., and Siebenmann, R. (1963). Addison's Disease With Cerebral Sclerosis in Childhood. A Hereditary Syndrome Transmitted Through Chromosome X? *Helv. Paediatr. Acta* *18*, 480-501.

Farmer, B.C., Kluemper, J., and Johnson, L.A. (2019). Apolipoprotein E4 Alters Astrocyte Fatty Acid Metabolism and Lipid Droplet Formation. *Cells* *8*.

Farmer, B.C., Walsh, A.E., Kluemper, J.C., and Johnson, L.A. (2020). Lipid Droplets in Neurodegenerative Disorders. *Front. Neurosci.* *14*.

Feige, J.N., and Auwerx, J. (2007). Transcriptional coregulators in the control of energy homeostasis. *Trends Cell Biol.* *17*, 292-301.

Ferdinandusse, S., Jimenez-Sanchez, G., Koster, J., Denis, S., Van Roermund, C.W., Silva-Zolezzi, I., Moser, A.B., Visser, W.F., Gulluoglu, M., Durmaz, O., et al. (2015). A novel bile acid biosynthesis defect due to a deficiency of peroxisomal ABCD3. *Hum. Mol. Genet.* *24*, 361-370.

Fernandez-Mejia, C. (2005). Pharmacological effects of biotin. *J. Nutr. Biochem.* *16*, 424-427.

Fernández de Mattos, S., Lam, E.W.F., and Tauler, A. (2002). An E2F-binding site mediates the activation of the proliferative isoform of 6-phosphofructo-2-kinase/fructose-2,6-bisphosphatase by phosphatidylinositol 3-kinase. *The Biochemical journal* *368*, 283-291.

Ferrer, I., Kapfhammer, J.P., Hindelang, C., Kemp, S., Troffer-Charlier, N., Broccoli, V., Callyzot, N., Mooyer, P., Selhorst, J., Vreken, P., et al. (2005). Inactivation of the peroxisomal ABCD2 transporter in the mouse leads to late-onset ataxia involving mitochondria, Golgi and endoplasmic reticulum damage. *Hum. Mol. Genet.* *14*, 3565-3577.

Fileiko, N.A., Kolar, C., West, J.T., Smith, S.A., Hassan, Y.I., Borgstahl, G.E.O., Zemleni, J., and Lyubchenko, Y.L. (2011). The Role of Histone H4 Biotinylation in the Structure of Nucleosomes. *PLoS One* *6*, e16299.

Fina, L., Molgaard, H.V., Robertson, D., Bradley, N.J., Monaghan, P., Delia, D., Sutherland, D.R., Baker, M.A., and Greaves, M.F. (1990). Expression of the CD34 gene in vascular endothelial cells. *Blood* *75*, 2417-2426.

Flavigny, E., Sanhaj, A., Aubourg, P., and Cartier, N. (1999). Retroviral-mediated adrenoleukodystrophy-related gene transfer corrects very long chain fatty acid metabolism in adrenoleukodystrophy fibroblasts: implications for therapy. *FEBS Lett.* *448*, 261-264.

Folch, J., Lees, M., and Sloane Stanley, G.H. (1957). A simple method for the isolation and purification of total lipides from animal tissues. *J. Biol. Chem.* *226*, 497-509.

Forss-Petter, S., Werner, H., Berger, J., Lassmann, H., Molzer, B., Schwab, M.H., Bernheimer, H., Zimmermann, F., and Nave, K.A. (1997). Targeted inactivation of the X-linked adrenoleukodystrophy gene in mice. *J. Neurosci. Res.* *50*, 829-843.

Fouquet, F., Zhou, J.M., Ralston, E., Murray, K., Troalen, F., Magal, E., Robain, O., Dubois-Dalcq, M., and Aubourg, P. (1997). Expression of the adrenoleukodystrophy protein in the human and mouse central nervous system. *Neurobiol. Dis.* *3*, 271-285.

Fourcade, S., Ferrer, I., and Pujol, A. (2015). Oxidative stress, mitochondrial and proteostasis malfunction in adrenoleukodystrophy: A paradigm for axonal degeneration. *Free Radic. Biol. Med.* *88*, 18-29.

Fourcade, S., Goicoechea, L., Parameswaran, J., Schlüter, A., Launay, N., Ruiz, M., Seyer, A., Colsch, B., Calingasan, N.Y., Ferrer, I., et al. (2020). High-dose biotin restores redox balance, energy and lipid homeostasis, and axonal health in a model of adrenoleukodystrophy. *Brain Pathol.* *30*, 945-963.

Fourcade, S., Lopez-Erauskin, J., Galino, J., Duval, C., Naudi, A., Jove, M., Kemp, S., Villarroja, F., Ferrer, I., Pamplona, R., et al. (2008). Early oxidative damage underlying neurodegeneration in X-adrenoleukodystrophy. *Hum. Mol. Genet.* *17*, 1762-1773.

Fourcade, S., Ruiz, M., Guilera, C., Hahnen, E., Brichta, L., Naudi, A., Portero-Otin, M., Dacremont, G., Cartier, N., Wanders, R., et al. (2010). Valproic acid induces antioxidant effects in X-linked adrenoleukodystrophy. *Hum. Mol. Genet.* *19*, 2005-2014.

Fourcade, S., Savary, S., Albet, S., Gauthé, D., Gondcaille, C., Pineau, T., Bellenger, J., Bentejac, M., Holzinger, A., Berger, J., et al. (2001). Fibrate induction of the adrenoleukodystrophy-related gene (ABCD2): promoter analysis and role of the peroxisome proliferator-activated receptor PPARalpha. *Eur. J. Biochem.* *268*, 3490-3500.

Fransen, M., Lismont, C., and Walton, P. (2017). The Peroxisome-Mitochondria Connection: How and Why? *Int. J. Mol. Sci.* *18*.

Frolov, M.V., and Dyson, N.J. (2004). Molecular mechanisms of E2F-dependent activation and pRB-mediated repression. *J. Cell Sci.* *117*, 2173-2181.

Füger, P., Hefendehl, J.K., Veeraraghavalu, K., Wendeln, A.-C., Schlosser, C., Obermüller, U., Wegenast-Braun, B.M., Neher, J.J., Martus, P., Kohsaka, S., et al. (2017). Microglia turnover

with aging and in an Alzheimer's model via long-term in vivo single-cell imaging. *Nat. Neurosci.* **20**, 1371-1376.

Funfschilling, U., Supplie, L.M., Mahad, D., Boretius, S., Saab, A.S., Edgar, J., Brinkmann, B.G., Kassmann, C.M., Tzvetanova, I.D., Mobius, W., et al. (2012). Glycolytic oligodendrocytes maintain myelin and long-term axonal integrity. *Nature* **485**, 517-521.

Furukawa, Y. (1999). [Enhancement of glucose-induced insulin secretion and modification of glucose metabolism by biotin]. *Nihon Rinsho* **57**, 2261-2269.

Gabalton, T., Snel, B., van Zimmeren, F., Hemrika, W., Tabak, H., and Huynen, M.A. (2006). Origin and evolution of the peroxisomal proteome. *Biol. Direct* **1**, 8.

Galbiati, L., Mendoza-Maldonado, R., Gutierrez, M.I., and Giacca, M. (2005). Regulation of E2F-1 after DNA damage by p300-mediated acetylation and ubiquitination. *Cell Cycle* **4**, 930-939.

Galea, E., Launay, N., Portero-Otin, M., Ruiz, M., Pamplona, R., Aubourg, P., Ferrer, I., and Pujol, A. (2012). Oxidative stress underlying axonal degeneration in adrenoleukodystrophy: a paradigm for multifactorial neurodegenerative diseases? *Biochim. Biophys. Acta* **1822**, 1475-1488.

Galino, J., Ruiz, M., Fourcade, S., Schluter, A., Lopez-Erauskin, J., Guilera, C., Jove, M., Naudi, A., Garcia-Arumi, E., Andreu, A.L., et al. (2011). Oxidative damage compromises energy metabolism in the axonal degeneration mouse model of X-adrenoleukodystrophy. *Antioxid Redox Signal* **15**, 2095-2107.

Garbuzova-Davis, S., Haller, E., Lin, R., and Borlongan, C.V. (2017). Intravenously Transplanted Human Bone Marrow Endothelial Progenitor Cells Engraft Within Brain Capillaries, Preserve Mitochondrial Morphology, and Display Pinocytotic Activity Toward Blood-Brain Barrier Repair in Ischemic Stroke Rats. *Stem Cells* **35**, 1246-1258.

Gaubatz, S., Wood, J.G., and Livingston, D.M. (1998). Unusual proliferation arrest and transcriptional control properties of a newly discovered E2F family member, E2F-6. *Proceedings of the National Academy of Sciences* **95**, 9190-9195.

Geillon, F., Gondcaille, C., Charbonnier, S., Van Roermund, C.W., Lopez, T.E., Dias, A.M., Pais de Barros, J.P., Arnould, C., Wanders, R.J., Trompier, D., et al. (2014). Structure-function analysis of peroxisomal ATP-binding cassette transporters using chimeric dimers. *J. Biol. Chem.* **289**, 24511-24520.

Geillon, F., Gondcaille, C., Raas, Q., Dias, A.M., Pecqueur, D., Truntzer, C., Lucchi, G., Ducoroy, P., Falson, P., Savary, S., et al. (2017). Peroxisomal ATP-binding cassette transporters form mainly tetramers. *J. Biol. Chem.*

Gemin, A., Sweet, S., Preston, T.J., and Singh, G. (2005). Regulation of the cell cycle in response to inhibition of mitochondrial generated energy. *Biochem. Biophys. Res. Commun.* **332**, 1122-1132.

Genin, E.C., Geillon, F., Gondcaille, C., Athias, A., Gambert, P., Trompier, D., and Savary, S. (2011). Substrate specificity overlap and interaction between adrenoleukodystrophy protein (ALDP/ABCD1) and adrenoleukodystrophy-related protein (ALDRP/ABCD2). *J. Biol. Chem.* **286**, 8075-8084.

Giese, K.P. (2009). GSK-3: A key player in neurodegeneration and memory. *IUBMB Life* **61**, 516-521.

Gieselmann, V. (2008). Metachromatic leukodystrophy: genetics, pathogenesis and therapeutic options. *Acta Paediatr.* **97**, 15-21.

Giguère, V. (2008). Transcriptional control of energy homeostasis by the estrogen-related receptors. *Endocr. Rev.* **29**, 677-696.

Gilg, A.G., Singh, A.K., and Singh, I. (2000). Inducible nitric oxide synthase in the central nervous system of patients with X-adrenoleukodystrophy. *J. Neuropathol. Exp. Neurol.* **59**, 1063-1069.

Ginhoux, F., Greter, M., Leboeuf, M., Nandi, S., See, P., Gokhan, S., Mehler, M.F., Conway, S.J., Ng, L.G., Stanley, E.R., et al. (2010). Fate mapping analysis reveals that adult microglia derive from primitive macrophages. *Science* **330**, 841-845.

Ginhoux, F., Lim, S., Hoeffel, G., Low, D., and Huber, T. (2013). Origin and differentiation of microglia. *Front. Cell. Neurosci.* 7, 45-45.

Giovanni, A., Keramaris, E., Morris, E.J., Hou, S.T., O'Hare, M., Dyson, N., Robertson, G.S., Slack, R.S., and Park, D.S. (2000). E2F1 mediates death of B-amyloid-treated cortical neurons in a manner independent of p53 and dependent on Bax and caspase 3. *J. Biol. Chem.* 275, 11553-11560.

Gnaiger, E. (2001). Bioenergetics at low oxygen: dependence of respiration and phosphorylation on oxygen and adenosine diphosphate supply. *Respir. Physiol.* 128, 277-297.

Goldberg, A.L. (2003). Protein degradation and protection against misfolded or damaged proteins. *Nature* 426, 895-899.

Goldfischer, S., Moore, C.L., Johnson, A.B., Spiro, A.J., Valsamis, M.P., Wisniewski, H.K., Ritch, R.H., Norton, W.T., Rapin, I., and Gartner, L.M. (1973). Peroxisomal and mitochondrial defects in the cerebro-hepato-renal syndrome. *Science* 182, 62-64.

Goldmann, T., Wieghofer, P., Jordão, M.J., Prutek, F., Hagemeyer, N., Frenzel, K., Amann, L., Staszewski, O., Kierdorf, K., Krueger, M., et al. (2016). Origin, fate and dynamics of macrophages at central nervous system interfaces. *Nat. Immunol.* 17, 797-805.

Gondcaille, C., Depreter, M., Fourcade, S., Lecca, M.R., Leclercq, S., Martin, P.G., Pineau, T., Cadepond, F., ElEtr, M., Bertrand, N., et al. (2005). Phenylbutyrate up-regulates the adrenoleukodystrophy-related gene as a nonclassical peroxisome proliferator. *J. Cell Biol.* 169, 93-104.

Gong, Y., Sasidharan, N., Laheji, F., Frosch, M., Musolino, P., Tanzi, R., Kim, D.Y., Biffi, A., El Khoury, J., and Eichler, F. (2017). Microglial dysfunction as a key pathological change in adrenomyeloneuropathy. *Ann. Neurol.* 82, 813-827.

Gonzalez-Romero, F., Mestre, D., Aurrekoetxea, I., O'Rourke, C.J., Andersen, J.B., Woodhoo, A., Tamayo-Caro, M., Varela Rey, M., Palomo-Irigoyen, M., Gómez-Santos, B., et al. (2021). E2F1 and E2F2-mediated repression of CPT2 establishes a lipid-rich tumor-promoting environment. *Cancer Res.*, canres.2052.2020.

Goto, Y., Hayashi, R., Kang, D., and Yoshida, K. (2006). Acute loss of transcription factor E2F1 induces mitochondrial biogenesis in HeLa cells. *J. Cell. Physiol.* 209, 923-934.

Gralla, M., Camporeale, G., and Zempleni, J. (2008). Holocarboxylase synthetase regulates expression of biotin transporters by chromatin remodeling events at the SMVT locus. *J. Nutr. Biochem.* 19, 400-408.

Gray, M.W., Burger, G., and Lang, B.F. (1999). Mitochondrial evolution. *Science* 283, 1476-1481.

Greenberg, A.S., Coleman, R.A., Kraemer, F.B., McManaman, J.L., Obin, M.S., Puri, V., Yan, Q.W., Miyoshi, H., and Mashek, D.G. (2011). The role of lipid droplets in metabolic disease in rodents and humans. *J. Clin. Invest.* 121, 2102-2110.

Griffin, D.E., Moser, H.W., Mendoza, Q., Moench, T.R., O'Toole, S., and Moser, A.B. (1985). Identification of the inflammatory cells in the central nervous system of patients with adrenoleukodystrophy. *Ann. Neurol.* 18, 660-664.

Griffin, J.W., Goren, E., Schaumburg, H., Engel, W.K., and Loriaux, L. (1977). Adrenomyeloneuropathy: a probable variant of adrenoleukodystrophy. I. Clinical and endocrinologic aspects. *Neurology* 27, 1107-1113.

Grunewald, S., Champion, M.P., Leonard, J.V., Schaper, J., and Morris, A.A. (2004). Biotinidase deficiency: a treatable leukoencephalopathy. *Neuropediatrics* 35, 211-216.

Guimaraes, C.P., Domingues, P., Aubourg, P., Fouquet, F., Pujol, A., Jimenez-Sanchez, G., Sa-Miranda, C., and Azevedo, J.E. (2004). Mouse liver PMP70 and ALDP: homomeric interactions prevail in vivo. *Biochim. Biophys. Acta* 1689, 235-243.

Hajra, A.K., and Bishop, J.E. (1982). Glycerolipid biosynthesis in peroxisomes via the acyl dihydroxyacetone phosphate pathway. *Ann. N. Y. Acad. Sci.* 386, 170-182.

Halliwell, B. (2006). Oxidative stress and neurodegeneration: where are we now? *J. Neurochem.* 97, 1634-1658.

Halliwell, B. (2007). Biochemistry of oxidative stress. *Biochem. Soc. Trans.* *35*, 1147-1150.

Halliwell, B., and Whiteman, M. (2004). Measuring reactive species and oxidative damage in vivo and in cell culture: how should you do it and what do the results mean? *Br. J. Pharmacol.* *142*, 231-255.

Handschin, C., Chin, S., Li, P., Liu, F., Maratos-Flier, E., Lebrasseur, N.K., Yan, Z., and Spiegelman, B.M. (2007). Skeletal muscle fiber-type switching, exercise intolerance, and myopathy in PGC-1alpha muscle-specific knock-out animals. *J. Biol. Chem.* *282*, 30014-30021.

Hao, S., Chen, C., and Cheng, T. (2016). Cell cycle regulation of hematopoietic stem or progenitor cells. *Int. J. Hematol.* *103*, 487-497.

Hashimoto, D., Chow, A., Noizat, C., Teo, P., Beasley, M.B., Leboeuf, M., Becker, C.D., See, P., Price, J., Lucas, D., et al. (2013). Tissue-resident macrophages self-maintain locally throughout adult life with minimal contribution from circulating monocytes. *Immunity* *38*, 792-804.

Healy, L., May, G., Gale, K., Grosveld, F., Greaves, M., and Enver, T. (1995). The stem cell antigen CD34 functions as a regulator of hemopoietic cell adhesion. *Proc. Natl. Acad. Sci. U. S. A.* *92*, 12240-12244.

Healy, S., Perez-Cadahia, B., Jia, D., McDonald, M.K., Davie, J.R., and Gravel, R.A. (2009). Biotin is not a natural histone modification. *Biochimica et Biophysica Acta (BBA) - Gene Regulatory Mechanisms* *1789*, 719-733.

Heinzer, A.K., Watkins, P.A., Lu, J.F., Kemp, S., Moser, A.B., Li, Y.Y., Mihalik, S., Powers, J.M., and Smith, K.D. (2003). A very long-chain acyl-CoA synthetase-deficient mouse and its relevance to X-linked adrenoleukodystrophy. *Hum. Mol. Genet.* *12*, 1145-1154.

Hemmati, M., Babaei, H., and Abdolsalehei, M. (2013). Survey of the effect of biotin on glycemic control and plasma lipid concentrations in type 1 diabetic patients in kermanshah in iran (2008-2009). *Oman Med. J.* *28*, 195-198.

Heneka, M.T., Sastre, M., Dumitrescu-Ozimek, L., Hanke, A., Dewachter, I., Kuiperi, C., O'Banion, K., Klockgether, T., Van Leuven, F., and Landreth, G.E. (2005). Acute treatment with the PPARgamma agonist pioglitazone and ibuprofen reduces glial inflammation and Abeta1-42 levels in APPV717I transgenic mice. *Brain* *128*, 1442-1453.

Hernandez-Vazquez, A., Ochoa-Ruiz, E., Ibarra-Gonzalez, I., Ortega-Cuellar, D., Salvador-Adriano, A., and Velazquez-Arellano, A. (2012). Temporal development of genetic and metabolic effects of biotin deprivation. A search for the optimum time to study a vitamin deficiency. *Mol. Genet. Metab.* *107*, 345-351.

Hernandez-Vazquez, A., Wolf, B., Pindolia, K., Ortega-Cuellar, D., Hernandez-Gonzalez, R., Heredia-Antunez, A., Ibarra-Gonzalez, I., and Velazquez-Arellano, A. (2013). Biotinidase knockout mice show cellular energy deficit and altered carbon metabolism gene expression similar to that of nutritional biotin deprivation: clues for the pathogenesis in the human inherited disorder. *Mol. Genet. Metab.* *110*, 248-254.

Hess, D.C., Hill, W.D., Martin-Studdard, A., Carroll, J., Brailer, J., and Carothers, J. (2002). Bone Marrow as a Source of Endothelial Cells and NeuN-Expressing Cells After Stroke. *Stroke* *33*, 1362-1368.

Hettema, E.H., van Roermund, C.W., Distel, B., van den Berg, M., Vilela, C., Rodrigues-Pousada, C., Wanders, R.J., and Tabak, H.F. (1996). The ABC transporter proteins Pat1 and Pat2 are required for import of long-chain fatty acids into peroxisomes of *Saccharomyces cerevisiae*. *EMBO J.* *15*, 3813-3822.

Hickey, W.F., and Kimura, H. (1988). Perivascular microglial cells of the CNS are bone marrow-derived and present antigen in vivo. *Science* *239*, 290-292.

Ho, J.K., Moser, H., Kishimoto, Y., and Hamilton, J.A. (1995). Interactions of a very long chain fatty acid with model membranes and serum albumin. Implications for the pathogenesis of adrenoleukodystrophy. *J. Clin. Invest.* *96*, 1455-1463.

Hoftberger, R., Kunze, M., Weinhofer, I., Aboul-Enein, F., Voigtlander, T., Oezen, I., Amann, G., Bernheimer, H., Budka, H., and Berger, J. (2007). Distribution and cellular localization of

adrenoleukodystrophy protein in human tissues: implications for X-linked adrenoleukodystrophy. *Neurobiol. Dis.* 28, 165-174.

Höglinger, G.U., Breunig, J.J., Depboylu, C., Rouaux, C., Michel, P.P., Alvarez-Fischer, D., Boutillier, A.L., Degregori, J., Oertel, W.H., Rakic, P., et al. (2007). The pRb/E2F cell-cycle pathway mediates cell death in Parkinson's disease. *Proc. Natl. Acad. Sci. U. S. A.* 104, 3585-3590.

Holzinger, A., Kammerer, S., Berger, J., and Roscher, A.A. (1997). cDNA cloning and mRNA expression of the human adrenoleukodystrophy related protein (ALDRP), a peroxisomal ABC transporter. *Biochem. Biophys. Res. Commun.* 239, 261-264.

Holzinger, A., Mayerhofer, P., Berger, J., Lichtner, P., Kammerer, S., and Roscher, A.A. (1999). Full length cDNA cloning, promoter sequence, and genomic organization of the human adrenoleukodystrophy related (ALDR) gene functionally redundant to the gene responsible for X-linked adrenoleukodystrophy. *Biochem. Biophys. Res. Commun.* 258, 436-442.

Hoozemans, J.J., van Haastert, E.S., Eikelenboom, P., de Vos, R.A., Rozemuller, J.M., and Scheper, W. (2007). Activation of the unfolded protein response in Parkinson's disease. *Biochem. Biophys. Res. Commun.* 354, 707-711.

Hoozemans, J.J., Veerhuis, R., Van Haastert, E.S., Rozemuller, J.M., Baas, F., Eikelenboom, P., and Scheper, W. (2005). The unfolded protein response is activated in Alzheimer's disease. *Acta Neuropathol.* 110, 165-172.

Hou, N.S., Gutschmidt, A., Choi, D.Y., Pather, K., Shi, X., Watts, J.L., Hoppe, T., and Taubert, S. (2014). Activation of the endoplasmic reticulum unfolded protein response by lipid disequilibrium without disturbed proteostasis in vivo. *Proc. Natl. Acad. Sci. U. S. A.* 111, E2271-2280.

Hsieh, M.C., Das, D., Sambandam, N., Zhang, M.Q., and Nahlé, Z. (2008). Regulation of the PDK4 isozyme by the Rb-E2F1 complex. *J. Biol. Chem.* 283, 27410-27417.

Hsieh, S.L., Liu, R.W., Wu, C.H., Cheng, W.T., and Kuo, C.M. (2003). cDNA nucleotide sequence coding for stearoyl-CoA desaturase and its expression in the zebrafish (*Danio rerio*) embryo. *Mol. Reprod. Dev.* 66, 325-333.

Hubbard, W.C., Moser, A.B., Liu, A.C., Jones, R.O., Steinberg, S.J., Lorey, F., Panny, S.R., Vogt, R.F., Jr., Macaya, D., Turgeon, C.T., et al. (2009). Newborn screening for X-linked adrenoleukodystrophy (X-ALD): validation of a combined liquid chromatography-tandem mass spectrometric (LC-MS/MS) method. *Mol. Genet. Metab.* 97, 212-220.

Hwang, W.Y., Samuel, M., Tan, D., Koh, L.P., Lim, W., and Linn, Y.C. (2007). A meta-analysis of unrelated donor umbilical cord blood transplantation versus unrelated donor bone marrow transplantation in adult and pediatric patients. *Biol. Blood Marrow Transplant.* 13, 444-453.

Hymes, J., and Wolf, B. (1996). Biotinidase and its roles in biotin metabolism. *Clin. Chim. Acta* 255, 1-11.

Hymes, J., and Wolf, B. (1999). Human biotinidase isn't just for recycling biotin. *J. Nutr.* 129, 485s-489s.

Hyun, D.H., Lee, M., Halliwell, B., and Jenner, P. (2003). Proteasomal inhibition causes the formation of protein aggregates containing a wide range of proteins, including nitrated proteins. *J. Neurochem.* 86, 363-373.

Igarashi, M., Schaumburg, H.H., Powers, J., Kishimoto, Y., Kolodny, E., and Suzuki, K. (1976). Fatty acid abnormality in adrenoleukodystrophy. *J. Neurochem.* 26, 851-860.

Imai, S., Armstrong, C.M., Kaeberlein, M., and Guarente, L. (2000). Transcriptional silencing and longevity protein Sir2 is an NAD-dependent histone deacetylase. *Nature* 403, 795-800.

Inloes, J.M., Hsu, K.L., Dix, M.M., Viader, A., Masuda, K., Takei, T., Wood, M.R., and Cravatt, B.F. (2014). The hereditary spastic paraplegia-related enzyme DDHD2 is a principal brain triglyceride lipase. *Proc. Natl. Acad. Sci. U. S. A.* 111, 14924-14929.

Inloes, J.M., Kiosses, W.B., Wang, H., Walther, T.C., Farese, R.V., Jr., and Cravatt, B.F. (2018). Functional Contribution of the Spastic Paraplegia-Related Triglyceride Hydrolase DDHD2 to the Formation and Content of Lipid Droplets. *Biochemistry* 57, 827-838.

Inoki, K., Ouyang, H., Zhu, T., Lindvall, C., Wang, Y., Zhang, X., Yang, Q., Bennett, C., Harada, Y., Stankunas, K., et al. (2006). TSC2 Integrates Wnt and Energy Signals via a Coordinated Phosphorylation by AMPK and GSK3 to Regulate Cell Growth. *Cell* *126*, 955-968.

Ioannou, M.S., Jackson, J., Sheu, S.-H., Chang, C.-L., Weigel, A.V., Liu, H., Pasolli, H.A., Xu, C.S., Pang, S., Matthies, D., et al. (2019). Neuron-Astrocyte Metabolic Coupling Protects against Activity-Induced Fatty Acid Toxicity. *Cell* *177*, 1522-1535.e1514.

Ito, M., Blumberg, B.M., Mock, D.J., Goodman, A.D., Moser, A.B., Moser, H.W., Smith, K.D., and Powers, J.M. (2001). Potential environmental and host participants in the early white matter lesion of adreno-leukodystrophy: morphologic evidence for CD8 cytotoxic T cells, cytolysis of oligodendrocytes, and CD1-mediated lipid antigen presentation. *J. Neuropathol. Exp. Neurol.* *60*, 1004-1019.

Jang, J., Kang, H.C., Kim, H.S., Kim, J.Y., Huh, Y.J., Kim, D.S., Yoo, J.E., Lee, J.A., Lim, B., Lee, J., et al. (2011). Induced pluripotent stem cell models from X-linked adrenoleukodystrophy patients. *Ann. Neurol.* *70*, 402-409.

Jang, J., Park, S., Jin Hur, H., Cho, H.J., Hwang, I., Pyo Kang, Y., Im, I., Lee, H., Lee, E., Yang, W., et al. (2016). 25-hydroxycholesterol contributes to cerebral inflammation of X-linked adrenoleukodystrophy through activation of the NLRP3 inflammasome. *Nature communications* *7*, 13129.

Jasper, H.H. (1969). *Jasper's Basic Mechanisms of the Epilepsies*. (Oxford University Press).

Jensen, P.K. (1966). Antimycin-insensitive oxidation of succinate and reduced nicotinamide-adenine dinucleotide in electron-transport particles. I. pH dependency and hydrogen peroxide formation. *Biochim. Biophys. Acta* *122*, 157-166.

Jha, M.K., and Morrison, B.M. (2018). Glia-neuron energy metabolism in health and diseases: New insights into the role of nervous system metabolic transporters. *Exp. Neurol.* *309*, 23-31.

Jin, Y., Tan, Y., Chen, L., Liu, Y., and Ren, Z. (2018). Reactive Oxygen Species Induces Lipid Droplet Accumulation in HepG2 Cells by Increasing Perilipin 2 Expression. *Int. J. Mol. Sci.* *19*.

Jitrapakdee, S., St Maurice, M., Rayment, I., Cleland, W.W., Wallace, J.C., and Attwood, P.V. (2008). Structure, mechanism and regulation of pyruvate carboxylase. *Biochem. J.* *413*, 369-387.

Johnson, A.C., Mc, N.A., and Rossiter, R.J. (1950). Chemistry of wallerian degeneration; a review of recent studies. *Arch. Neurol. Psychiatry* *64*, 105-121.

Jones, R.G., and Pearce, E.J. (2017). MenTORing Immunity: mTOR Signaling in the Development and Function of Tissue-Resident Immune Cells. *Immunity* *46*, 730-742.

Jordan-Sciutto, K.L., Malaiyandi, L.M., and Bowser, R. (2002). Altered distribution of cell cycle transcriptional regulators during Alzheimer disease. *J. Neuropathol. Exp. Neurol.* *61*, 358-367.

Jung, E.M., Ka, M., and Kim, W.Y. (2016). Loss of GSK-3 Causes Abnormal Astrogenesis and Behavior in Mice. *Mol. Neurobiol.* *53*, 3954-3966.

Ka, M., Condorelli, G., Woodgett, J.R., and Kim, W.-Y. (2014). mTOR regulates brain morphogenesis by mediating GSK3 signaling. *Development (Cambridge, England)* *141*, 4076-4086.

Kamijo, K., Taketani, S., Yokota, S., Osumi, T., and Hashimoto, T. (1990). The 70-kDa peroxisomal membrane protein is a member of the Mdr (P-glycoprotein)-related ATP-binding protein superfamily. *J. Biol. Chem.* *265*, 4534-4540.

Kansanen, E., Jyrkkanen, H.K., and Levonen, A.L. (2012). Activation of stress signaling pathways by electrophilic oxidized and nitrated lipids. *Free Radic. Biol. Med.* *52*, 973-982.

Kashiwayama, Y., Seki, M., Yasui, A., Murasaki, Y., Morita, M., Yamashita, Y., Sakaguchi, M., Tanaka, Y., and Imanaka, T. (2009). 70-kDa peroxisomal membrane protein related protein (P70R/ABCD4) localizes to endoplasmic reticulum not peroxisomes, and NH2-terminal hydrophobic property determines the subcellular localization of ABC subfamily D proteins. *Exp. Cell Res.* *315*, 190-205.

Kee, N., Sivalingam, S., Boonstra, R., and Wojtowicz, J.M. (2002). The utility of Ki-67 and BrdU as proliferative markers of adult neurogenesis. *J. Neurosci. Methods* *115*, 97-105.

Keller, G.A., Warner, T.G., Steimer, K.S., and Hallewell, R.A. (1991). Cu,Zn superoxide dismutase is a peroxisomal enzyme in human fibroblasts and hepatoma cells. *Proc. Natl. Acad. Sci. U. S. A.* *88*, 7381-7385.

Keller, J.N., Hanni, K.B., and Markesbery, W.R. (2000). Possible involvement of proteasome inhibition in aging: implications for oxidative stress. *Mech. Ageing Dev.* *113*, 61-70.

Kemp, S., Berger, J., and Aubourg, P. (2012). X-linked adrenoleukodystrophy: clinical, metabolic, genetic and pathophysiological aspects. *Biochim. Biophys. Acta* *1822*, 1465-1474.

Kemp, S., Ligtenberg, M.J., van Geel, B.M., Barth, P.G., Wolterman, R.A., Schoute, F., Sarde, C.O., Mandel, J.L., van Oost, B.A., and Bolhuis, P.A. (1994). Identification of a two base pair deletion in five unrelated families with adrenoleukodystrophy: a possible hot spot for mutations. *Biochem. Biophys. Res. Commun.* *202*, 647-653.

Kemp, S., Pujol, A., Waterham, H.R., van Geel, B.M., Boehm, C.D., Raymond, G.V., Cutting, G.R., Wanders, R.J., and Moser, H.W. (2001). ABCD1 mutations and the X-linked adrenoleukodystrophy mutation database: role in diagnosis and clinical correlations. *Hum. Mutat.* *18*, 499-515.

Kemp, S., Valianpour, F., Denis, S., Ofman, R., Sanders, R.J., Mooyer, P., Barth, P.G., and Wanders, R.J. (2005). Elongation of very long-chain fatty acids is enhanced in X-linked adrenoleukodystrophy. *Mol. Genet. Metab.* *84*, 144-151.

Kemp, S., Wei, H.M., Lu, J.F., Braiterman, L.T., McGuinness, M.C., Moser, A.B., Watkins, P.A., and Smith, K.D. (1998). Gene redundancy and pharmacological gene therapy: implications for X-linked adrenoleukodystrophy. *Nat. Med.* *4*, 1261-1268.

Kemper, A.R., Brosco, J., Comeau, A.M., Green, N.S., Grosse, S.D., Jones, E., Kwon, J.M., Lam, W.K., Ojodu, J., Prosser, L.A., et al. (2017). Newborn screening for X-linked adrenoleukodystrophy: evidence summary and advisory committee recommendation. *Genet. Med.* *19*, 121-126.

Kennedy, D.W., and Abkowitz, J.L. (1997). Kinetics of central nervous system microglial and macrophage engraftment: analysis using a transgenic bone marrow transplantation model. *Blood* *90*, 986-993.

Khan, M., Pahan, K., Singh, A.K., and Singh, I. (1998). Cytokine-induced accumulation of very long-chain fatty acids in rat C6 glial cells: implication for X-adrenoleukodystrophy. *J. Neurochem.* *71*, 78-87.

Khatchadourian, A., Bourque, S.D., Richard, V.R., Titorenko, V.I., and Maysinger, D. (2012). Dynamics and regulation of lipid droplet formation in lipopolysaccharide (LPS)-stimulated microglia. *Biochimica et Biophysica Acta (BBA) - Molecular and Cell Biology of Lipids* *1821*, 607-617.

Kierdorf, K., and Prinz, M. (2013). Factors regulating microglia activation. *Front. Cell. Neurosci.* *7*, 44.

Kim, K.H., Song, M.J., Yoo, E.J., Choe, S.S., Park, S.D., and Kim, J.B. (2004). Regulatory role of glycogen synthase kinase 3 for transcriptional activity of ADD1/SREBP1c. *J. Biol. Chem.* *279*, 51999-52006.

Kishimoto, Y., Moser, H.W., Kawamura, N., Platt, M., Pallante, S.L., and Fenselau, C. (1980). Adrenoleukodystrophy: evidence that abnormal very long chain fatty acids of brain cholesterol esters are of exogenous origin. *Biochem. Biophys. Res. Commun.* *96*, 69-76.

Kitada, T., Asakawa, S., Hattori, N., Matsumine, H., Yamamura, Y., Minoshima, S., Yokochi, M., Mizuno, Y., and Shimizu, N. (1998). Mutations in the parkin gene cause autosomal recessive juvenile parkinsonism. *Nature* *392*, 605-608.

Klemm, R.W., Norton, J.P., Cole, R.A., Li, C.S., Park, S.H., Crane, M.M., Li, L., Jin, D., Boye-Doe, A., Liu, T.Y., et al. (2013). A conserved role for atlastin GTPases in regulating lipid droplet size. *Cell Rep.* *3*, 1465-1475.

Knazek, R.A., Rizzo, W.B., Schulman, J.D., and Dave, J.R. (1983). Membrane microviscosity is increased in the erythrocytes of patients with adrenoleukodystrophy and adrenomyeloneuropathy. *J. Clin. Invest.* *72*, 245-248.

Knoll, S., Emmrich, S., and Pützer, B.M. (2013). The E2F1-miRNA cancer progression network. *Adv. Exp. Med. Biol.* *774*, 135-147.

Kobayashi, T., Shinnoh, N., Kondo, A., and Yamada, T. (1997). Adrenoleukodystrophy protein-deficient mice represent abnormality of very long chain fatty acid metabolism. *Biochem. Biophys. Res. Commun.* *232*, 631-636.

Kobza, K., Sarath, G., and Zempleni, J. (2008). Prokaryotic BirA ligase biotinylates K4, K9, K18 and K23 in histone H3. *BMB reports* *41*, 310-315.

Kontaki, H., and Talianidis, I. (2010). Lysine methylation regulates E2F1-induced cell death. *Mol. Cell* *39*, 152-160.

Koppaka, V., Paul, C., Murray, I.V., and Axelsen, P.H. (2003). Early synergy between Abeta42 and oxidatively damaged membranes in promoting amyloid fibril formation by Abeta40. *J. Biol. Chem.* *278*, 36277-36284.

Korenke, G.C., Christen, H.J., Kruse, B., Hunneman, D.H., and Hanefeld, F. (1997). Progression of X-linked adrenoleukodystrophy under interferon-beta therapy. *J. Inherit. Metab. Dis.* *20*, 59-66.

Korenke, G.C., Fuchs, S., Krasemann, E., Doerr, H.G., Wilichowski, E., Hunneman, D.H., and Hanefeld, F. (1996). Cerebral adrenoleukodystrophy (ALD) in only one of monozygotic twins with an identical ALD genotype. *Ann. Neurol.* *40*, 254-257.

Korhonen, J.A., Pham, X.H., Pellegrini, M., and Falkenberg, M. (2004). Reconstitution of a minimal mtDNA replisome in vitro. *EMBO J.* *23*, 2423-2429.

Koutsikos, D., Agroyannis, B., and Tzanatos-Exarchou, H. (1990). Biotin for diabetic peripheral neuropathy. *Biomed. Pharmacother.* *44*, 511-514.

Kovesdi, I., Reichel, R., and Nevins, J.R. (1986). Identification of a cellular transcription factor involved in E1A trans-activation. *Cell* *45*, 219-228.

Krause, D., Fackler, M.J., Civin, C.I., and May, M.D.P.W. (1996). CD34: Structure, biology, and clinical utility. *Blood* *87*, 1-13.

Krause, K.H., Bonjour, J.P., Berlit, P., and Kochen, W. (1985). Biotin status of epileptics. *Ann. N. Y. Acad. Sci.* *447*, 297-313.

Kreilaus, F., Spiro, A.S., McLean, C.A., Garner, B., and Jenner, A.M. (2016). Evidence for altered cholesterol metabolism in Huntington's disease post mortem brain tissue. *Neuropathol. Appl. Neurobiol.* *42*, 535-546.

Kressler, D., Hock, M.B., and Kralli, A. (2007). Coactivators PGC-1 β and SRC-1 Interact Functionally to Promote the Agonist Activity of the Selective Estrogen Receptor Modulator Tamoxifen. *J. Biol. Chem.* *282*, 26897-26907.

Krivot, W., Sung, J.H., Shapiro, E.G., and Lockman, L.A. (1995). Microglia: the effector cell for reconstitution of the central nervous system following bone marrow transplantation for lysosomal and peroxisomal storage diseases. *Cell Transplant.* *4*, 385-392.

Kruska, N., Schonfeld, P., Pujol, A., and Reiser, G. (2015). Astrocytes and mitochondria from adrenoleukodystrophy protein (ABCD1)-deficient mice reveal that the adrenoleukodystrophy-associated very long-chain fatty acids target several cellular energy-dependent functions. *Biochim. Biophys. Acta* *1852*, 925-936.

Kuhl, J.S., Suarez, F., Gillett, G.T., Hemmati, P.G., Snowden, J.A., Stadler, M., Vuong, G.L., Aubourg, P., Kohler, W., and Arnold, R. (2017). Long-term outcomes of allogeneic haematopoietic stem cell transplantation for adult cerebral X-linked adrenoleukodystrophy. *Brain* *140*, 953-966.

Kumar, M., and Axelrod, A.E. (1978). Cellular antibody synthesis in thiamin, riboflavin, biotin and folic acid-deficient rats. *Proc. Soc. Exp. Biol. Med.* *157*, 421-423.

Kuroishi, T., Rios-Avila, L., Pestinger, V., Wijeratne, S.S.K., and Zempleni, J. (2011). Biotinylation is a natural, albeit rare, modification of human histones. *Mol. Genet. Metab.* *104*, 537-545.

Ladu, S., Calvisi, D.F., Conner, E.A., Farina, M., Factor, V.M., and Thorgeirsson, S.S. (2008). E2F1 inhibits c-Myc-driven apoptosis via PIK3CA/Akt/mTOR and COX-2 in a mouse model of human liver cancer. *Gastroenterology* *135*, 1322-1332.

Lannuzel, A., Aubourg, P., and Tardieu, M. (1998). Excessive production of tumour necrosis factor alpha by peripheral blood mononuclear cells in X-linked adrenoleukodystrophy. *Eur. J. Paediatr. Neurol.* *2*, 27-32.

Larrieta, E., Velasco, F., Vital, P., Lopez-Aceves, T., Lazo-de-la-Vega-Monroy, M.L., Rojas, A., and Fernandez-Mejia, C. (2010). Pharmacological concentrations of biotin reduce serum triglycerides and the expression of lipogenic genes. *Eur. J. Pharmacol.* *644*, 263-268.

Larsson, N.G., Wang, J., Wilhelmsson, H., Oldfors, A., Rustin, P., Lewandoski, M., Barsh, G.S., and Clayton, D.A. (1998). Mitochondrial transcription factor A is necessary for mtDNA maintenance and embryogenesis in mice. *Nat. Genet.* *18*, 231-236.

Launay, N., Aguado, C., Fourcade, S., Ruiz, M., Grau, L., Riera, J., Guilera, C., Giros, M., Ferrer, I., Knecht, E., et al. (2015). Autophagy induction halts axonal degeneration in a mouse model of X-adrenoleukodystrophy. *Acta Neuropathol.* *129*, 399-415.

Launay, N., Ruiz, M., Fourcade, S., Schluter, A., Guilera, C., Ferrer, I., Knecht, E., and Pujol, A. (2013). Oxidative stress regulates the ubiquitin-proteasome system and immunoproteasome functioning in a mouse model of X-adrenoleukodystrophy. *Brain* *136*, 891-904.

Launay, N., Ruiz, M., Grau, L., Ortega, F.J., Ilieva, E.V., Martinez, J.J., Galea, E., Ferrer, I., Knecht, E., Pujol, A., et al. (2017). Tauroursodeoxycholic bile acid arrests axonal degeneration by inhibiting the unfolded protein response in X-linked adrenoleukodystrophy. *Acta Neuropathol.* *133*, 283-301.

Lawson, L.J., Perry, V.H., and Gordon, S. (1992). Turnover of resident microglia in the normal adult mouse brain. *Neuroscience* *48*, 405-415.

Lazarow, P.B., and De Duve, C. (1976). A fatty acyl-CoA oxidizing system in rat liver peroxisomes; enhancement by clofibrate, a hypolipidemic drug. *Proc. Natl. Acad. Sci. U. S. A.* *73*, 2043-2046.

Lazo, O., Contreras, M., Hashmi, M., Stanley, W., Irazu, C., and Singh, I. (1988). Peroxisomal lignoceroyl-CoA ligase deficiency in childhood adrenoleukodystrophy and adrenomyeloneuropathy. *Proc. Natl. Acad. Sci. U. S. A.* *85*, 7647-7651.

Lazarino, G., Amorini, A.M., Eikelenboom, M.J., Killestein, J., Belli, A., Di Pietro, V., Tavazzi, B., Barkhof, F., Polman, C.H., Uitdehaag, B.M., et al. (2010). Cerebrospinal fluid ATP metabolites in multiple sclerosis. *Mult. Scler.* *16*, 549-554.

Lee, C.A.A., Seo, H.S., Armien, A.G., Bates, F.S., Tolar, J., and Azarin, S.M. (2018). Modeling and rescue of defective blood-brain barrier function of induced brain microvascular endothelial cells from childhood cerebral adrenoleukodystrophy patients. *Fluids Barriers CNS* *15*, 9.

Lee, D.K., Long, N.P., Jung, J., Kim, T.J., Na, E., Kang, Y.P., Kwon, S.W., and Jang, J. (2019). Integrative lipidomic and transcriptomic analysis of X-linked adrenoleukodystrophy reveals distinct lipidome signatures between adrenomyeloneuropathy and childhood cerebral adrenoleukodystrophy. *Biochem. Biophys. Res. Commun.* *508*, 563-569.

Lee, J., Giordano, S., and Zhang, J. (2012). Autophagy, mitochondria and oxidative stress: cross-talk and redox signalling. *Biochem. J.* *441*, 523-540.

Lee, J.H., Yu, W.H., Kumar, A., Lee, S., Mohan, P.S., Peterhoff, C.M., Wolfe, D.M., Martinez-Vicente, M., Massey, A.C., Sovak, G., et al. (2010). Lysosomal proteolysis and autophagy require presenilin 1 and are disrupted by Alzheimer-related PS1 mutations. *Cell* *141*, 1146-1158.

Lee, S.-J., Zhang, J., Choi, A.M.K., and Kim, H.P. (2013). Mitochondrial dysfunction induces formation of lipid droplets as a generalized response to stress. *Oxid. Med. Cell. Longev.* *2013*, 327167-327167.

Lee, S., Clinard, K., Young, S.P., Rehder, C.W., Fan, Z., Calikoglu, A.S., Bali, D.S., Bailey, D.B., Jr., Gehlert, L.M., Millington, D.S., et al. (2020). Evaluation of X-Linked Adrenoleukodystrophy Newborn Screening in North Carolina. *JAMA network open* *3*, e1920356.

Lee, Y.S., Kennedy, W.D., and Yin, Y.W. (2009). Structural insight into processive human mitochondrial DNA synthesis and disease-related polymerase mutations. *Cell* *139*, 312-324.

León-Del-Río, A., Leclerc, D., Akerman, B., Wakamatsu, N., and Gravel, R.A. (1995). Isolation of a cDNA encoding human holocarboxylase synthetase by functional complementation of a biotin auxotroph of *Escherichia coli*. *Proceedings of the National Academy of Sciences* *92*, 4626-4630.

Leonardsson, G., Steel, J.H., Christian, M., Pocock, V., Milligan, S., Bell, J., So, P.W., Medina-Gomez, G., Vidal-Puig, A., White, R., et al. (2004). Nuclear receptor corepressor RIP140 regulates fat accumulation. *Proc. Natl. Acad. Sci. U. S. A.* *101*, 8437-8442.

Leone, G., Nuckolls, F., Ishida, S., Adams, M., Sears, R., Jakoi, L., Miron, A., and Nevins, J.R. (2000). Identification of a novel E2F3 product suggests a mechanism for determining specificity of repression by Rb proteins. *Mol. Cell. Biol.* *20*, 3626-3632.

Leone, T.C., Lehman, J.J., Finck, B.N., Schaeffer, P.J., Wende, A.R., Boudina, S., Courtois, M., Wozniak, D.F., Sambandam, N., Bernal-Mizrachi, C., et al. (2005). PGC-1alpha deficiency causes multi-system energy metabolic derangements: muscle dysfunction, abnormal weight control and hepatic steatosis. *PLoS Biol.* *3*, e101.

Li, F.X., Zhu, J.W., Hogan, C.J., and DeGregori, J. (2003). Defective gene expression, S phase progression, and maturation during hematopoiesis in E2F1/E2F2 mutant mice. *Mol. Cell. Biol.* *23*, 3607-3622.

Li, J., Ran, C., Li, E., Gordon, F., Comstock, G., Siddiqui, H., Cleghorn, W., Chen, H.-Z., Kornacker, K., Liu, C.-G., et al. (2008). Synergistic Function of E2F7 and E2F8 Is Essential for Cell Survival and Embryonic Development. *Dev. Cell* *14*, 62-75.

Li, Y., Malkaram, S.A., Zhou, J., and Zemleni, J. (2014). Lysine biotinylation and methionine oxidation in the heat shock protein HSP60 synergize in the elimination of reactive oxygen species in human cell cultures. *J. Nutr. Biochem.* *25*, 475-482.

Li, Y., Tan, W., Neo, T.W., Aung, M.O., Wasser, S., Lim, S.G., and Tan, T.M. (2009). Role of the miR-106b-25 microRNA cluster in hepatocellular carcinoma. *Cancer Sci.* *100*, 1234-1242.

Liberti, M.V., and Locasale, J.W. (2016). The Warburg Effect: How Does it Benefit Cancer Cells? *Trends Biochem. Sci.* *41*, 211-218.

Lim, C.A., Yao, F., Wong, J.J., George, J., Xu, H., Chiu, K.P., Sung, W.K., Lipovich, L., Vega, V.B., Chen, J., et al. (2007). Genome-wide mapping of RELA(p65) binding identifies E2F1 as a transcriptional activator recruited by NF-kappaB upon TLR4 activation. *Mol. Cell* *27*, 622-635.

Lin, J., Wu, P.H., Tarr, P.T., Lindenberg, K.S., St-Pierre, J., Zhang, C.Y., Mootha, V.K., Jager, S., Vianna, C.R., Reznick, R.M., et al. (2004). Defects in adaptive energy metabolism with CNS-linked hyperactivity in PGC-1alpha null mice. *Cell* *119*, 121-135.

Lin, W., and Popko, B. (2009). Endoplasmic reticulum stress in disorders of myelinating cells. *Nat. Neurosci.* *12*, 379-385.

Lin, Y.T., Seo, J., Gao, F., Feldman, H.M., Wen, H.L., Penney, J., Cam, H.P., Gjoneska, E., Raja, W.K., Cheng, J., et al. (2018). APOE4 Causes Widespread Molecular and Cellular Alterations Associated with Alzheimer's Disease Phenotypes in Human iPSC-Derived Brain Cell Types. *Neuron* *98*, 1141-1154.e1147.

Linnebank, M., Kemp, S., Wanders, R.J., Kleijer, W.J., van der Sterre, M.L., Gartner, J., Fliessbach, K., Semmler, A., Sokolowski, P., Kohler, W., et al. (2006). Methionine metabolism and phenotypic variability in X-linked adrenoleukodystrophy. *Neurology* *66*, 442-443.

Liu, D.-Z., Ander, B.P., and Sharp, F.R. (2010a). Cell cycle inhibition without disruption of neurogenesis is a strategy for treatment of central nervous system diseases. *Neurobiol. Dis.* *37*, 549-557.

Liu, D., and Zemleni, J. (2014). Holocarboxylase synthetase interacts physically with nuclear receptor co-repressor, histone deacetylase 1 and a novel splicing variant of histone deacetylase 1 to repress repeats. *The Biochemical journal* *461*, 477-486.

Liu, D.Z., Ander, B.P., and Sharp, F.R. (2010b). Cell cycle inhibition without disruption of neurogenesis is a strategy for treatment of central nervous system diseases. *Neurobiol. Dis.* *37*, 549-557.

Liu, L., Zhang, K., Sandoval, H., Yamamoto, S., Jaiswal, M., Sanz, E., Li, Z., Hui, J., Graham, B.H., Quintana, A., et al. (2015). Glial lipid droplets and ROS induced by mitochondrial defects promote neurodegeneration. *Cell* *160*, 177-190.

Liu, L.X., Janvier, K., Berteaux-Lecellier, V., Cartier, N., Benarous, R., and Aubourg, P. (1999). Homo- and heterodimerization of peroxisomal ATP-binding cassette half-transporters. *J. Biol. Chem.* *274*, 32738-32743.

Loes, D.J., Fatemi, A., Melhem, E.R., Gupte, N., Bezman, L., Moser, H.W., and Raymond, G.V. (2003). Analysis of MRI patterns aids prediction of progression in X-linked adrenoleukodystrophy. *Neurology* *61*, 369-374.

Loes, D.J., Hite, S., Moser, H., Stillman, A.E., Shapiro, E., Lockman, L., Latchaw, R.E., and Krivit, W. (1994). Adrenoleukodystrophy: a scoring method for brain MR observations. *AJNR Am. J. Neuroradiol.* *15*, 1761-1766.

Lombard-Platet, G., Savary, S., Sarde, C.O., Mandel, J.L., and Chimini, G. (1996). A close relative of the adrenoleukodystrophy (ALD) gene codes for a peroxisomal protein with a specific expression pattern. *Proc. Natl. Acad. Sci. U. S. A.* *93*, 1265-1269.

Lopez-Atalaya, J.P., Askew, K.E., Sierra, A., and Gomez-Nicola, D. (2018). Development and maintenance of the brain's immune toolkit: Microglia and non-parenchymal brain macrophages. *Dev. Neurobiol.* *78*, 561-579.

Lopez-Erauskin, J., Ferrer, I., Galea, E., and Pujol, A. (2013a). Cyclophilin D as a potential target for antioxidants in neurodegeneration: the X-ALD case. *Biol. Chem.* *394*, 621-629.

Lopez-Erauskin, J., Fourcade, S., Galino, J., Ruiz, M., Schluter, A., Naudi, A., Jove, M., Portero-Otin, M., Pamplona, R., Ferrer, I., et al. (2011). Antioxidants halt axonal degeneration in a mouse model of X-adrenoleukodystrophy. *Ann. Neurol.* *70*, 84-92.

Lopez-Erauskin, J., Galino, J., Bianchi, P., Fourcade, S., Andreu, A.L., Ferrer, I., Munoz-Pinedo, C., and Pujol, A. (2012). Oxidative stress modulates mitochondrial failure and cyclophilin D function in X-linked adrenoleukodystrophy. *Brain* *135*, 3584-3598.

Lopez-Erauskin, J., Galino, J., Ruiz, M., Cuezva, J.M., Fabregat, I., Cacabelos, D., Boada, J., Martinez, J., Ferrer, I., Pamplona, R., et al. (2013b). Impaired mitochondrial oxidative phosphorylation in the peroxisomal disease X-linked adrenoleukodystrophy. *Hum. Mol. Genet.* *22*, 3296-3305.

Lopez-Mejia, I.C., and Fajas, L. (2015). Cell cycle regulation of mitochondrial function. *Curr. Opin. Cell Biol.* *33*, 19-25.

Lu, J.F., Lawler, A.M., Watkins, P.A., Powers, J.M., Moser, A.B., Moser, H.W., and Smith, K.D. (1997). A mouse model for X-linked adrenoleukodystrophy. *Proc.Natl.Acad.Sci.U.S.A* *94*, 9366-9371.

Lukas, J., Bartkova, J., and Bartek, J. (1996). Convergence of mitogenic signalling cascades from diverse classes of receptors at the cyclin D-cyclin-dependent kinase-pRb-controlled G1 checkpoint. *Mol. Cell. Biol.* *16*, 6917-6925.

Lv, Y., Xiao, J., Liu, J., and Xing, F. (2017). E2F8 is a Potential Therapeutic Target for Hepatocellular Carcinoma. *J. Cancer* *8*, 1205-1213.

Ma, T., Hoeffler, C.A., Capetillo-Zarate, E., Yu, F., Wong, H., Lin, M.T., Tampellini, D., Klann, E., Blitzer, R.D., and Gouras, G.K. (2010). Dysregulation of the mTOR pathway mediates impairment of synaptic plasticity in a mouse model of Alzheimer's disease. *PLoS One* *5*, e12845.

Ma, T., Tzavaras, N., Tsokas, P., Landau, E.M., and Blitzer, R.D. (2011). Synaptic Stimulation of mTOR Is Mediated by Wnt Signaling and Regulation of Glycogen Synthetase Kinase-3. *The Journal of Neuroscience* *31*, 17537-17546.

MacManus, J.P., Jian, M., Preston, E., Rasquinha, I., Webster, J., and Zurakowski, B. (2003). Absence of the transcription factor E2F1 attenuates brain injury and improves behavior after focal ischemia in mice. *J. Cereb. Blood Flow Metab.* *23*, 1020-1028.

Mahad, D., Ziabreva, I., Lassmann, H., and Turnbull, D. (2008). Mitochondrial defects in acute multiple sclerosis lesions. *Brain* *131*, 1722-1735.

Maier, E.M., Mayerhofer, P.U., Asheuer, M., Kohler, W., Rothe, M., Muntau, A.C., Roscher, A.A., Holzinger, A., Aubourg, P., and Berger, J. (2008). X-linked adrenoleukodystrophy phenotype is independent of ABCD2 genotype. *Biochem. Biophys. Res. Commun.* *377*, 176-180.

Mammucari, C., Patron, M., Granatiero, V., and Rizzuto, R. (2011). Molecules and roles of mitochondrial calcium signaling. *Biofactors* *37*, 219-227.

Marschallinger, J., Iram, T., Zardeneta, M., Lee, S.E., Lehallier, B., Haney, M.S., Pluvinage, J.V., Mathur, V., Hahn, O., Morgens, D.W., et al. (2020). Lipid-droplet-accumulating microglia represent a dysfunctional and proinflammatory state in the aging brain. *Nat. Neurosci.* *23*, 194-208.

Martinez-Vicente, M., and Cuervo, A.M. (2007). Autophagy and neurodegeneration: when the cleaning crew goes on strike. *Lancet Neurol.* *6*, 352-361.

Martinez-Vicente, M., Tallozy, Z., Wong, E., Tang, G., Koga, H., Kaushik, S., de Vries, R., Arias, E., Harris, S., Sulzer, D., et al. (2010). Cargo recognition failure is responsible for inefficient autophagy in Huntington's disease. *Nat. Neurosci.* *13*, 567-576.

Mastroeni, R., Bensadoun, J.C., Charvin, D., Aebischer, P., Pujol, A., and Raoul, C. (2009). Insulin-like growth factor-1 and neurotrophin-3 gene therapy prevents motor decline in an X-linked adrenoleukodystrophy mouse model. *Ann. Neurol.* *66*, 117-122.

Matsukawa, T., Asheuer, M., Takahashi, Y., Goto, J., Suzuki, Y., Shimozawa, N., Takano, H., Onodera, O., Nishizawa, M., Aubourg, P., et al. (2011). Identification of novel SNPs of ABCD1, ABCD2, ABCD3, and ABCD4 genes in patients with X-linked adrenoleukodystrophy (ALD) based on comprehensive resequencing and association studies with ALD phenotypes. *Neurogenetics* *12*, 41-50.

Matsukawa, T., Yamamoto, T., Honda, A., Toya, T., Ishiura, H., Mitsui, J., Tanaka, M., Hao, A., Shinohara, A., Ogura, M., et al. (2020). Clinical efficacy of haematopoietic stem cell transplantation for adult adrenoleukodystrophy. *Brain Communications* *2*.

Matus, S., Glimcher, L.H., and Hetz, C. (2011). Protein folding stress in neurodegenerative diseases: a glimpse into the ER. *Curr. Opin. Cell Biol.* *23*, 239-252.

McBride, H.M., Neuspiel, M., and Wasiak, S. (2006). Mitochondria: more than just a powerhouse. *Curr. Biol.* *16*, R551-560.

McCart, E.A., Thangapazham, R.L., Lombardini, E.D., Mog, S.R., Panganiban, R.A.M., Dickson, K.M., Mansur, R.A., Nagy, V., Kim, S.Y., Selwyn, R., et al. (2017). Accelerated senescence in skin in a murine model of radiation-induced multi-organ injury. *J Radiat Res* *58*, 636-646.

McGarry, J.D., and Brown, N.F. (1997). The mitochondrial carnitine palmitoyltransferase system. From concept to molecular analysis. *Eur. J. Biochem.* *244*, 1-14.

McGuinness, M.C., Powers, J.M., Bias, W.B., Schmeckpeper, B.J., Segal, A.H., Gowda, V.C., Wesselingh, S.L., Berger, J., Griffin, D.E., and Smith, K.D. (1997). Human leukocyte antigens and cytokine expression in cerebral inflammatory demyelinating lesions of X-linked adrenoleukodystrophy and multiple sclerosis. *J. Neuroimmunol.* *75*, 174-182.

McGuinness, M.C., Zhang, H.P., and Smith, K.D. (2001). Evaluation of pharmacological induction of fatty acid beta-oxidation in X-linked adrenoleukodystrophy. *Mol. Genet. Metab.* *74*, 256-263.

McKercher, S.R., Torbett, B.E., Anderson, K.L., Henkel, G.W., Vestal, D.J., Baribault, H., Klemsz, M., Feeney, A.J., Wu, G.E., Paige, C.J., et al. (1996). Targeted disruption of the PU.1 gene results in multiple hematopoietic abnormalities. *EMBO J.* *15*, 5647-5658.

McNaught, K.S., and Jenner, P. (2001). Proteasomal function is impaired in substantia nigra in Parkinson's disease. *Neurosci. Lett.* *297*, 191-194.

Mehlem, A., Hagberg, C.E., Muhl, L., Eriksson, U., and Falkevall, A. (2013). Imaging of neutral lipids by oil red O for analyzing the metabolic status in health and disease. *Nat. Protoc.* *8*, 1149-1154.

Melo, R.C., D'Avila, H., Bozza, P.T., and Weller, P.F. (2011). Imaging lipid bodies within leukocytes with different light microscopy techniques. *Methods Mol. Biol.* *689*, 149-161.

Meo-Evoli, N., Almacellas, E., Massucci, F.A., Gentilella, A., Ambrosio, S., Kozma, S.C., Thomas, G., and Tauler, A. (2015). V-ATPase: a master effector of E2F1-mediated lysosomal trafficking, mTORC1 activation and autophagy. *Oncotarget* 6, 28057-28070.

Michel, S., Wanet, A., De Pauw, A., Rommelaere, G., Arnould, T., and Renard, P. (2012). Crosstalk between mitochondrial (dys)function and mitochondrial abundance. *J. Cell. Physiol.* 227, 2297-2310.

Migeon, B.R., Moser, H.W., Moser, A.B., Axelman, J., Sillence, D., and Norum, R.A. (1981). Adrenoleukodystrophy: evidence for X linkage, inactivation, and selection favoring the mutant allele in heterozygous cells. *Proc. Natl. Acad. Sci. U. S. A.* 78, 5066-5070.

Mihaylova, M.M., and Shaw, R.J. (2011). The AMPK signalling pathway coordinates cell growth, autophagy and metabolism. *Nat. Cell Biol.* 13, 1016-1023.

Miike, T., Taku, K., Tamura, T., Ohta, J., Ozaki, M., Yamamoto, C., Sakai, T., Antoku, Y., and Yadomi, C. (1989). Clinical improvement of adrenoleukodystrophy following intravenous gammaglobulin therapy. *Brain Dev.* 11, 134-137.

Mildner, A., Schmidt, H., Nitsche, M., Merkler, D., Hanisch, U.K., Mack, M., Heikenwalder, M., Brück, W., Priller, J., and Prinz, M. (2007). Microglia in the adult brain arise from Ly-6ChiCCR2+ monocytes only under defined host conditions. *Nat. Neurosci.* 10, 1544-1553.

Milenkovic, D., Matic, S., Kuhl, I., Ruzzenente, B., Freyer, C., Jemt, E., Park, C.B., Falkenberg, M., and Larsson, N.G. (2013). TWINKLE is an essential mitochondrial helicase required for synthesis of nascent D-loop strands and complete mtDNA replication. *Hum. Mol. Genet.* 22, 1983-1993.

Miller, W.P., Rothman, S.M., Nascene, D., Kivisto, T., DeFor, T.E., Ziegler, R.S., Eisengart, J., Leiser, K., Raymond, G., Lund, T.C., et al. (2011). Outcomes after allogeneic hematopoietic cell transplantation for childhood cerebral adrenoleukodystrophy: the largest single-institution cohort report. *Blood* 118, 1971-1978.

Min, K.T., and Benzer, S. (1999). Preventing neurodegeneration in the *Drosophila* mutant bubblegum. *Science* 284, 1985-1988.

Mock, D.M., and Dyken, M.E. (1997). Biotin catabolism is accelerated in adults receiving long-term therapy with anticonvulsants. *Neurology* 49, 1444-1447.

Montine, T.J., Neely, M.D., Quinn, J.F., Beal, M.F., Markesbery, W.R., Roberts, L.J., and Morrow, J.D. (2002). Lipid peroxidation in aging brain and Alzheimer's disease. *Free Radic. Biol. Med.* 33, 620-626.

Mootha, V.K., Lindgren, C.M., Eriksson, K.F., Subramanian, A., Sihag, S., Lehar, J., Puigserver, P., Carlsson, E., Ridderstrale, M., Laurila, E., et al. (2003). PGC-1alpha-responsive genes involved in oxidative phosphorylation are coordinately downregulated in human diabetes. *Nat. Genet.* 34, 267-273.

Morato, L., Galino, J., Ruiz, M., Calingasan, N.Y., Starkov, A.A., Dumont, M., Naudi, A., Martinez, J.J., Aubourg, P., Portero-Otin, M., et al. (2013). Pioglitazone halts axonal degeneration in a mouse model of X-linked adrenoleukodystrophy. *Brain* 136, 2432-2443.

Morato, L., Ruiz, M., Boada, J., Calingasan, N.Y., Galino, J., Guilera, C., Jove, M., Naudi, A., Ferrer, I., Pamplona, R., et al. (2015). Activation of sirtuin 1 as therapy for the peroxisomal disease adrenoleukodystrophy. *Cell Death Differ.* 22, 1742-1753.

Mori, K., Uchida, T., Fukumura, M., Tamiya, S., Higurashi, M., Sakai, H., Ishikawa, F., and Shibamura, M. (2016). Linkage of E2F1 transcriptional network and cell proliferation with respiratory chain activity in breast cancer cells. *Cancer Sci.* 107, 963-971.

Morita, M., Kaizawa, T., Yoda, T., Oyama, T., Asakura, R., Matsumoto, S., Nagai, Y., Watanabe, Y., Watanabe, S., Kobayashi, H., et al. (2020). Bone marrow transplantation into *Abcd1*-deficient mice: Distribution of donor derived-cells and biological characterization of the brain of the recipient mice. *J. Inherit. Metab. Dis.* *n/a*.

Morrison, S.J., and Scadden, D.T. (2014). The bone marrow niche for haematopoietic stem cells. *Nature* 505, 327-334.

Moser, A.B., Borel, J., Odone, A., Naidu, S., Cornblath, D., Sanders, D.B., and Moser, H.W. (1987). A new dietary therapy for adrenoleukodystrophy: biochemical and preliminary clinical results in 36 patients. *Ann. Neurol.* *21*, 240-249.

Moser, A.B., and Fatemi, A. (2018). Newborn Screening and Emerging Therapies for X-Linked Adrenoleukodystrophy. *JAMA Neurol* *75*, 1175-1176.

Moser, A.B., Kreiter, N., Bezman, L., Lu, S., Raymond, G.V., Naidu, S., and Moser, H.W. (1999). Plasma very long chain fatty acids in 3,000 peroxisome disease patients and 29,000 controls. *Ann. Neurol.* *45*, 100-110.

Moser, A.B., and Moser, H.W. (1999). The prenatal diagnosis of X-linked adrenoleukodystrophy. *Prenat. Diagn.* *19*, 46-48.

Moser, H., Smith, KD, Watkins, PA, Powers, J, Moser, AB (2001). X-linked adrenoleukodystrophy. In *The Metabolic and Molecular Bases of Inherited disease*. C. Scriver, ed. (New-York: McGraw-Hill), pp. 3257-3301.

Moser, H.W., Mahmood, A., and Raymond, G.V. (2007). X-linked adrenoleukodystrophy. *Nat. Clin. Pract. Neurol.* *3*, 140-151.

Moser, H.W., Moser, A.B., Frayer, K.K., Chen, W., Schulman, J.D., O'Neill, B.P., and Kishimoto, Y. (1981). Adrenoleukodystrophy: increased plasma content of saturated very long chain fatty acids. *Neurology* *31*, 1241-1249.

Moser, H.W., Moser, A.B., Kawamura, N., Murphy, J., Suzuki, K., Schaumburg, H., and Kishimoto, Y. (1980). Adrenoleukodystrophy: elevated C26 fatty acid in cultured skin fibroblasts. *Ann. Neurol.* *7*, 542-549.

Moser, H.W., Moser, A.B., Smith, K.D., Bergin, A., Borel, J., Shankroff, J., Stine, O.C., Merette, C., Ott, J., Krivit, W., et al. (1992). Adrenoleukodystrophy: phenotypic variability and implications for therapy. *J. Inherit. Metab. Dis.* *15*, 645-664.

Moser, H.W., Tutschka, P.J., Brown, F.R., 3rd, Moser, A.E., Yeager, A.M., Singh, I., Mark, S.A., Kumar, A.A., McDonnell, J.M., White, C.L., 3rd, et al. (1984). Bone marrow transplant in adrenoleukodystrophy. *Neurology* *34*, 1410-1417.

Mosser, J., Douar, A.M., Sarde, C.O., Kioschis, P., Feil, R., Moser, H., Poustka, A.M., Mandel, J.L., and Aubourg, P. (1993). Putative X-linked adrenoleukodystrophy gene shares unexpected homology with ABC transporters. *Nature* *361*, 726-730.

Mosser, J., Lutz, Y., Stoeckel, M.E., Sarde, C.O., Kretz, C., Douar, A.M., Lopez, J., Aubourg, P., and Mandel, J.L. (1994). The gene responsible for adrenoleukodystrophy encodes a peroxisomal membrane protein. *Hum. Mol. Genet.* *3*, 265-271.

Motonaga, K., Itoh, M., Hirayama, A., Hirano, S., Becker, L.E., Goto, Y., and Takashima, S. (2001). Up-regulation of E2F-1 in Down's syndrome brain exhibiting neuropathological features of Alzheimer-type dementia. *Brain Res.* *905*, 250-253.

Muffat, J., Li, Y., Yuan, B., Mitalipova, M., Omer, A., Corcoran, S., Bakiasi, G., Tsai, L.H., Aubourg, P., Ransohoff, R.M., et al. (2016). Efficient derivation of microglia-like cells from human pluripotent stem cells. *Nat. Med.* *22*, 1358-1367.

Murabe, Y., and Sano, Y. (1982). Morphological studies on neuroglia. V. Microglial cells in the cerebral cortex of the rat, with special reference to their possible involvement in synaptic function. *Cell Tissue Res.* *223*, 493-506.

Murabe, Y., and Sano, Y. (1983). Morphological studies on neuroglia. VII. Distribution of "brain macrophages" in brains of neonatal and adult rats, as determined by means of immunohistochemistry. *Cell Tissue Res.* *229*, 85-95.

Murphy, M.P. (2009). How mitochondria produce reactive oxygen species. *Biochem. J.* *417*, 1-13.

Musolino, P.L., Gong, Y., Snyder, J.M., Jimenez, S., Lok, J., Lo, E.H., Moser, A.B., Grabowski, E.F., Frosch, M.P., and Eichler, F.S. (2015). Brain endothelial dysfunction in cerebral adrenoleukodystrophy. *Brain* *138*, 3206-3220.

Musolino, P.L., Rapalino, O., Caruso, P., Caviness, V.S., and Eichler, F.S. (2012). Hypoperfusion predicts lesion progression in cerebral X-linked adrenoleukodystrophy. *Brain* *135*, 2676-2683.

Mutemberezi, V., Guillemot-Legris, O., and Muccioli, G.G. (2016). Oxysterols: From cholesterol metabolites to key mediators. *Prog. Lipid Res.* *64*, 152-169.

Nagy, Z., and Tora, L. (2007). Distinct GCN5/PCAF-containing complexes function as co-activators and are involved in transcription factor and global histone acetylation. *Oncogene* *26*, 5341-5357.

Naidu, S., Bresnan, M.J., Griffin, D., O'Toole, S., and Moser, H.W. (1988). Childhood adrenoleukodystrophy. Failure of intensive immunosuppression to arrest neurologic progression. *Arch. Neurol.* *45*, 846-848.

Naik, E., and Dixit, V.M. (2011). Mitochondrial reactive oxygen species drive proinflammatory cytokine production. *J. Exp. Med.* *208*, 417-420.

Nassif, M., Matus, S., Castillo, K., and Hetz, C. (2010). Amyotrophic lateral sclerosis pathogenesis: a journey through the secretory pathway. *Antioxid Redox Signal* *13*, 1955-1989.

Nave, K.A., and Werner, H.B. (2014). Myelination of the nervous system: mechanisms and functions. *Annu. Rev. Cell Dev. Biol.* *30*, 503-533.

Nelson, T.J., and Alkon, D.L. (2005). Oxidation of cholesterol by amyloid precursor protein and beta-amyloid peptide. *J. Biol. Chem.* *280*, 7377-7387.

Netik, A., Forss-Petter, S., Holzinger, A., Molzer, B., Unterrainer, G., and Berger, J. (1999). Adrenoleukodystrophy-related protein can compensate functionally for adrenoleukodystrophy protein deficiency (X-ALD): implications for therapy. *Hum. Mol. Genet.* *8*, 907-913.

Nevins, J.R. (2001). The Rb/E2F pathway and cancer. *Hum. Mol. Genet.* *10*, 699-703.

Nevins, J.R., Chellappan, S.P., Mudryj, M., Hiebert, S., Devoto, S., Horowitz, J., Hunter, T., and Pines, J. (1991). E2F transcription factor is a target for the RB protein and the cyclin A protein. *Cold Spring Harb. Symp. Quant. Biol.* *56*, 157-162.

Nielsen, J.S., and McNagny, K.M. (2008). Novel functions of the CD34 family. *J. Cell Sci.* *121*, 3683-3692.

Nielsen, J.S., and McNagny, K.M. (2009). CD34 is a key regulator of hematopoietic stem cell trafficking to bone marrow and mast cell progenitor trafficking in the periphery. *Microcirculation* *16*, 487-496.

Niki, E., Yoshida, Y., Saito, Y., and Noguchi, N. (2005). Lipid peroxidation: mechanisms, inhibition, and biological effects. *Biochem. Biophys. Res. Commun.* *338*, 668-676.

Nisoli, E., Clementi, E., Moncada, S., and Carruba, M.O. (2004). Mitochondrial biogenesis as a cellular signaling framework. *Biochem. Pharmacol.* *67*, 1-15.

Nunnari, J., and Suomalainen, A. (2012). Mitochondria: in sickness and in health. *Cell* *148*, 1145-1159.

Nury, T., Zarrouk, A., Ragot, K., Debbabi, M., Riedinger, J.-M., Vejux, A., Aubourg, P., and Lizard, G. (2017). 7-Ketocholesterol is increased in the plasma of X-ALD patients and induces peroxisomal modifications in microglial cells: Potential roles of 7-ketocholesterol in the pathophysiology of X-ALD. *The Journal of Steroid Biochemistry and Molecular Biology* *169*, 123-136.

Oezen, I., Rossmanith, W., Forss-Petter, S., Kemp, S., Voigtlander, T., Moser-Thier, K., Wanders, R.J., Bittner, R.E., and Berger, J. (2005). Accumulation of very long-chain fatty acids does not affect mitochondrial function in adrenoleukodystrophy protein deficiency. *Hum. Mol. Genet.* *14*, 1127-1137.

Ofir, M., Hacohen, D., and Ginsberg, D. (2011). MiR-15 and miR-16 are direct transcriptional targets of E2F1 that limit E2F-induced proliferation by targeting cyclin E. *Mol. Cancer Res.* *9*, 440-447.

Ofman, R., Dijkstra, I.M., van Roermund, C.W., Burger, N., Turkenburg, M., van Cruchten, A., van Engen, C.E., Wanders, R.J., and Kemp, S. (2010). The role of ELOVL1 in very long-chain fatty acid homeostasis and X-linked adrenoleukodystrophy. *EMBO Mol. Med.* *2*, 90-97.

Onal, G., Kutlu, O., Gozuacik, D., and Dokmeci Emre, S. (2017). Lipid Droplets in Health and Disease. *Lipids Health Dis.* *16*, 128.

- Orchard, P.J., Lund, T., Miller, W., Rothman, S.M., Raymond, G., Nascene, D., Basso, L., Cloyd, J., and Tolar, J. (2011). Chitotriosidase as a biomarker of cerebral adrenoleukodystrophy. *J. Neuroinflammation* 8, 144.
- Ortega-Cuellar, D., Hernandez-Mendoza, A., Moreno-Arriola, E., Carvajal-Aguilera, K., Perez-Vazquez, V., Gonzalez-Alvarez, R., and Velazquez-Arellano, A. (2010). Biotin starvation with adequate glucose provision causes paradoxical changes in fuel metabolism gene expression similar in rat (*Rattus norvegicus*), nematode (*Caenorhabditis elegans*) and yeast (*Saccharomyces cerevisiae*). *Journal of nutrigenetics and nutrigenomics* 3, 18-30.
- Osuga, H., Osuga, S., Wang, F.H., Fetni, R., Hogan, M., Slack, R., Hakim, A., Ikeda, J.-E., and Park, D. (2000). Cyclin-dependent kinases as a therapeutic target for stroke. *Proc. Natl. Acad. Sci. U. S. A.* 97, 10254-10259.
- Outeiro, T.F., and Lindquist, S. (2003). Yeast Cells Provide Insight into Alpha-Synuclein Biology and Pathobiology. *Science* 302, 1772-1775.
- Ouyang, Z., Zhou, Q., and Wong, W.H. (2009). ChIP-Seq of transcription factors predicts absolute and differential gene expression in embryonic stem cells. *Proc. Natl. Acad. Sci. U. S. A.* 106, 21521-21526.
- Owen, J.L., Zhang, Y., Bae, S.H., Farooqi, M.S., Liang, G., Hammer, R.E., Goldstein, J.L., and Brown, M.S. (2012). Insulin stimulation of SREBP-1c processing in transgenic rat hepatocytes requires p70 S6-kinase. *Proc. Natl. Acad. Sci. U. S. A.* 109, 16184-16189.
- Ozand, P.T., Gascon, G.G., Al Essa, M., Joshi, S., Al Jishi, E., Bakheet, S., Al Watban, J., Al-Kawi, M.Z., and Dabbagh, O. (1998). Biotin-responsive basal ganglia disease: a novel entity. *Brain* 121 (Pt 7), 1267-1279.
- Pacheco-Alvarez, D., Solorzano-Vargas, R., Gravel, R., Cervantes-Roldán, R., Velázquez-Arellano, A., and León Del Río, A. (2005). Paradoxical Regulation of Biotin Utilization in Brain and Liver and Implications for Inherited Multiple Carboxylase Deficiency. *The Journal of biological chemistry* 279, 52312-52318.
- Pacheco-Alvarez, D., Solórzano-Vargas, R.S., and Del Río, A.L. (2002). Biotin in Metabolism and Its Relationship to Human Disease. *Arch. Med. Res.* 33, 439-447.
- Park, J., Choi, H., Min, J.S., Park, S.J., Kim, J.H., Park, H.J., Kim, B., Chae, J.I., Yim, M., and Lee, D.S. (2013). Mitochondrial dynamics modulate the expression of pro-inflammatory mediators in microglial cells. *J. Neurochem.* 127, 221-232.
- Patel, M.S. (1974). THE RELATIVE SIGNIFICANCE OF CO₂-FIXING ENZYMES IN THE METABOLISM OF RAT BRAIN. *J. Neurochem.* 22, 717-724.
- Pavlova, N.N., and Thompson, C.B. (2016). The Emerging Hallmarks of Cancer Metabolism. *Cell Metab.* 23, 27-47.
- Peeters, A., Shinde, A.B., Dirx, R., Smet, J., De Bock, K., Espeel, M., Vanhorebeek, I., Vanlander, A., Van Coster, R., Carmeliet, P., et al. (2015). Mitochondria in peroxisome-deficient hepatocytes exhibit impaired respiration, depleted DNA, and PGC-1alpha independent proliferation. *Biochim. Biophys. Acta* 1853, 285-298.
- Penfield, W. (1932). *Cytology & cellular pathology of the nervous system.* (New York: P.B. Hoeber, inc.).
- Pennetta, G., and Welte, M.A. (2018). Emerging Links between Lipid Droplets and Motor Neuron Diseases. *Dev. Cell* 45, 427-432.
- Perissi, V., Jepsen, K., Glass, C.K., and Rosenfeld, M.G. (2010). Deconstructing repression: evolving models of co-repressor action. *Nature reviews. Genetics* 11, 109-123.
- Perluigi, M., Di Domenico, F., and Butterfield, D.A. (2015). mTOR signaling in aging and neurodegeneration: At the crossroad between metabolism dysfunction and impairment of autophagy. *Neurobiol. Dis.* 84, 39-49.
- Petrillo, S., Piemonte, F., Pastore, A., Tozzi, G., Aiello, C., Pujol, A., Cappa, M., and Bertini, E. (2013). Glutathione imbalance in patients with X-linked adrenoleukodystrophy. *Mol. Genet. Metab.* 109, 366-370.

Pickering, M.T., Stadler, B.M., and Kowalik, T.F. (2009). miR-17 and miR-20a temper an E2F1-induced G1 checkpoint to regulate cell cycle progression. *Oncogene* 28, 140-145.

Polager, S., and Ginsberg, D. (2008). E2F – at the crossroads of life and death. *Trends Cell Biol.* 18, 528-535.

Polager, S., Kalma, Y., Berkovich, E., and Ginsberg, D. (2002). E2Fs up-regulate expression of genes involved in DNA replication, DNA repair and mitosis. *Oncogene* 21, 437-446.

Poppy Roworth, A., Ghari, F., and La Thangue, N.B. (2015). To live or let die - complexity within the E2F1 pathway. *Mol Cell Oncol* 2, e970480-e970480.

Porstmann, T., Santos, C.R., Griffiths, B., Cully, M., Wu, M., Leever, S., Griffiths, J.R., Chung, Y.L., and Schulze, A. (2008). SREBP activity is regulated by mTORC1 and contributes to Akt-dependent cell growth. *Cell Metab.* 8, 224-236.

Potten, C.S. (1970). Radiation depigmentation of mouse hair: effect of the hair growth cycle on the sensitivity. *J. Invest. Dermatol.* 55, 410-418.

Powelka, A.M., Seth, A., Virbasius, J.V., Kiskinis, E., Nicoloso, S.M., Guilherme, A., Tang, X., Straubhaar, J., Cherniack, A.D., Parker, M.G., et al. (2006). Suppression of oxidative metabolism and mitochondrial biogenesis by the transcriptional corepressor RIP140 in mouse adipocytes. *J. Clin. Invest.* 116, 125-136.

Powers, J.M., DeCiero, D.P., Cox, C., Richfield, E.K., Ito, M., Moser, A.B., and Moser, H.W. (2001). The dorsal root ganglia in adrenomyeloneuropathy: neuronal atrophy and abnormal mitochondria. *J. Neuropathol. Exp. Neurol.* 60, 493-501.

Powers, J.M., Liu, Y., Moser, A.B., and Moser, H.W. (1992). The inflammatory myelinopathy of adreno-leukodystrophy: cells, effector molecules, and pathogenetic implications. *J. Neuropathol. Exp. Neurol.* 51, 630-643.

Powers, J.M., Pei, Z., Heinzer, A.K., Deering, R., Moser, A.B., Moser, H.W., Watkins, P.A., and Smith, K.D. (2005). Adreno-leukodystrophy: oxidative stress of mice and men. *J. Neuropathol. Exp. Neurol.* 64, 1067-1079.

Powers, J.M., and Schaumburg, H.H. (1974). Adreno-leukodystrophy. Similar ultrastructural changes in adrenal cortical and Schwann cells. *Arch. Neurol.* 30, 406-408.

Prasad, P.D., Ramamoorthy, S., Leibach, F.H., and Ganapathy, V. (1997). Characterization of a sodium-dependent vitamin transporter mediating the uptake of pantothenate, biotin and lipoate in human placental choriocarcinoma cells. *Placenta* 18, 527-533.

Pryor, W.A., Houk, K.N., Foote, C.S., Fukuto, J.M., Ignarro, L.J., Squadrito, G.L., and Davies, K.J. (2006). Free radical biology and medicine: it's a gas, man! *Am. J. Physiol. Regul. Integr. Comp. Physiol.* 291, R491-511.

Puigserver, P., Wu, Z., Park, C.W., Graves, R., Wright, M., and Spiegelman, B.M. (1998). A cold-inducible coactivator of nuclear receptors linked to adaptive thermogenesis. *Cell* 92, 829-839.

Pujol, A. (2016). Novel Therapeutic Targets and Drug Candidates for Modifying Disease Progression in Adrenoleukodystrophy. *Endocr. Dev.* 30, 147-160.

Pujol, A., Ferrer, I., Camps, C., Metzger, E., Hindelang, C., Callizot, N., Ruiz, M., Pampols, T., Giros, M., and Mandel, J.L. (2004). Functional overlap between ABCD1 (ALD) and ABCD2 (ALDR) transporters: a therapeutic target for X-adrenoleukodystrophy. *Hum.Mol.Genet.* 13, 2997-3006.

Pujol, A., Hindelang, C., Callizot, N., Bartsch, U., Schachner, M., and Mandel, J.L. (2002). Late onset neurological phenotype of the X-ALD gene inactivation in mice: a mouse model for adrenomyeloneuropathy. *Hum. Mol. Genet.* 11, 499-505.

Pulikkan, J.A., Dengler, V., Peramangalam, P.S., Peer Zada, A.A., Müller-Tidow, C., Bohlander, S.K., Tenen, D.G., and Behre, G. (2010). Cell-cycle regulator E2F1 and microRNA-223 comprise an autoregulatory negative feedback loop in acute myeloid leukemia. *Blood* 115, 1768-1778.

Qin, J., Goswami, R., Balabanov, R., and Dawson, G. (2007). Oxidized phosphatidylcholine is a marker for neuroinflammation in multiple sclerosis brain. *J. Neurosci. Res.* 85, 977-984.

Raimundo, N., Song, L., Shutt, T.E., McKay, S.E., Cotney, J., Guan, M.X., Gilliland, T.C., Hohuan, D., Santos-Sacchi, J., and Shadel, G.S. (2012). Mitochondrial stress engages E2F1 apoptotic signaling to cause deafness. *Cell* *148*, 716-726.

Ranea-Robles, P., Launay, N., Ruiz, M., Calingasan, N.Y., Dumont, M., Naudi, A., Portero-Otin, M., Pamplona, R., Ferrer, I., Beal, M.F., et al. (2018). Aberrant regulation of the GSK-3beta/NRF2 axis unveils a novel therapy for adrenoleukodystrophy. *EMBO Mol. Med.* *10*.

Ranganathan, S., and Bowser, R. (2003). Alterations in G(1) to S phase cell-cycle regulators during amyotrophic lateral sclerosis. *The American journal of pathology* *162*, 823-835.

Ransohoff, R.M., and Cardona, A.E. (2010). The myeloid cells of the central nervous system parenchyma. *Nature* *468*, 253-262.

Rasmussen, M., Moser, A.B., Borel, J., Khangoora, S., and Moser, H.W. (1994). Brain, liver, and adipose tissue erucic and very long chain fatty acid levels in adrenoleukodystrophy patients treated with glyceryl trierucate and trioleate oils (Lorenzo's oil). *Neurochem. Res.* *19*, 1073-1082.

Rasola, A., and Bernardi, P. (2011). Mitochondrial permeability transition in Ca(2+)-dependent apoptosis and necrosis. *Cell Calcium* *50*, 222-233.

Raymond, G.V., Seidman, R., Monteith, T.S., Kolodny, E., Sathe, S., Mahmood, A., and Powers, J.M. (2010). Head trauma can initiate the onset of adreno-leukodystrophy. *J. Neurol. Sci.* *290*, 70-74.

Reed, T.T. (2011). Lipid peroxidation and neurodegenerative disease. *Free Radic. Biol. Med.* *51*, 1302-1319.

Rhodin, J. (1954). Correlation of Ultrastructural Organization and Function in Normal and Experimentally Changed Proximal Convoluted Tubule Cells of the Mouse Kidney: An Electron Microscopic Study Including an Experimental Analysis of the Conditions for Fixation of the Renal Tissue for High Resolution Electron Microscopy. In *Anatomy* (Sweden: Karolinska Universitet).

Richmond, P.A., van der Kloet, F., Vaz, F.M., Lin, D., Uzozie, A., Graham, E., Kobor, M., Mostafavi, S., Moerland, P.D., Lange, P.F., et al. (2020). Multi-Omic Approach to Identify Phenotypic Modifiers Underlying Cerebral Demyelination in X-Linked Adrenoleukodystrophy. *Frontiers in cell and developmental biology* *8*, 520.

Rodriguez-Melendez, R., Schwab, L.D., and Zemleni, J. (2004). Jurkat cells respond to biotin deficiency with increased nuclear translocation of NF-kappaB, mediating cell survival. *Int. J. Vitam. Nutr. Res.* *74*, 209-216.

Romero-Navarro, G., Cabrera-Valladares, G., German, M.S., Matschinsky, F.M., Velazquez, A., Wang, J., and Fernandez-Mejia, C. (1999). Biotin Regulation of Pancreatic Glucokinase and Insulin in Primary Cultured Rat Islets and in Biotin- Deficient Rats¹. *Endocrinology* *140*, 4595-4600.

Ron, D., and Walter, P. (2007). Signal integration in the endoplasmic reticulum unfolded protein response. *Nat. Rev. Mol. Cell Biol.* *8*, 519-529.

Ross, B.M., Mamalias, N., Moszczyńska, A., Rajput, A.H., and Kish, S.J. (2001). Elevated activity of phospholipid biosynthetic enzymes in substantia nigra of patients with Parkinson's disease. *Neuroscience* *102*, 899-904.

Ruffert, K. (2012). European Society of Gene and Cell Therapy French Society of Cell and Gene Therapy Collaborative Congress 2012 October 25–29, 2012 Palais des Congrès de Versailles Versailles, France. In *Hum. Gene Ther.*, pp. A1-A173.

Ruiz, M., Jove, M., Schluter, A., Casasnovas, C., Villarroya, F., Guilera, C., Ortega, F.J., Naudi, A., Pamplona, R., Gimeno, R., et al. (2015). Altered glycolipid and glycerophospholipid signaling drive inflammatory cascades in adrenomyeloneuropathy. *Hum. Mol. Genet.* *24*, 6861-6876.

Safiulina, D., Kaasik, A., Seppet, E., Peet, N., Zharkovsky, A., and Seppet, E. (2004). Method for in situ detection of the mitochondrial function in neurons. *J. Neurosci. Methods* *137*, 87-95.

Sahin, K., Tuzcu, M., Orhan, C., Sahin, N., Kucuk, O., Ozercan, I.H., Juturu, V., and Komorowski, J.R. (2013). Anti-diabetic activity of chromium picolinate and biotin in rats with type 2 diabetes induced by high-fat diet and streptozotocin. *Br. J. Nutr.* *110*, 197-205.

Said, H., Redha, R., and Nylander, W. (1989). Biotin transport in the human intestine: Inhibition by anticonvulsant drugs. *The American journal of clinical nutrition* *49*, 127-131.

Sánchez, I., Balagué, E., and Matilla-Dueñas, A. (2016). Ataxin-1 regulates the cerebellar bioenergetics proteome through the GSK3 β -mTOR pathway which is altered in Spinocerebellar ataxia type 1 (SCA1). *Hum. Mol. Genet.* *25*, 4021-4040.

Sanhueza, M., Chai, A., Smith, C., McCray, B.A., Simpson, T.I., Taylor, J.P., and Pennetta, G. (2015). Network analyses reveal novel aspects of ALS pathogenesis. *PLoS Genet.* *11*, e1005107.

Sankaran, V.G., Orkin, S.H., and Walkley, C.R. (2008). Rb intrinsically promotes erythropoiesis by coupling cell cycle exit with mitochondrial biogenesis. *Genes Dev.* *22*, 463-475.

Sarruf, D.A., Iankova, I., Abella, A., Assou, S., Miard, S., and Fajas, L. (2005). Cyclin D3 promotes adipogenesis through activation of peroxisome proliferator-activated receptor gamma. *Mol. Cell. Biol.* *25*, 9985-9995.

Saxena, S., Cabuy, E., and Caroni, P. (2009). A role for motoneuron subtype-selective ER stress in disease manifestations of FALS mice. *Nat. Neurosci.* *12*, 627-636.

Saxton, R.A., and Sabatini, D.M. (2017). mTOR Signaling in Growth, Metabolism, and Disease. *Cell* *168*, 960-976.

Scarpulla, R.C. (2006). Nuclear control of respiratory gene expression in mammalian cells. *J. Cell. Biochem.* *97*, 673-683.

Schatteman, G.C., Dunnwald, M., and Jiao, C. (2007). Biology of bone marrow-derived endothelial cell precursors. *American Journal of Physiology-Heart and Circulatory Physiology* *292*, H1-H18.

Schaumburg, H.H., Powers, J.M., Raine, C.S., Suzuki, K., and Richardson, E.P., Jr. (1975). Adrenoleukodystrophy. A clinical and pathological study of 17 cases. *Arch. Neurol.* *32*, 577-591.

Schilder, P. (1924). Die Encephalitis periaxialis diffusa. *Arch Psychiatr. Nervenkr.* *71*, 327-356.

Schluter, A., Espinosa, L., Fourcade, S., Galino, J., Lopez, E., Ilieva, E., Morato, L., Asheuer, M., Cook, T., McLaren, A., et al. (2012). Functional genomic analysis unravels a metabolic-inflammatory interplay in adrenoleukodystrophy. *Hum. Mol. Genet.* *21*, 1062-1077.

Schluter, A., Fourcade, S., Ripp, R., Mandel, J.L., Poch, O., and Pujol, A. (2006). The evolutionary origin of peroxisomes: an ER-peroxisome connection. *Mol. Biol. Evol.* *23*, 838-845.

Schluter, A., Real-Chicharro, A., Gabaldon, T., Sanchez-Jimenez, F., and Pujol, A. (2010). PeroxisomeDB 2.0: an integrative view of the global peroxisomal metabolome. *Nucleic Acids Res.* *38*, D800-805.

Schluter, A., Sandoval, J., Fourcade, S., Diaz-Lagares, A., Ruiz, M., Casaccia, P., Esteller, M., and Pujol, A. (2018). Epigenomic signature of adrenoleukodystrophy predicts compromised oligodendrocyte differentiation. *Brain Pathol.* *28*, 902-919.

Schmidt, S., Marrosu, G.M., Kolsch, H., Haase, C.G., Ferenczik, S., Sokolowski, P., Kohler, W., Schmidt, M., Papassotiropoulos, A., Heun, R., et al. (2003). Genetic variations and humoral immune responses to myelin oligodendroglia glycoprotein in adult phenotypes of X-linked adrenoleukodystrophy. *J. Neuroimmunol.* *135*, 148-153.

Schneider, C., Pratt, D.A., Porter, N.A., and Brash, A.R. (2007). Control of oxygenation in lipoxygenase and cyclooxygenase catalysis. *Chem. Biol.* *14*, 473-488.

Schoenfeld, R., Wong, A., Silva, J., Li, M., Itoh, A., Horiuchi, M., Itoh, T., Pleasure, D., and Cortopassi, G. (2010). Oligodendroglial differentiation induces mitochondrial genes and inhibition of mitochondrial function represses oligodendroglial differentiation. *Mitochondrion* *10*, 143-150.

Schrader, M., Costello, J., Godinho, L.F., and Islinger, M. (2015). Peroxisome-mitochondria interplay and disease. *J. Inherit. Metab. Dis.* *38*, 681-702.

Schrader, M., and Fahimi, H.D. (2004). Mammalian peroxisomes and reactive oxygen species. *Histochem. Cell Biol.* *122*, 383-393.

Schroder, J.M., Mayer, M., and Weis, J. (1996). Mitochondrial abnormalities and intrafamilial variability of sural nerve biopsy findings in adrenomyeloneuropathy. *Acta Neuropathol.* *92*, 64-69.

Schulz, C., Gomez Perdiguero, E., Chorro, L., Szabo-Rogers, H., Cagnard, N., Kierdorf, K., Prinz, M., Wu, B., Jacobsen, S.E., Pollard, J.W., et al. (2012). A lineage of myeloid cells independent of Myb and hematopoietic stem cells. *Science* *336*, 86-90.

Schuurs-Hoeijmakers, J.H., Geraghty, M.T., Kamsteeg, E.J., Ben-Salem, S., de Bot, S.T., Nijhof, B., van de V., II, van der Graaf, M., Nobau, A.C., Otte-Holler, I., et al. (2012). Mutations in DDHD2, encoding an intracellular phospholipase A(1), cause a recessive form of complex hereditary spastic paraplegia. *Am. J. Hum. Genet.* *91*, 1073-1081.

Sedel, F., Papeix, C., Bellanger, A., Touthou, V., Lebrun-Frenay, C., Galanaud, D., Gout, O., Lyon-Caen, O., and Tourbah, A. (2015). High doses of biotin in chronic progressive multiple sclerosis: a pilot study. *Mult Scler Relat Disord* *4*, 159-169.

Selkoe, D.J. (2003). Folding proteins in fatal ways. *Nature* *426*, 900-904.

Semmler, A., Bao, X., Cao, G., Kohler, W., Weller, M., Aubourg, P., and Linnebank, M. (2009). Genetic variants of methionine metabolism and X-ALD phenotype generation: results of a new study sample. *J. Neurol.* *256*, 1277-1280.

Seth, A., Steel, J.H., Nichol, D., Pocock, V., Kumaran, M.K., Fritah, A., Mobberley, M., Ryder, T.A., Rowlerson, A., Scott, J., et al. (2007). The Transcriptional Corepressor RIP140 Regulates Oxidative Metabolism in Skeletal Muscle. *Cell Metab.* *6*, 236-245.

Seyer, A., Boudah, S., Broudin, S., Junot, C., and Colsch, B. (2016). Annotation of the human cerebrospinal fluid lipidome using high resolution mass spectrometry and a dedicated data processing workflow. *Metabolomics* *12*, 91.

Shah, N., and Singh, I. (2017). MicroRNA Profiling Identifies miR-196a as Differentially Expressed in Childhood Adrenoleukodystrophy and Adult Adrenomyeloneuropathy. *Mol. Neurobiol.* *54*, 1392-1403.

Shani, N., Jimenez-Sanchez, G., Steel, G., Dean, M., and Valle, D. (1997). Identification of a fourth half ABC transporter in the human peroxisomal membrane. *Hum. Mol. Genet.* *6*, 1925-1931.

Shani, N., Watkins, P.A., and Valle, D. (1995). PXA1, a possible *Saccharomyces cerevisiae* ortholog of the human adrenoleukodystrophy gene. *Proc. Natl. Acad. Sci. U. S. A.* *92*, 6012-6016.

Shen, H., and Shi, L.Z. (2019). Metabolic regulation of TH17 cells. *Mol. Immunol.* *109*, 81-87.

Shichiri, M. (2014). The role of lipid peroxidation in neurological disorders. *J. Clin. Biochem. Nutr.* *54*, 151-160.

Shimabukuro, M.K., Langhi, L.G., Cordeiro, I., Brito, J.M., Batista, C.M., Mattson, M.P., and Mello Coelho, V. (2016). Lipid-laden cells differentially distributed in the aging brain are functionally active and correspond to distinct phenotypes. *Sci. Rep.* *6*, 23795.

Shimano, H., and Sato, R. (2017). SREBP-regulated lipid metabolism: convergent physiology - divergent pathophysiology. *Nat. Rev. Endocrinol.* *13*, 710-730.

Shin, S., Wolgamott, L., Tcherkezian, J., Vallabhapurapu, S., Yu, Y., Roux, P.P., and Yoon, S.O. (2014). Glycogen synthase kinase-3 β positively regulates protein synthesis and cell proliferation through the regulation of translation initiation factor 4E-binding protein 1. *Oncogene* *33*, 1690-1699.

Shin, S., Wolgamott, L., Yu, Y., Blenis, J., and Yoon, S.O. (2011). Glycogen synthase kinase (GSK)-3 promotes p70 ribosomal protein S6 kinase (p70S6K) activity and cell proliferation. *Proc. Natl. Acad. Sci. U. S. A.* *108*, E1204-1213.

Shinnoh, N., Yamada, T., Yoshimura, T., Furuya, H., Yoshida, Y., Suzuki, Y., Shimosawa, N., Orii, T., and Kobayashi, T. (1995). Adrenoleukodystrophy: the restoration of peroxisomal beta-oxidation by transfection of normal cDNA. *Biochem. Biophys. Res. Commun.* *210*, 830-836.

Siemerling, E., and Creutzfeldt, H.G. (1923). Bronzkrankheit und sklerosierende encephalomyelitis. *Arch. Psychiatr Nervenkr.* *68*, 217-244.

Silva, J.M., Wong, A., Carelli, V., and Cortopassi, G.A. (2009). Inhibition of mitochondrial function induces an integrated stress response in oligodendroglia. *Neurobiol. Dis.* *34*, 357-365.

Simsek, T., Kocabas, F., Zheng, J., Deberardinis, R.J., Mahmoud, A.I., Olson, E.N., Schneider, J.W., Zhang, C.C., and Sadek, H.A. (2010). The distinct metabolic profile of hematopoietic stem cells reflects their location in a hypoxic niche. *Cell Stem Cell* *7*, 380-390.

Singh, A.K., Dhaunsi, G.S., Gupta, M.P., Orak, J.K., Asayama, K., and Singh, I. (1994). Demonstration of glutathione peroxidase in rat liver peroxisomes and its intraorganellar distribution. *Arch. Biochem. Biophys.* *315*, 331-338.

Singh, A.K., Dobashi, K., Gupta, M.P., Asayama, K., Singh, I., and Orak, J.K. (1999). Manganese superoxide dismutase in rat liver peroxisomes: biochemical and immunochemical evidence. *Mol. Cell. Biochem.* *197*, 7-12.

Singh, I., Khan, M., Key, L., and Pai, S. (1998a). Lovastatin for X-linked adrenoleukodystrophy. *N. Engl. J. Med.* *339*, 702-703.

Singh, I., Moser, A.E., Goldfischer, S., and Moser, H.W. (1984a). Lignoceric acid is oxidized in the peroxisome: implications for the Zellweger cerebro-hepato-renal syndrome and adrenoleukodystrophy. *Proc. Natl. Acad. Sci. U. S. A.* *81*, 4203-4207.

Singh, I., Moser, A.E., Moser, H.W., and Kishimoto, Y. (1984b). Adrenoleukodystrophy: impaired oxidation of very long chain fatty acids in white blood cells, cultured skin fibroblasts, and amniocytes. *Pediatr. Res.* *18*, 286-290.

Singh, I., Pahan, K., and Khan, M. (1998b). Lovastatin and sodium phenylacetate normalize the levels of very long chain fatty acids in skin fibroblasts of X- adrenoleukodystrophy. *FEBS Lett.* *426*, 342-346.

Singh, I., and Pujol, A. (2010). Pathomechanisms underlying X-adrenoleukodystrophy: a three-hit hypothesis. *Brain Pathol.* *20*, 838-844.

Singh, J., and Giri, S. (2014). Loss of AMP-activated protein kinase in X-linked adrenoleukodystrophy patient-derived fibroblasts and lymphocytes. *Biochem. Biophys. Res. Commun.* *445*, 126-131.

Singh, J., Olle, B., Suhail, H., Felicella, M.M., and Giri, S. (2016). Metformin-induced mitochondrial function and ABCD2 up-regulation in X-linked adrenoleukodystrophy involves AMP-activated protein kinase. *J. Neurochem.* *138*, 86-100.

Sivachenko, A., Gordon, H.B., Kimball, S.S., Gavin, E.J., Bonkowsky, J.L., and Letsou, A. (2016). Neurodegeneration in a Drosophila model of adrenoleukodystrophy: the roles of the Bubblegum and Double bubble acyl-CoA synthetases. *Dis. Model. Mech.* *9*, 377-387.

Smith, A.C., and Cronan, J.E. (2012). Dimerization of the bacterial biotin carboxylase subunit is required for acetyl coenzyme A carboxylase activity in vivo. *J. Bacteriol.* *194*, 72-78.

Smith, E.M., Hoi, J.T., Eissenberg, J.C., Shoemaker, J.D., Neckameyer, W.S., Ilvarsonn, A.M., Harshman, L.G., Schlegel, V.L., and Zemleni, J. (2007). Feeding Drosophila a biotin-deficient diet for multiple generations increases stress resistance and lifespan and alters gene expression and histone biotinylation patterns. *The Journal of nutrition* *137*, 2006-2012.

Smith, J.J., and Aitchison, J.D. (2013). Peroxisomes take shape. *Nat. Rev. Mol. Cell Biol.* *14*, 803-817.

Soliman, G.A. (2011). The integral role of mTOR in lipid metabolism. *Cell Cycle* *10*, 861-862.

St-Pierre, J., Drori, S., Uldry, M., Silvaggi, J.M., Rhee, J., Jager, S., Handschin, C., Zheng, K., Lin, J., Yang, W., et al. (2006). Suppression of reactive oxygen species and neurodegeneration by the PGC-1 transcriptional coactivators. *Cell* *127*, 397-408.

Stavrovskaya, I.G., and Kristal, B.S. (2005). The powerhouse takes control of the cell: is the mitochondrial permeability transition a viable therapeutic target against neuronal dysfunction and death? *Free Radic. Biol. Med.* *38*, 687-697.

Stevens, C., and La Thangue, N.B. (2004). The emerging role of E2F-1 in the DNA damage response and checkpoint control. *DNA repair* *3*, 1071-1079.

Stevens, C., Smith, L., and La Thangue, N.B. (2003). Chk2 activates E2F-1 in response to DNA damage. *Nat. Cell Biol.* 5, 401-409.

Stolz, D.B., Zamora, R., Vodovotz, Y., Loughran, P.A., Billiar, T.R., Kim, Y.M., Simmons, R.L., and Watkins, S.C. (2002). Peroxisomal localization of inducible nitric oxide synthase in hepatocytes. *Hepatology* 36, 81-93.

Strachan, L.R., Stevenson, T.J., Freshner, B., Keefe, M.D., Miranda Bowles, D., and Bonkowsky, J.L. (2017). A zebrafish model of X-linked adrenoleukodystrophy recapitulates key disease features and demonstrates a developmental requirement for *abcd1* in oligodendrocyte patterning and myelination. *Hum. Mol. Genet.* 26, 3600-3614.

Stumpf, D.A., Hayward, A., Haas, R., Frost, M., and Schaumburg, H.H. (1981). Adrenoleukodystrophy. Failure of immunosuppression to prevent neurological progression. *Arch. Neurol.* 38, 48-49.

Sugita, Y., Shirakawa, H., Sugimoto, R., Furukawa, Y., and Komai, M. (2008). Effect of Biotin Treatment on Hepatic Gene Expression in Streptozotocin-Induced Diabetic Rats. *Biosci. Biotechnol. Biochem.* 72, 1290-1298.

Sugiura, A., Mattie, S., Prudent, J., and McBride, H.M. (2017). Newly born peroxisomes are a hybrid of mitochondrial and ER-derived pre-peroxisomes. *Nature* 542, 251-254.

Sundqvist, A., Bengoechea-Alonso, M.T., Ye, X., Lukiyanchuk, V., Jin, J., Harper, J.W., and Ericsson, J. (2005). Control of lipid metabolism by phosphorylation-dependent degradation of the SREBP family of transcription factors by SCF(Fbw7). *Cell Metab.* 1, 379-391.

Tan, P.Y., Chang, C.W., Duan, K., Poidinger, M., Ng, K.L., Chong, Y.S., Gluckman, P.D., and Stünkel, W. (2016). E2F1 Orchestrates Transcriptomics and Oxidative Metabolism in Wharton's Jelly-Derived Mesenchymal Stem Cells from Growth-Restricted Infants. *PLoS One* 11, e0163035-e0163035.

Tansey, F.A., Thampy, K.G., and Cammer, W. (1988). Acetyl-CoA carboxylase in rat brain. II. Immunocytochemical localization. *Brain Res.* 471, 131-138.

Tarangelo, A., Lo, N., Teng, R., Kim, E., Le, L., Watson, D., Furth, E.E., Raman, P., Ehmer, U., and Viatour, P. (2015). Recruitment of Pontin/Reptin by E2f1 amplifies E2f transcriptional response during cancer progression. *Nature communications* 6, 10028.

Tay, T.L., Mai, D., Dautzenberg, J., Fernández-Klett, F., Lin, G., Sagar, Datta, M., Drougard, A., Stempfl, T., Ardura-Fabregat, A., et al. (2017). A new fate mapping system reveals context-dependent random or clonal expansion of microglia. *Nat. Neurosci.* 20, 793-803.

Tesio, M., and Trumpp, A. (2011). Breaking the Cell Cycle of HSCs by p57 and Friends. *Cell Stem Cell* 9, 187-192.

Theda, C., Moser, A.B., Powers, J.M., and Moser, H.W. (1992). Phospholipids in X-linked adrenoleukodystrophy white matter: fatty acid abnormalities before the onset of demyelination. *J. Neurol. Sci.* 110, 195-204.

Ting, J.H., Marks, D.R., Schleidt, S.S., Wu, J.N., Zyskind, J.W., Lindl, K.A., Blendy, J.A., Pierce, R.C., and Jordan-Sciutto, K.L. (2014). Targeted gene mutation of E2F1 evokes age-dependent synaptic disruption and behavioral deficits. *J. Neurochem.* 129, 850-863.

Tong, L. (2013). Structure and function of biotin-dependent carboxylases. *Cell. Mol. Life Sci.* 70, 863-891.

Tourbah, A., Lebrun-Frenay, C., Edan, G., Clanet, M., Papeix, C., Vukusic, S., De Seze, J., Debouverie, M., Gout, O., Clavelou, P., et al. (2016). MD1003 (high-dose biotin) for the treatment of progressive multiple sclerosis: A randomised, double-blind, placebo-controlled study. *Mult. Scler.* 22, 1719-1731.

Trapp, B.D., and Stys, P.K. (2009). Virtual hypoxia and chronic necrosis of demyelinated axons in multiple sclerosis. *Lancet Neurol.* 8, 280-291.

Tremblay, M.E., Stevens, B., Sierra, A., Wake, H., Bessis, A., and Nimmerjahn, A. (2011). The role of microglia in the healthy brain. *J. Neurosci.* 31, 16064-16069.

Trikha, P., Sharma, N., Opavsky, R., Reyes, A., Pena, C., Ostrowski, M.C., Roussel, M.F., and Leone, G. (2011). E2f1-3 are critical for myeloid development. *J. Biol. Chem.* 286, 4783-4795.

Trimarchi, J.M., Fairchild, B., Verona, R., Moberg, K., Andon, N., and Lees, J.A. (1998). E2F-6, a member of the E2F family that can behave as a transcriptional repressor. *Proc. Natl. Acad. Sci. U. S. A.* *95*, 2850-2855.

Troffer-Charlier, N., Doerflinger, N., Metzger, E., Fouquet, F., Mandel, J.L., and Aubourg, P. (1998). Mirror expression of adrenoleukodystrophy and adrenoleukodystrophy related genes in mouse tissues and human cell lines. *Eur. J. Cell Biol.* *75*, 254-264.

Turgeon, C.T., Moser, A.B., Morkrid, L., Magera, M.J., Gavrilov, D.K., Oglesbee, D., Raymond, K., Rinaldo, P., Matern, D., and Tortorelli, S. (2015). Streamlined determination of lysophosphatidylcholines in dried blood spots for newborn screening of X-linked adrenoleukodystrophy. *Mol. Genet. Metab.* *114*, 46-50.

Turk, B.R., Theisen, B.E., Nemeth, C.L., Marx, J.S., Shi, X., Rosen, M., Jones, R.O., Moser, A.B., Watkins, P.A., Raymond, G.V., et al. (2017). Antioxidant Capacity and Superoxide Dismutase Activity in Adrenoleukodystrophy. *JAMA Neurol.*

Urbanska, M., Gozdz, A., Macias, M., Cymerman, I.A., Liszewska, E., Kondratiuk, I., Devijver, H., Lechat, B., Van Leuven, F., and Jaworski, J. (2018). GSK3 β Controls mTOR and Prosurvival Signaling in Neurons. *Mol. Neurobiol.* *55*, 6050-6062.

Uto, T., Contreras, M.A., Gilg, A.G., and Singh, I. (2008). Oxidative imbalance in nonstimulated X-adrenoleukodystrophy-derived lymphoblasts. *Dev. Neurosci.* *30*, 410-418.

van Ballegoij, W.J.C., van de Stadt, S.I.W., Huffnagel, I.C., Kemp, S., Willemsse, E.A.J., Teunissen, C.E., and Engelen, M. (2020). Plasma NFL and GFAP as biomarkers of spinal cord degeneration in adrenoleukodystrophy. *Ann Clin Transl Neurol* *7*, 2127-2136.

van den Heuvel, S., and Dyson, N.J. (2008). Conserved functions of the pRB and E2F families. *Nat. Rev. Mol. Cell Biol.* *9*, 713-724.

van der Vlies, D., Makkinje, M., Jansens, A., Braakman, I., Verkleij, A.J., Wirtz, K.W., and Post, J.A. (2003). Oxidation of ER resident proteins upon oxidative stress: effects of altering cellular redox/antioxidant status and implications for protein maturation. *Antioxid Redox Signal* *5*, 381-387.

van der Zand, A., Gent, J., Braakman, I., and Tabak, H.F. (2012). Biochemically distinct vesicles from the endoplasmic reticulum fuse to form peroxisomes. *Cell* *149*, 397-409.

van Engen, C.E., Ofman, R., Dijkstra, I.M., van Goethem, T.J., Verheij, E., Varin, J., Vidaud, M., Wanders, R.J., Aubourg, P., Kemp, S., et al. (2016). CYP4F2 affects phenotypic outcome in adrenoleukodystrophy by modulating the clearance of very long-chain fatty acids. *Biochim. Biophys. Acta* *1862*, 1861-1870.

van Geel, B.M., Assies, J., Haverkort, E.B., Koelman, J.H., Verbeeten, B., Jr., Wanders, R.J., and Barth, P.G. (1999). Progression of abnormalities in adrenomyeloneuropathy and neurologically asymptomatic X-linked adrenoleukodystrophy despite treatment with "Lorenzo's oil". *J. Neurol. Neurosurg. Psychiatry* *67*, 290-299.

van Geel, B.M., Bezman, L., Loes, D.J., Moser, H.W., and Raymond, G.V. (2001). Evolution of phenotypes in adult male patients with X-linked adrenoleukodystrophy. *Ann. Neurol.* *49*, 186-194.

van Geel, B.M., Poll-The, B.T., Verrips, A., Boelens, J.J., Kemp, S., and Engelen, M. (2015). Hematopoietic cell transplantation does not prevent myelopathy in X-linked adrenoleukodystrophy: a retrospective study. *J. Inherit. Metab. Dis.* *38*, 359-361.

van Roermund, C.W., Ijlst, L., Wagemans, T., Wanders, R.J., and Waterham, H.R. (2014). A role for the human peroxisomal half-transporter ABCD3 in the oxidation of dicarboxylic acids. *Biochim. Biophys. Acta* *1841*, 563-568.

van Roermund, C.W., Visser, W.F., Ijlst, L., van Cruchten, A., Boek, M., Kulik, W., Waterham, H.R., and Wanders, R.J. (2008). The human peroxisomal ABC half transporter ALDP functions as a homodimer and accepts acyl-CoA esters. *FASEB J.* *22*, 4201-4208.

Vargas, C.R., Wajner, M., Sirtori, L.R., Goulart, L., Chiochetta, M., Coelho, D., Latini, A., Llesuy, S., Bello-Klein, A., Giugliani, R., et al. (2004). Evidence that oxidative stress is increased in patients with X-linked adrenoleukodystrophy. *Biochim. Biophys. Acta* *1688*, 26-32.

Vaziri, H., Dessain, S.K., Ng Eaton, E., Imai, S.I., Frye, R.A., Pandita, T.K., Guarente, L., and Weinberg, R.A. (2001). hSIR2(SIRT1) functions as an NAD-dependent p53 deacetylase. *Cell* *107*, 149-159.

Velazquez-Arellano, A., Ortega-Cuellar, D., Hernandez-Mendoza, A., and Moreno-Arriola, E. (2011). A heuristic model for paradoxical effects of biotin starvation on carbon metabolism genes in the presence of abundant glucose. *Mol. Genet. Metab.* *102*, 69-77.

Viader, A., Sasaki, Y., Kim, S., Strickland, A., Workman, C.S., Yang, K., Gross, R.W., and Milbrandt, J. (2013). Aberrant Schwann cell lipid metabolism linked to mitochondrial deficits leads to axon degeneration and neuropathy. *Neuron* *77*, 886-898.

Viatour, P. (2012). Bridges between Cell Cycle Regulation and Self-Renewal Maintenance. *Genes Cancer* *3*, 670-677.

Vidal, R., Caballero, B., Couve, A., and Hetz, C. (2011). Converging pathways in the occurrence of endoplasmic reticulum (ER) stress in Huntington's disease. *Curr. Mol. Med.* *11*, 1-12.

Vincent, I., Jicha, G., Rosado, M., and Dickson, D.W. (1997). Aberrant expression of mitotic cdc2/cyclin B1 kinase in degenerating neurons of Alzheimer's disease brain. *The Journal of neuroscience : the official journal of the Society for Neuroscience* *17*, 3588-3598.

Wallace, D.C., Fan, W., and Procaccio, V. (2010). Mitochondrial energetics and therapeutics. *Annu. Rev. Pathol.* *5*, 297-348.

Wallberg, A.E., Yamamura, S., Malik, S., Spiegelman, B.M., and Roeder, R.G. (2003). Coordination of p300-mediated chromatin remodeling and TRAP/mediator function through coactivator PGC-1alpha. *Mol. Cell* *12*, 1137-1149.

Walther, T.C., Chung, J., and Farese, R.V., Jr. (2017). Lipid Droplet Biogenesis. *Annu. Rev. Cell Dev. Biol.* *33*, 491-510.

Wanders, R.J. (2003). Defects in mitochondrial and peroxisomal fatty acid oxidation. In *Advances in Molecular and Cell Biology* (Elsevier), pp. 295-317.

Wanders, R.J., van Roermund, C.W., van Wijland, M.J., Nijenhuis, A.A., Tromp, A., Schutgens, R.B., Brouwer-Kelder, E.M., Schram, A.W., Tager, J.M., van den Bosch, H., et al. (1987). X-linked adrenoleukodystrophy: defective peroxisomal oxidation of very long chain fatty acids but not of very long chain fatty acyl-CoA esters. *Clin. Chim. Acta* *165*, 321-329.

Wanders, R.J., van Roermund, C.W., van Wijland, M.J., Schutgens, R.B., Schram, A.W., Tager, J.M., van den Bosch, H., and Schalkwijk, C. (1988). X-linked adrenoleukodystrophy: identification of the primary defect at the level of a deficient peroxisomal very long chain fatty acyl-CoA synthetase using a newly developed method for the isolation of peroxisomes from skin fibroblasts. *J. Inher. Metab. Dis.* *11 Suppl 2*, 173-177.

Wanders, R.J., and Waterham, H.R. (2006). Biochemistry of mammalian peroxisomes revisited. *Annu. Rev. Biochem.* *75*, 295-332.

Wang, C., Li, Z., Lu, Y., Du, R., Katiyar, S., Yang, J., Fu, M., Leader, J.E., Quong, A., Novikoff, P.M., et al. (2006). Cyclin D1 repression of nuclear respiratory factor 1 integrates nuclear DNA synthesis and mitochondrial function. *Proceedings of the National Academy of Sciences* *103*, 11567-11572.

Wang, L.Y., Hung, C.L., Chen, Y.R., Yang, J.C., Wang, J., Campbell, M., Izumiya, Y., Chen, H.W., Wang, W.C., Ann, D.K., et al. (2016). KDM4A Coactivates E2F1 to Regulate the PDK-Dependent Metabolic Switch between Mitochondrial Oxidation and Glycolysis. *Cell Rep.* *16*, 3016-3027.

Wang, W., Bu, B., Xie, M., Zhang, M., Yu, Z., and Tao, D. (2009). Neural cell cycle dysregulation and central nervous system diseases. *Prog. Neurobiol.* *89*, 1-17.

Wang, Y., Busin, R., Reeves, C., Bezman, L., Raymond, G., Toomer, C.J., Watkins, P.A., Snowden, A., Moser, A., Naidu, S., et al. (2011). X-linked adrenoleukodystrophy: ABCD1 de novo mutations and mosaicism. *Mol. Genet. Metab.* *104*, 160-166.

Wang, Y., Santa-Cruz, K., DeCarli, C., and Johnson, J.A. (2000). NAD(P)H:quinone oxidoreductase activity is increased in hippocampal pyramidal neurons of patients with alzheimer's disease. *Neurobiol. Aging* *21*, 525-531.

Wang, Y., Yang, J., and Yi, J. (2012). Redox sensing by proteins: oxidative modifications on cysteines and the consequent events. *Antioxid Redox Signal* *16*, 649-657.

Wang, Z., Fan, M., Candas, D., Zhang, T.-Q., Qin, L., Eldridge, A., Wachsmann-Hogiu, S., Ahmed, Kazi M., Chromy, Brett A., Nantajit, D., et al. (2014). Cyclin B1/Cdk1 Coordinates Mitochondrial Respiration for Cell-Cycle G2/M Progression. *Dev. Cell* *29*, 217-232.

Ward, R.J., Dexter, D.T., and Crichton, R.R. (2012). Chelating agents for neurodegenerative diseases. *Curr. Med. Chem.* *19*, 2760-2772.

Warg, L.A., Oakes, J.L., Burton, R., Neidermyer, A.J., Rutledge, H.R., Groshong, S., Schwartz, D.A., and Yang, I.V. (2012). The role of the E2F1 transcription factor in the innate immune response to systemic LPS. *Am. J. Physiol. Lung Cell Mol. Physiol.* *303*, L391-400.

Watanabe-Kamiyama, M., Kamiyama, S., Horiuchi, K., Ohinata, K., Shirakawa, H., Furukawa, Y., and Komai, M. (2008). Antihypertensive effect of biotin in stroke-prone spontaneously hypertensive rats. *Br. J. Nutr.* *99*, 756-763.

Waterham, H.R., Ferdinandusse, S., and Wanders, R.J. (2016). Human disorders of peroxisome metabolism and biogenesis. *Biochim. Biophys. Acta* *1863*, 922-933.

Weber, F.D., Wiesinger, C., Forss-Petter, S., Regelsberger, G., Einwich, A., Weber, W.H., Köhler, W., Stockinger, H., and Berger, J. (2014). X-linked adrenoleukodystrophy: very long-chain fatty acid metabolism is severely impaired in monocytes but not in lymphocytes. *Hum. Mol. Genet.* *23*, 2542-2550.

Weinhofer, I., Rommer, P., Zierfuss, B., Altmann, P., Foiani, M., Heslegrave, A., Zetterberg, H., Gleiss, A., Musolino, P.L., Gong, Y., et al. (2021). Neurofilament light chain as a potential biomarker for monitoring neurodegeneration in X-linked adrenoleukodystrophy. *Nature communications* *12*, 1816.

Weinhofer, I., Zierfuss, B., Hametner, S., Wagner, M., Popitsch, N., Machacek, C., Bartolini, B., Zlabinger, G., Ohradanova-Repic, A., Stockinger, H., et al. (2018). Impaired plasticity of macrophages in X-linked adrenoleukodystrophy. *Brain* *141*, 2329-2342.

Weller, M., Liedtke, W., Petersen, D., Opitz, H., and Poremba, M. (1992). Very-late-onset adrenoleukodystrophy: possible precipitation of demyelination by cerebral contusion. *Neurology* *42*, 367-370.

Welte, M.A. (2015). Expanding roles for lipid droplets. *Curr. Biol.* *25*, R470-481.

Wenk, M.R. (2005). The emerging field of lipidomics. *Nat Rev Drug Discov* *4*, 594-610.

Whitcomb, R.W., Linehan, W.M., and Knazek, R.A. (1988). Effects of long-chain, saturated fatty acids on membrane microviscosity and adrenocorticotropin responsiveness of human adrenocortical cells in vitro. *J. Clin. Invest.* *81*, 185-188.

White, R., Morganstein, D., Christian, M., Seth, A., Herzog, B., and Parker, M.G. (2008). Role of RIP140 in metabolic tissues: connections to disease. *FEBS Lett.* *582*, 39-45.

Wiesinger, C., Kunze, M., Regelsberger, G., Forss-Petter, S., and Berger, J. (2013). Impaired very long-chain acyl-CoA beta-oxidation in human X-linked adrenoleukodystrophy fibroblasts is a direct consequence of ABCD1 transporter dysfunction. *J. Biol. Chem.* *288*, 19269-19279.

Wilkinson, K.D. (2000). Ubiquitination and deubiquitination: targeting of proteins for degradation by the proteasome. *Semin. Cell Dev. Biol.* *11*, 141-148.

Wolf, B. (2011). The neurology of biotinidase deficiency. *Mol. Genet. Metab.* *104*, 27-34.

Wong, E., and Cuervo, A.M. (2010). Autophagy gone awry in neurodegenerative diseases. *Nat. Neurosci.* *13*, 805-811.

Wongkittichote, P., Ah Mew, N., and Chapman, K.A. (2017). Propionyl-CoA carboxylase - A review. *Mol. Genet. Metab.* *122*, 145-152.

Wood, J.G., and Dawson, R.M. (1974). Lipid and protein changes in sciatic nerve during Wallerian degeneration. *J. Neurochem.* *22*, 631-635.

Wu, J., Kharebava, G., Piao, C., Stoica, B.A., Dinizo, M., Sabirzhanov, B., Hanscom, M., Guanciale, K., and Faden, A.I. (2012). Inhibition of E2F1/CDK1 pathway attenuates neuronal apoptosis in vitro and confers neuroprotection after spinal cord injury in vivo. *PLoS One* *7*, e42129.

Wu, J., Sabirzhanov, B., Stoica, B.A., Lipinski, M.M., Zhao, Z., Zhao, S., Ward, N., Yang, D., and Faden, A.I. (2015). Ablation of the transcription factors E2F1-2 limits neuroinflammation and associated neurological deficits after contusive spinal cord injury. *Cell Cycle* 14, 3698-3712.

Wyss-Coray, T., and Mucke, L. (2002). Inflammation in neurodegenerative disease--a double-edged sword. *Neuron* 35, 419-432.

Xiong, T., Qu, Y., Wang, H., Chen, H., Zhu, J., Zhao, F., Zou, R., Zhang, L., and Mu, D. (2018). GSK-3 β /mTORC1 Couples Synaptogenesis and Axonal Repair to Reduce Hypoxia Ischemia-Mediated Brain Injury in Neonatal Rats. *J. Neuropathol. Exp. Neurol.* 77, 383-394.

Xu, S., Tao, J., Yang, L., Zhang, E., Boriboun, C., Zhou, J., Sun, T., Cheng, M., Huang, K., Shi, J., et al. (2018). E2F1 Suppresses Oxidative Metabolism and Endothelial Differentiation of Bone Marrow Progenitor Cells. *Circ. Res.* 122, 701-711.

Yamamoto, H., Williams, E.G., Mouchiroud, L., Canto, C., Fan, W., Downes, M., Heligon, C., Barish, G.D., Desvergne, B., Evans, R.M., et al. (2011). NCoR1 is a conserved physiological modulator of muscle mass and oxidative function. *Cell* 147, 827-839.

Yamashita, H., Avraham, S., Jiang, S., London, R., Van Veldhoven, P.P., Subramani, S., Rogers, R.A., and Avraham, H. (1999). Characterization of human and murine PMP20 peroxisomal proteins that exhibit antioxidant activity in vitro. *J. Biol. Chem.* 274, 29897-29904.

Yang, I.V., Alper, S., Lackford, B., Rutledge, H., Warg, L.A., Burch, L.H., and Schwartz, D.A. (2011). Novel regulators of the systemic response to lipopolysaccharide. *Am. J. Respir. Cell Mol. Biol.* 45, 393-402.

Yang, Y., and Herrup, K. (2007). Cell division in the CNS: Protective response or lethal event in post-mitotic neurons? *Biochimica et Biophysica Acta (BBA) - Molecular Basis of Disease* 1772, 457-466.

Yu, H., Li, Z., and Wang, M. (2020). Expression and prognostic role of E2F transcription factors in high-grade glioma. *CNS Neurosci. Ther.* 26, 741-753.

Zarrouk, A., Vejux, A., Mackrill, J., O'Callaghan, Y., Hammami, M., O'Brien, N., and Lizard, G. (2014). Involvement of oxysterols in age-related diseases and ageing processes. *Ageing research reviews* 18, 148-162.

Zarrouk, A., Vejux, A., Nury, T., El Hajj, H.I., Haddad, M., Cherkaoui-Malki, M., Riedinger, J.M., Hammami, M., and Lizard, G. (2012). Induction of mitochondrial changes associated with oxidative stress on very long chain fatty acids (C22:0, C24:0, or C26:0)-treated human neuronal cells (SK-NB-E). *Oxid. Med. Cell. Longev.* 2012, 623257.

Zecca, L., Youdim, M.B., Riederer, P., Connor, J.R., and Crichton, R.R. (2004). Iron, brain ageing and neurodegenerative disorders. *Nat. Rev. Neurosci.* 5, 863-873.

Zempleni, J., Liu, D., Camara, D.T., and Cordonier, E.L. (2014). Novel roles of holocarboxylase synthetase in gene regulation and intermediary metabolism. *Nutr. Rev.* 72, 369-376.

Zempleni, J., and Mock, D.M. (2000). Marginal biotin deficiency is teratogenic. *Proc. Soc. Exp. Biol. Med.* 223, 14-21.

Zempleni, J., Teixeira, D.C., Kuroishi, T., Cordonier, E.L., and Baier, S. (2012). Biotin requirements for DNA damage prevention. *Mutation Research/Fundamental and Molecular Mechanisms of Mutagenesis* 733, 58-60.

Zempleni, J., Wijeratne, S.S., and Hassan, Y.I. (2009). Biotin. *Biofactors* 35, 36-46.

Zempleni, J., Wolf, B., Cannon, M., Jennings, M., Cress, S., Boylan, J., Roth, S., Cederbaum, S., and Mock, D. (2002). Biotin dependency due to a defect in biotin transport. *The Journal of clinical investigation* 109, 1617-1623.

Zhang, H., Osada, K., Maebashi, M., Ito, M., Komai, M., and Furukawa, Y. (1996). A high biotin diet improves the impaired glucose tolerance of long-term spontaneously hyperglycemic rats with non-insulin-dependent diabetes mellitus. *J. Nutr. Sci. Vitaminol. (Tokyo)* 42, 517-526.

Zheng, S., Moehlenbrink, J., Lu, Y.C., Zalmas, L.P., Sagum, C.A., Carr, S., McGouran, J.F., Alexander, L., Fedorov, O., Munro, S., et al. (2013). Arginine methylation-dependent reader-writer interplay governs growth control by E2F-1. *Mol. Cell* 52, 37-51.

Zhou, Y., Kim, Y.S., Yan, X., Jacobson, O., Chen, X., and Liu, S. (2011). ⁶⁴Cu-labeled lissamine rhodamine B: a promising PET radiotracer targeting tumor mitochondria. *Mol. Pharm.* *8*, 1198-1208.

Zhu, X., Lee, H.G., Perry, G., and Smith, M.A. (2007). Alzheimer disease, the two-hit hypothesis: an update. *Biochim. Biophys. Acta* *1772*, 494-502.

Ziabreva, I., Campbell, G., Rist, J., Zamboni, J., Rorbach, J., Wydro, M.M., Lassmann, H., Franklin, R.J., and Mahad, D. (2010). Injury and differentiation following inhibition of mitochondrial respiratory chain complex IV in rat oligodendrocytes. *Glia* *58*, 1827-1837.

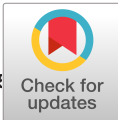
Zyskind, J.W., Wang, Y., Cho, G., Ting, J.H., Kolson, D.L., Lynch, D.R., and Jordan-Sciutto, K.L. (2015). E2F1 in neurons is cleaved by calpain in an NMDA receptor-dependent manner in a model of HIV-induced neurotoxicity. *J. Neurochem.* *132*, 742-755.

APPENDIX I

† **This appendix corresponds to:**

Stéphane Fourcade; **Leire Goicoechea**; Janani Parameswaran; Agatha Schlüter; Nathalie Launay; Montserrat Ruiz; Alexandre Seyer; Benoit Colsch; Noel Ylagan Calingasan; Isidre Ferrer; M. Flint Beal; Frédéric Sedel; Aurora Pujol (2020). High-dose biotin restores redox balance, energy and lipid homeostasis, and axonal health in a model of adrenoleukodystrophy. *Brain Pathology* 1015-6305.

Research Article



RESEARCH ARTICLE

High-dose biotin restores redox balance, energy and lipid homeostasis, and axonal health in a model of adrenoleukodystrophy

Stéphane Fourcade^{1,2*} ; Leire Goicoechea^{1,2#}; Janani Parameswaran^{1,2#}; Agatha Schlüter^{1,2}; Nathalie Launay^{1,2}; Montserrat Ruiz^{1,2}; Alexandre Seyer³; Benoit Colsch⁴; Noel Ylagan Calingasan⁵; Isidre Ferrer^{6,7,8} ; M. Flint Beal⁵; Frédéric Sedel³; Aurora Pujol^{1,2,9,*}

¹ Neurometabolic Diseases Laboratory, IDIBELL, Barcelona, Spain.

² CIBERER U759, Center for Biomedical Research on Rare Diseases, Barcelona, Spain.

³ Medday Pharmaceuticals SA, Paris, France.

⁴ Service de Pharmacologie et Immuno-Analyse (SPI), Laboratoire d'Etude du Métabolisme des Médicaments, CEA, INRA, Université Paris Saclay, MetaboHUB, Gif-sur-Yvette, F-91191, France.

⁵ Feil Family Brain and Mind Research Institute, Weill Cornell Medical College, New York, NY 10065, USA.

⁶ Department of Pathology and Experimental Therapeutics, IDIBELL, Faculty of Medicine, University of Barcelona, L'Hospitalet de Llobregat, Barcelona, 08907, Spain.

⁷ Center for Biomedical Research on Neurodegenerative Diseases (CIBERNED), ISCIII, Madrid, Spain.

⁸ Institute of Neurosciences, University of Barcelona, Barcelona, Spain.

⁹ Catalan Institution of Research and Advanced Studies (ICREA), Barcelona, Spain.

Keywords

axonal degeneration, biotin, mTORC1, multiple sclerosis, NRF2, redox homeostasis, SREBP-1c.

Corresponding author

Aurora Pujol and Stéphane Fourcade, Neurometabolic Diseases Laboratory, Institut de Neuropatologia de Bellvitge, IDIBELL, Gran Via, 199, L'Hospitalet de Llobregat, Barcelona 08908, Spain (Email: sfourcade@idibell.cat and apujol@idibell.cat)

Received 28 February 2020

Accepted 26 May 2020

Published Online Article

Accepted 00 Month 2020

#Contributed equally to this work.

doi:10.1111/bpa.12869

Abstract

Biotin is an essential cofactor for carboxylases that regulates the energy metabolism. Recently, high-dose pharmaceutical-grade biotin (MD1003) was shown to improve clinical parameters in a subset of patients with chronic progressive multiple sclerosis. To gain insight into the mechanisms of action, we investigated the efficacy of high-dose biotin in a genetic model of chronic axonopathy caused by oxidative damage and bioenergetic failure, the *Abcd1*⁻ mouse model of adrenomyeloneuropathy. High-dose biotin restored redox homeostasis driven by NRF-2, mitochondria biogenesis and ATP levels, and reversed axonal demise and locomotor impairment. Moreover, we uncovered a concerted dysregulation of the transcriptional program for lipid synthesis and degradation in the spinal cord likely driven by aberrant SREBP-1c/mTORC1 signaling. This resulted in increased triglyceride levels and lipid droplets in motor neurons. High-dose biotin normalized the hyperactivation of mTORC1, thus restoring lipid homeostasis. These results shed light into the mechanism of action of high-dose biotin of relevance for neurodegenerative and metabolic disorders.

INTRODUCTION

Biotin is an essential B-complex vitamin that controls energy metabolism through its role as a cofactor for five carboxylases: pyruvate carboxylase (PC), 3-methylcrotonyl-CoA carboxylase (MCC), propionyl-CoA carboxylase (PCC), and the two isoforms of acetyl-CoA carboxylase (ACC1 and ACC2) (69). ACC1 is the rate-limiting enzyme that generates malonyl-CoA, the two-carbon building block for the synthesis of fatty acids, which are essential components of the myelin sheath (9,68). PC, PCC, and MCC generate intermediates of the tricarboxylic acid cycle and thus increase the levels of cellular ATP at the rate of one molecule of ATP produced

per one molecule of acetyl-CoA used by the TCA cycle. Indeed, nutritional biotin deficiency and biotin deficiency induced by the loss of the recycling enzyme biotinidase causes severe ATP depletion (24). The importance of biotin in the brain is best manifested by inherited errors of biotin metabolism, which lead to severe neurological impairments involving myelin, as seen in biotinidase deficiency, which is reversible to some extent with biotin treatment (76) in the same manner as biotin-thiamine responsive basal ganglia disease (53).

Recently, treatment with a formulation of high-dose pharmaceutical-grade biotin (MD1003, 10 000 times the recommended daily intake) resulted in improvement of

clinical markers in a subset of patients suffering from progressive multiple sclerosis (MS) (70). Thereby, we set out to investigate its possible mechanisms of action as the first step in developing a rationale for broadening its application to other neurodegenerative diseases. We chose an X-ALD mouse model since its hallmarks, that is, redox imbalance of mitochondrial origin intertwined with energy deficiency that leads to axonal degeneration, are shared by MS and the most common neurodegenerative disorders, such as Alzheimer, Parkinson's disease, and ALS (22).

X-ALD is the most common peroxisomal disease, with an incidence of 1:14 700 live births (50). It is caused by mutations in the *ABCD1* gene (51) located on Xq.28, which encodes a peroxisomal transporter that imports very long-chain fatty acids (VLCFAs) into the peroxisome for degradation by β -oxidation (61,75). As a consequence, VLCFAs, especially C26:0, accumulate in tissues and plasma and constitute pathognomonic biomarkers for diagnosis. There are two main forms of the disease (14,15): (i) cALD or cAMN, a rapidly progressing cerebral demyelinating leukodystrophy that leads to death (35–40% of cases) and (ii) adrenomyeloneuropathy (AMN), which makes up 60% of cases and affects adult men and heterozygous women over the age of 40 (13) and is characterized by distal axonopathy involving the corticospinal tract in the spinal cord and peripheral neuropathy. For the cerebral form of the disease, current therapeutic options are restricted to bone marrow transplantation (47) and for childhood cALD, hematopoietic stem cell gene therapy (5,12). No treatment is currently available for the AMN phenotype, although a phase II pilot trial of a combination of high-dose antioxidants recently showed some promise (6). The mouse model of X-ALD (*Abcd1*⁻) develops axonopathy and locomotor impairment very late in life, at 20 months of age, and thus resembled AMN, the most common X-ALD phenotype (58). The closest *Abcd1* homolog, *Abcd2*, exhibits overlapping metabolic functions (20), shows a complementary expression pattern (16,71), and has thus been postulated as a modifier of the biochemical defects (52,57). Double mutant *Abcd1*⁻/*Abcd2*⁻ mice develop more substantial accumulation of VLCFAs and more severe, earlier onset axonopathy starting at 12 months of age, which makes this model better suited for therapeutic assays (57). Indeed, this mouse model was instrumental in pinpointing early oxidative damage, mitochondrial depletion and bioenergetic failure as early, intertwined culprits of axonal degeneration (23,39,40) and in identifying therapeutic targets along the way (32,33,48,49,59). This knowledge aligns X-ALD physiopathogenesis with that of the most prevalent neurodegenerative disorders, including MS (22).

Here, we used X-ALD patient's primary fibroblasts and two mouse models of X-ALD (*Abcd1*⁻ and *Abcd1*⁻/*Abcd2*⁻ mice) to investigate the preclinical efficacy and mode of action of high-dose biotin on the established biochemical hallmarks of redox dyshomeostasis and energetic failure, as well as axonal damage and locomotor function (41,49,59). Moreover, we uncovered novel alterations that results from the loss of the *Abcd1* transporter, specifically profound dysregulation of the lipogenesis and fatty acid degradation

pathways governed by mTOR/SREBP-1c in the spinal cord concomitant with global increases in triglycerides and lipid droplets. High-dose biotin restores metabolic balance and rescues axonal degeneration, indicating that it is a promising therapeutic option for X-ALD and similar neurometabolic conditions.

MATERIALS AND METHODS

Cell culture experiments

Human X-ALD fibroblasts were obtained at the Bellvitge University Hospital after informed consent. Control and X-ALD cells were grown in DMEM containing 1 g/L glucose, pyruvate, L-glutamine, 10% foetal calf serum (FCS), 100 U/mL penicillin and 100 mg streptomycin and maintained at 37°C in humidified 95% air/5% CO₂ (40). The compounds tested were added to 80%–90% confluent cells in medium containing 10% FCS at the following concentrations: 50 μ M C26:0 and 0.25 to 10 μ M pharmaceutical-grade biotin (MD1003).

Evaluation of intracellular ROS

Intracellular H₂O₂ levels were estimated using the ROS-sensitive probe H₂DCFDA (DCF) as previously described (19). Following incubation with 10 μ M DCF for 30 minutes, the cells were washed twice with PBS and scraped into water. Intracellular and mitochondrial superoxide anion levels were estimated using DHE probes and MitoSOXTM Red (Molecular Probes), respectively (41). Following incubation with 5 μ M DHE for 10 minutes or 5 μ M MitoSOX for 10 minutes, the cells were washed twice with PBS and scraped into water. The homogenate was transferred to a 96-well plate for fluorescence detection with a spectrofluorimeter. The fluorescence of DCF-, DHE-, and MitoSOX-stained cells was measured with a spectrofluorimeter (excitation wavelength of 493 nm and emission wavelength of 527 nm for DCF; excitation wavelength of 530 nm and emission wavelength of 590 nm for DHE and MitoSOX). The fluorescence values were corrected for protein content. Fatty acids were dissolved in ethanol and added to the medium for 24 h, and biotin was dissolved in DMSO. The final concentration of ethanol and DMSO was, respectively, 0.83% and 0.01% in each well. Antimycin A (Ant A; 200 μ M for 1 h) was used as a positive control.

Evaluation of reduced glutathione

The intracellular content of GSH was determined using monochlorobimane, a thiol-reactive probe. Following incubation for 30 minutes with 100 μ M monochlorobimane, the cells were washed twice with PBS and scraped into water. The fluorescence of monochlorobimane-stained cells was measured with a spectrofluorimeter (excitation wavelength of 380 nm and emission wavelength of 460 nm). L-Buthionine sulfoximine (BSO) (500 μ M) was used as a positive control.

Inner mitochondrial membrane potential quantification by flow cytometry

Treated cells were washed with PBS and incubated with 50 nM TMRE (Molecular Probes) in pre-warmed PBS for 30 minutes at 37°C. Cells were trypsinized, centrifuged at $1000 \times g$ for 5 minutes, and resuspended in pre-warmed PBS. All samples were captured by a FACSCanto™ flow cytometer, which recorded 20 000 cells for each condition and genotype tested. FCCP (200 μ M for 10 minutes) was used as a positive control. Histograms showing the inner mitochondrial membrane potential levels ($\Delta\psi_m$) were obtained after gating live cells. The data were analyzed with FlowJo Tree Star software.

Quantitative real-time PCR

Total RNA was extracted using the RNeasy Kit (Qiagen). Total DNA was extracted using the Gentra Puragene Tissue Kit (Qiagen). Gene expression and mtDNA levels were measured by TaqMan quantitative real-time PCR as previously described (49).

Mouse strains

The methods for generating and genotyping of *Abcd1*⁻ (*Abcd1*^{Tm1Kds}) and *Abcd2*^{-/-} (*Abcd2*^{Tm1Apuj}) mice were previously described (16,42,57,58). We used male mice of a pure C57BL/6J background. All methods employed in this study were in accordance with the ARRIVE guidelines, the Guide for the Care and Use of Laboratory Animals (Guide, 8th edition, 2011, NIH), European (2010/63/UE) and Spanish (RD 53/2013) legislation. Experimental protocols were approved by IDIBELL, IACUC (Institutional Animal Care and Use Committee) and regional authority (3546 DMAH). IDIBELL animal facility is accredited by The Association for Assessment and Accreditation of Laboratory Animal Care (AAALAC, Unit 1155). Animals were housed at 22°C on specific-pathogen-free conditions, in a 12-hour light/dark cycle, and *ad libitum* access to food and water. Cages contained three to four animals.

Mouse experiments

Two X-ALD mouse models were used in this study. The first model was the *Abcd1*⁻ mouse model, which exhibits *molecular* signs of pathology, including oxidative stress (19) and altered energy homeostasis (23); however, the first clinical signs of AMN (axonopathy and locomotor impairment) appear at 20 months (57,58). We characterized the molecular signs of adult AMN in these mice. The second model was a mouse with double gene knockout of both the *Abcd1* and *Abcd2* transporters (*Abcd1*⁻/*Abcd2*^{-/-}). Compared with the *Abcd1*⁻ mice, the *Abcd1*⁻/*Abcd2*^{-/-} mice display enhanced VLCFA accumulation in the spinal cord (57), higher levels of oxidative damage to proteins (21), and a more severe AMN-like pathology with an earlier onset at 12 months of age (16,57,58); therefore, this is the preferred model for assaying therapeutic strategies. Notably, no disease-causative role of *ABCD2* has been demonstrated; however, its absence

induces a partially overlapping fatty acid pattern compared with that of the *Abcd1*-dependent biochemical phenotype (20,37). We assessed the *clinical* signs of AMN in these *Abcd1*⁻/*Abcd2*^{-/-} mice.

Rationale for dose selection

The dose (60 mg/kg/day) was selected for use in mice because it is equivalent to the human therapeutic dose used in clinical trials (300 mg/day) (65).

Treatment duration

Treated animals had free access to AIN-76A + 0.06% high-dose pharmaceutical-grade biotin (MD1003), which was distributed twice a week so that a dose of 60 mg/kg/day was reached. To measure the biochemical alterations, animals were treated for 3.5 months and sacrificed at 13 months of age. The animals were randomly assigned to one of the following dietary groups: group I, WT mice that received normal AIN-76A chow (n = 18); group II, *Abcd1*⁻ mice that received normal AIN-76A chow (n = 18); or group III, *Abcd1*⁻ mice that received AIN-76A chow containing high-dose biotin (n = 18). To measure the clinical signs of the disease (locomotor dysfunction and axonal degeneration), 12-month-old animals were treated for 6 months. The animals were randomly assigned to one of the following dietary groups: group I, WT mice that received normal AIN-76A chow (n = 14); group II, *Abcd1*⁻/*Abcd2*^{-/-} mice that received normal AIN-76A chow (n = 15); or group III, *Abcd1*⁻/*Abcd2*^{-/-} mice that received AIN-76A chow containing high-dose biotin (n = 16).

Morbidity and mortality

Each animal was checked for mortality and morbidity once every 3 days during the acclimation period and treatment period, including on weekends and public holidays.

Body weight

The body weight of the animals was recorded twice a week during the study. No change was observed.

ATP levels

Mice were sacrificed by cervical dislocation, and the spinal cords were immediately frozen in liquid nitrogen and stored at -80°C. ATP was extracted and quantified as reported (23).

Motor function tests

Locomotor function was analyzed in WT and *Abcd1*⁻/*Abcd2*^{-/-} mice at 18 months of age under blinded conditions as previously described (32,33,39,48,49,57).

Treadmill test

The treadmill apparatus (Panlab, Barcelona, Spain) consisted of a belt (50 cm long and 20 cm wide) with variable speed capacity (5 to 150 cm/s) and slope (0–25°) enclosed in a

plexiglass chamber. An electrified grid was located to the rear of the belt, and footshocks (0.2 mA) were administered whenever the mice fell off the belt. The mice were placed on the top of the already moving belt facing away from the electrified grid and in the direction opposite to the movement of the belt. Thus, to avoid footshocks, the mice had to locomote forward. The latency to fall off the belt (time of shocks in seconds) and the number of shocks received were measured as previously described (32,33,39,48,49,57).

Horizontal bar cross test

The bar cross test was carried out using a wooden bar that was 100 cm in length and 2 cm in width (diameter). In each experimental session, the number of hind limb lateral slips and falls from the bar was counted in four consecutive trials (32,33,39,48,49,57).

Clasping

For behavioral testing, hindlimb clasping was assessed; WT and *Abcd1*⁻¹/*Abcd2*⁻¹ mice were suspended from their tails until they reached a vertical position but were allowed to grab the grill of the lid of the cage with their forelimbs, as adapted from Dumser *et al.* (10). Hindlimb reflexes were analyzed for 10 s in three consecutive trials separated by 5 minutes of rest.

Terminal euthanasia

The mice were anesthetized with Dolethal and perfused with 4% paraformaldehyde (PFA) solution.

Immunohistochemistry

Tissue preparation

Spinal cords were harvested from 18-month-old WT, *Abcd1*⁻¹/*Abcd2*⁻¹ and *Abcd1*⁻¹/*Abcd2*⁻¹ mice treated with high-dose biotin after perfusion with 4% PFA as previously described (16,32,33,39,48,49,57). The spinal cords were embedded in paraffin, and serial sections (5- μ m thick) were cut in the transverse or longitudinal (1-cm long) plane. The number of abnormal specific profiles in every 10 sections was counted for each stain. At least three sections of the spinal cord per animal per stain were analyzed.

Staining

The sections were stained with hematoxylin and eosin and Sudan black or processed for immunohistochemistry with a rabbit anti-Iba1 antibody (diluted 1/1000; Wako; 019-19741); a rabbit anti-glial fibrillary acidic protein (GFAP) antibody (diluted 1/300; Dako; Z-0334); a mouse anti-synaptophysin antibody (diluted 1/500; Leica; SYNAP-299-L-CE); a rabbit anti-amyloid precursor protein (APP) antibody (diluted 1/100; Serotec; AHP538); a mouse anti-cytochrome c antibody (diluted 1/100; BD Pharmigen; 55643); a mouse anti-non-phosphorylated neurofilament

H (SMI32) antibody (diluted 1/3000; Covance Inc.; SMI-32P); and a rabbit anti-malondialdehyde (MDA) antibody (diluted 1/1000; (16,39,48).

Microscopic examination

Photos were taken with an Olympus BX51 conventional light microscope coupled to an Olympus DP71 color digital camera. The software used to analyze the photos was Cell[^]B from Olympus. APP and synaptophysin were quantified as previously described (16,32,33,39,48,49,57). The number of GFAP⁺ cells (astrocytes) and Iba1⁺ positive cells (microglia) per mm² in the spinal cord ventral horn of WT, *Abcd1*⁻¹/*Abcd2*⁻¹ and high-dose biotin-treated *Abcd1*⁻¹/*Abcd2*⁻¹ mice (n = 5) was determined. The number of brown cells was counted with the Cell Counter ImageJ plugin. The data are presented as the average of the data obtained from two 20x images per animal for each group.

Lipidomic analysis

Lipidomic analyses of the mouse spinal cord were performed according to the modified Folch method (17). For each sample, the solvent volume was adjusted to the weight of the fresh tissue. In brief, 190 μ L of CHCl₃/MeOH 2:1 (v/v) and 10 μ L of internal standard mixture were added to 10 mg of spinal cord. The samples were vortexed for 60 s and then, sonicated for 30 s using a sonication probe. Extraction was performed after incubation for 2 h at 4°C and centrifugation at 15 000 \times g for 10 minutes at 4°C. The upper phase (aqueous phase), which contained ganglioside species and several lysophospholipids, was transferred and dried under a stream of nitrogen. The protein interphase was discarded, and the lower lipid-rich phase (organic phase) was pooled with the dried upper phase. The samples were then reconstituted in 200 μ L of CHCl₃/MeOH 2:1, vortexed for 30 s, and sonicated for 60 s, and these total lipid extracts (TLEs) were then stored at -80°C until analysis. Before analysis, the samples were diluted 100 times in MeOH/IPA/H₂O 65:35:5 (v/v/v) before injection.

The samples were separated on an HTC PAL system (CTC Analytics AG) coupled with a Transcend 1250 liquid chromatographic system (Thermo Fisher Scientific, Inc.) using a Kinetex C8 2.6 μ m 2.1 \times 150 mm column (Phenomenex, Sydney, NSW, Australia). High-resolution mass spectrometry using a Q-Exactive mass spectrometer (Thermo Fisher Scientific, Inc.) was performed as previously described (66). The relative amount of each lipid was semi-quantified as the area of its corresponding chromatographic peak.

LPC 26:0 absolute quantification

A total of 400 μ L of CHCl₃/MeOH 2:1 followed by 75 μ L of pure water was added to 100 μ L of total lipid extract. The samples were then centrifuged at 15 000 \times g for 10 minutes. The lower phase, which contained phospholipids, was transferred, dried under a stream of nitrogen, and reconstituted in 200 μ L of CHCl₃.

Glycerophospholipids were further purified by solid phase extraction (SPE) using Supelclean™ LC-NH2 cartridges (Sigma-Aldrich; ref: 57014) (3). The cartridges were first conditioned in 2 mL of hexane and loaded with 200 µL of samples reconstituted in CHCl₃. Four different washing steps with 2 mL of diethylether, 1.6 mL of CHCl₃/MeOH 23:1 (v/v), 1.8 mL of diisopropyl ether/acetic acid 98:4 (v/v) and 2 mL of acetone/MeOH 9:1.2 (v/v) were then performed. Finally, 2 mL of CHCl₃/MeOH 2:1 (v/v) was added, and the corresponding eluent was dried under a stream of nitrogen and reconstituted in MeOH/IPA/H₂O 65:35:5 (v/v/v) before injection. LC-HRMS experiments were performed in positive ionization mode using the same system as that used for the lipidomic method described above.

Absolute quantification of LPC 26:0 in the mouse spinal cord was performed using the standard addition method. A calibration curve was obtained by adding increasing quantities (0, 10, 40, and 100 ng/mg of tissue in triplicate) of pure LPC 26:0 standard (Avanti Polar Lipids; ref: 855810P) to pooled of mouse spinal cord tissues. The calibration curves were analyzed in duplicate, that is, at the beginning of the analytical batch containing the mouse spinal cord samples and at the end. The endogenous concentration of LPC 26:0 in the mouse spinal cord samples was then evaluated by measuring the area under the curve of the protonated [M + H]⁺ ion and calculated according to calibration curves and the standard addition procedure.

Triglyceride levels

Spinal cords (~10 mg) were homogenized in 100 mL of solution containing 5% NP-40 in water, and then, the samples were slowly heated to 80–100°C in a water bath for 2–5 minutes or until the NP-40 became cloudy and cooled to room temperature. The heating was repeated one more time to solubilize all TAG. The samples were centrifuged for 2 minutes (top speed in a microcentrifuge) to remove any insoluble material. The TAG levels were quantified with a triglyceride quantification kit according to the manufacturer's protocol (BioVision, ref: K622-100). The absorbance was measured at 570 nm. All assays were performed in duplicate.

Oil red O staining and quantification of lipid droplets (LDs)

Spinal cords were harvested from mice after perfusion with 4% PFA and embedded in Tissue-Tek® OCT (optimum cutting temperature). Serial sections (12-µm thick) were then cut in the transverse plane at -20°C using a cryostat.

Oil red O (ORO) staining was used to measure lipid accumulation. A stock ORO solution was generated by diluting 0.35 g ORO (Sigma-Aldrich; ref: 000625) in 100 mL of isopropanol. To prepare the staining solution, the ORO stock solution was filtered, mixed with dH₂O at a 6:4 ratio and then, filtered using a 0.2-micron syringe filter. Spinal cord sections were incubated in ORO staining solution for 15 minutes at room temperature, washed in dH₂O and

immediately covered with Fluoromount™ Aqueous mounting medium (Sigma-Aldrich; ref: F4680). Brightfield microscopy images were acquired using a Nikon Eclipse 80I microscope equipped with a Nikon DS-R1i camera operated by NIS-Elements BR software. An average of six images per animal was acquired.

To assess LDs, images were edited using Adobe Photoshop CS5 software. The area corresponding to the neuronal soma was selected and saved as the region of interest (an average of 25 selections/animal). Then, the total area of LDs accumulated in each neuronal soma was analyzed using ImageJ software. For each measurement, the data were normalized to the tissue area to exclude unwanted biases and to determine the ratio of LD area to tissue area.

Immunoblotting

Mice spinal cords were homogenized in RIPA buffer (50 mM Tris-HCl, pH 8, 12 mM deoxycholic acid, 150 mM NaCl and 1% NP40) supplemented with Complete Protease Inhibitor Cocktail (Roche) and PhosSTOP EASYpack Phosphatase Inhibitor Cocktail (Roche), sonicated for 2 minutes in 10-s intervals and centrifuged for 10 minutes at maximum speed. The protein concentration was determined using a BCA protein assay kit (Thermo Fisher Scientific, Inc.). The samples were heated for 10 minutes at 70°C after adding 4X NuPAGE LDS Sample Buffer (Invitrogen, Thermo Fisher Scientific, Inc.). A total of 30–60 µg of protein was loaded onto a 10% Novex NuPAGE SDS-PAGE gel system (Invitrogen, Thermo Fisher Scientific, Inc.) and run for 60–90 minutes at 120 V in NuPAGE MOPS SDS Running Buffer (Invitrogen, Thermo Fisher Scientific, Inc.) supplemented with 5 mM sodium bisulfite (Sigma-Aldrich; ref: 243973). SeeBlue Plus2 Pre-Stained (Invitrogen, Thermo Fisher Scientific Inc.) was used as a ladder. Immunoblotting was carried out with the avidin–biotin peroxidase method, as reported earlier (59).

Antibodies

The following antibodies were used for Western blotting: phospho-mTOR (diluted 1/1000; Cell Signaling [Beverly, MA, USA]; 5536S); γ-tubulin (diluted 1/10000; Sigma-Aldrich); and horseradish peroxidase-conjugated goat anti-rabbit IgG (diluted 1/10000; Invitrogen; 81-6520) and horseradish peroxidase-conjugated goat anti-mouse IgG (diluted 1/10000; Invitrogen; 81-6120) secondary antibodies.

Quantification and Statistical analysis

Statistical analysis was carried out in GraphPad Prism6. The values are expressed as the mean ± standard deviation (SD). Significant differences between comparing two groups were determined by two-tailed unpaired Student's *t*-test (**P* < 0.05, ***P* < 0.01, ****P* < 0.001). When comparing more than two groups, significant differences were determined by one-way ANOVA followed by Fisher *post hoc* or Sidak *post hoc* test (**P* < 0.05, ***P* < 0.01, ****P* < 0.001).

RESULTS

Biotin counteracts redox imbalance in human fibroblasts

We first investigated whether biotin is efficient in addressing a core problem of X-ALD, the increased ROS production generated by an excess of hexacosanoic acid C26:0. We previously showed that excess C26:0 triggers mitochondrial reactive oxygen species (ROS) production by electron transport chain (ETC) complexes while depleting the reduced glutathione (GSH) pool and decreasing membrane potential ($\Delta\Psi_m$) (41).

At doses of 0.5 to 5 μM , biotin successfully prevented ROS production induced by excess 26:0, as visualized using the dichlorodihydrofluorescein diacetate (DCF) and dihydroethidium (DHE) fluorescent probes, to assess total intracellular H_2O_2 and superoxide anion, respectively (Figure 1A,B). The same doses of biotin were efficacious at preventing mitochondrial ROS production assessed by MitoSOX (Figure 1C). Moreover, biotin treatment also reduced the mitochondrial ROS produced by the inhibitor of complex III antimycin, indicating that the precise mechanism of protection against ROS may not be restricted to excess fatty acids (Supporting Figure S1A). The mechanism might be indirect, as incubation with biotin for a short period of time (1 h) was not sufficient to abolish the increase in ROS levels (Supporting Figure S1B).

Further, incubation for 24 h with biotin at 0.5 to 5 μM prevented GSH reduction in fibroblasts challenged with C26:0 excess, in both X-ALD and control fibroblasts (Figure 1D). In contrast, incubation of 1 h was insufficient (Supporting Figure S1C).

Biotin did not exert any effects on the mitochondrial membrane potential decrease provoked by excess C26:0 (Supporting Figure S1D). We next explored whether biotin would influence transcription of genes governing GSH biosynthesis. As earlier reported, incubation with C26:0 was not inducing NRF2-target genes (*GCLC*, *GCLM*, and *GSRI*) in X-ALD fibroblasts, caused by a blunted response of the NRF-2 pathway driven by dysregulated AKT/GSK3 β signaling (76). Upon biotin treatment, the expression of the first rate-limiting enzyme in GSH biosynthesis, glutamate-cysteine ligase (GCL), was increased. This was true for both subunits, namely, the catalytic subunit (*GCLC*) and the modifier subunit (*GCLM*). Additionally, the expression of glutathione reductase (*GSRI*) was increased in X-ALD fibroblasts only (Figure 1E). These results suggest that biotin reactivates the NRF2 pathway in X-ALD fibroblasts.

High-dose biotin rescues mitochondrial biogenesis and energy failure in *Abcd1*⁻ mice

Based on these positive results, we felt prompted to treat *Abcd1*⁻ mice (58) with a dose of biotin equivalent to the dose administered to MS patients (70); the mice were fed 60 mg/kg/day biotin for 3.5 months, from the age of 9.5 months to 13 months.

We then evaluated the following parameters of altered pathways in the spinal cord in X-ALD: (i) target genes of NRF2, a transcription factor that governs the endogenous antioxidant response and shows a blunted response in X-ALD (59); (ii) mtDNA copy number and the master regulators of mitochondrial biogenesis, which are also reduced in X-ALD (18,48); and (iii) ATP levels, which are reduced in X-ALD (41) (Figure 2). Treatment with high-dose biotin normalized the expression of NRF2 targets (*Hmox1*, *Nqo1*, *Gsta3*, and *Gclc*) (Figure 2A). In agreement with previous data on fibroblasts, the enzymes GSTA3 and GCLC may have directly contributed to preserving redox potential (Figure 1E). Next, we quantified mitochondrial biogenesis based on the mitochondrial DNA/nuclear DNA (mtDNA/nDNA) ratio (Figure 2B) and the induction of PGC-1 α and TFAM mRNA in *Abcd1*⁻ mice (Figure 2C), which were normalized by the treatment. We also observed that high-dose biotin reversed the drop in ATP levels (Figure 2D).

High-dose biotin prevents locomotor deficits in *Abcd1*⁻/*Abcd2*⁻ mice

Our next step was to evaluate the preclinical efficacy of high-dose biotin in alleviating axonopathy and the associated locomotor dysfunction exhibited by the X-ALD mouse model (57). We used mice with complete loss of *Abcd1* and its closest homolog, *Abcd2* (*Abcd1*⁻/*Abcd2*⁻), as they represent an improved model of AMN-like phenotypes, showing an onset of axonal degeneration at approximately 12 months of age, which is amenable to therapeutic testing. The *Abcd1*⁻/*Abcd2*⁻ mice were treated for 6 months with high-dose biotin and then, challenged with three locomotor tests. In the treadmill test, the total number and duration of shocks received by the *Abcd1*⁻/*Abcd2*⁻ mice were higher than those received by the WT mice under conditions of high speed and high slope, indicating that the mutants reached exhaustion earlier than WT. Remarkably, the animals fed high-dose biotin performed the same as control mice (Figure 3A). In the bar cross experiment, while the double knockout mice slipped off the bar more frequently and needed a longer time to reach the opposite platform, the *Abcd1*⁻/*Abcd2*⁻ + high-dose biotin mice performed the task the same as their WT littermates and were statistically similar (Figure 3B). In the clasping test, the best score for each animal was used for statistical analysis. *Abcd1*⁻/*Abcd2*⁻ mice presented a lower score than WT mice, demonstrating a locomotor deficit. In this test, high-dose biotin treatment also significantly improved this score (Figure 3C). In conclusion, high-dose biotin rescued locomotor deficits in *Abcd1*⁻/*Abcd2*⁻ mice.

High-dose biotin prevents axonal damage in *Abcd1*⁻/*Abcd2*⁻ mice

We then evaluated the correlation between the observed improvements in locomotor dysfunction and arrested axonal degeneration. *Abcd1*⁻/*Abcd2*⁻ mice presented an overt neuropathological phenotype characterized by the following: (i)

microgliosis (Figure 3D,E, Supporting Figure S2A) and astrogliosis (Figure 3G-H, Supporting Figure S2B), as detected by Iba1 and GFAP staining, respectively; (ii) axonal damage suggested by the accumulation of synaptophysin (Figure 3J,K, Supporting Figure S2C) and amyloid precursor protein (APP) in axonal swellings (Figure 3M,N,

Supporting Figure S2C); (iii) scattered myelin debris around the axonal ovoids, probably secondary to axonal degeneration, as detected by Sudan black (Figure 3P,Q); (iv) reduced SMI-32 staining in motor neurons, an indicator of disturbed neurofilament status (Figure 3S,T); (v) a diminished amount of cytochrome c (Figure 3V,W), which is a marker of

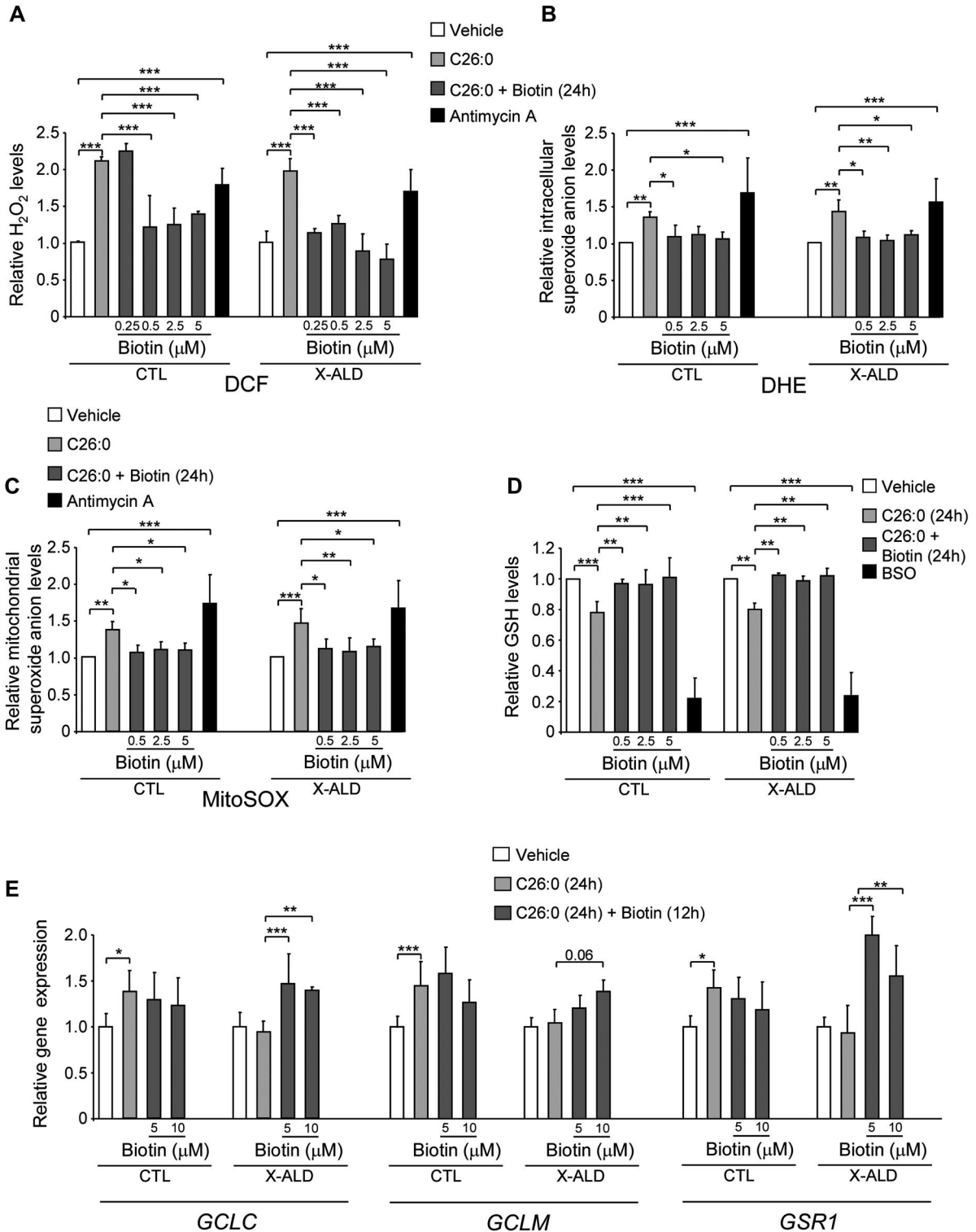


Figure 1. Biotin prevents ROS production of mitochondrial origin and normalizes GSH levels and GSH biosynthesis genes in X-ALD fibroblasts.

A. Intracellular H₂O₂ (DCF probe) was quantified in control (CTL) (n = 3) and X-ALD human fibroblasts (n = 3) after 24 h of treatment with vehicle (as a control), C26:0 or C26:0 with biotin (0.25, 0.5, 2.5 or 5 μM). For this and the experiments in **B** and **C**, C26:0 was used at 50 μM. Antimycin A (200 μM for 1 h) was used as a positive control. **B.** Intracellular superoxide anions (DHE probe) were quantified in CTL (n = 4 to 5 by condition) and X-ALD human fibroblasts (n = 3 to 5 by condition) after 24 h of treatment with vehicle (as a control), C26:0 or C26:0 with biotin (0.5, 2.5, or 5 μM). **C.** Mitochondrial superoxide anions (MitoSOX probe) was quantified in CTL (n = 4 to 5 by condition) and X-ALD human fibroblasts (n = 3 to 5 by condition) after 24 h of treatment with vehicle (as a control), C26:0 or C26:0 with biotin (0.5, 2.5 or 5 μM). **D.** Relative

GSH levels were quantified in CTL (n = 4) and X-ALD human fibroblasts (n = 4) after 24 h of treatment with vehicle (as a control), C26:0 or C26:0 with biotin (0.5, 2.5, or 5 μM). For this and the subsequent experiments, C26:0 was used at 50 μM. Buthionine sulfoximine (BSO; 500 μM for 24 h) was used as a positive control, since it inhibits the rate-limiting enzyme on GSH biosynthesis. **E.** Relative *GCLC*, *GCLM*, and *GSR1* gene expression was measured in CTL (n = 4 to 5 by condition) and X-ALD human fibroblasts (n = 3 to 5 by condition) after 24 h of treatment with vehicle (as a control) or C26:0. Biotin (5 or 10 μM) was added 12 h after C26:0 treatment for 12 h. Gene expression normalized to *RPLP0*. Quantification presented as the fold change relative to vehicle-treated fibroblasts. The experiments were done in triplicates. The values are expressed as the mean ± SD [one-way ANOVA followed by Fisher *post hoc* test (**P* < 0.05, ***P* < 0.01 and ****P* < 0.001)].

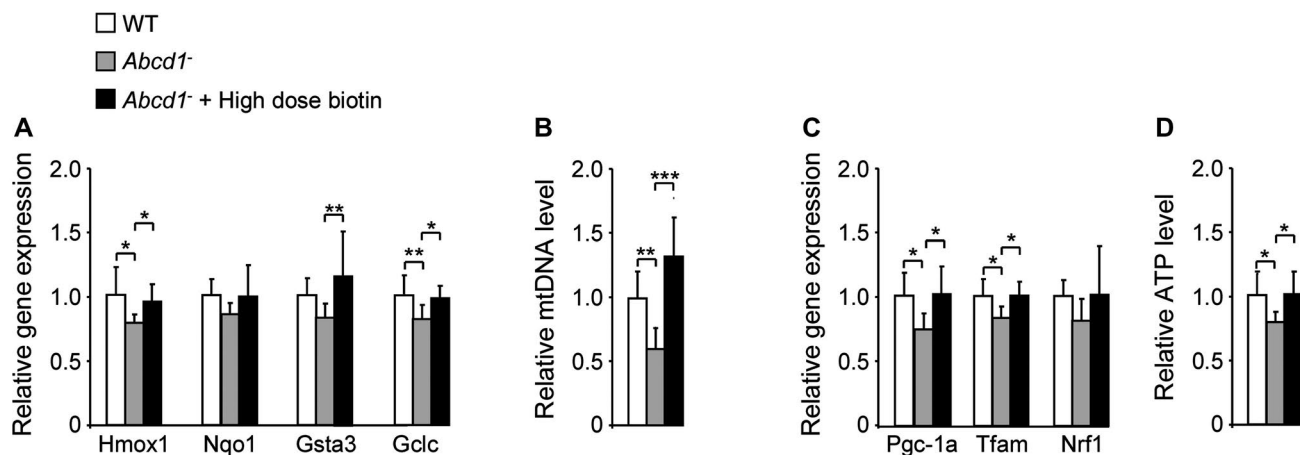


Figure 2. High-dose biotin rescues mitochondrial biogenesis and prevents energy failure in the *Abcd1*⁻ mouse spinal cord. Experiments were performed on the spinal cord of 13-month-old WT, *Abcd1*⁻ and *Abcd1*⁻ mice treated with high-dose biotin (*Abcd1*⁻ + high-dose biotin) (A-D). **A.** Relative gene expression of NRF2 target genes (*Hmox1*, *Nqo1*, *Gsta3*, and *Gclc*) was analyzed by quantitative RT-PCR in WT, *Abcd1*⁻ and *Abcd1*⁻ + high-dose biotin mice (n = 5 to 11 per genotype and condition). **B.** mtDNA content was analyzed by quantitative RT-PCR and

is expressed as the ratio of mtDNA to nuclear DNA (mtDNA/nDNA) (n = 6 to 7 per genotype and condition). **C.** Relative gene expression of *Pgc-1a*, *Tfam*, and *Nrf1* was analyzed by quantitative RT-PCR (n = 6 to 11 per genotype and condition). **D.** ATP levels (n = 7 to 8 per genotype and condition). Gene expression normalized to mouse *Rplp0* and presented as the fold change relative to that in WT mice. The values are expressed as the mean ± SD [one-way ANOVA followed by Fisher *post hoc* test (**P* < 0.05, ***P* < 0.01 and ****P* < 0.001)].

mitochondrial depletion; and (vi) increased staining for malondialdehyde (MDA), a marker of lipoxidation (Figure 3Y,Z) (16,32,33,39,48,49,57,59). We found that treatment with high-dose biotin in *Abcd1*⁻/*Abcd2*^{-/-} mice efficaciously suppressed microgliosis (Figure 3D-F, Supporting Figure S2A) and astrogliosis (Figure 3G-I, Supporting Figure S2B). Moreover, synaptophysin (Figure 3J-L, Supporting Figure S2C) and APP accumulation (Figure 3M-O, Supporting Figure S2C) and myelin debris were prevented (Figure 3P-R), demonstrating that high-dose biotin halted axonal damage in this X-ALD mouse model. It is worth noting that the current experimental setting does not discriminate between disturbed axonal trafficking or axonal transection. Moreover, the treated cohort presented healthier motor neurons (Figure 3S-U), normalized mitochondrial content (Figure 3V-X) and reduced signs of lipoperoxidation (Figure 3Y-A'), confirming the role of high-dose biotin in

maintaining redox and metabolic homeostasis in the nervous system in this model.

Increased triglyceride levels in the spinal cord of *Abcd1*⁻ mice and restoration by high-dose biotin

Knowing the effects of biotin on fatty acid synthesis as a cofactor of the enzymes ACC1 and ACC2, we generated an untargeted lipidomic profile of the spinal cord of 13-month-old WT, *Abcd1*⁻ and *Abcd1*⁻ + high-dose biotin mice to evaluate the possible global effects of the treatment using liquid chromatography coupled to a high-resolution mass spectrometer (LC-HRMS). We identified and annotated 747 unique lipid species belonging to different lipid classes: free fatty acids (FA), fatty acylcarnitines (FA-Carn), cholesteryl esters (Chol. Ester), diacylglycerols (DG), triacylglycerols (TAG), lyso-glycerophosphocholines (LPC),

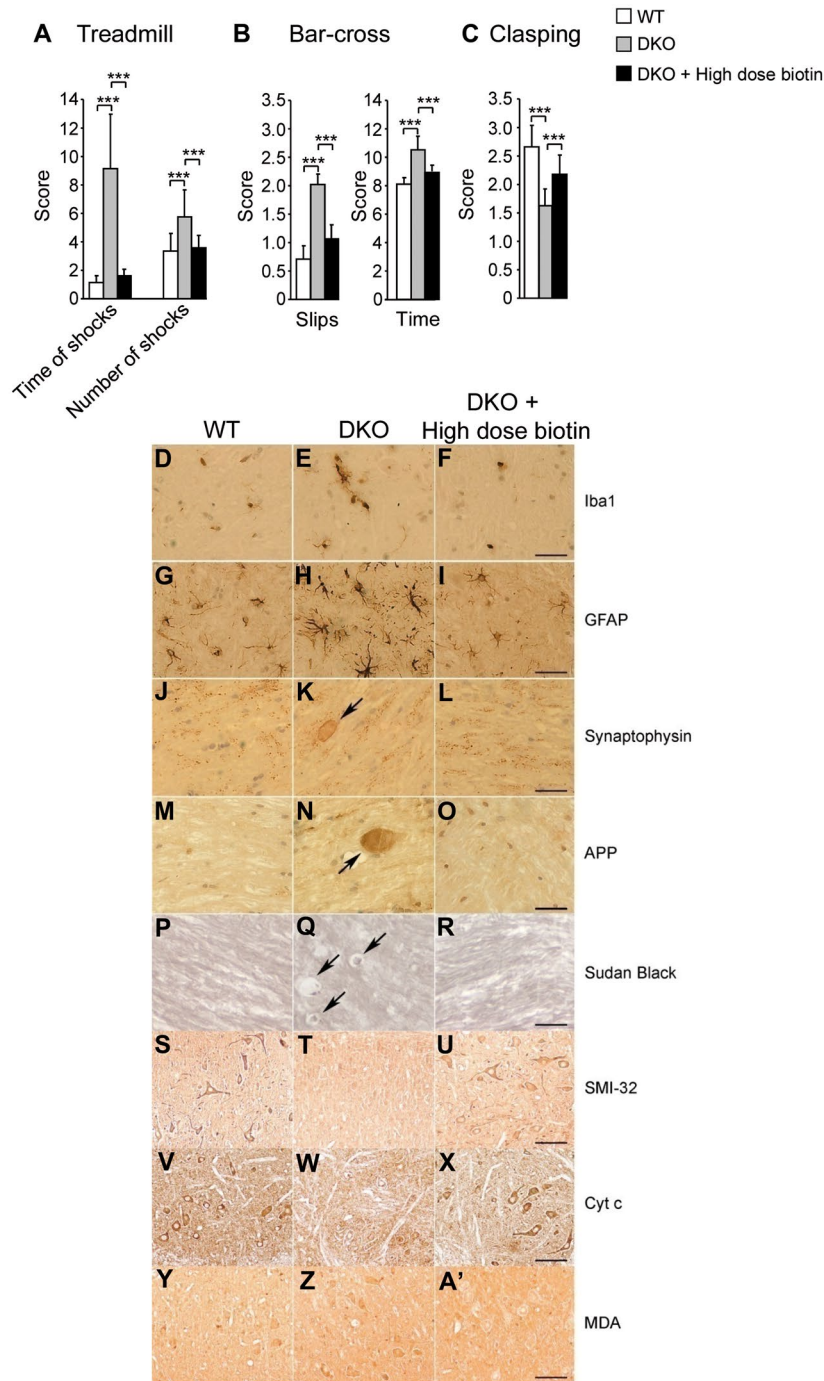


Figure 3. High-dose biotin halts axonal degeneration and locomotor dysfunction in *Abcd1*^{-/-}/*Abcd2*^{-/-} mice. **A.** The treadmill test and **(B)** bar cross test, and **(C)** clasping test were carried out in 18-month-old WT, DKO and DKO + high-dose biotin mice (n = 13 to 16 by genotype and condition). **A.** The latency to fall off the belt (time of shocks) and the number of shocks received were computed after 5 minutes. **B.** The time required to cross the bar and the number of slips were quantified. **C.** The best score for each animal was used for analysis (10). **D-A'.** Immunohistochemical analysis of axonal pathology was performed in 18-month-old WT, *Abcd1*^{-/-}/*Abcd2*^{-/-} (DKO) and *Abcd1*^{-/-}/*Abcd2*^{-/-} plus high-dose biotin (DKO + high-

dose biotin) mice (n = 6/genotype and condition). Spinal cord immunohistological sections were processed for **(D-F)** Iba1, **(G-I)** GFAP, **(J-L)** synaptophysin, **(M-O)** APP, **(P-R)** Sudan black, **(S-U)** SMI-32, **(V-X)** Cytochrome c, and **(Y-A')** MDA. Representative images **(D, G, J, M, P, S, V, and Y)** for WT, **(E, H, K, N, Q, T, W, and Z)** DKO **(F, I, L, O, R, U, X, and A')** and DKO + high-dose biotin mice are shown. Scale bar = 25 μm. The values are expressed as the mean ± SD [one-way ANOVA followed by Fisher *post hoc* test (**P* < 0.05, ***P* < 0.01 and ****P* < 0.001)].

lyso-glycerophosphoethanolamines (LPE), lyso-glycerophosphoinositols (LPI), lyso-glycerophosphoserines (LPS), glycerophosphocholines (PC), glycerophosphoethanolamines (PE), glycerophosphoglycerols (PG), glycerophosphoinositols (PI), glycerophosphoserines (PS), ceramides (Cer),

hexosylceramides (HexCer), dihexosylceramides (DiHexCer), sphingomyelins (SM), sulfoglycosphingolipids (Su), and gangliosides (GSL). The only class significantly altered in *Abcd1*^{-/-} mice was TAG (Figure 4A). This is in line with the increased TAG detected in the peripheral blood mononuclear cells

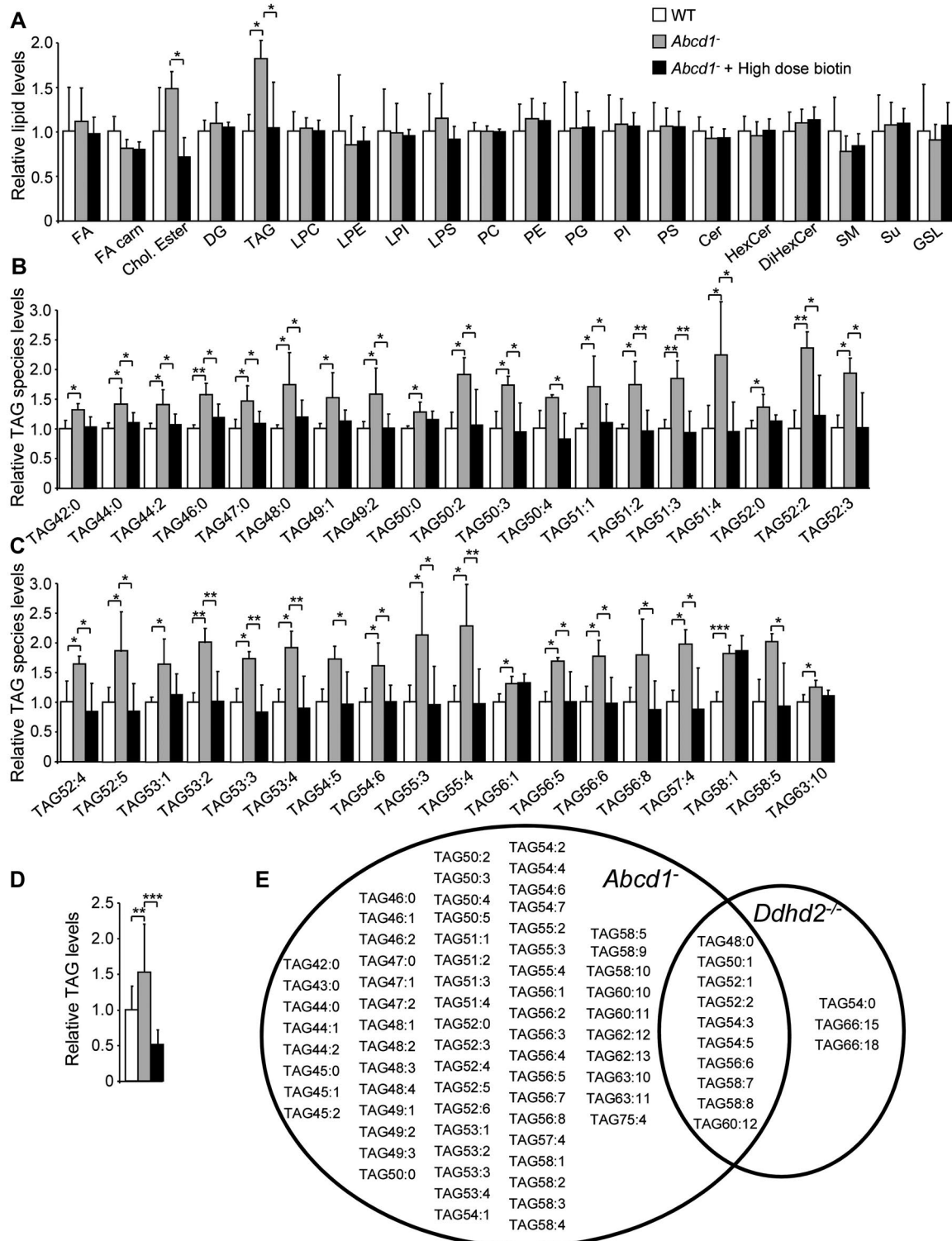


Figure 4. High-dose biotin rescues TAG levels in *Abcd1*⁻ mice spinal cords. **A.** Lipidomic experiments were performed in the spinal cord of 13-month-old WT (n = 5), *Abcd1*⁻ (n = 3) and *Abcd1*⁻ + high-dose biotin (n = 6) mice, and all lipid species annotated are represented (FA = free fatty acids, FA-Carn = fatty acyl carnitines, Chol. Ester = cholesterol esters, DG = diacylglycerols, TAG = triacylglycerols, LPC = lyso-glycerophosphocholines, LPE = lyso-glycerophosphoethanolamines, LPI = lyso-glycerophosphoinositols, LPS = lyso-glycerophosphoserines, PC = glycerophosphocholines, PE = glycerophosphoethanolamines, PG = glycerophosphoglycerols, PI = glycerophosphoinositols, PS = glycerophosphoserines, Cer = ceramides, HexCer = hexosylceramides, DiHexCer = dihexosylceramides,

SM = sphingomyelins, Su = sulfoglycosphingolipids and GSL = gangliosides). **B** and **C.** Species of TAG annotated by lipidomic analysis which are significantly altered in *Abcd1*⁻ or *Abcd1*⁻ + high-dose biotin mice. They are represented in function of the numbers of both total carbons and double bonds. Relative lipid levels were normalized to WT mice. **D.** TAG levels in the spinal cord of 13-month-old WT (n = 5-6 per genotype and condition). **E.** A Venn diagram depicting TAG species that have been annotated by untargeted lipidomic experiments in the spinal cord of *Abcd1*⁻ mice and *Ddhd2*^{-/-} mice (25). The values are expressed as the mean ± [for **A**, **B**, **C** and **E**: one-way followed by Sidak *post hoc* test (**P* < 0.05, ***P* < 0.01 and ****P* < 0.001); for **D**: one-way followed by Fisher *post hoc* test (**P* < 0.05, ***P* < 0.01 and ****P* < 0.001)].

(PBMC) of a cohort of patients with AMN (62) and more recently in the fibroblasts of cALD patients (34). Seventy-nine different TAG species, ranging from a TAG with 42 carbons and 0 double bonds (TAG 42:0) to a TAG with 75 carbons and four double bonds (TAG 75:4), were annotated. Of these, 61 species of TAG accumulated over 1.3-fold, with 33 of these 61 species reaching statistical significance. Strikingly, the levels of all of these different species of TAG were normalized by treatment with high-dose biotin (Figure 4B-D, Supporting Figure S3A,B).

We noticed that a similar untargeted lipidomic study was undertaken in brain of adult mice with knockout of the TAG hydrolase *DDHD2*, the main enzyme that degrades TAGs in nervous tissue (25). The brains of *Ddhd2*^{-/-} mice accumulated 13 species of TAGs ranging from TAG 48:0 to TAG 66:18, and 11 of these species were significantly increased (2.07- to 5.45-fold). We observed that a high number of species identified in the previous study were also identified in the *Abcd1*⁻ mice based on our lipidomic data, with 1.08- to 2.33-fold accumulation in the *Abcd1*⁻ mice (Figure 4E).

We also detected a tendency for cholesterol esters (CE) to be increased in the *Abcd1*⁻ mice, albeit nonsignificantly (Figure 4A). Both, CE and TAG alterations were normalized by high-dose biotin (Figure 4A).

However, when we specifically investigated the effects of high-dose biotin on lysophosphatidylcholine C26:0, a phospholipid species widely used as a pathognomonic marker for the diagnosis of X-ALD (72), we found no amelioration of the profile (Supporting Figure S3C).

Increased size and number of LDs accumulated in motor neurons of *Abcd1*⁻/*Abcd2*^{-/-} mice and restoration by high-dose biotin

TAG and sterol esters are mostly stored in cells as LDs, which act as reservoirs to be used in case of insufficient energy sources (73). We, therefore, decided to visualize possible LD accumulation at the cellular level in the spinal cord by performing classical ORO staining on spinal cord sections. This histological stain is specific for neutral lipids and does not stain the polarized phospholipids of the cell membrane (45), enabling clear visualization of LDs by bright-field microscopy (46). ORO staining revealed an increase in LDs in neuronal somas in the ventral horn of *Abcd1*⁻ and *Abcd1*⁻/*Abcd2*^{-/-} mice, with no differential staining in glial

cells. Quantitative analysis using ImageJ software to assess the area occupied by LDs relative to the area of the motoneuronal soma indicated an augmented surface in mutant animals, in *Abcd1*⁻ mice at 12 months of age (Supporting Figure S4), and in *Abcd1*⁻/*Abcd2*^{-/-} mice at 18 months of age (Figure 5A,B,D,E). This accumulation of LDs was normalized in *Abcd1*⁻/*Abcd2*^{-/-} mice after 6 months of treatment with high-dose biotin (Figure 5A-G).

Transcriptional dysregulation of lipid homeostasis in the *Abcd1*⁻ spinal cord and restoration by high-dose biotin

We set out to gain insight into the origin of the increased TAG levels in X-ALD and the mechanisms of normalization by high-dose biotin to assess whether the effects were caused by an increase in biosynthesis or a decrease in the degradation of TAG. We thus measured a set of genes involved in the main lipid homeostatic pathways: (i) the synthesis of fatty acids (Figure 6A) and (ii) the degradation of fatty acids via β -oxidation (FAO) in mitochondria and peroxisomes (Figure 6B). At baseline, we observed an induction of lipogenesis in the *Abcd1*⁻ spinal cord, which characterized by an upregulation of sterol regulatory element binding protein 1c (SREBP-1c) and its targets *Fas*, *Scd1*, *Scd2*, *Scd3*, *Acs11*, *Acs13*, *Acs14*, *Acs15*, and *Acs16* (Figure 6A). SREBP-1c belongs to the basic-helix-loop-helix-leucine zipper (bHLH-LZ) family of transcription factors and controls lipogenesis (67). Moreover, the FAO genes, in particular *Cpt2*, *Acadm*, *Acadl*, *Acadvl*, *Echs1*, *Hadha*, *Acaa2*, *Acox1*, and *Ehhadh*, showed decreased expression (Figure 6B).

High-dose biotin exerted a striking effect in modulating the transcription of core lipid homeostatic pathways; the treatment repressed SREBP-1c and thus reduced the lipogenesis gene expression (Figure 6A) while inducing fatty acid beta-oxidation by normalizing the levels of enzymes in both peroxisomes and mitochondria (Figure 6B), which may explain the correction of total TAG levels in treated X-ALD mice (Figure 4A-D). Intrigued by this concerted dysregulation of both anabolic and catabolic lipid pathways, we investigated mTOR, the mammalian target of rapamycin and nutrient sensor. This kinase is activated by anabolic signals and governs global lipid metabolism, including SREBP-1c, in response to nutrition (56). When induced, mTOR facilitates the accumulation of TAGs by promoting lipogenesis while inhibiting the beta-oxidation of fatty acids

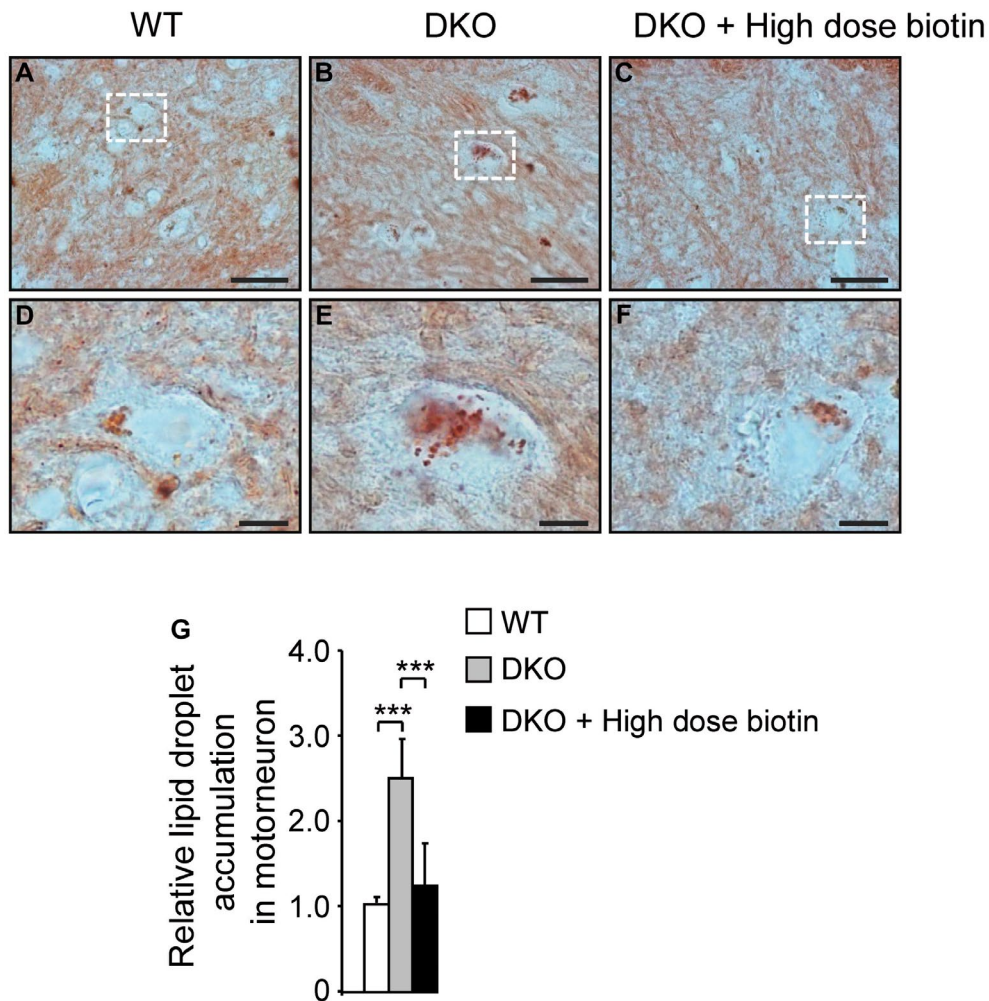


Figure 5. High-dose biotin normalizes excess lipid droplet accumulation in motorneurons in *Abcd1*⁻¹/*Abcd2*⁻¹ mice. A-G. Histological analysis performed in 18-month-old (A and D) WT, (B and E) *Abcd1*⁻¹/*Abcd2*⁻¹ (DKO) and (C and F) *Abcd1*⁻¹/*Abcd2*⁻¹ plus high-dose biotin (DKO + high-dose biotin) mice. Spinal cord histological sections were processed for oil red O (ORO) staining (n = 4 to 5 per genotype and condition). G.

Quantification of lipid droplet accumulation in spinal cord histological sections from 18-month-old WT, DKO, and DKO + high-dose biotin mice by ImageJ. Scale bar = 25 μm (A-C); scale bar = 5 μm (D-F). The values are expressed as the mean ± SD (one-way ANOVA followed by Fisher *post hoc* test (**P* < 0.05, ***P* < 0.01 and ****P* < 0.001).

and lipolysis (4). Here, we detected increased levels of P-mTOR, the active form of mTOR. Importantly, treatment with high-dose biotin restored the levels of activated mTOR (Figure 6C).

In summary, in X-ALD, high-dose biotin is efficacious in correcting the molecular drivers of disrupted lipid homeostasis in the nervous system, which may eventually lead to halted axonal demise (Figure 7).

DISCUSSION

This study provides novel insights into the mode of action of high-dose biotin on redox homeostasis and energy metabolism at multiple levels. Our data shows that treatment with high-dose biotin halts axonal damage and locomotor dysfunction while preventing a decrease in ATP, mitochondrial

DNA depletion, and oxidative damage in the spinal cord of X-ALD mice. Moreover, it unveils a general dysregulation of lipid metabolism as a novel culprit that drives axonal demise in an X-ALD model, also restored upon high-dose biotin treatment. This has direct implications for X-ALD as well as MS and other metabolic axonopathies since mitochondrial dysfunction has been reported in the chronically demyelinated axons of MS patients (11) and in acute MS lesions (43).

Biotin prevented total ROS and mitochondrial ROS production *in vitro*. To the best of our knowledge, this is the first time that biotin or high-dose biotin was shown to induce the endogenous antioxidant response of NRF-2. A different mechanism of action of the antioxidant role of biotin dependent on the biotinylation of HSP60 at its lysines,

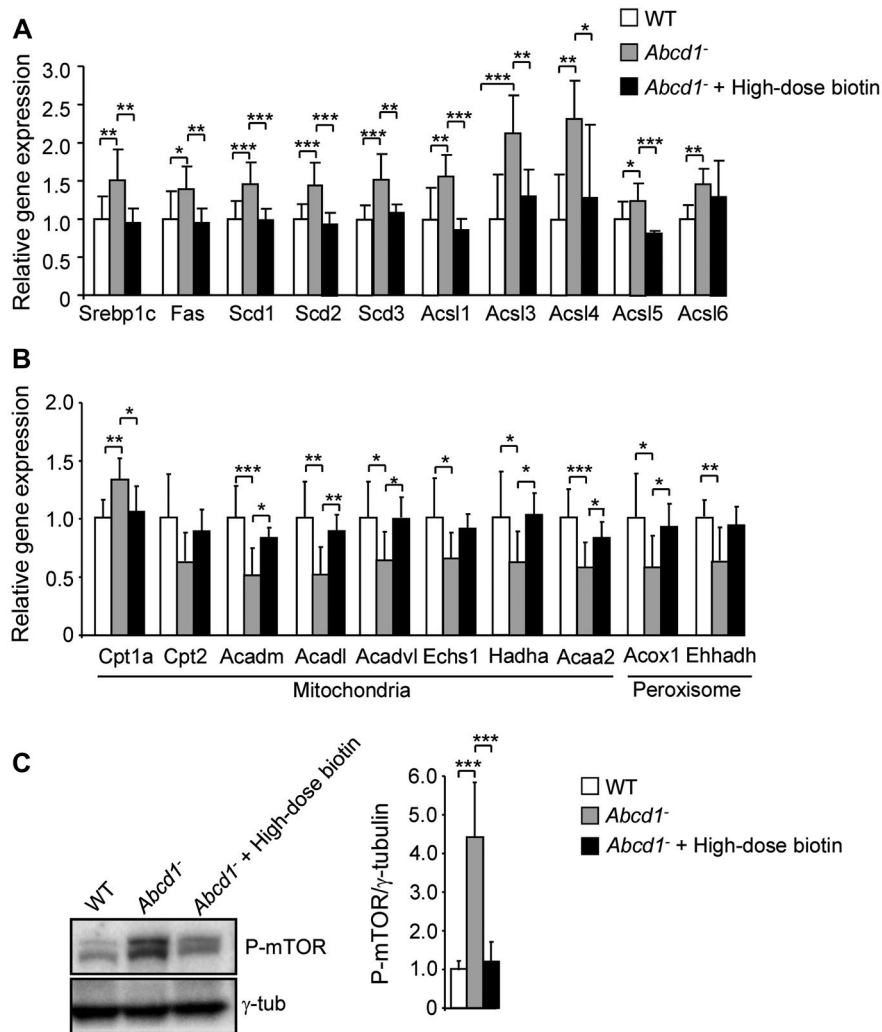


Figure 6. High-dose biotin restores lipid homeostasis through SREBP-1c/mTOR in *Abcd1*⁻ mice spinal cords. Experiments were performed in the spinal cord of 13-month-old WT, *Abcd1*⁻ and *Abcd1*⁻ + high-dose biotin mice. Relative gene expression of enzymes involved in (A) lipogenesis (*Srebp1c*, *Fas*, *Scd1*, *Scd2*, *Scd3*, *Acs1*, *Acs3*, *Acs4*, *Acs5*, and *Acs6*) in WT, *Abcd1*⁻ and *Abcd1*⁻ + high-dose biotin mice (n = 7 to 11 per genotype and condition) and (B) mitochondrial and peroxisomal fatty acid β-oxidation (*Cpt1a*, *Cpt2*, *Acadm*, *Acadl*, *Acadvl*, *Echs1*, *Hadha*,

Acaa2, *Acox1*, and *Ehhadh*) in WT, *Abcd1*⁻ and *Abcd1*⁻ + high-dose biotin mice. Gene expression was normalized to mouse *Rplp0* and is presented as the fold change to relative to that in WT mice (n = 5 to 7 per genotype and condition). C. P-mTOR protein level (n = 4 per genotype and condition). Protein content was normalized relative to γ-tubulin and quantification depicted as fold change to WT mice. The values are expressed as the mean ± SD [one-way ANOVA followed by Fisher *post hoc* test (**P* < 0.05, ***P* < 0.01 and ****P* < 0.001)].

a mitochondrial heat-shock protein that ameliorates oxidative stress in cells, was previously reported (36).

Biotin is a cofactor for five carboxylases. ACC1 is the cytosolic rate-limiting carboxylase of the synthesis of malonyl-CoA, the two-carbon building block for fatty acid synthesis and subsequent lipogenesis (9,68). Malonyl-CoA is also a well-known inhibitor of carnitine palmitoyltransferase I (CPT1) (44), the first enzyme required in the process of mitochondrial FAO. CPT1 inhibition is mainly caused by ACC2-derived malonyl-CoA, as ACC2 (1) is bound to the mitochondrial outer membrane where CPT1 acts. Surprisingly, treating *Abcd1*⁻ mice with high-dose biotin upregulated the FAO pathway, and repressed the lipogenesis pathway, thereby decreasing triglyceride accumulation. These results suggest

that the observed effects go beyond the actions of biotin on ACC1/ACC2 carboxylases in favor of a general effect on lipid homeostasis.

In addition, the recovery of ATP levels may also suggest that high-dose biotin enhanced FAO in *Abcd1*⁻ mice. To enter the TCA cycle, fatty acid-derived acetyl-CoAs are bound to oxaloacetate by citrate synthase. Additional oxaloacetate may be directly provided by other biotin-dependent carboxylases, such as pyruvate carboxylase (PC) (28) or indirectly provided by refurbishing TCA cycle intermediates through the action of propionyl-CoA carboxylase (PCC) (77), thereby boosting the efficiency of FAO in producing ATP. Thus, the effects of biotin on PC and PCC rather

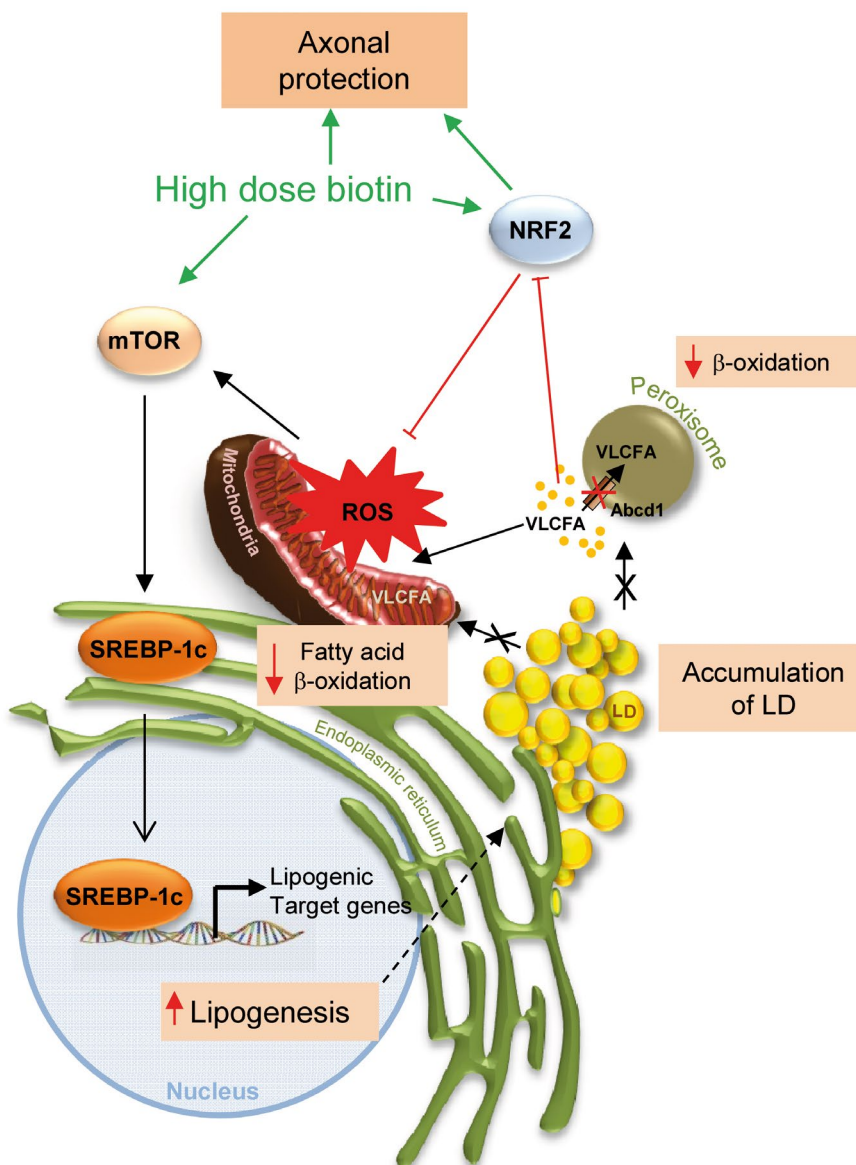


Figure 7. Model recapitulating the mode of action of High-dose biotin in X-ALD. High-dose biotin restores redox through reactivation of the NRF2 response, and normalizes the mTOR/SREBP1 transcriptional program, thus re-establishing lipid homeostasis. The lipid droplet accumulation in X-ALD may be caused by a combination of factors: (i) An increase in the formation of lipid droplets via increased lipid synthesis driven by mTOR/

SREBP-1; (ii) A decrease in the mitochondrial capacity to degrade lipid droplets caused by fewer mitochondria and lower fatty acid beta-oxidation: the latter driven by mTOR/SREBP1, and (iii) The decreased capacity of the peroxisome to degrade TAG caused by the loss of ABCD1: shown to be a key element in the tethering of LD to the peroxisomes.

than the enzymes ACC1/ACC2 could contribute to the restoration of metabolic homeostasis we see in this model.

Beyond the possible impact of biotin on its well-known carboxylase targets, the effect of high-dose biotin on the mTOR/SREBP-1c axis is intriguing, as it may have broad implications beyond the field of neurodegenerative diseases given its role as master regulator of metabolism, cell growth, autophagy, and innate immunity (29,55). We propose that mTOR overactivity in the nervous system of X-ALD mice is neutralized by high-dose biotin, igniting a cascade of compensatory effects that lead to restored lipid homeostasis,

improved metabolic function and the axonal maintenance. Restoring the expression levels of SREBP-1c and its targets, the lipogenic enzymes FAS, Δ9-desaturases, acyl-CoA synthetases and, moreover, the genes involved in mitochondrial fatty acid oxidation, may have direct consequences on axonal function. Indeed, knockout of SREBP-1c in the mouse induced the development of peripheral neuropathy and decreased myelin synthesis, along with blunted fatty acid synthesis and increased fatty acid oxidation, establishing a direct link between SREBP-1c function and axonal health (7).

Thus, normalization of the mTOR/SREBP-1c axis by high-dose biotin led to a reduction in total TAG levels in *Abcd1*^{-/-} spinal cords, although the levels of LPC C26:0 were maintained, indicating that there was no direct action on ABCD1 or other peroxisomal transporters potentially bypassing ABCD1 loss. The normalization of TAG levels by biotin was previously observed in a study of WT mice fed pharmacological doses of biotin (31). The treated mice showed a similar reduction in SREBP-1c-dependent lipid synthesis in the liver and adipose tissue along with decreased serum levels of TAG. Compared to our study, the experimental setting in that work was shorter (8 weeks), the mice were younger (3 months) and were of a different genetic background (Balbc), and lower doses of biotin were used (13.5 mg/kg/day vs. 60 mg/kg/day in our study), which underscores the robust effect in different organs and treatment conditions. Notably, the hypotriglyceridemic effect of biotin supplementation was also observed in nondiabetic and diabetic human probands in the absence of effects on cholesterol, glucose, or insulin levels (60). Taken together, these findings suggest a broader indication of high-dose biotin to treat systemic metabolic conditions.

The accumulation of LDs in the spinal motoneurons of X-ALD mouse models may have detrimental consequences. This appears to be an undescribed pathogenic factor inherent to X-ALD underappreciated to date, although LDs were recently detected in an *in vitro* endothelial model mimicking the blood brain barrier (35). Based on this observation, the authors suggested that metabolic lipid dysfunction not only contributes to chronic axonal degeneration in the mouse model (63) but is also implicated in the cerebral ALD phenotype.

There is a long-held view of LDs as inert intracellular storages for neutral lipids in all living organisms and cells; however, early indications of the accumulation of TAGs and sterol esters as consequence of membrane remodeling in neurodegenerative disorders and neural injury also exist, suggesting that LDs would merely be transient indicators of disease states (78). More recently, however, the direct impact of impaired LD dynamics on energy homeostasis and the overall physiology of organisms have begun to emerge (74). Later, advances have argued for a driving role of LDs in protection against oxidative stress. LDs may allow cells to safely sequester otherwise toxic lipids, in particular in cases of overabundant fatty acids, which may pose a threat to membrane integrity and peroxidability (2). Once these fatty acids become triglycerides, they incorporate into LDs and become relatively harmless (74). Indeed, in *Drosophila* larvae, LDs are substantially increased in the CNS as a result of oxidative stress originating from either hypoxic conditions or excess free radicals. By abolishing droplets specifically in glia, the capacity of neuronal stem cells to proliferate under oxidative stress *milieu* is arrested. The role played by these glial LDs is thought to be protective and has been attributed to the sequestration of vulnerable membrane fatty acids away from free radicals, thus avoiding the vicious cycle of lipid peroxidation (2). This view is further supported by work in flies, as elevated

mitochondrial ROS in neurons induce lipid synthesis via JNK/SREBP in these cells (38). Neuronal fatty acids are then transferred to astrocytes to form LDs, where they are oxidized in mitochondria (27). The accumulation of peroxidized lipids induces neurodegeneration, supporting LDs as both markers and protective agents rather than causes of neuronal demise. Furthermore, antioxidants reduced LD accumulation, thereby delaying neurodegeneration in mice (38). Moreover, a primary, causative role of disrupted LD dynamics in neuronal dysfunction is underscored by examining the consequence of loss of function of genes that are responsible for a number of hereditary cortical motoneuron diseases (the hereditary spastic paraplegias), such as atlastin, REEP1, seipin, spartin, and kinesin-1. These proteins play crucial roles in LD biology, such as mediating the fusion of ER tubules or controlling the size of LDs (30,54). More precise insights are derived from the study of DDHD2, the principal brain TAG lipase, which is defective in patients with spastic paraplegia 54 (SPG54) (64). DDHD2 patients exhibit a thin corpus callosum and periventricular myelin abnormalities in MRI, features reminiscent of other leukodystrophies, including X-ALD. In *Ddhd2*^{-/-} mice, a greater amount of TAGs in the form of LDs accumulates in the brain and spinal cord (25). The disruption of TAG hydrolase activity impairs the capacity to protect cells from LD accumulation following free fatty acid exposure (26). These results converge into a strong body of evidence directly connecting the dysfunction of LDs to decreased protection from lipid-caused oxidative stress, leading to motoneuron disease.

In sum, we believe the LD accumulation in X-ALD may constitute a protective mechanism against excess VLCFAs, which does not rule out a direct contribution of the increased LD to axonal demise when the situation becomes chronic. This increased size of the LD compartment is most likely caused by multifactorial mechanisms: (i) an increase in the biogenesis of LDs through increased lipid synthesis driven by mTOR/SREBP-1 and oxidative stress; (ii) a decrease in LD degradation capacity through impaired mitochondrial function caused by lower mitochondrial mass and lower fatty acid beta-oxidation expression, the latter driven by mTOR/SREBP-1; and (iii) the incapacity of peroxisomes to degrade at least some of the TAG fatty acids caused by the loss of ABCD1, which was shown very recently to be a key element in the tethering of LDs to the peroxisomes (8) (Figure 7). Consequently, LD accumulation in the spinal cord and increased TAG levels, which are also detectable in the periphery (PBMCs) of AMN patients (62), may be considered new biomarkers of X-ALD.

Taken together, our findings strongly suggest that interventional treatment using high-dose biotin may be an attractive therapeutic option for patients with X-AMN. The biological effects could be easily monitored by quantitatively measuring TAG levels in the PBMC of patients with X-AMN, as previously described (62). Moreover, these data open new perspectives for other diseases that exhibit axonal degeneration as a significant component of clinical progression, together with redox dyshomeostasis, mitochondrial depletion and/or alterations in lipid metabolism.

ACKNOWLEDGMENTS

We thank Laia Grau, Juanjo Martínez, and Cristina Guilera from the Neurometabolic Diseases Laboratory, IDIBELL, for technical assistance.

CONFLICT OF INTEREST

This study was supported by grants from Medday Pharmaceuticals SA who provided high-dose pharmaceutical-grade Biotin. High-dose Pharmaceutical-grade Biotin, MD1003, is a not approved investigational product being developed for use in patients with progressive MS.

FUNDING INFORMATION

We thank CERCA Program/Generalitat de Catalunya for institutional support. This study was supported by grants from Medday Pharmaceuticals SA to AP, the Autonomous Government of Catalonia [SGR 2014SGR1430; 2017SGR1206], and Instituto de Salud Carlos III [PI17/00916] (Co-funded by European Regional Development Fund. ERDF, a way to build Europe) to AP; by Instituto de Salud Carlos III through the grants [Miguel Servet program CPII16/00016] to SF (Co-funded by European Social Fund. ESF investing in your future); and the Center for Biomedical Research on Rare Diseases (CIBERER) to MR and NL. Locomotor experiments were performed by the SEFALer unit F5 (CIBERER) led by AP. Writing and editorial assistance was provided by Jean Fiber funded by MedDay Pharmaceuticals.

DATA AVAILABILITY STATEMENT

All data used and/or analyzed during the current study are available from the corresponding author on reasonable request.

REFERENCES

1. Abu-Elheiga L, Matzuk MM, Abo-Hashema KA, Wakil SJ (2001) Continuous fatty acid oxidation and reduced fat storage in mice lacking acetyl-CoA carboxylase 2. *Science* **291**:2613–2616.
2. Bailey AP, Koster G, Guillermier C, Hirst EM, MacRae JJ, Lechene CP *et al* (2015) Antioxidant role for lipid droplets in a stem cell niche of drosophila. *Cell* **163**:340–353.
3. Bodennec J, Koul O, Aguado I, Brichon G, Zwingelstein G, Portoukalian J (2000) A procedure for fractionation of sphingolipid classes by solid-phase extraction on aminopropyl cartridges. *J Lipid Res* **41**:1524–1531.
4. Caron A, Richard D, Laplante M (2015) The roles of mTOR complexes in lipid metabolism. *Annu Rev Nutr* **35**:321–348.
5. Cartier N, Hacein-Bey-Abina S, Bartholomae CC, Veres G, Schmidt M, Kutschera I *et al* (2009) Hematopoietic stem cell gene therapy with a lentiviral vector in X-linked adrenoleukodystrophy. *Science* **326**:818–823.
6. Casasnovas C, Ruiz M, Schluter A, Naudi A, Fourcade S, Veciana M *et al* (2019) Biomarker identification, safety, and efficacy of high-dose antioxidants for adrenomyeloneuropathy: a phase II pilot study. *Neurotherapeutics* **16**:1167–1182.
7. Cermentati G, Audano M, Giatti S, Carozzi V, Porretta-Serapiglia C, Pettinato E *et al* (2015) Lack of sterol regulatory element binding factor-1c imposes glial Fatty Acid utilization leading to peripheral neuropathy. *Cell Metab* **21**:571–583.
8. Chang CL, Weigel AV, Ioannou MS, Pasolli HA, Xu CS, Peale DR *et al* (2019) Spastin tethers lipid droplets to peroxisomes and directs fatty acid trafficking through ESCRT-III. *J Cell Biol* **218**:2583–2599.
9. DeWille JE, Horrocks LA (1992) Synthesis and Turnover of Myelin Phospholipids and Cholesterol. CRC Press: Boca Raton, FL.
10. Dumser M, Bauer J, Lassmann H, Berger J, Forss-Petter S (2007) Lack of adrenoleukodystrophy protein enhances oligodendrocyte disturbance and microglia activation in mice with combined Abcd1/Mag deficiency. *Acta Neuropathol* **114**:573–586.
11. Dutta R, McDonough J, Yin X, Peterson J, Chang A, Torres T *et al* (2006) Mitochondrial dysfunction as a cause of axonal degeneration in multiple sclerosis patients. *Ann Neurol* **59**:478–489.
12. Eichler F, Duncan C, Musolino PL, Orchard PJ, De Oliveira S, Thrasher AJ *et al* (2017) Hematopoietic stem-cell gene therapy for cerebral adrenoleukodystrophy. *N Engl J Med* **377**:1630–1638.
13. Engelen M, Barbier M, Dijkstra IM, Schur R, de Bie RM, Verhamme C *et al* (2014) X-linked adrenoleukodystrophy in women: a cross-sectional cohort study. *Brain* **137**(Pt 3):693–706.
14. Engelen M, Kemp S, de Visser M, van Geel BM, Wanders RJ, Aubourg P, Poll-The BT (2012) X-linked adrenoleukodystrophy (X-ALD): clinical presentation and guidelines for diagnosis, follow-up and management. *Orphanet J Rare Dis* **7**:51.
15. Ferrer I, Aubourg P, Pujol A (2010) General aspects and neuropathology of X-linked adrenoleukodystrophy. *Brain Pathol* **20**:817–830.
16. Ferrer I, Kapfhammer JP, Hindelang C, Kemp S, Troffer-Charlier N, Broccoli V *et al* (2005) Inactivation of the peroxisomal ABCD2 transporter in the mouse leads to late-onset ataxia involving mitochondria, Golgi and endoplasmic reticulum damage. *Hum Mol Genet* **14**:3565–3577.
17. Folch J, Lees M, Sloane Stanley GH (1957) A simple method for the isolation and purification of total lipides from animal tissues. *J Biol Chem* **226**:497–509.
18. Fourcade S, Ferrer I, Pujol A (2015) Oxidative stress, mitochondrial and proteostasis malfunction in adrenoleukodystrophy: A paradigm for axonal degeneration. *Free Radic Biol Med* **88**(Pt A):18–29.
19. Fourcade S, Lopez-Erauskin J, Galino J, Duval C, Naudi A, Jove M *et al* (2008) Early oxidative damage underlying neurodegeneration in X-adrenoleukodystrophy. *Hum Mol Genet* **17**:1762–1773.
20. Fourcade S, Ruiz M, Camps C, Schluter A, Houten SM, Mooyer PA *et al* (2009) A key role for the peroxisomal ABCD2 transporter in fatty acid homeostasis. *Am J Physiol Endocrinol Metab* **296**:E211–E221.
21. Fourcade S, Ruiz M, Guilera C, Hahnen E, Brichta L, Naudi A *et al* (2010) Valproic acid induces antioxidant effects in X-linked adrenoleukodystrophy. *Hum Mol Genet* **19**:2005–2014.

22. Galea E, Launay N, Portero-Otin M, Ruiz M, Pamplona R, Aubourg P *et al* (2012) Oxidative stress underlying axonal degeneration in adrenoleukodystrophy: a paradigm for multifactorial neurodegenerative diseases? *Biochim Biophys Acta* **1822**:1475–1488.
23. Galino J, Ruiz M, Fourcade S, Schluter A, Lopez-Erauskin J, Guilera C *et al* (2011) Oxidative damage compromises energy metabolism in the axonal degeneration mouse model of X-adrenoleukodystrophy. *Antioxid Redox Signal* **15**:2095–2107.
24. Hernandez-Vazquez A, Wolf B, Pindolia K, Ortega-Cuellar D, Hernandez-Gonzalez R, Heredia-Antunez A *et al* (2013) Biotinidase knockout mice show cellular energy deficit and altered carbon metabolism gene expression similar to that of nutritional biotin deprivation: clues for the pathogenesis in the human inherited disorder. *Mol Genet Metab* **110**:248–254.
25. Inloes JM, Hsu KL, Dix MM, Viader A, Masuda K, Takei T *et al* (2014) The hereditary spastic paraplegia-related enzyme DDHD2 is a principal brain triglyceride lipase. *Proc Natl Acad Sci U S A* **111**:14924–14929.
26. Inloes JM, Kiosses WB, Wang H, Walther TC, Farese RV Jr, Cravatt BF (2018) Functional contribution of the spastic paraplegia-related triglyceride hydrolase DDHD2 to the formation and content of lipid droplets. *Biochemistry* **57**:827–838.
27. Ioannou MS, Jackson J, Sheu SH, Chang CL, Weigel AV, Liu H *et al* (2019) Neuron-astrocyte metabolic coupling protects against activity-induced fatty acid toxicity. *Cell* **177**:1522–1535.e14.
28. Jitrapakdee S, St Maurice M, Rayment I, Cleland WW, Wallace JC, Attwood PV (2008) Structure, mechanism and regulation of pyruvate carboxylase. *Biochem J* **413**:369–387.
29. Jones RG, Pearce EJ (2017) mTOR signaling in the development and function of tissue-resident immune cells. *Immunity* **46**:730–742.
30. Klemm RW, Norton JP, Cole RA, Li CS, Park SH, Crane MM *et al* (2013) A conserved role for atlastin GTPases in regulating lipid droplet size. *Cell Rep* **3**:1465–1475.
31. Larrieta E, Velasco F, Vital P, Lopez-Aceves T, Lazo-de-la-Vega-Monroy ML, Rojas A, Fernandez-Mejia C (2010) Pharmacological concentrations of biotin reduce serum triglycerides and the expression of lipogenic genes. *Eur J Pharmacol* **644**:263–268.
32. Launay N, Aguado C, Fourcade S, Ruiz M, Grau L, Riera J *et al* (2015) Autophagy induction halts axonal degeneration in a mouse model of X-adrenoleukodystrophy. *Acta Neuropathol* **129**:399–415.
33. Launay N, Ruiz M, Grau L, Ortega FJ, Ilieva EV, Martinez JJ *et al* (2017) Tauroursodeoxycholic bile acid arrests axonal degeneration by inhibiting the unfolded protein response in X-linked adrenoleukodystrophy. *Acta Neuropathol* **133**:283–301.
34. Lee DK, Long NP, Jung J, Kim TJ, Na E, Kang YP *et al* (2019) Integrative lipidomic and transcriptomic analysis of X-linked adrenoleukodystrophy reveals distinct lipidome signatures between adrenomyeloneuropathy and childhood cerebral adrenoleukodystrophy. *Biochem Biophys Res Commun* **508**:563–569.
35. Lee CAA, Seo HS, Armién AG, Bates FS, Tolar J, Azarin SM (2018) Modeling and rescue of defective blood-brain barrier function of induced brain microvascular endothelial cells from childhood cerebral adrenoleukodystrophy patients. *Fluids Barriers CNS* **15**:9.
36. Li Y, Malkaram SA, Zhou J, Zempleni J (2014) Lysine biotinylation and methionine oxidation in the heat shock protein HSP60 synergize in the elimination of reactive oxygen species in human cell cultures. *J Nutr Biochem* **25**:475–482.
37. Liu J, Sabeva NS, Bhatnagar S, Li XA, Pujol A, Graf GA (2010) ABCD2 is abundant in adipose tissue and opposes the accumulation of dietary erucic acid (C22:1) in fat. *J Lipid Res* **51**:162–168.
38. Liu L, Zhang K, Sandoval H, Yamamoto S, Jaiswal M, Sanz E *et al* (2015) Glial lipid droplets and ROS induced by mitochondrial defects promote neurodegeneration. *Cell* **160**:177–190.
39. Lopez-Erauskin J, Fourcade S, Galino J, Ruiz M, Schluter A, Naudi A *et al* (2011) Antioxidants halt axonal degeneration in a mouse model of X-adrenoleukodystrophy. *Ann Neurol* **70**:84–92.
40. Lopez-Erauskin J, Galino J, Bianchi P, Fourcade S, Andreu AL, Ferrer I *et al* (2012) Oxidative stress modulates mitochondrial failure and cyclophilin D function in X-linked adrenoleukodystrophy. *Brain* **135**(Pt 12):3584–3598.
41. Lopez-Erauskin J, Galino J, Ruiz M, Cuezva JM, Fabregat I, Cacabelos D *et al* (2013) Impaired mitochondrial oxidative phosphorylation in the peroxisomal disease X-linked adrenoleukodystrophy. *Hum Mol Genet* **22**:3296–3305.
42. Lu JF, Lawler AM, Watkins PA, Powers JM, Moser AB, Moser HW, Smith KD (1997) A mouse model for X-linked adrenoleukodystrophy. *Proc Natl Acad Sci U S A* **94**:9366–9371.
43. Mahad D, Ziabreva I, Lassmann H, Turnbull D (2008) Mitochondrial defects in acute multiple sclerosis lesions. *Brain* **131**(Pt 7):1722–1735.
44. McGarry JD, Brown NF (1997) The mitochondrial carnitine palmitoyltransferase system. From concept to molecular analysis. *Eur J Biochem* **244**:1–14.
45. Mehlem A, Hagberg CE, Muhl L, Eriksson U, Falkevall A (2013) Imaging of neutral lipids by oil red O for analyzing the metabolic status in health and disease. *Nat Protoc* **8**:1149–1154.
46. Melo RC, D'Avila H, Bozza PT, Weller PF (2011) Imaging lipid bodies within leukocytes with different light microscopy techniques. *Methods Mol Biol* **689**:149–161.
47. Miller WP, Rothman SM, Nascene D, Kivisto T, DeFor TE, Ziegler RS *et al* (2011) Outcomes after allogeneic hematopoietic cell transplantation for childhood cerebral adrenoleukodystrophy: the largest single-institution cohort report. *Blood* **118**:1971–1978.
48. Morato L, Galino J, Ruiz M, Calingasan NY, Starkov AA, Dumont M *et al* (2013) Pioglitazone halts axonal degeneration in a mouse model of X-linked adrenoleukodystrophy. *Brain* **136**(Pt 8):2432–2443.
49. Morato L, Ruiz M, Boada J, Calingasan NY, Galino J, Guilera C *et al* (2015) Activation of sirtuin 1 as therapy for the peroxisomal disease adrenoleukodystrophy. *Cell Death Differ* **22**:1742–1753.
50. Moser AB, Fatemi A (2018) Newborn screening and emerging therapies for X-linked adrenoleukodystrophy. *JAMA Neurol* **75**:1175–1176.
51. Mosser J, Douar AM, Sarde CO, Kioschis P, Feil R, Moser H *et al* (1993) Putative X-linked adrenoleukodystrophy gene shares unexpected homology with ABC transporters. *Nature* **361**(6414):726–730.
52. Muneer Z, Wiesinger C, Voigtlander T, Werner HB, Berger J, Forss-Petter S (2014) Abcd2 is a strong modifier of the metabolic impairments in peritoneal macrophages of ABCD1-deficient mice. *PLoS One* **9**:e108655.

53. Ozand PT, Gascon GG, Al Essa M, Joshi S, Al Jishi E, Bakheet S *et al* (1998) Biotin-responsive basal ganglia disease: a novel entity. *Brain* **121**(Pt 7):1267–1279.
54. Pennetta G, Welte MA (2018) Emerging links between lipid droplets and motor neuron diseases. *Dev Cell* **45**: 427–432.
55. Perluigi M, Di Domenico F, Butterfield DA (2015) mTOR signaling in aging and neurodegeneration: at the crossroad between metabolism dysfunction and impairment of autophagy. *Neurobiol Dis* **84**:39–49.
56. Porstmann T, Santos CR, Griffiths B, Cully M, Wu M, Leever S *et al* (2008) SREBP activity is regulated by mTORC1 and contributes to Akt-dependent cell growth. *Cell Metab* **8**:224–236.
57. Pujol A, Ferrer I, Camps C, Metzger E, Hindelang C, Callizot N *et al* (2004) Functional overlap between ABCD1 (ALD) and ABCD2 (ALDR) transporters: a therapeutic target for X-adrenoleukodystrophy. *Hum Mol Genet* **13**:2997–3006.
58. Pujol A, Hindelang C, Callizot N, Bartsch U, Schachner M, Mandel JL (2002) Late onset neurological phenotype of the X-ALD gene inactivation in mice: a mouse model for adrenomyeloneuropathy. *Hum Mol Genet* **11**:499–505.
59. Ranea-Robles P, Launay N, Ruiz M, Calingasan NY, Dumont M, Naudi A *et al* (2018) Aberrant regulation of the GSK-3 β /NRF2 axis unveils a novel therapy for adrenoleukodystrophy. *EMBO Mol Med* **10**:e8604.
60. Revilla-Monsalve C, Zendejas-Ruiz I, Islas-Andrade S, Baez-Saldana A, Palomino-Garibay MA, Hernandez-Quiroz PM, Fernandez-Mejia C (2006) Biotin supplementation reduces plasma triacylglycerol and VLDL in type 2 diabetic patients and in nondiabetic subjects with hypertriglyceridemia. *Biomed Pharmacother* **60**:182–185.
61. van Roermund CW, Visser WF, Ijlst L, van Cruchten A, Boek M, Kulik W *et al* (2008) The human peroxisomal ABC half transporter ALDP functions as a homodimer and accepts acyl-CoA esters. *FASEB J* **22**:4201–4208.
62. Ruiz M, Jove M, Schluter A, Casanovas C, Villarroya F, Guilera C *et al* (2015) Altered glycolipid and glycerophospholipid signaling drive inflammatory cascades in adrenomyeloneuropathy. *Hum Mol Genet* **24**:6861–6876.
63. Schluter A, Espinosa L, Fourcade S, Galino J, Lopez E, Ilieva E *et al* (2012) Functional genomic analysis unravels a metabolic-inflammatory interplay in adrenoleukodystrophy. *Hum Mol Genet* **21**:1062–1077.
64. Schuurs-Hoeijmakers JH, Geraghty MT, Kamsteeg EJ, Ben-Salem S, de Bot ST, Nijhof B *et al* (2012) Mutations in DDHD2, encoding an intracellular phospholipase A(1), cause a recessive form of complex hereditary spastic paraplegia. *Am J Hum Genet* **91**:1073–1081.
65. Sedel F, Papeix C, Bellanger A, Touitou V, Lebrun-Frenay C, Galanaud D *et al* (2015) High doses of biotin in chronic progressive multiple sclerosis: a pilot study. *Mult Scler Relat Disord* **4**:159–169.
66. Seyer A, Boudah S, Broudin S, Junot C, Colsch B (2016) Annotation of the human cerebrospinal fluid lipidome using high resolution mass spectrometry and a dedicated data processing workflow. *Metabolomics* **12**:91.
67. Shimano H, Sato R (2017) SREBP-regulated lipid metabolism: convergent physiology - divergent pathophysiology. *Nat Rev Endocrinol* **13**:710–730.
68. Tansey FA, Thampy KG, Cammer W (1988) Acetyl-CoA carboxylase in rat brain. II. Immunocytochemical localization. *Brain Res* **471**:131–138.
69. Tong L (2013) Structure and function of biotin-dependent carboxylases. *Cell Mol Life Sci* **70**:863–891.
70. Tourbah A, Lebrun-Frenay C, Edan G, Clanet M, Papeix C, Vukusic S *et al* (2016) MD1003 (high-dose biotin) for the treatment of progressive multiple sclerosis: a randomised, double-blind, placebo-controlled study. *Mult Scler* **22**:1719–1731.
71. Troffer-Charlier N, Doerflinger N, Metzger E, Fouquet F, Mandel JL, Aubourg P (1998) Mirror expression of adrenoleukodystrophy and adrenoleukodystrophy related genes in mouse tissues and human cell lines. *Eur J Cell Biol* **75**:254–264.
72. Turgeon CT, Moser AB, Morkrid L, Magera MJ, Gavrilov DK, Oglesbee D *et al* (2015) Streamlined determination of lysophosphatidylcholines in dried blood spots for newborn screening of X-linked adrenoleukodystrophy. *Mol Genet Metab* **114**:46–50.
73. Walther TC, Chung J, Farese RV Jr (2017) Lipid droplet biogenesis. *Annu Rev Cell Dev Biol* **33**:491–510.
74. Welte MA (2015) Expanding roles for lipid droplets. *Curr Biol* **25**:R470–R481.
75. Wiesinger C, Kunze M, Regelsberger G, Forss-Petter S, Berger J (2013) Impaired very long-chain acyl-CoA beta-oxidation in human X-linked adrenoleukodystrophy fibroblasts is a direct consequence of ABCD1 transporter dysfunction. *J Biol Chem* **288**:19269–19279.
76. Wolf B (2011) The neurology of biotinidase deficiency. *Mol Genet Metab* **104**:27–34.
77. Wongkittichote P, Ah Mew N, Chapman KA (2017) Propionyl-CoA carboxylase - A review. *Mol Genet Metab* **122**:145–152.
78. Wood JG, Dawson RM (1974) Lipid and protein changes in sciatic nerve during Wallerian degeneration. *J Neurochem* **22**:631–635.

SUPPORTING INFORMATION

Additional supporting information may be found in the online version of this article at the publisher's web site:

Figure S1. (A) CTL (n = 3 to 4 by condition) and X-ALD human fibroblasts (n = 4 to 5 by condition) were pretreated with biotin (0.5, 2.5, or 5 μ M) for 24 h, and then, antimycin A (200 μ M) was added to the medium for 1 h. Next, H₂O₂ (DCF probe) was quantified. (B) CTL (n = 4) and X-ALD human fibroblasts (n = 5) were pretreated with biotin (0.5, 2.5 or 5 μ M) for 1 h, and then, antimycin A (200 μ M) was added to the medium for 1 h. Next, H₂O₂ (DCF probe) was quantified. (C) Relative GSH levels were quantified in CTL (n = 5) and X-ALD human fibroblasts (n = 3) after 24 h of treatment with vehicle (as a control) or C26:0. The cells were incubated with biotin (0.5, 2.5, or 5 μ M) for the last hour. (D) The relative inner mitochondrial potential ($\Delta\Psi$ m) was measured in CTL (n = 4 to 5 by condition) and X-ALD human fibroblasts (n = 3 to 4 by condition) after 24 h of treatment with vehicle (as a control), C26:0 or C26:0 with biotin (5 or 10 μ M), with C26:0 being added to medium containing 10% FCS. FCCP (200 μ M for 10 minutes) was used as a positive control. Quantification presented as the fold change relative to vehicle-treated fibroblasts. n = 4–5 per genotype and condition, with experiments done in triplicates. The values are expressed as the mean \pm SD (one-way ANOVA followed by Fisher *post hoc* test (**P* < 0.05, ***P* < 0.01 and ****P* < 0.001).

Fig S2

Figure S2. Quantification of (A) Iba1⁺ density (cells/mm²) (n = 4 to 5 per genotype and condition), (B) GFAP⁺ density (cells/mm²) (n = 4 to 5 per genotype and condition), and (C) synaptophysin and APP accumulation (n = 7 to 8 per genotype and condition) in spinal cord immunohistological sections from WT, DKO and DKO + high-dose biotin mice. The values are expressed as the mean \pm SD [one-way ANOVA followed by Fisher's *post hoc* test (**P* < 0.05, ***P* < 0.01 and ****P* < 0.001)].

Fig S3

Figure S3. Experiments were performed in the spinal cord of 13-month-old WT, *Abcd1*⁻ and *Abcd1*⁻ + high-dose biotin mice. (A-B) Species of TAG annotated by lipidomic analysis (n = 3 to 6 per genotype and condition) are represented based on the numbers of both total carbons and double bonds. The relative lipid levels were normalized to WT mice. The number is the relative fold change in the corresponding TAG species in

(A) *Abcd1*⁻ and (B) *Abcd1*⁻ + high-dose biotin mice compared with WT mice. In bold, species of TAG which are significantly different with (A) WT and (B) *Abcd1*⁻. Scale from red to blue represents the relative levels of each TAG species compared with WT. (C) LPC-26:0 levels (ng/mg of tissue) WT (n = 5), *Abcd1*⁻ (n = 3) and *Abcd1*⁻ + High-dose biotin (n = 6). Values are expressed as mean \pm SD (One-way followed by Fisher's *post hoc* test (**P* < 0.05, ***P* < 0.01 and ****P* < 0.001).

Fig S4

Figure S4. (A-D) Histological analysis performed in 13-month-old (A, C) WT (n = 5) and (B, D) *Abcd1*⁻ mice, (n = 5). Spinal cord histological sections were processed for ORO staining. (E) Quantification of lipid droplet accumulation in spinal cord immunohistological sections from 13-month-old WT and *Abcd1*⁻ mice. Scale bar = 25 μ m (A-B); scale bar = 5 μ m (C-D). The values are expressed as the mean \pm SD [Student's t-test (**P* < 0.05, ***P* < 0.01 and ****P* < 0.001)].



UNIVERSITAT_{DE}
BARCELONA